



IUSS

Scuola Universitaria Superiore Pavia

Scuola Universitaria Superiore IUSS Pavia

Università degli Studi di Pavia

Dipartimento di Biologia e Biotecnologie
'L. Spallanzani'

**Going on the road of antimycobacterial drug discovery: new,
old, repurposed drugs and mechanisms of action**

A Thesis Submitted in Partial Fulfilment of the Requirements
for the Degree of Doctor of Philosophy in

BIOMOLECULAR SCIENCES AND BIOTECHNOLOGIES

Obtained in the framework of the Doctoral Programme in
Biomolecular Sciences and Biotechnologies

by

Josè Camilla Sammartino

Supervised by
**Proff. Riccardi Giovanna,
Chiarelli Laurent Roberto, Pasca Maria Rosalia**

XXXIII° Cycle A.A. 2017-2021



Scuola Universitaria Superiore IUSS Pavia

Università degli Studi di Pavia

Dipartimento di Biologia e Biotecnologie

'L. Spallanzani'

**Going on the road of antimycobacterial drug discovery: new,
old, repurposed drugs and mechanisms of action**

A Thesis Submitted in Partial Fulfilment of the Requirements
for the Degree of Doctor of Philosophy in

BIOMOLECULAR SCIENCES AND BIOTECHNOLOGIES

Obtained in the framework of the Doctoral Programme in
Biomolecular Sciences and Biotechnologies

by

Josè Camilla Sammartino

Supervised by
**Proff. Riccardi Giovanna,
Chiarelli Laurent Roberto, Pasca Maria Rosalia**

XXXIII° Cycle A.A. 2017-2021

ABSTRACT

Since the beginning of 2020, the SARS-CoV-2 pandemic has drawn the world's attention to the danger of infectious agents, and to the need for ready-to-use therapies that are effective, with low risks and side effects for the patients. Despite the drama of today's situation, it is necessary to realize that there are many other infectious diseases in the world, which every year lead to the death of millions of people.

Tuberculosis (TB), caused by the bacillus *Mycobacterium tuberculosis* (*Mtb*), remains a worldwide spread disease. TB is the first cause of death from a single pathogen, and its therapy requires daily doses of multiple antibiotics over a period of 6 months but can be extended due to the onset of drug-resistant *Mtb* strains. For years, the efforts of our laboratory have focused on the characterization of the mechanism of action of new compounds with antitubercular activity, as well as on the understanding of the molecular and biochemical mechanisms of *Mtb* drug resistance.

In this thesis, we proceeded along the same path, following two complementary approaches: the “Target-to-Drug” and the “Drug-to-Target”. Firstly, through screening of compound libraries, we identified new anti-TB compounds, and studied their possible mechanism of action. In addition, we proceeded with a repurposing study of the Avermectins, which are anthelmintic compounds used in veterinary practice; among them, Selamectin showed the greatest anti-TB activity. This study revealed that selamectin has an inhibitory effect on the well-known drug target decaprenylphosphoryl-beta-D-ribose oxidase (DprE1), which is essential for the biosynthesis of the mycobacterial cell wall. Furthermore, because DprE1 works in concert with the decaprenylphosphoryl-2-keto-beta-D-erythro-pentose reductase (DprE2), the DprE1-DprE2 complex activity was in depth investigated.

On the other hand, we studied the polymorphisms associated with bedaquiline resistance, to deepen the knowledge on this mechanism of resistance and to help to overcome the spreading of bedaquiline-resistant *Mtb* strains in clinical settings.

This project expanded towards the study of new drugs against non-tuberculous mycobacteria (NTM), in particular *Mycobacterium abscessus* (*Mab*), which is an emerging pathogen among Cystic Fibrosis (CF) patients. In our work, we looked for new drugs against *Mab*. The hit compound 11326083 showed to be active, not only against *Mab*, but also against other NTMs and MDR clinical isolates. Its mechanism of action is still under investigation. Furthermore, by *in silico* molecular docking we identified some putative MmpL3 inhibitors active against *Mab* growth for which the characterization is still in progress.

TABLE OF CONTENTS

ABSTRACT.....	i
TABLE OF CONTENTS.....	iv
1. INTRODUCTION	1
1.1 <i>MYCOBACTERIUM TUBERCULOSIS</i> COMPLEX.....	3
1.1.1 Epidemiology and Drug-Susceptible TB therapy.....	5
1.1.2 <i>Mtb</i> Drug resistance: current therapy and drug development	8
1.1.3 Focus on bedaquiline, a new antitubercular drug.....	15
1.1.4 Drug repurposing	17
1.1.5 Mycobacterial cell envelope.....	18
1.1.6 Mycolic acid biosynthesis and direct inhibitors	20
1.1.7 Arabinogalactan biosynthesis effectors as molecular targets.....	22
1.2 CYSTIC FIBROSIS AND NONTUBERCULOUS MYCOBACTERIA.....	25
1.2.1 NTM morphology and pathophysiology	27
1.2.2 Therapy, and drug-resistance.....	30
1.2.3 New drugs and possible molecular targets.....	34
2. AIMS OF THE RESEARCH.....	37
3. MATERIALS AND METHODS.....	39
4. RESULTS AND DISCUSSION.....	48
5. CONCLUSIONS	86
REFERENCES	i
LIST OF ORIGINAL WORKS.....	xix

1. INTRODUCTION

During the last year, the Severe Acute Respiratory Syndrome - Coronavirus - 2 (SARS-CoV-2) pandemic has opened the eyes of the entire world on how dangerous infectious agents can be. As reported by the World Health Organization (WHO), each year millions of people die worldwide due to respiratory diseases, in particular Tuberculosis (TB) and acute lower respiratory infections (LRI) [WHO estimates, 2018]. Respiratory diseases make up five of the 30 most common causes of death: Chronic obstructive pulmonary disease (COPD) is third; LRI is fourth; tracheal, bronchial and lung cancer is sixth; TB is twelfth; and asthma is twenty-eighth [GBD, 2016; WHO, 2017]. LRI during childhood, and particularly before age 5, has been associated with and increased risk of developing asthma and reduced lung function in children, further posing a risk to their lives in the future [van Meel *et al.*, 2019]. Moreover, LRI gathering information process can be difficult, especially from low-income countries, proving a proper and valid estimation of the burden challenging [Murdoch and Howie, 2018; Ruopp *et al.*, 2015]. Even though the LRIs are caused by different viruses, *Haemophilus influenzae* and *Streptococcus pneumoniae* [Murdoch and Howie, 2018], mycobacterial lung infections need to be carefully assessed due to the unique characteristics of these bacteria [Cosma *et al.*, 2003].

TB is the first cause of death worldwide by a single pathogen, *Mycobacterium tuberculosis* (*Mtb*) [Banuls *et al.*, 2015].

As of today, there are more than 170 recognized species of mycobacteria [Forbes, 2016], which characterization in regards of the interaction with humans is vary, ranging from strictly pathogenic (*Mycobacterium tuberculosis*, *Mycobacterium leprae*, and *Mycobacterium ulcerans*), to environmental saprophytes (*Mycobacterium smegmatis*) mycobacteria [Bottai *et al.*, 2014]. *Mycobacterium* genus can be classified in two distinct groups: *Mycobacterium tuberculosis* Complex (MTBC) and Non-tuberculous mycobacteria (NTM). NTM do not cause tuberculosis or leprosy and are further subdivided into 4 categories based on phenotypic traits (Table 1), following Runyon classification [Simner *et al.*, 2016].

Mycobacteria are aerobic, nonmotile and do not form spores (with the exception of *Mycobacterium marinum*); the cell morphology is small rod-shaped. The colonies have different morphologies and colours depending on the type of mycobacteria or the exposure to external factors (light, minimal or rich media, anaerobic conditions, acidification) (Table 1) [Pfyffer, 2015; Wu and Dick, 2015]. Mycobacteria are widely spread in the environment, specifically due to their adaptive capabilities developed through genomic

INTRODUCTION

evolution and are characterized by a GC-rich genome with a peculiar lipid-rich cell-wall, which confers unique characteristics of drug/immuno resistance [Bottai *et al.*, 2014]. Host-pathogen interaction between Mycobacteria and humans has been the focus of research in the last years, unravelling the intricate infection pathways.

Table 1. Runyon classification of mycobacteria. Adapted from Simner *et al.*, 2016.

Group	Growth time on solid media (days)	Colony appearance	Mycobacterial species
<i>M. tuberculosis</i> complex	> 7	Rough, buff (light and dark)	<i>M. tuberculosis</i> , <i>M. africanum</i> , <i>M. bovis</i>
Runyon Group I Photochromogens	> 7	Smooth or rough, buff (dark), becoming lemon yellow or orange when exposed to light	<i>M. simiae</i> , <i>M. marinum</i> , <i>M. kansasii</i> , <i>M. asiaticum</i>
Runyon Group II Scotochromogens	> 7	Smooth or rough, yellow to orange (light or dark)	<i>M. goodii</i> , <i>M. scrofulaceum</i> , <i>M. szulgai</i>
Runyan Group 3 Nonchromogens	> 7	Smooth or rough, nonpigmented, buff (light or dark), colour may intensify with age	<i>M. avium</i> complex, <i>M. haemophilum</i> , <i>M. ulcerans</i> , <i>M. genavense</i>
Runyon Group IV Rapid Growers	< 7	Smooth or rough, buff or orange (light and dark)	<i>M. abscessus</i> , <i>M. chelonae</i> , <i>M. fortuitum</i> , <i>M. mucogenicum</i>

While *Mtb* is an obligate human pathogen, NTM have been considered, at most, opportunistic up until the 1980s where the human immunodeficiency virus (HIV) epidemic showed critical clinical interaction. Co-morbidity with other pathologies, such as HIV infection, Diabete Melitus, Rheumatoid Arthritis, Cystic Fibrosis, immunocompromisation and overall structural lung disease are strictly linked with more invasive mycobacterial disease and poor clinical outcomes [Degiacomi *et al.*, 2019]. Mycobacterial infections caused by *Mtb* or opportunistic mycobacteria (*Mycobacterium abscessus*, *Mycobacterium avium*) can interest not only lungs, but also different host's organs. Notably, the most cases of *Mtb* infections are pulmonary, while the other ones can involve different organs and host body districts [Aygun *et al.*, 2019; Sunnetcioglu *et al.*, 2015]. Furthermore, *Mtb* pulmonary infection, even post-treatment and resolution, has been linked to lung disfunction, fibrosis and higher risk of developing COPD [Ravimohan *et al.*, 2018]. Similarly, for NTM infection over 70% are pulmonary, mostly depending on the host immunological conditions, and are principally caused by *Mycobacterium avium* (*Mav*), followed by *Mycobacterium abscessus* (*Mab*) and *Mycobacterium kansasii* (*Mkan*) [Henkle and Winthrop, 2016].

1.1 MYCOBACTERIUM TUBERCULOSIS COMPLEX

Tuberculosis (TB), is an ancient disease, historically known as the “Consumption disease”, and dates back in the years with the first officially reported case about 3000 years ago [Barberis *et al.*, 2017]. In humans and animals, TB is caused by members of the *Mycobacterium tuberculosis* Complex (MTBC), which is a group of acid-fast bacteria with a high percentage of identity (99.9%) and comprises: *Mycobacterium tuberculosis*, *Mycobacterium africanum*, *Mycobacterium bovis* (and *Mycobacterium bovis* bacillus Calmette-Guérin), *Mycobacterium canettii*, *Mycobacterium microti*, *Mycobacterium pinnipedii*, *Mycobacterium mungi*, *Mycobacterium caprae*, *Mycobacterium orygis* and *Mycobacterium suricattae* [Brites and Gagneux, 2017; Malone and Gordon, 2017]. Among the species belonging to MTBC, 7 lineages are human host-specific: *Mycobacterium tuberculosis* lineages 1, 2, 3, 4 and 7; *Mycobacterium africanum* lineages 5 and 6; the other species cannot sustain the entire infective cycle only relying on the human host [Brites and Gagneux, 2017].

To this date, TB caused by *Mtb* still represents a serious health issue with over 10 million people affected in 2019, which resulted in about 1.4 million death worldwide [WHO, 2020]. To ultimately eradicate TB, in 2015 started the EndTB strategy, which aim is the 90% reduction of mortality and incidence of this disease by 2035 [Chakaya *et al.*, 2020]. Quick diagnosis protocols, management of TB latent form, immediate therapy administration and research funding are fundamental in order to reach the goal [Chakaya *et al.*, 2020]. Owing to its virulence and airborne transmission, *Mtb* is classified as a risk group 3 agent; as stated by the European Centre for Disease Prevention and Control (ECDC), manipulation of this microorganism, for diagnosis or research purposes, needs to be carried out at a Biosafety Level 3 laboratory (BSL3) [ECDC handbook, 2018]. The identification and characterization of the infective *Mtb* strain is fundamental for the appropriate therapy [Unubol *et al.*, 2019]. In this regard, genotyping and spoligotyping are established methodologies [Gori *et al.*, 2005], but new techniques are being developed to further reduce analysis time and laboratory expenses [Khosravi *et al.*, 2017; Unubol *et al.*, 2019]. Particularly in high burden countries, where TB is still endemic, understanding *Mtb* transmission, infection mechanisms and survival is pivotal [WHO report, 2020].

Upon exposure to infective agents, the human immune system is brought into action through recognition of specific pathogen-associated molecular patterns (PAMPs) by the pattern recognition Toll-like receptors (TLRs). However, *Mtb* can evade the immune response thanks to cell surface associated phthiocerol dimycocoserate (PDIM) lipids that mask PAMPs preventing signalling during the initial infective phase [Cambier *et al.*, 2014]. Furthermore, even when phagocytised, *Mtb* can counter the phagosome acidification through the activation of stress-response genes and perforate the phagosome activating its Type VII/ ESX-1 protein secretion system [Simeone *et al.*, 2015]. *Mtb* can survive in the macrophage for a long period of time stimulating the formation of the granuloma through

INTRODUCTION

cytokines induction by the phosphatidylinositol mannosides, and lipomannans present in the mycobacterial cell membrane [Dulberger *et al.*, 2019]. The granuloma structure, which is composed of a central necrotic core, surrounded by macrophages and lymphocytes, is a control mechanism, that can lead to the resolution of the infection, successfully eradicating *Mtb*. In some cases, it can also fail, allowing *Mtb* survival, leading to lung parenchyma disruption, cavitation of the airways and onset of the active disease, allowing *Mtb* transmission [Cadena *et al.*, 2017]. Consequently, upon *Mtb* exposure, only 5-10% of patients will immediately develop active TB, while the majority will have a persistent immune response to *Mtb* antigens in absence of clinical symptoms known as latent TB infection (LTBI) [Huang *et al.*, 2019]. LTBI can be diagnosed using the Tuberculin Skin Test (TST) and the Interferon- γ release assay (IGRA); neither of these tests has the power to help predicting the possibility of LTBI progression in the active TB form [Auguste *et al.*, 2017]. Nonetheless, a correct diagnosis is crucial for starting the therapy and ultimately eradicate TB, because LTBI can switch into the active form of the disease in case of immune system debilitation, such can occur in co-morbidities that modulate the patient immune system [Sia and Rengarajan, 2019].

Unfortunately, the only licenced vaccine available is Bacillus Calmette-Guérin (BCG), which is an attenuated strain of *M. bovis* [Calmet, 1931]. The efficacy of BCG in preventing *Mtb* infections varies widely between adults and children, being effective mostly only for the latter; the low efficacy of BCG could be explained considering that its antigenic composition is loosely related to *Mtb* [Ernst, 2018]. Currently, there are 14 new vaccine candidates in the Pipeline (Figure 1), of which 3 are in phase I, 8 in phase II (4 in phase IIa and 4 in phase IIb) and 3 in phase III clinical trials [WHO report, 2019]. However, only the vaccine candidate M72/AS01_E showed an unprecedented efficacy [WHO report, 2019]. M72/AS01_E comprises a recombinant fused protein (M72) of 2 highly immunogenic *Mtb* antigens (Mtb32A and Mtb39A), and the adjuvant AS01_E, that helps boosting the immune system cytotoxic response [Ji *et al.*, 2019]. This vaccine was designed to prevent pulmonary TB in subjects infected with *Mtb*. Clinical trials show that M72/AS01_E has a 54% efficacy in adult patients, and a 57% efficacy in LTBI patients in preventing pulmonary TB. Furthermore, this vaccine candidate can be safely used with HIV-infected patients and a second dose vaccination allows for a longer-term protection, with scarce adverse effects, deeming M72/AS01_E an interesting and safe candidate vaccine [Ji *et al.*, 2019].

Nonetheless, the progresses made are still far from what needed to eradicate *Mtb*. Various reasons hide behind the challenges for the development of a valid *Mtb* vaccine: scarce knowledge of *Mtb* epitopes, insufficient availability of valid animal models, need of infected human (or humanized) cells, higher equipment sensitivity and facilities that can sustain biosafety risk [Ernst, 2018].

INTRODUCTION

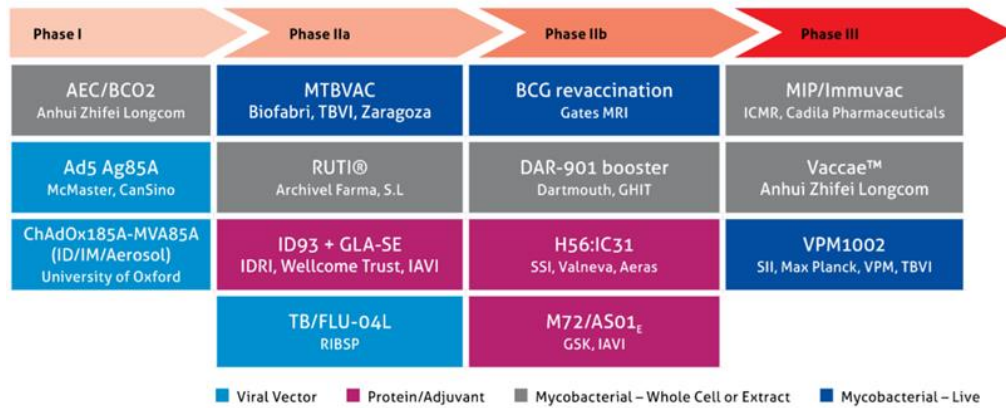


Figure 1. Vaccine Pipeline 2019 [WHO report, 2019].

1.1.1 Epidemiology and Drug-Susceptible TB therapy

The incidence trend since the EndTB strategy started, shows a gradual reduction over the years: 142:100000 in 2015 [WHO report, 2016], 140:100000 in 2016 [WHO report, 2017], 133:100000 in 2017 [WHO report, 2018], 130:100000 in 2018 [WHO report, 2019]. Over the last 4 years there has been a 6.3% reduction of TB incidence, which is far from the 20% reduction goal for 2020 [WHO report, 2019]. However, the distribution of the disease is not equally spread out in the world (Figure 2), because of the 87% of all registered TB cases in 2018 came from 30 high burden country, of which roughly the 67% were from just 8 of those: India (27%), China (9%), Indonesia (8%), the Philippines (6%), Pakistan (6%), Nigeria (4%), Bangladesh (4%) and South Africa (3%) [WHO report, 2019]. Furthermore, *Mtb* lineages are differently distributed in the world: lineages 2 (East Asia Lineage) and 4 (Euro-American Lineage) are broadly spread out; lineage 1 (Indo-Oceanic Strain) is commonly found in the regions of the Indian Ocean and lineage 3 is mostly distributed in East Africa, Central Asia and South Asia; lineages 5 (West Africa 1), 6 (West Africa 2) and 7 are specific of different African regions [Correa-Macedo *et al.*, 2019; Coscolla and Gagneux, 2014].

INTRODUCTION

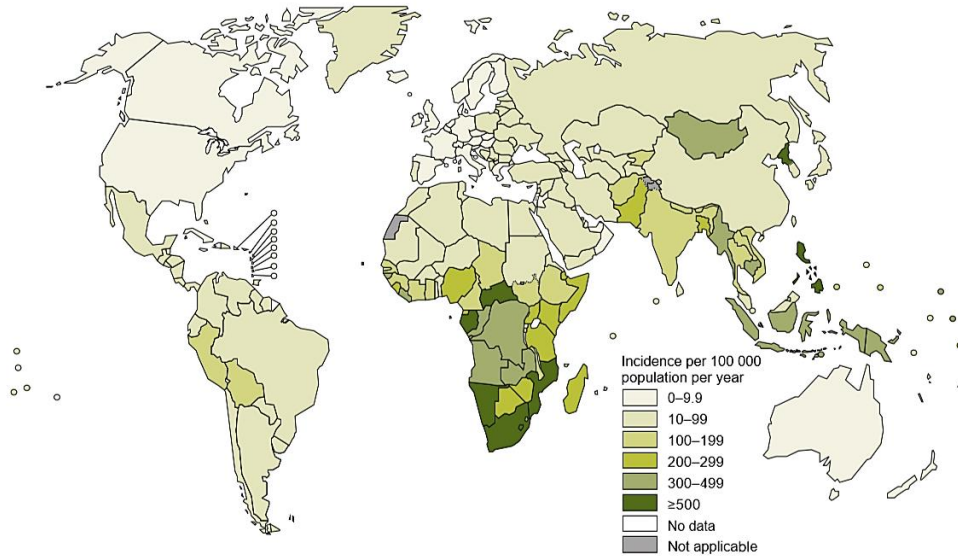


Figure 2. Estimates TB incidence rates in 2018 [WHO report, 2019].

The lineage identification could be beneficial for treatment, patient care and TB epidemiology, as *Mtb* lineages showed different behaviors in terms of virulence, stimulation of the host pro-inflammatory response and site of infection (pulmonary or extra-pulmonary) [Coscolla and Gagneux, 2014]. Moreover, TB progression depends on a plethora of factors, such as socioeconomic status, nutrition, smoke or alcohol abuse, co-morbidity with other pathologies, living conditions (overcrowding, poor ventilation, scarce hygiene) and intravenous drug usage [Duarte *et al.*, 2018]. Delineate the correct therapy and immediately start the patient on antibiotics are the most important actions to take.

Drug-susceptible TB (DS-TB) therapy is a two-phase treatment that last up to 6 months. During the first phase, the patient is administrated with 4 different first-line antibiotics daily, over a period of 2 months: isoniazid, rifampicin, pyrazinamide, and ethambutol; during the second phase that lasts 4 months, the patient is given rifampicin and isoniazid daily. The treatment has a low cost (about US\$20 in total) and an average success rate of 85% [Tiberi *et al.*, 2018].

Whereas for LTBI, different treatment options are available, and more are being tested in clinical trials. The three main optional treatments available are: (i) isoniazid and rifapentine once a week for 4 months; (ii) daily rifapentine for 4 months; (iii) daily isoniazid for 9 months [Lee *et al.*, 2020].

INTRODUCTION

Rifampicin and rifapentine are part of the same drug class and act by inhibiting transcription through binding of the mycobacterial RNA polymerase β subunit. Most of the mutations that confer resistance to these drugs are in the *rpoB* gene, coding for the RNA polymerase β subunit [Riccardi and Pasca, 2014]. Since its first use for TB treatment in the 1970s, not much has changed in terms of its administration, due to the dose-dependent complications that could arise [Grobbelaar *et al.*, 2019]. Furthermore, the use of rifampicin for over 40 years has led to the development of compensatory mutations in other genes, that allow *Mtb* rifampicin-resistant strains to have higher fitness and infectivity [Dookie *et al.*, 2018].

Isoniazid is a prodrug that once activated by the *Mtb* catalase-peroxidase KatG inhibits the NADH-dependent enoyl-ACP reductase by blocking mycolic acid synthesis, which is essential for *Mtb* survival, virulence and drug-resistance [Unissa *et al.*, 2016]. Since its first use in TB therapy in the 1950', isoniazid has been defined as the 'magic drug' by the media, and it is still one of the most powerful and used drugs in TB treatment [Riccardi and Pasca, 2014]. Most drug-resistant mutations reported are in *katA* and *inhA* genes that code respectively for the overmentioned activator and target of the drug; isoniazid-resistance mechanism is far more complex and can involve multiple genes and types of mutations at once [Hameed *et al.*, 2018].

The other first-line prodrug in TB treatment is the pyrazinamide; this compound is activated by the bacterial pyrazinamidase into pyrazinoic acid and acts by blocking mycobacterial translation through the binding of RpsA, coded by the *rspA* gene [Riccardi and Pasca, 2014]. Mutations in *rspA* gene are linked to pyrazinamide-resistance, as well as mutations in *pncA* gene (coding for the activator pyrazinamidase), but new resistance-linked genes are being discovered, highlighting the complexity of the mechanisms behind pyrazinamide-resistance [Hameed *et al.*, 2018].

The last one first-line drug, which is routinely utilised in DS-TB therapy, is ethambutol [Riccardi and Pasca, 2014]. This compound inhibits *Mtb* cell wall biosynthesis by targeting the arabinosyltransferase complex through the binding of the active sites of EmbC and EmbB [Zhang *et al.*, 2020]. The arabinosyltransferase complex is comprised of the heterodimer EmbA-EmbB and the homodimer EmbC₂; mutations in each one of the genes encoding for the complex subunits have been linked to *Mtb* ethambutol resistance [Hameed *et al.*, 2018; Zhang *et al.*, 2020].

Therapy success rate, for both DS-TB and LTBI, depends on diverse factors such as treatment drop-out, availability of counseling during treatment and follow-up, high-risk populations (refugees, poor, alcohol abusers, smokers), spread of *Mtb* drug resistant strains and co-morbidity with other pathologies [Lee *et al.*, 2020]. Particularly, HIV/*Mtb* coinfection (Figure 3) is the most represented and lethal comorbidity worldwide with over

INTRODUCTION

862000 coinfecting subject and 251000 deaths in 2018 [WHO report, 2019]. In patient HIV-positive, the risk of *Mtb* infection, reinfection and switching from LTBI to active TB is higher than the healthy population [Bruchfeld *et al.*, 2015]. However, the co-administration of TB and HIV antiviral therapies can produce alarming side effects, such as in case of rifampicin-based TB therapy co-administrated with Lopinavir/Ritonavir antivirals which could result in an increased hepatotoxicity with gastrointestinal involvement [Bruchfeld *et al.*, 2015]. In this regard, new therapies are being developed to overcome the problems related to co-administration, using a dual-target approach that allows for the targeting of both *Mtb* and HIV simultaneously [Alexandrova *et al.*, 2017].

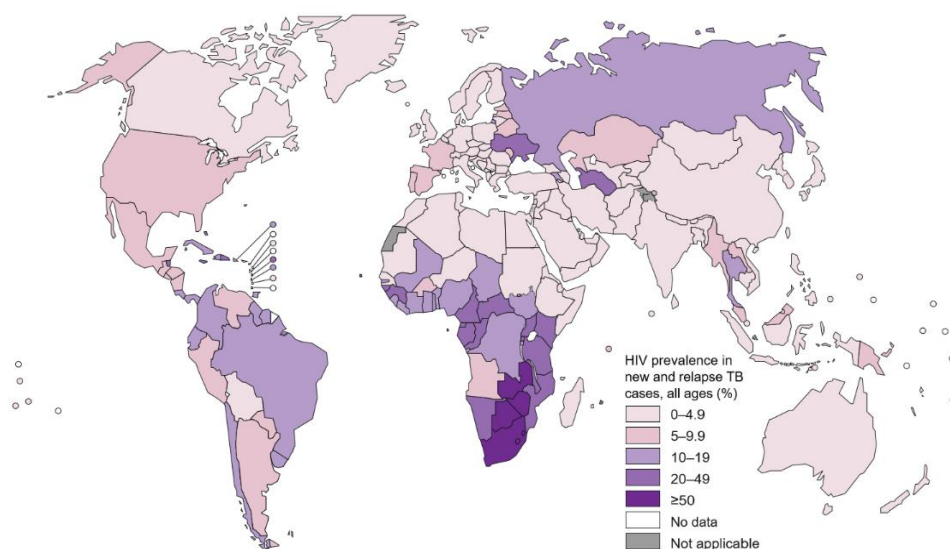


Figure 3. Estimated HIV prevalence in new and relapse TB cases, 2018 [WHO report, 2019].

Despite all the efforts for TB control and management, the situation is still extraordinarily complex. All the risk factors associated with contracting TB are the same as those related to the progression and resolution of the disease, which outline the effect of a 'dog chasing its tail'. Furthermore, apart from comorbidities, even more worrisome is the spreading of *Mtb* drug-resistant strains, as their appearance increases the variables against the resolution of the disease more than anything else.

1.1.2 *Mtb* Drug resistance: current therapy and drug development

Insurgence of drug resistance may derive from diverse factors, such as wrong antibiotics administration, treatment drop-out, late diagnosis, limited access to the therapy [Hameed *et al.*, 2018]. The first reported case of drug-resistant TB (DR-TB) was in the

INTRODUCTION

1950s, and ever since there has been an alarming increase in DR and Multi DR *Mtb* (MDR-*Mtb*) strains worldwide. *Mtb* drug resistant strains are categorized as it follows: (i) Mono-resistant (resistant to one antitubercular drug); (ii) Poly-resistant (resistant to at least 2 First-line drugs but rifampicin or isoniazid susceptible); (iii) Rifampicin-resistant (RR); (iv) MDR (resistant to both rifampicin and isoniazid); (v) Extensively Drug Resistant (XDR; an MDR strain also resistant to a fluoroquinolone and a second-line drug); (vi) Pre-XDR (MDR resistant to a fluoroquinolone or a second-line drug) [Hameed *et al.*, 2018; Shah *et al.*, 2020]. Furthermore, in recent years there have been reports of XDR *Mtb* strains resistant to all second-line drugs, which were classified as Totally drug resistant (TDR) *Mtb* [Migliori *et al.*, 2007; Velayati *et al.*, 2009; Udwadia *et al.*, 2012].

Early identification and monitoring of mono-resistant *Mtb* strains are pivotal to prevent the development of additional drug resistances; furthermore, particular attention should be given to anti-TB compounds used in the treatment of bacterial infections other than TB, as the over-exposition to these drugs can lead to the development of additional antibiotic-resistances [Mogashoa *et al.*, 2019]. Since treatment recommendations for DR-TB have changed throughout the years, the therapy should be carefully addressed; in particular, the patient must be supported and thoroughly followed during and after therapy administration [Tiberi *et al.*, 2017]. Clinicians should seek advertisement from TB experts in case of a suspected or confirmed case of DR-TB; then, molecular analysis for the identification of the *Mtb* drug resistance profile should be performed before and during TB treatment, to adapt the therapy to the patient needs [Nahid *et al.*, 2019]. Table 2 reports the latest classification of second-line drugs officially recommended by WHO [WHO consolidated guidelines, 2019].

Table 2. Second-line Drugs [WHO consolidated guidelines, 2019].

Group	Drugs
A	Fluoroquinolones (Levofloxacin, Moxifloxacin) Bedaquiline Linezolid
B	Clofazimine Cycloserine or Terizidone
C	Ethambutol Delamanid Pyrazinamide Imipenem-Cilastatin [†] or Meropenem [†] Amikacin or Streptomycin [‡] Ethionamide or Prothionamide p-Aminosalicylic acid

[†] Are administrated in association with Clavulanic acid, or Amoxicillin-Clavulanic acid.

[‡] Streptomycin is administrated only in case of Amikacin resistance or unavailability.

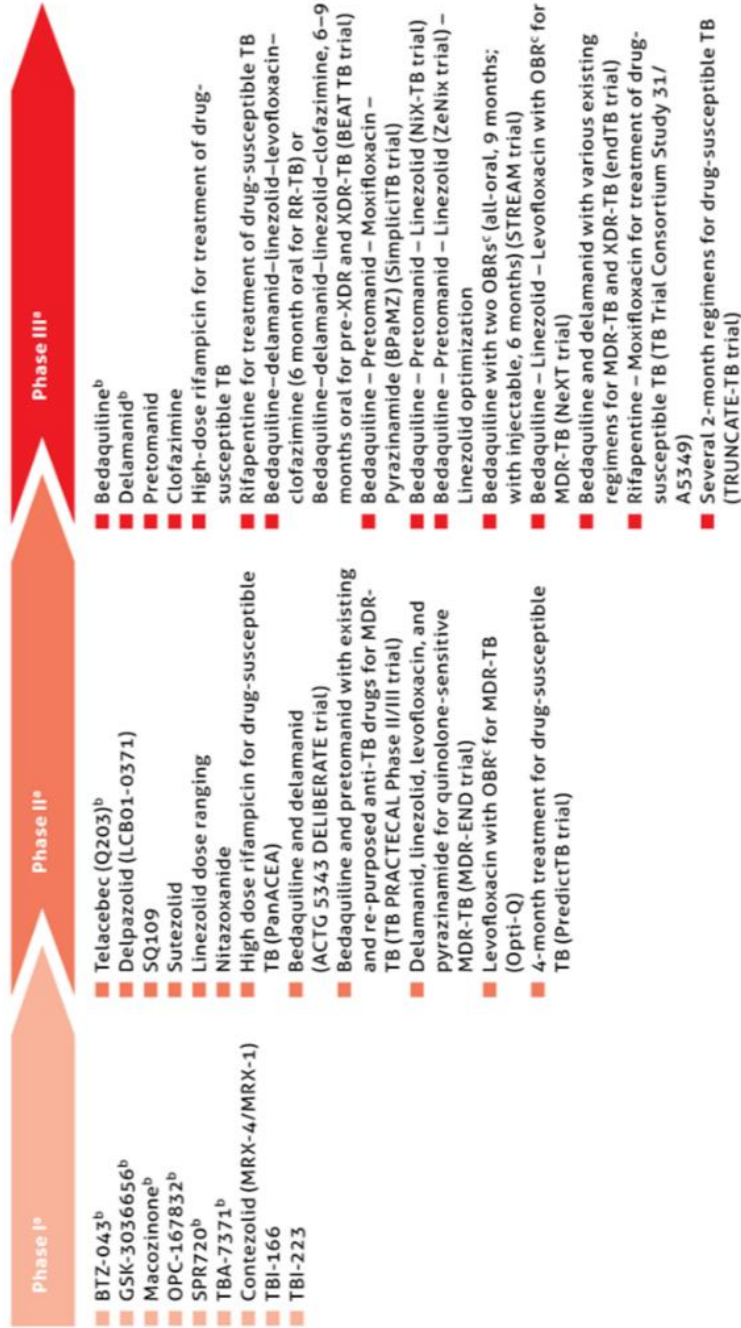
INTRODUCTION

Patients with isoniazid-resistant TB should be administered with rifampicin, ethambutol, pyrazinamide and levofloxacin daily for 6 months without streptomycin or other injectable drugs. Streptomycin should be used in MDR/RR-TB treatment only in the case of amikacin unavailability as it can correlate with lower treatment success rate [WHO consolidated guidelines, 2019].

For MDR/RR-TB the recommended treatment includes all Group A plus one from Group B drugs; Group C agents should be used only in the case of multiple resistances to Group A and B drugs (Table 2). Pyrazinamide should be administered for the entirety of the treatment, associated with fluoroquinolones, injectable anti-TB drugs, ethionamide and cycloserine in the intensive phase. In the eventuality of cycloserine unavailability, the p-Aminosalicylic acid should be used instead [WHO consolidated guidelines, 2019]. MDR/RR-TB treatment duration depends on the patient condition; the suggested period is of 18-20 months but can be shortened to 9-12 months if the patient has not already been treated for more than 1 month and resistance to fluoroquinolones or second-line injectable drugs has not been observed [WHO consolidated guidelines, 2019].

Treatment success for DR-TB depends on multiple factors; results from a meta-analysis of 87 studies from 25 countries, show an overall success rate of 65%, definitely lower than the 87% success rate of DS-TB therapy, but higher than previously reported (54%) for DR-TB [Collaborative Group, 2018]. The authors hypothesized that the introduction in the therapy of new drugs and the use of later generation fluoroquinolones may be the key factors for the higher success of currently DR-TB treatment compared to the past [Collaborative Group, 2018]. Developing new anti-TB drugs is necessary to contrast the spreading of *Mtb* DR strains and build a better treatment. In figure 4 it is reported the latest TB Drug pipeline, while the characteristics of recently approved drugs as well as that in clinical trials are overviewed in table 3.

A new anti-TB drug should have the following features: (i) safety usage; (ii) less to no side effects; (iii) be effective for shorter treatment time; (iv) cheaper; (v) have different targets from previously used drugs, so to avoid existing drug-resistance mechanisms; (vi) be compatible for the co-administration with antivirals and other anti-TB drugs [Bahuguna and Rawat, 2020].



^a New drug compounds are listed first, followed by repurposed drugs and then by regimens.

^b New chemical class.

^c Optimized background regimen.

Figure 4. TB Drug Pipeline 2019 [WHO report, 2019].

INTRODUCTION

Table 3. Overview of recent anti-TB drugs and development status. Adapted from Bahuguna and Rawat, 2019.

	Drug	Chemical class	Target	Effect	Clinical status
Recently approved	Bedaquiline	Diarylquinoline	ATP synthase	Inhibits cell energy metabolism	Phase III
	Delamanid	Nitroimidazole	Not known	Inhibits mycolic acid synthesis	Phase III
In clinical trials	Pretomanid	Nitroimidazole	Not known	Inhibition of cell wall synthesis	Phase III
	Delpazolid	Oxazolidinone	50S ribosome subunit	Inhibits protein synthesis	Phase II
	Sutezolid	Oxazolidinone	50S ribosome subunit	Inhibits protein synthesis	Phase II
	SQ109	Diamine	MmpL3	Inhibits cell wall synthesis	Phase II
	PBTZ169	Benzothiazinone	DprE1	Inhibits cell wall synthesis	Phase II
	Q203	Imidazopyridine	Cytochrome <i>bc1</i> complex	Inhibits ATP synthesis	Phase II
Repurposed	Clofazimine	Riminophenazine	Not known	Transmembrane penetration and intracellular redox cycling	
	Levofloxacin	Fluoroquinolone	DNA gyrase	Inhibits DNA replication	
	Moxifloxacin	Fluoroquinolone	DNA gyrase	Inhibits DNA replication	
	Linezolid	Oxazolidinone	50S ribosome subunit	Inhibits protein synthesis	

Bedaquiline was the first anti-TB drug approved by Food and Drug Administration (FDA) in the last 50 years; it is a potent bactericidal and sterilizing agent that inhibits the activity of *Mtb* ATP synthase. Bedaquiline activity can be enhanced if administrated with other anti-TB drugs, such as third-generation fluoroquinolones, pretomanid or pyrazinamide. Even though in recent years there has been a rising in

INTRODUCTION

bedaquiline-resistant *Mtb* strains, this drug is included in the second-line Group A drugs due to its relevance in treating DR-TB [Li *et al.*, 2019].

Levofloxacin is a third-generation fluoroquinolone used for a broad spectrum of bacterial infections, approved in the 1996 by the FDA and repurposed for TB therapy as a second-line drug. Levofloxacin achieves bactericidal activity through inhibition of the DNA gyrase, which results in blocking DNA synthesis in susceptible pathogens [Podder and Sadiq, 2019].

A fourth-generation fluoroquinolone approved for TB treatment is moxifloxacin, which is an 8-methoxy fluoroquinolone with bactericidal activity against Gram-positive/negative bacteria and *Mtb*. It is recommended in monoresistant TB therapy, but its plasma concentration is drastically reduced when co-administered with rifamycins. The mechanism of action is the same as the other fluoroquinolones. Moxifloxacin is generally tolerated in therapy, with rare serious adverse events, and its bactericidal efficacy is similar to isoniazid, making this drug an appealing substitute in TB therapy [Naidoo *et al.*, 2017].

Delamanid, which belongs to Nitroimidazole class, was approved for TB treatment in 2014 by the European Medicines Agency but it is yet to be approved by FDA. This compound inhibits the biosynthesis of mycolic acids; recent studies show very variable treatment success rates (from 53.8% to over 70%), demonstrating that an exhaustive validation of delamanid efficacy is yet to be obtained [Li *et al.*, 2019].

Another Nitroimidazole in phase III clinical trial is pretomanid. This compound is a prodrug that once activated by the deazaflavin-dependent nitroreductase Ddn, has bactericidal activity against replicating and non-replicating bacilli. Studies have shown synergistic effects in the combination pretomanid-bedaquiline-linezolid (PBL) with or without moxifloxacin (PBL±M), but the coadministration of PBL and clofazimine has antagonistic effects. Nonetheless, the synergy of PBL±M allows for a stronger sterilizing effect and shorten the treatment time in murine models [Xu *et al.*, 2019].

Linezolid belonging to Oxazolidinones class was just recommended by WHO as a Group A agent in 2018. Linezolid binds the 70S ribosomal subunit inhibiting *Mtb* protein synthesis. It also can target human mitochondria, leading to severe adverse effects such as bone marrow suppression, neuropathy and gastrointestinal involvement. Nonetheless, different studies reported the higher efficacy of linezolid in DR-TB treatment, but more work and assessments are necessary [Singh *et al.*, 2019].

Sutezolid is a thiomorpholinyl oxazolidinone, currently in phase II clinical trials [Bahuguna and Rawat, 2020]. This compound is generally safe and well tolerated; then, it showed superior efficacy against *Mtb* than linezolid in clinical trials and can shorten the

INTRODUCTION

treatment time in murine model. Furthermore, *in vitro* its sulfoxide metabolite has extracellular killing activity while the parent one is active against intracellular mycobacteria, making this compound promising for complete *Mtb* eradication [Wallis *et al.*, 2014].

Delpazolid is a synthetic oxazolidinone with a cyclic amidrazone group and inhibits early protein translation through the binding the 23S rRNA V domain of the 50S ribosomal subunit. Retrospective analysis showed that its activity is comparable to other oxazolidinones used in TB therapy, but with a fewer delpazolid-resistance rate, probably implying that its mechanism of action may differ in part from other oxazolidinones [Zong *et al.*, 2018].

Q203 is an imidazopyridine amide that inhibits *Mtb* growth *in vitro* and in murine models, by targeting the Cytochrome *bc1* complex. Even though nanomolar concentration of the compound are needed to explicate its activity, Q203 lacks bactericidal activity against *Mtb*. However, simultaneously targeting other effectors of the respiratory chain or its use in combination with other anti-TB drugs may help weakening *Mtb* defenses and efficiently kill the pathogen [Lu *et al.*, 2018].

Another synthetic drug in the development is SQ109. Its structure is based on a N,N'-isopropyl ethylenediamine core. SQ109 derives from ethambutol but has a different mechanism of action; in fact, ethambutol-resistant *Mtb* strains are SQ109-susceptible. This compound blocks the integration of mycolic acids into *Mtb* cell wall through the inhibition of MmpL3, which is the membrane transporter of trehalose monomycolate [Tahlan *et al.*, 2012].

Targeting mycobacterial cell wall biosynthesis is a desirable mechanism of action for anti-TB drugs, as it leads to integrity disruption of the cell and consequently to mycobacterial death. In this regard in 2009 BTZ043 was synthesized [Makarov *et al.*, 2009]. This compound blocks arabinogalactan synthesis, which is essential for *Mtb* cell wall biosynthesis, through the inhibition of the decaprenylphosphoryl- β -D-ribose 2-epimerase (DprE1) even at nanomolar concentrations [Makarov *et al.*, 2009].

In 2014 the piperazine derivative of BTZ043, PBTZ169, was synthesized. This compound, which is currently in phase II clinical trials, showed higher efficacy against both DS and DR *Mtb* strains and lower cytotoxicity [Makarov *et al.*, 2014]. Moreover, PBTZ169 has additive effects in combination with isoniazid, moxifloxacin, pretomanid and rifampicin, and synergistic effect in combination with bedaquiline *in vitro*. Also, in a chronic TB murine model, the combination of PBTZ169-bedaquiline-pyrazinamide was more effective in comparison to the canonical isoniazid-rifampicin-pyrazinamide [Makarov *et al.*, 2014].

INTRODUCTION

Clofazimine, is a repurposed drug used for leprosy treatment since the 1980'. The exact mechanism of action of clofazimine is yet to be fully elucidated, but it probably targets *Mtb* outer membrane. Clofazimine has shown synergistic effects with other anti-TB drugs, such as ethambutol, pyrazinamide, PBTZ169 and SQ109. Clofazimine has in its structure phenazine nucleus that can spontaneously oxidize, producing electron attractors elements, that can compete with NADH oxidization, reducing ATP production, and ultimately inhibiting the respiratory chain and ion transporters in mycobacteria [Mirnejad *et al.*, 2018].

1.1.3 Focus on bedaquiline, a new antitubercular drug

Approved in 2012 for TB treatment, bedaquiline (Figure 5) is a diarylquinoline, which targets the F₀ subunit of the ATP synthase (Figure 6) [Andries *et al.*, 2005; Li *et al.*, 2019]. Bedaquiline is active against different mycobacterial species but has scarce efficacy against Gram-positive and Gram-negative bacteria, proving its specificity to *Mycobacterium* genus [Andries *et al.*, 2005]. Bedaquiline is very active *in vitro* against fully susceptible *Mtb* strains and drug-resistant clinical isolates (comprising MDR and XDR) (MIC = 0.03-0.12 µg/mL) [Andries *et al.*, 2005].

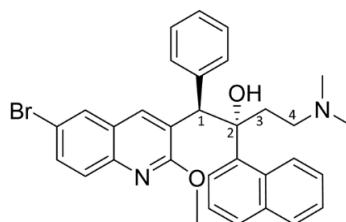


Figure 5. Bedaquiline chemical structure.

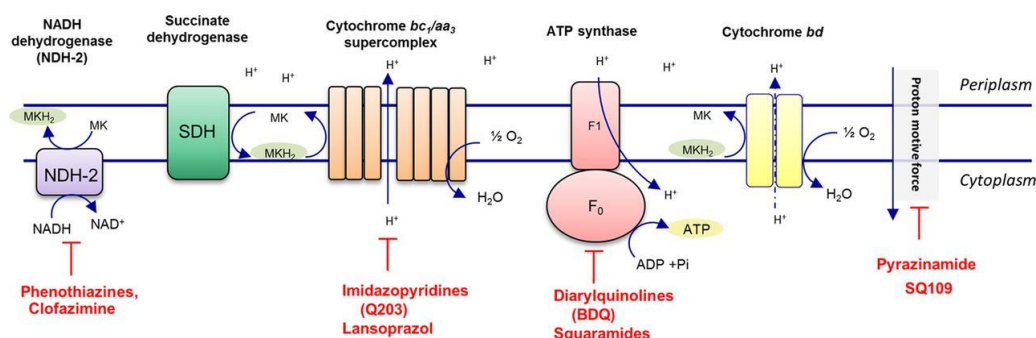


Figure 6. Drug targets in the *Mtb* electron transport chain. [Bald *et al.*, 2017].

Furthermore, bedaquiline bactericidal activity is time-dependent, more than dose-dependent, making this drug very appealing for TB treatment [Andries *et al.*, 2005]. Using

INTRODUCTION

a metabolomic approach, it was discovered that it is primarily metabolized by the CYP3A4 through N-demethylation, producing 8 different metabolites; CYP2C8 and CYP2C19 are also involved in this process [Liu *et al.*, 2014]. Moreover, CYP3A4 is also responsible for bedaquiline N-dealkylation, which produces an aldehyde metabolite with potential high toxicity [Liu *et al.*, 2014]. Consequently, as TB treatment requires the co-administration of various drugs over a long period of time, it is important to understand the pathways involved in the drugs metabolism to avoid adverse effects or treatment failure. In this regard, rifampicin is a well-known CYP3A4 inducer, while isoniazid inhibits both CYP3A4 and CYP2C19 [Desta *et al.*, 2001; Thijs *et al.*, 2019]. Furthermore, CYP3A4 is also inhibited by the antiviral ritonavir used to treat HIV infections and by clofazimine, which also inhibits CYP2C8 [Jungmann *et al.*, 2019; Sangana *et al.*, 2018]. Co-administration of these drugs should be carefully evaluated.

Bedaquiline has a long half-life (5-6 months), in part attributed to its high lipophilic structure, modulable by the modification of the naphthalene ring in C2, the phenyl ring in C1 and the Bromine (Br) in position 6 of the methoxy-quinoline moiety [Patel *et al.*, 2019] (Figure 5). Moreover, the diethylamino group in C4 enhances lipophilicity, but can also target the human cardiac potassium channel hERG (KCNH2), inhibiting its activity, and consequently prolonging the QT interval [Patel *et al.*, 2019]. Oral administered high lipophilicity drugs have been linked to increased risk of liver toxicity damage, which still explains why bedaquiline should be administered under strict patient control [Cohen and Martens, 2019; McEuen *et al.*, 2017].

The use of bedaquiline for treating MDR- and (pre)XDR-TB is crucial as it can shorten sputum culture conversion time, increase cure rates, and reduce mortality [Cohen and Maartens, 2019]. Bedaquiline, altogether with linezolid, clofazimine or delamanid, is recommended for longer DR-TB treatment (18-24 months) by the WHO for patients aged 6 or more [WHO consolidated guidelines, 2019]. Moreover, different ongoing studies are evaluating the efficacy of bedaquiline on shorter regimens and in association with other anti-TB drugs [WHO report, 2019]. In particular, NIX-TB and TB-PRACTECAL trials are evaluating a 6-month regimen with bedaquiline, pretomanid and linezolid (BPL) [ClinicalTrials.gov; Conradie *et al.*, 2020]. In the NIX-TB trial, results showed that 90% of the 109 enrolled patients (71 XDR and 38 MDR) had favorable therapy outcomes, while the TB-PRACTECAL, which started in January 2017, is ongoing [ClinicalTrials.gov; Conradie *et al.*, 2020]. The TB-PRACTECAL enrolled 630 patients (almost 6:1 in comparison to NIX-TB) and compared 3 regimens: (i) BPL; (ii) BPL + moxifloxacin; (iii) BPL + clofazimine [ClinicalTrials.gov].

Unfortunately, primary bedaquiline resistance has already been reported in *Mtb* clinical isolates [Veziris *et al.*, 2017; Villelas *et al.*, 2017; Zimenkov *et al.*, 2017; Ismail *et al.*, 2018]. The most represented bedaquiline-resistance mutations among *Mtb* clinical isolates

are in the following genes: *Rv0678*, coding for the repressor of the MmpS5-MmpL5 efflux pump; *atpE*, coding for the ATP synthase subunit c [Degiacomi *et al.*, 2020]. Mutations in *atpE* increase bedaquiline MIC in *Mtb* resistant strains, from 10 to 128 times, while mutations in *Rv0678* have a 2 to 8-fold higher MIC in comparison with the susceptible strain, and cause additional cross-resistance to clofazimine [Nguyen *et al.*, 2018]. Moreover, in association with *Rv0678*, other mutations in *pepQ* gene, coding for the cytoplasmatic peptidase PepQ, and in *Rv1979c*, coding an uncharacterized transporter, have also been linked to clofazimine-bedaquiline cross-resistance [Nieto *et al.*, 2020]. For these reasons, a quick and specific characterization of *Mtb* bedaquiline resistant strains is pivotal for the definition of the correct and safest therapy for TB patients, particularly in case of drug resistant *Mtb* infections [Nguyen *et al.*, 2017]. In this regard, repurposing already available drugs for TB treatment is an appealing strategy to contrast the shortage of ready-to-use compounds in the TB drug pipeline.

1.1.4 Drug repurposing

Drug repurposing (or-reprofiling) is the study of previously approved drugs, which are aimed at specific diseases or conditions, and redirects them to a new purpose. This approach is based on the already available knowledge of approved drugs, which can be readily authorized by the FDA bypassing the early expensive stages of research [Gns *et al.*, 2019]. Knowing the involved actors, metabolic pathways, protein interactions, side effects, mechanisms of action and more, can help to identify different drugs with the same effect/target and repurpose those to cure a different disease with same molecular, biochemical characteristics [Gns *et al.*, 2019]. In this regard, recently it was found that avermectins (Figure 7) have bactericidal activity against DS-, MDR- and XDR-*Mtb* strains [Lim *et al.*, 2013].

Avermectins are macrocyclic lactones which are used as veterinary and human drugs for the control of parasitic infections [Bishop *et al.*, 2000; Laing *et al.*, 2017]. Furthermore, this class is also used as insecticides, that block neural transmission and muscular activity through the binding of glutamate-gated chloride ion channels [Giannetti *et al.*, 2011]. It is worth noting that mammals have ligand-gated chloride channels, which are the γ -aminobutyric acid type A (GABA), located in the central nervous system. Macrolides could potentially bind them and activate the inhibitory neurotransmission, but the presence of the hematoencephalic barrier prevents macrolides diffusion into the brain and consequently their action [Merola and Eubig, 2018]. The repurposing of these drugs could be extremely beneficial due to the possible oral administration, reducing therapy burden for those infections treated with intravenous drugs daily [Omansens *et al.*, 2015]. Furthermore, in recent studies, preliminary data show that both ivermectin and selamectin can strongly inhibit the cytopathogenic effect in cells infected with SARS-CoV-2 *in vitro* [Caly *et al.*, 2020; Fan *et al.*, 2020]. In mammal, evidence showed that selamectin is a P-gp

INTRODUCTION

modulator. P-gp is a drug efflux transporter of the ABC superfamily linked to drug resistance in tumoral cells; in fact, selamectin oral administration inhibits P-gp activity, reducing the transport in the outer-membrane space in Caco-2 monolayer cells *in vitro* [Griffin *et al.*, 2005].

Interestingly, avermectins appear to target mycobacteria, which is promising for human clinical practice, as the gut flora would not be dramatically affected by their prolonged use [Lim *et al.*, 2013]. Selamectin has been proven the most effective avermectin with bactericidal time-dependent activity against mycobacteria [Scherr *et al.*, 2015].

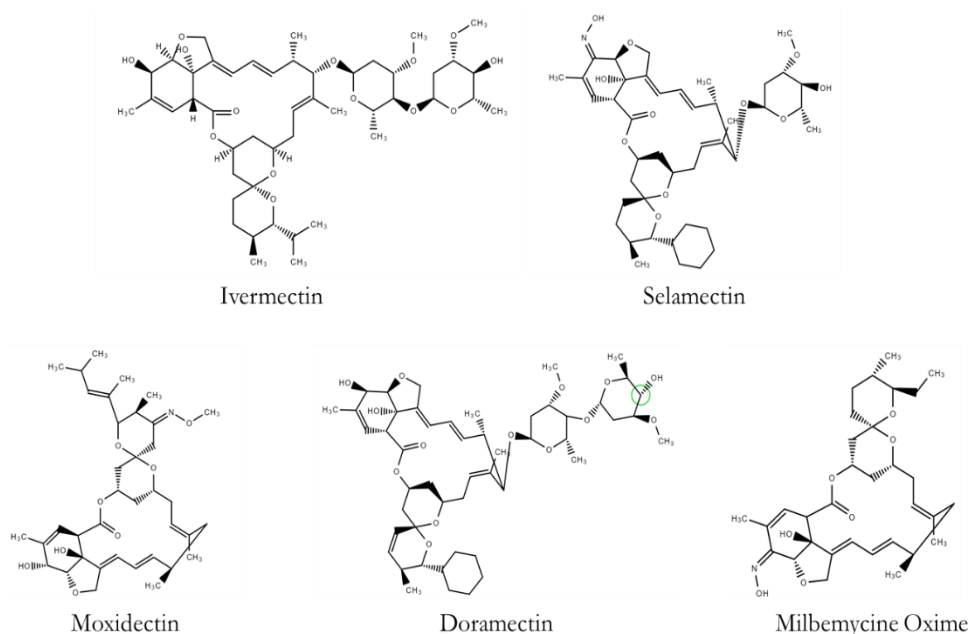


Figure 7. Macrolides used in veterinary practice and as insecticides.

1.1.5 Mycobacterial cell envelope

Mycobacteria have a peculiar cell envelope composition, that greatly differs from Gram-positive and Gram-negative bacteria (Figure 8), both in the structure and in the responsiveness to external factors. The plasma membrane has a high presence of glycoconjugates and functional proteins and is quite similar between fast and slow growing mycobacteria [Daffè and Marrakchi, 2019]. The cell wall is composed of mycolyl-arabinogalactan-peptidoglycan, which is a large thick structure of 7-8 nm where the mycolic

INTRODUCTION

acid chains are folded and intercalated with glycosylated proteins, transferases, and membrane channel proteins [Daffè and Marrakchi, 2019].

The hallmark of mycobacterial cell wall is the high lipids content, which translates in a largely developed lipids metabolism machinery with at least 5-fold more enzymes involved in the process, in comparison to the laboratory reference *Escherichia coli* [Cole *et al.*, 1998].

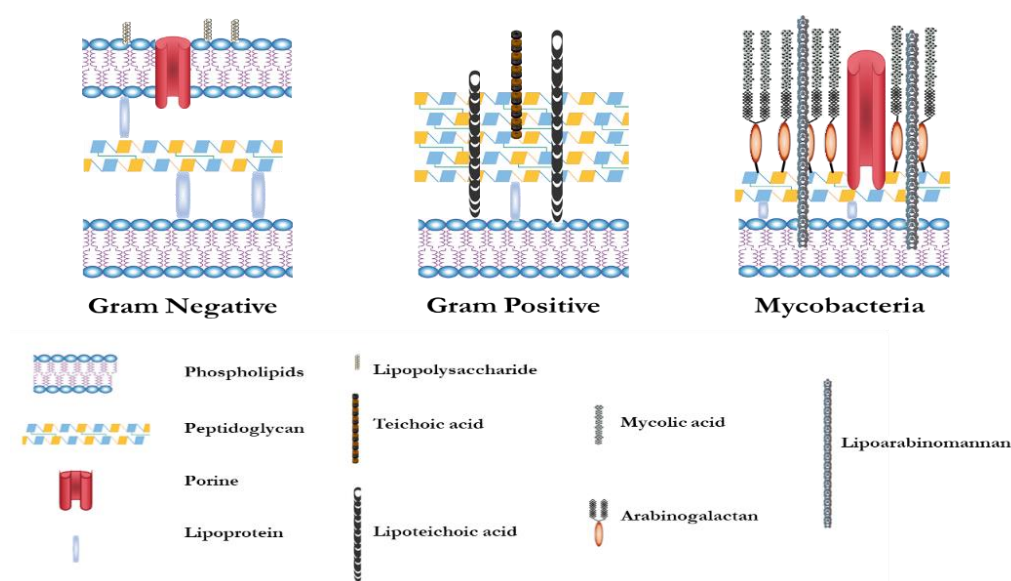


Figure 8. Graphical representation of Gram-positive, Gram-negative, and mycobacterial envelopes.

The outermost layer is represented by the capsule, composed of glycopeptidolipids, polysaccharides, glucans and polypeptides that can be secreted or linked to the cell wall [Daffè and Marrakchi, 2019]. Furthermore, mycobacterial cell division is not symmetrical, leading to different cell daughters, making the understanding of where and how the new constituents are inserted hard to decipher [Baranowski *et al.*, 2019]. Nevertheless, considering that the cell envelope is the first point-of-contact between the pathogen and the human host during infection, and that its integrity is fundamental for mycobacterial survival and virulence, its components and effectors are important drug targets for the development of new anti-TB drugs [Dulberger *et al.*, 2020].

In designing a new compound, deep understanding of the plausible target is fundamental. Thus far, different mycobacterial cell wall targets have been identified, and specific drugs to inhibit the biosynthesis pathways involved have been designed, but to

overcome the rising of *Mtb* drug resistant-strains, new efforts need to be made [Bhat *et al.*, 2017].

1.1.5.1 Mycolic acid biosynthesis and direct inhibitors

Mycolic acids are composed of multiple long-chain fatty acids that can be linked to trehalose sugars or extractable with organic solvents; they are disposed in the outermost layer of the mycobacterial cell envelope just beneath the loose matrix of glucans and proteins that composes the capsule [Dulberger *et al.*, 2020]. Their biosynthesis involves the iterating action of the fatty acid synthase type I (FAS-I) and the fatty acid synthase type II (FAS-II) systems. The first biosynthetic step is carried out by the FAS-I system through the condensation of acetyl-CoA units to form malonyl-CoA, that is further elongated by FAS-I up to C₁₆-C₁₈ or C₂₄-C₂₆ fatty acid chains. The C₁₆-C₁₈ chains are condensed with Malonyl-ACP to form β -ketoacyl-ACP, which is modified and elongated 2 carbons per cycle through the FAS-II system. The Acyl-ACP formed is then elongated, desaturated and modified to obtain a C₄₈-C₅₂ activated meromycolate; it can be condensed with the carboxylated C₂₄-C₂₆ chain produced by FAS-I, generating a mycolic β -ketoester. Finally, the trehalose ester can be transported through the trehalose monomycolate transporter MmpL3 from the cytosol to the cell wall [Marrakchi *et al.*, 2014].

Several enzymes are involved in the fatty acid biosynthesis process, but only that coded by *fas*, *inhA*, *fabG1*, *badB* and *kasA* genes are essential for *Mtb* growth. In particular, *fas* gene codes for the fatty acid synthase type I, while the other ones are part of the FAS-II system; *inhA* codes for the NADH-dependent enoyl-ACP reductase, that reduces the enoyl chain to produce acyl-ACP; *fabG1* codes for the 3-oxoacyl-ACP reductase that catalyses the first reduction of the FAS-II cycle; *badB* codes for one of the subunits of the (3R)-hydroxyacyl-ACP dehydratase that removes one molecule of H₂O from the elongating fatty acid; *kasA* codes for the 3-oxoacyl-ACP synthase 1 that starts a new FAS-II cycle through the addition of another Malonyl-ACP unit to the fatty acid chain [Marrakchi *et al.*, 2014]. The expression of the fatty acid synthase I is promoted by the TetR-like regulator FasR, which binding to the *fas* promoter is modulated by the pool of C₁₆-C_{>16} fatty acids chains, while the expression of the FAS-II enzymes is regulated by the binding of MabR to the FAS-II operon promoter. Interestingly, MabR appears to also have a role in modulating FasR, as the repression of the FAS-II promoter from MabR yields the accumulation of C₁₆-C_{>16} fatty acid chains that inhibit FasR binding to the *fas* promoter [Salzman *et al.*, 2010; Mondino *et al.*, 2013].

Taking into consideration all the different effectors and steps in the biosynthesis of mycolic acids, many compounds that target this process are already available or in development.

INTRODUCTION

As already mentioned, isoniazid is a first-line prodrug that after its activation inhibits the NADH-dependent enoyl-ACP reductase (InhA). The insurgence of resistance-inducing mutations in both the activator and the target is posing a great problem for the public health [Garg *et al.*, 2019]. For this reason, finding a new compound that does not need to be activated, while still targets InhA is appealing.

In this regard, triclosan and its derivatives are promising candidates as they directly interact with InhA active site, competing both with the NADH and the substrate for the binding of the reductase and consequently inhibiting its function [Vosátka *et al.*, 2018]. Triclosan is a biocide widely used as a sterilizing agent in veterinary, industrial care and house care; its bactericidal activity is dose-dependent. Furthermore, it is not toxic nor mutagenic in mammals but its scarce solubility in water and bioavailability limits its therapy use [Vosátka *et al.*, 2018]. For these reasons, the development of derivative is an appealing strategy to overcome the issues of triclosan administration while keeping the positive effects of this compound. Triclosan has a two-ring structure composed of a 5-chlorophenol (A-ring) and a 2,4-dichlorophenoxy in 2 (B-ring); substituents on its rings have proven to alter its efficacy and chemical characteristics (Figure 9) [Vosátka *et al.*, 2018].

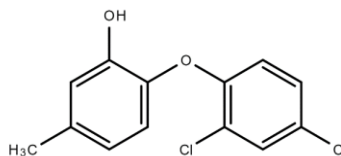


Figure 9. Triclosan molecular structure.

Triclosan alkyl diphenyl ethers substituted at the A-ring are less cytotoxic *in vitro*, have higher affinity to InhA and are well tolerated in murine model. The higher affinity can be explained because the bulkier substituent may produce more interactions with the active lipophilic site of the reductase; on the other hand, bulk substitutions on the B-ring proved a reduced affinity to the target, with lower antimicrobial activity. Therefore, the A-ring may play an important role in the interaction with InhA, and in particular the substitution of Cl in 5 seems to be crucial, as longer chain substituents in 5 have an increased inhibitory potency against InhA [Vosátka *et al.*, 2018]. Nevertheless, *ortho*-substitution in the B-ring showed a slow-onset inhibition of InhA, which is preferable as it correlates with stronger activity *in vivo* [Vosátka *et al.*, 2018]. In particular, the substitution in *ortho* of a methyl moiety produces more hydrophilic interactions with the reductase, making the binding to InhA more stable and long, yielding to a better inhibition [Vosátka *et al.*, 2018]. Furthermore, the removal of the hydroxyl group coupled with substitutions in either *ortho*, *meta* or *para* showed higher efficacy *in vitro* and good efficacy *in vivo* in a murine model of *M. bovis* BCG infection [Vosátka *et al.*, 2018]. In conclusion, the direct inhibition of the InhA achieved by using triclosan, and the possibility to modulate its action through substitutions on its

scaffold paves the way for the design of new and more powerful derivatives that could bypass the issue of drug-resistant *Mtb* strains [Vosátka *et al.*, 2018].

1.1.5.2 Arabinogalactan biosynthesis effectors as molecular targets

Arabinogalactan is a fundamental component of the mycobacterial cell wall, which structure comprises arabinose and galactose sugars intertwined and interlinked to peptidoglycan on one end and to mycolic acids on the other [Alderwick *et al.*, 2015]. The binding to peptidoglycan is allowed through linker units composed of two types of glycolipids (GL-1 and GL-2), while the mycolic acids are esterified to the arabinan component of arabinogalactan [Alderwick *et al.*, 2015]. The galactan precursors are synthesized through epimerization and ring contraction reactions starting from the UDP-D-glucopyranose to obtain the UDP-D-galactofuranosyl, while the arabinan precursors derive from the 5-phosphoribosyl-1-pyrophosphate (pRpp) a nonoxidative pentose shunt pathway metabolite [Alderwick *et al.*, 2015]. In *Mtb*, UbiA transferase uses pRpp to produce decaprenylphosphoryl-5- β -D-phosphoribofuranose (DPPR), which is then dephosphorylated by Rv3807c to obtain decaprenylphosphoryl- β -D-ribofuranose (DPR). Subsequently, DPR is epimerized to decaprenylphosphoryl- β -D-arabinofuranose (DPA), which is the fundamental activated D-arabinofuranosyl substrate for arabinan biosynthesis (Figure 10) [Alderwick *et al.*, 2015]. This two-step epimerization process involves the enzymes decaprenylphosphoryl- β -D-ribose 2'-oxidase (DprE1 coded by *Rv3790*) and the decaprenylphosphoryl-D-2-keto erythropentose reductase (DprE2 coded by *Rv3791*). DprE1 catalyses the oxidation of DPR into decaprenylphosphoryl-D-2'-keto-erythropentofuranose (DPX), which is an intermediate that is the substrate for DprE2 to be reduced and forms DPA [Mikusova *et al.*, 2005]. This last biosynthetic step is essential, as its inhibition leads to cell death by accumulation of DPR in the cytoplasmic membrane [Alderwick *et al.*, 2015].

Indeed, DprE1 has been demonstrated to be a pharmacological target, whose inhibition leads to mycobacterial cell death. Moreover, this enzyme is the cellular target of more than 15 different classes of inhibitors, and for this reason has earned the title of 'promiscuous target'. Such title had a negative connotation in the past, due to the possibility of developing more compounds resistances with just one target mutated, but lately it has been reconsidered as a valid option to reduce the treatment time in TB therapy [Degiacomi *et al.*, 2020].

INTRODUCTION

The already mentioned nitrobenzothiazinones (BTZ) as well as other classes of nitro compounds such as dinitrobenzamides (DNB), have been demonstrated to target DprE1, with a peculiar mechanism of action [Makarov *et al.*, 2009; Christophe *et al.*, 2009]. In particular, the cysteine in position 387 (Cys387) of DprE1 is fundamental for BTZs activity (Figure 11), as proved by the *in vitro* isolation of BTZ043 resistant *Mtb* mutants, harbouring Cys387 serine/glycine substitutions [Makarov *et al.*, 2009]. The crystallographic structure of *Mycobacterium smegmatis* (Figure 12) and *Mtb* DprE1 proved that the Cys387 (Cys394 in *M. smegmatis*) is fundamental for the interaction with BTZ and DNB forming a covalent adduct with these compounds [Batt *et al.*, 2012; Neres *et al.*, 2012]. Indeed, the inhibitory activity of BTZs requires their activation through reduction of their nitro moiety in the nitroso state that can covalently bind the Cys387 through a semimercaptal adduct [Trefzer *et al.*, 2012; Neres *et al.*, 2012].

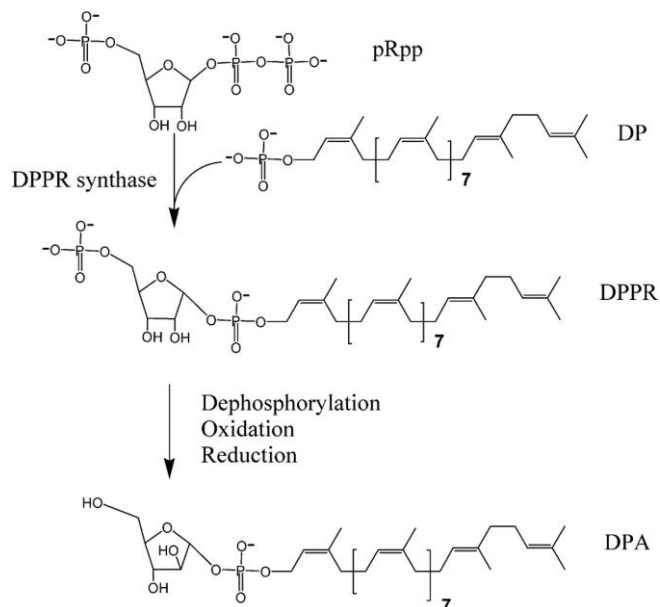


Figure 10. Overview of the pathway for DPA biosynthesis in *Mtb*. [Huang *et al.*, 2008].

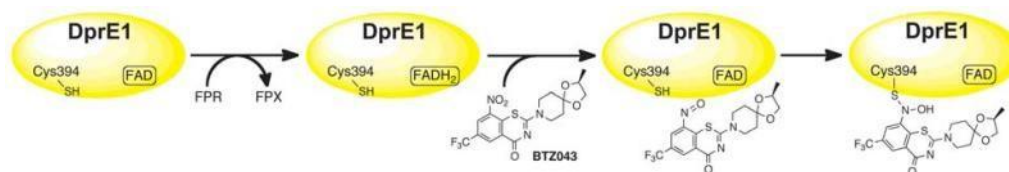


Figure 11. Structure and mechanism of action of BTZ043 against DprE1 in *Mtb*. [Neres *et al.*, 2013]

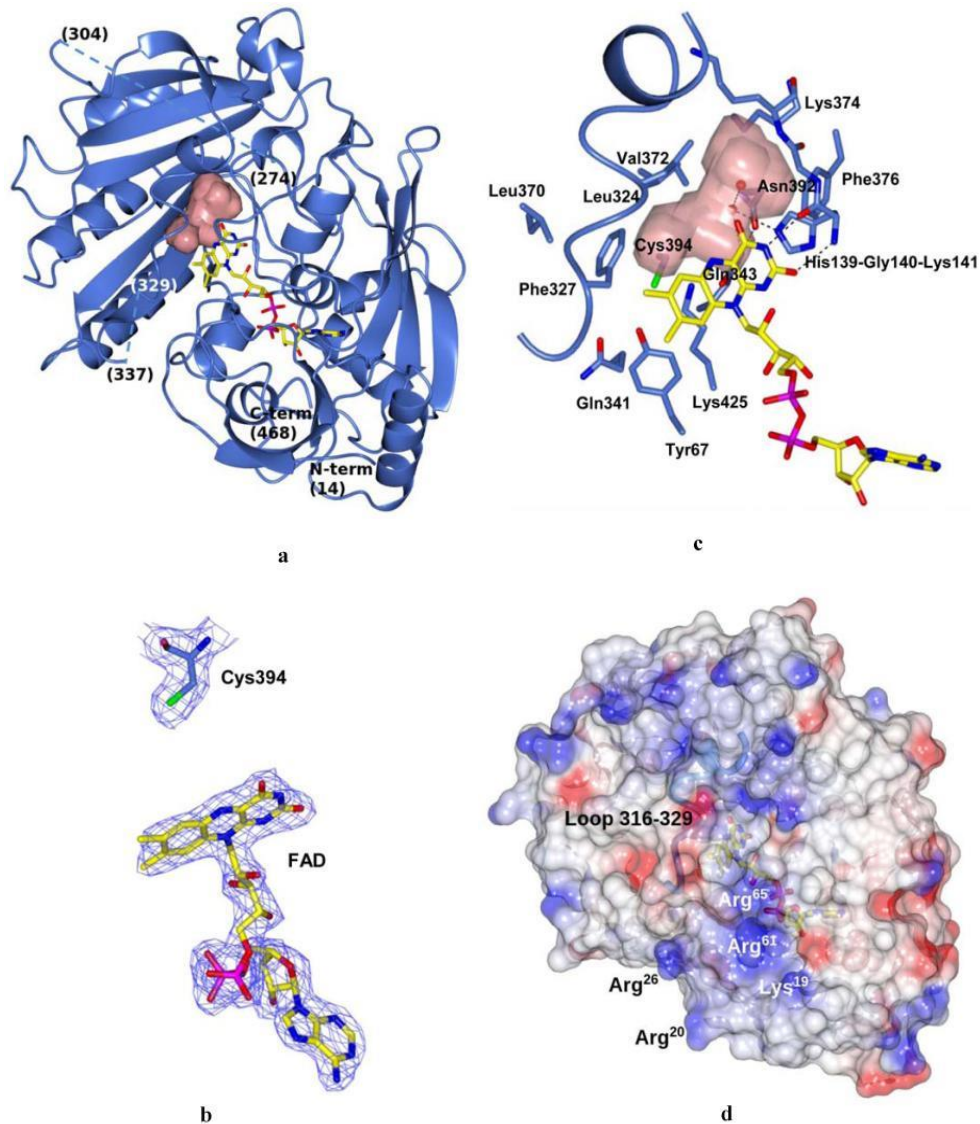


Figure 12. DprE1 3D structure bound to the FAD cofactor. A) Ribbon diagram of *M. smegmatis* DprE1 structure. B) Electron density map for the FAD cofactor and the Cys394 residue of DprE1. C) DprE1 active site. D) Electrostatic surface potential of DprE1. [Adapted from Neres *et al.*, 2012]

DprE1 is a flavin adenine dinucleotide (FAD)-dependent oxidoreductase, with the cofactor binding site, which stretches along the DprE1 substrate-binding site, being accommodated in the proximity of the Cys387 residue. As BTZ043 needs to be activated through reduction of its nitro moiety, it has been proven that FADH₂, which is the reduced

INTRODUCTION

form of FAD, is actually responsible for its activation, thus demonstrating that BTZ043 acts as a suicide inhibitor being activated by its own target cofactor [Trefzer *et al.*, 2012; Neres *et al.*, 2012]. The FAD-binding site is highly conserved and composed of various α -helices and two β -sheets that allows for a deep accommodation of the cofactor. On the other hand, the substrate-binding site is composed of a long antiparallel β -sheet with three α -helices on the back. Moreover, in correspondence with the substrate-binding site there are two distorted regions, which suggested that DprE1 may have formed an homocomplex; in fact, it was not possible to detect DprE1 dimerization in solution, highlighting that this enzyme does not present as a homodimer (Figure 12) [Batt *et al.*, 2012].

In *Corynebacterium glutamicum* it was shown through the bacterial adenylate cyclase two-hybrid (BACTH) system, that DprE1 directly interacts with DprE2 to perform the conversion of DPR into DPA [Jankute *et al.*, 2014]. As the genus *Corynebacterium* is closely related to *Mycobacterium*, it was postulated that the DprE1-DprE2 interaction described may also be present in *Mtb*, but to date, there still is no definitive proof that DprE1 and DprE2 form a complex in *Mtb* [Jankute *et al.*, 2014].

Nonetheless, computational homology modelling investigated the structural and dynamic features of DprE1, particularly of the two distorted regions at the substrate-binding site, thus strengthening the assumption of their physical interaction [Bhutani *et al.*, 2015]. Considering that both DprE1 and DprE2 are required for DPA production and that are fundamental for *Mtb* survival, the hypothesis of the DprE1-DprE2 heterocomplex is positively plausible [Mikusova *et al.*, 2005; Kolly *et al.*, 2014].

1.2 CYSTIC FIBROSIS AND NONTUBERCULOUS MYCOBACTERIA

Cystic Fibrosis (CF) is a multisystem autosomal recessive genetic disease caused by mutations in the gene that codes for the CF transmembrane conductance regulator (CFTR), which is a cAMP-regulated anion channel [Egan, 2016]. CF incidence ranges from 1 in 2800 to 1 in 3500 live births with prevalence in subject of European descent. To this day, over 2000 different mutations have been identified linked to CF and are subdivided into 6 different classes based on the type of mutation and clinical outcome (Table 4). The most represented CFTR mutation is the deletion of a single phenylalanine at position 508 that accounts for over the 80% of single mutations and 50% homozygotes CF European descent patients [Egan, 2016].

INTRODUCTION

Table 4. Overview of CFTR mutations Classes [adapted from Egan, 2016].

	CFTR Defect	Mutation Type	Major Problem
Class I	No functional CFTR protein	Nonsense, Splicing, Frameshift	Truncated unstable RNA
Class II	CFTR trafficking/processing	Missense, SNP, single Deletion	Unstable protein degraded
Class III	Defective CFTR protein	Missense, SNP, single Deletion	Abnormal CFTR channel regulation
Class IV	Defective CFTR protein	Missense, SNP, single Deletion	Decreased CFTR channel conductance
Class V	Reduced synthesis of CFTR protein	Splicing, Missense	Decreased amount of normal CFTR at the cell surface
Class VI	Reduced CFTR protein (instability)	Missense, SNP	Unstable CFTR protein

In most cases, mutations of this channel predispose patients to chronic respiratory infections with dysfunction of the respiratory, gastrointestinal, and genitourinary tracts. In particular, in the respiratory tract these mutations are translated in dysregulation of the airway's epithelial cells, with variation in the pH, mucus composition and airway surface liquid volume, with a neutrophil-driven inflammation [Ramsey *et al.*, 2019]. Activation of the neutrophil inflammatory response can stimulate the progression of the pulmonary disease that can lead to respiratory failure, which is to this day, the most common cause of death in FC patients [King *et al.*, 2016]. Despite the high prevalence of neutrophils, there are various factors that cause phagocyte dysfunction in CF patients making the microenvironment of CF lung airways favourable for microbial survival and persistence [Ramsey *et al.*, 2019].

The most common pathogens associated with pulmonary infections in CF patients are: *Staphylococcus aureus*, *Pseudomonas aeruginosa*, *Burkholderia cepacia* complex, *Haemophilus influenzae* and emerging pathogens such as *Stenotrophomonas maltophilia*, and nontuberculous mycobacteria (NTM) [Scoffone *et al.*, 2019]. Usually, NTM are not classified as human pathogens, but they can become opportunistic pathogens and infect the human host causing among others TB-like pulmonary diseases, skin and central nervous system infections [Lee *et al.*, 2015]. In recent years, NTM are emerging as important pathogens for CF patients; in particular, *Mycobacterium avium* complex (MAC) and *Mycobacterium abscessus* complex (MABSC) are the most represented NTM species in CF patients [Martiniانو *et al.*, 2018]. The MAC historically comprises the species *Mycobacterium avium* (*Mav*) and *Mycobacterium intracellulare*. However the advancement of molecular identification tools identified new species strictly related to *M. intracellulare* that could be included into the

INTRODUCTION

MAC, even though they differ in terms of virulence and therapy success rate: *Mycobacterium chimaera*, *Mycobacterium colombiense*, *Mycobacterium arosiense*, *Mycobacterium vulneris*, *Mycobacterium marseillense*, *Mycobacterium timonense*, *Mycobacterium bouchehurbonense*, *Mycobacterium mantenii*, *Mycobacterium yongonense*, “*Mycobacterium indicus pranii*”, *Mycobacterium paraintracellulare*, and *Mycobacterium lepraemurium*. On the other end, MABSC includes the three *Mycobacterium abscessus* subspecies: *Mycobacterium abscessus* subsp. *abscessus* (*Mab*), *Mycobacterium abscessus* subsp. *bolletii*, and *Mycobacterium abscessus* subsp. *massiliense* [Koh, 2017; Turenne, 2019]. Among the NTM affecting CF patients (3.3-22.6%), *Mab* is the most represented worldwide and the one with the lowest cure rate (25–58%). *Mab*-infected CF patients can benefit from the surgical resection of the colonized lung tissue, but unsuccessful *Mab* eradication is a contraindication for lung transplantation [Wu *et al.*, 2018; Lopeman *et al.*, 2019; Degiacomi *et al.*, 2019]. Since its first isolation in 1952, *Mab* has been identified as widespread in the environment, generally found in the soil, dust, plants and water sources. It is a rapid growing mycobacterium, which is able to produce biofilm. The insurgence of *Mab* infections is associated with various risk factors, such as age of the CF patient, lower values of body mass index (BMI), worse values of forced expiratory volume (FEV₁), *Pseudomonas aeruginosa* and *Stenotrophomonas maltophilia* pre-existing infections, pneumothorax, chest drain, use of inhaled antibiotics and overall compromising of the immune system [Lopeman *et al.*, 2019]. Furthermore, *Mab* can resist harsh environmental conditions thanks to its ability of forming biofilm, which in association with its characteristic mycobacteria cell wall, further enhances its survival both in the environment and in the human host [Lopeman *et al.*, 2019]. *Mab* mode of transmission is yet to be fully elucidated, but recently it was unveiled through whole-genome sequencing (WGS) of *Mab* isolates from CF centres worldwide that human-to-human transmission is possible [van Dorn, 2017; Bryant *et al.*, 2016; Yan *et al.*, 2020]. Moreover, Bryant *et al.* (2016) grouped *Mab* subspecies into three circulating clusters: *Mycobacterium abscessus* isolate 1 and 2 and *Mycobacterium massiliense* isolate 1. Interestingly, these 3 clusters of *Mab* isolates were identified in CF centres in different countries, proving that transcontinental spreading is possible [Bryant *et al.*, 2016]. Consequently, are not just the environmental sources of *Mab* that should be addressed, but it is pivotal to prevent the human-to-human spreading between CF patients as well [Stephenson, 2019; Ramsey *et al.*, 2019].

1.2.1 NTM morphology and pathophysiology

Even if the WGS and the RNA 16S typing are available, to this day the phenotypic characterization of NTM still remains valid, with the Runyon classical subdivision that divides NTM in Rapid Growing Mycobacteria (RGM) and Slow Growing Mycobacteria (SGM) [Turenne, 2019]. NTM are aerobic, non-motile acid-fast bacilli with a high content of GC in their genome. Moreover, NTM have the same complex and peculiar cell wall structure as other mycobacteria [Turenne, 2019]. Cell wall lipids can help escaping the host immune response through suppression of the cytokine signalling fundamental to control

INTRODUCTION

NTM infections. In particular, the surface glycopeptidolipids (GPL; Figure 13) are required for intracellular survival, biofilm formation, host-pathogen interactions, and modulation of the inflammatory response [Johansen *et al.*, 2020]. Variations in the level of expression of GPL leads to changes in the colonies morphotype, from smooth (high level of GPL) to rough (low to no level of GPL) and are correlated to NTM virulence with the rough morphotype being the most virulent [Johansen *et al.*, 2020]. NTM can display both the smooth and the rough phenotype, the latter correlated to a more virulent phenotype [Johansen *et al.*, 2020].

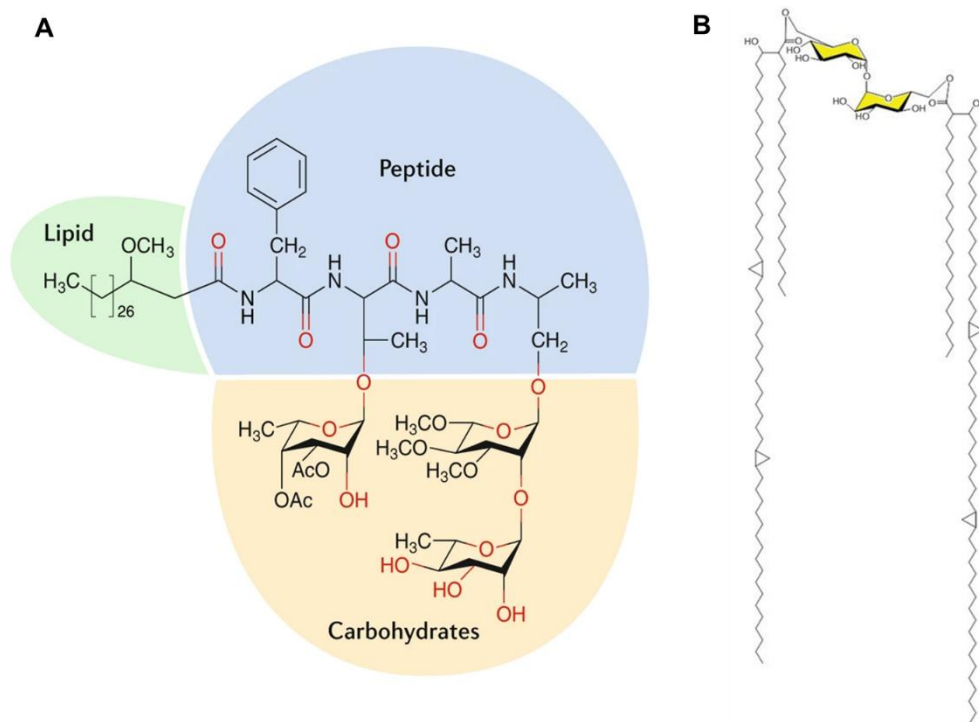


Figure 13. GPL and TDM structures. A) Exemplificative structure of a mycobacterial glycopeptidolipids [Johansen *et al.*, 2020]. B) Structure of the mycobacterial trehalose dimycolate [Norbe *et al.*, 2012].

GPLs can be subdivided into alkali-stable (or C-type GPL) an alkali-labile serine-containing GPL; the first ones are more common in saprophytes and opportunistic NTM. The C-type GPL have a lipopeptidyl core of C₂₈-C₃₀ fatty acid chains amidated by a tripeptide-amino-alcohol core of D-Phe-D-allo-Thr-D-Ala-L-alaninol. The C-type core is glycosylated with the allo-Thr linked to a 6-deoxy- α -L-talose and the alaninol linked to an

INTRODUCTION

a-L-rhamnose. *Mav* C-type GPL can be not-methylated in the 6-deoxytalose or 3-O-methylated and can also be O-acetylated at various locations. In contrast, *Mab* has a diglycosylated GPL with a 3,4-di-O-acetylated 6-deoxytalose and a 3,4-di-O-methylated or 2,3,4-tri-O-methylated rhamnose [Gutiérrez *et al.*, 2018]. The *gpl* locus is highly conserved among NTM and contains several genes coding for proteins essential for GPL biosynthesis and transport across the plasma membrane. *mps1* and *mps2* genes code for the effectors of the tripeptide amino-alcohol moiety GPL formation, while *gtf1* and *gtf2* encoding proteins catalyse the glycosylation of the lipopeptide core and Gtf3 adds the extra rhamnose. Rmt2, Rmt3, and Rmt4 are involved in the O-methylation of the rhamnose while *fmt* encoding protein is involved in O-methylation of the lipid moiety. The products of *atf1* and *atf2* genes are necessary for the acetylation of the deoxytalose while Mmps4, Mmpl4a and Mmpl4b are involved in GPL biosynthesis and transport [Gutiérrez *et al.*, 2018]. NTM can switch between the smooth and rough morphotype through the development of mutations in the genes involved in GPL biosynthesis and transport. In fact, in *M. boletii* it was shown that point mutations in Mmpl4a at Tyr842 or Mmpl4b at Tyr854 drastically impaired GPL production [Bernut *et al.*, 2016]. In addition to GPL, another fundamental component of NTM cell wall is the trehalose dimycolate (TDM; Figure 13). TDM is known to be involved in *Mtb* virulence, and even though its role in virulence has yet to be in depth studied in NTM, its level of expression varies inversely proportional to GPL values in the smooth and rough morphotype underling a possible relation between TDM, GPL and virulence [Hunt-Serracin *et al.*, 2019]. Furthermore, TDM is necessary for the cording phenotype, fundamental for increasing NTM virulence and a more invasive infection; indeed, the lack of the cording phenotype in the smooth morphotype could be explained by the high presence of GPL that could mask the TDM residues [Howard *et al.*, 2006; Hunt-Serracin *et al.*, 2019].

NTM, and particularly *Mab*, can persist in the lungs stimulating the formation of the granuloma, similarly to what happens during *Mtb* infection. After inhalation by the host, *Mab* is phagocytised by the immune system cells (macrophages and neutrophils) but can escape the intracellular disruption and establish the continuous stimulation of cytokines and TNF secretion, which recruits more immunity cells, leading to the formation of the granuloma. Moreover, once in the granuloma, *Mab* can maintain the smooth form and persist or switch from the smooth to the rough morphotype, leading to the disruption of the granuloma and its release in the lung with consequent lung disease onset [Johansen *et al.*, 2020].

NTM lung disease has two major different radiographic manifestations: the fibrocavitary and the nodular bronchiectatic forms. The first form has cavitary lesions predominantly in the upper lobes, similar to pulmonary TB, and it generally occurs in older individuals with pre-existent pulmonary disease or smoking habit. On the other end, the nodular bronchiectatic disease can occur as a multifocal bronchiectasis, with clusters of

small nodules, and branching linear structures that generally involve the right middle lobe and the lingular segment of the left upper lobe [Koh, 2017]. For the right diagnosis of NTM infections, the physician should keep in consideration the clinical findings (e.g.: pulmonary symptoms, radiographic evidence, high-resolution computed tomography) altogether with the microbiological findings (e.g.: positive sputum cultures, positive bronchial wash); when possible, the molecular identification is the most reliable because it allows for a correct differentiation between NTM and *Mtb* [Koh, 2017]. It is important to correctly identify the NTM, particularly in case of infected CF patients, because the therapy design is fundamental for its success. In CF patients *Mab* therapy can last up to 2 years, but the success rate is incredibly low (30%), and not achieving the total eradication of the pathogen leads to an accelerated deterioration of lung function in these patients [van Dorn, 2017].

1.2.2 Therapy and drug-resistance

Treatment of *Mab* lung infections can be challenging due to the lack of specific drugs against this pathogen and its innate resistance to the commonly used antibiotics for Gram-positive/negative bacteria and for most of the anti-TB drugs [Luthra *et al.*, 2018]. Moreover, particularly in CF patients where the secretions of thick mucus can cause an increase in the renal clearance of the drug and a possible reduced gastrointestinal absorption, a completely resolute treatment can be difficult to achieve [Chopra *et al.*, 2011]. Furthermore, *Mab* can resist the antibiotics effect due to their inability of passing through the biofilm and the complex, GPL, mycolic acid rich cell wall [Estepan and Garcia-Coca, 2018; Howard *et al.*, 2006; Hunt-Serracin *et al.*, 2019].

The antibiotic therapy reported in the guidelines for *Mab* infections in CF patients consists of a first intensive phase that lasts from 3 to 12 weeks, followed by a continuation phase that can last up to 12 months after culture conversion. During the intensive phase, the patient is given daily doses of oral macrolides, preferably azithromycin, in combination with intravenous amikacin (IV) and one or more of the following antibiotics: tigecycline IV, imipenem or ceftazidime. For the continuation phase, the patient is given inhaled amikacin and 2 or 3 oral antibiotics chosen from minocycline, clofazimine, moxifloxacin and linezolid [Floto *et al.*, 2016]. In figure 14, the chemical structures of the drugs commonly used in *Mab* therapy for CF patients are reported. Clarithromycin and azithromycin should always be administered in combination with other antibiotics to prevent the insurgence of macrolides resistance; considering that CF patients can be under different medicaments at the same time, interactions with other drugs should be carefully evaluated for each patient [Floto *et al.*, 2016; Skolnik *et al.*, 2016].

Macrolides are a large family of natural and synthetic antibiotics, which show a 14-16 lactones structure with sugar residues. They inhibit protein biosynthesis through the binding of the ribosome, successfully blocking the peptide elongation [Hansen *et al.*, 2002].

INTRODUCTION

A frequent cause of macrolide resistance among *Mab* clinical isolates, are mutations in the peptidyl-transferase region of the rRNA 23S, particularly at the positions 2058 and 2059 of the *rrl* gene (encoding the 23S rRNA), which are involved in the binding to the drugs [Nash *et al.*, 2009]. Furthermore, another mechanism of macrolide resistance is due to the presence of the macrolide-inducible gene *erm(41)*, coding for the inactivating enzyme Erm(41), responsible for the post-transcriptional methylation of the Ala2058 of the peptidyl-transferase region [Hansen *et al.*, 2002; Nash *et al.*, 2009]. In this case, the T28C polymorphism in *erm(41)* is responsible for the macrolides-inducible phenotype [Nessar *et al.*, 2011]. However, the mechanism of *erm(41)* inducible macrolides-resistance is not commonly shared across different NTM, as in *M. massiliense* this gene is completely deleted, consequently this NTM is macrolide-susceptible [Nash *et al.*, 2009].

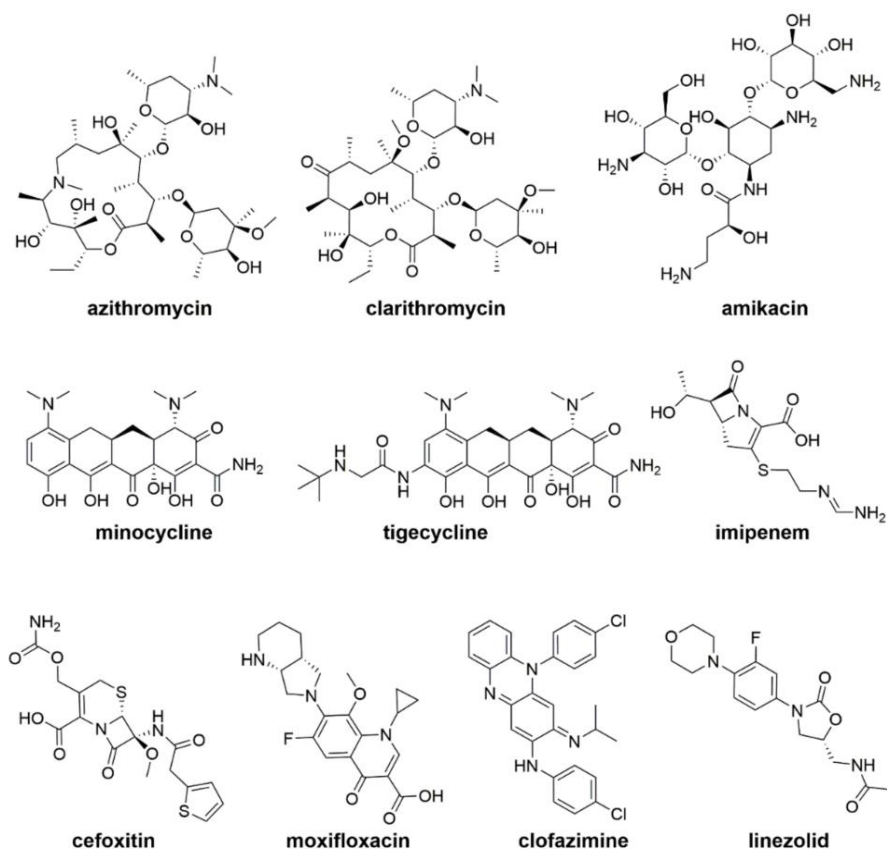


Figure 14. Chemical structures of the drugs used in *Mab* therapy.

In *Mab* the mechanism of aminoglycosides resistance is mainly based on the modification of the ribosome 30S subunit; in fact, in 90% of *Mab* clinical isolates resistant

INTRODUCTION

to aminoglycosides, the gene *rrs* (coding rRNA 16S) and the gene *rpsL* are mutated. In particular, the mutation A1408G in *rrs* results in high amikacin resistance in *Mab* isolates. [Nessar *et al.*, 2011; Prammananan *et al.*, 1998]. Interestingly, another aminoglycoside resistance mechanism could be linked to enzymatic drug modification. Several aminoglycosides could be acetylated by the 20-Nacetyltransferase (AAC(20)), encoded by *MAB_4395* gene. So, *Mab* strains harbouring mutations (or complete deletion) in this gene show higher sensitivity to aminoglycosides. Another N-acetyltransferase, named Eis2 (coded by *MAB_4532c*), is able to acetylate aminoglycosides, conferring *Mab* resistance [Luthra *et al.*, 2018].

The only β -lactams used in *Mab* therapy are cefoxitin and imipenem. The low activity of β -lactams depends on the presence in *Mab* of the constitutively expressed Class A β -lactamase, Bla_Mab coded by *MAB_2875* gene. Bla_Mab hydrolyses cefoxitin and imipenem at very low level, not compromising their therapeutic efficacy [Soroka *et al.*, 2014]. Avibactam is a β -lactamase inhibitor approved by the FDA in 2014 [Dubee *et al.*, 2015]. Recently, 5 combinations of avibactam with β -lactams were tested against *Mab*; the activity of three β -lactams (cefuroxime, imipenem and biapenem) was reduced below the therapeutic level, in presence of avibactam [Story-Roller *et al.*, 2018].

Tetracycline inhibits protein biosynthesis through the binding to the ribosomal 30S subunit. In *Mab* tetracycline resistance can be caused by enhanced activity of MabTetX enzyme, which is a monooxygenase coded by the *MAB_1496c*, that inactivate tetracycline. It was shown in *Mab* strains hypersensitive to tetracycline harbouring a deletion of *MAB_1496c* gene. MabTeX expression appears to be induced by the WhiB7 regulator after tetracycline exposure [Rudra *et al.*, 2018].

WhiB7, coded by *MAB_3508c*, is a transcriptional regulator that regulates many intrinsic mechanisms of drug resistance not only in *Mab*, but also in *Mtb* [Hurst-Hess *et al.*, 2017]. Furthermore, *Mab* WhiB7 also regulates the expression of genes that confer resistance to aminoglycosides and macrolides. Its expression is strongly induced after exposure to antibiotics affecting the ribosome (erythromycin, tetracycline, clarithromycin and amikacin). In fact, deletions in *MAB_3508c* gene coding for WhiB7 results in an increased sensitivity to amikacin and clarithromycin [Hurst-Hess *et al.*, 2017; Wu *et al.*, 2018].

Clofazimine is a repurposed drug which is used in the treatment of both leprosy and MDR-TB. It was recently introduced in *Mab* therapy despite its mechanism of resistance already known in *Mtb* and caused by mutations in *MAB_2299c* gene (homologous to *Rv0678* in *Mtb*) coding for the repressor of MmpS5-MmpL5 efflux pump [Hartkoorn *et al.*, 2014; Richard *et al.*, 2018].

INTRODUCTION

Moxifloxacin is a bactericidal fluoroquinolone used in TB treatment. Moxifloxacin inhibits the DNA gyrase blocking DNA replication and leading to cell death. The genes involved in moxifloxacin resistance are *gyrA* and *gyrB* coding for the target gyrase [Dookie *et al.*, 2018]. In *Mab*, resistance to moxifloxacin is caused by mutations in *gyrA*, coding for the A subunit of DNA gyrase [Guillemin *et al.*, 1998]. However, in a recent study, no clear correlation was found between mutations in *gyrA/gyrB* genes and fluoroquinolone resistance, suggesting that there could be an additional mechanism involved in *Mab* fluoroquinolone resistance [Kim *et al.*, 2018].

Linezolid is an oxazolidinone active against *Mab* and *Mtb*. The resistance mechanism involves mutations in the target rRNA 23S, and in the ribosomal proteins L3, L4 and L22 [Ye *et al.*, 2019]. Linezolid was the first oxazolidinone to be used in NTM treatment. Tedizolid and delpazolid are two others more active oxazolidinones and with less side effect (Figure 15) [Kim *et al.*, 2017].

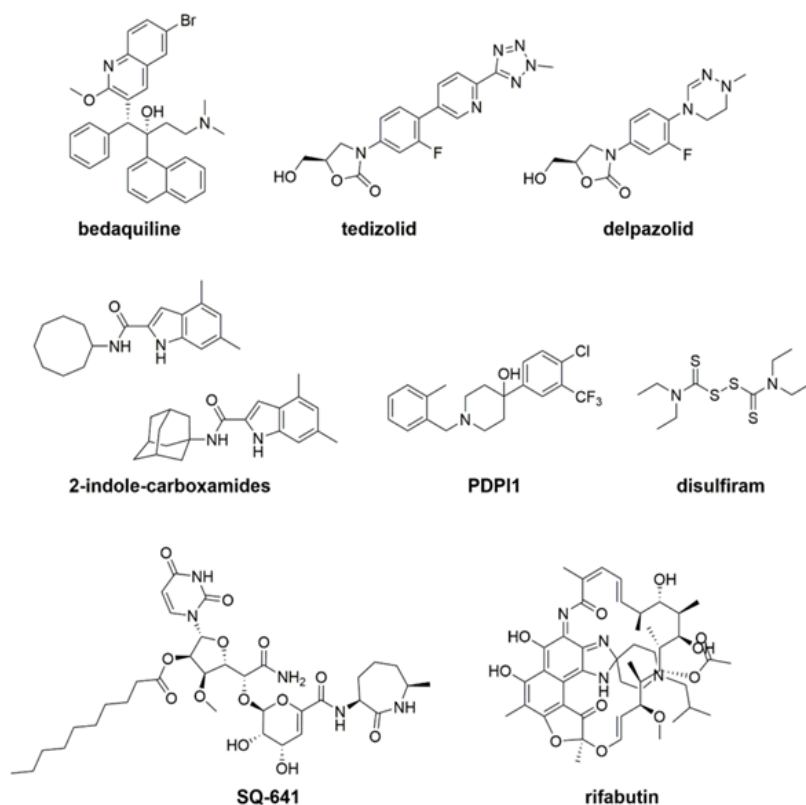


Figure 15. Chemical structures of new and repurposed drugs for in *Mab* therapy.

1.2.3 New drugs and possible molecular targets

There is an urgent need to discover and to develop novel and more effective agents to contrast the spreading of *Mab* drug resistant isolates. Considering in *Mab* the presence of intrinsic (biofilm formation, cell wall complexity), adaptative (*erm*(41) inducibility) and acquired (mutations in target genes) drug resistance, unfortunately the NTM drug pipeline is nearly empty in comparison with that of TB [Johansen *et al.*, 2020]. Indeed, most current antibiotics and lead candidates are derived either from existing drugs or taken directly from the TB Drug Pipeline. The hypothetical repurposing of anti-TB drugs in *Mab* therapy is based on the knowledge that *Mab* and *Mtb* share a strong genome similarity; however, just some anti-TB drugs actually are effective against *Mab* growth [Choo *et al.*, 2014]. In figure 15 the structures of new and repurposed drugs against *Mab* are reported.

Bedaquiline is a recently approved anti-TB drug already described [Andries *et al.*, 2005] (Figure 15). Unfortunately, controversial results were observed when bedaquiline was tested *in vivo*, probably due to its bacteriostatic activity against *Mab* [Lerat *et al.*, 2014; Obregón-Henao *et al.*, 2015]. However, the activity of bedaquiline can be enhanced by coadministration with verapamil, an efflux pump inhibitor, both *in vitro* and *ex vivo* [Viljoen *et al.*, 2019].

SQ641 belongs to capuramycins, which is a class of antibiotics targeting the Trslocase 1, an enzyme essential for peptidoglycan synthesis (Figure 15). SQ641 is bactericidal against *Mab* with a MIC of 0.25–1 µg/mL. Furthermore, when administered in combination with rifabutin and streptomycin has synergistic effects against *Mab* (Figure 15) [Dubuisson *et al.*, 2010].

Tigecycline is a tetracycline glycyclcycline which is in phase II clinical development (Figure 15). Preliminary data report that tigecycline administered on its own, is associated with a favourable treatment outcome, and in association with other compounds, such as rifabutin, has synergistic effects [Wallace *et al.*, 2014; Cheng *et al.*, 2019].

Rifabutin, a rifampicin derivative, has been found to be bactericidal against *Mab in vitro* and *ex vivo*. Furthermore, rifabutin has synergistic activity in combination with amikacin, cefoxitin, linezolid, clarithromycin (in triple combination with tigecycline) and azithromycin [Aziz *et al.*, 2017; Ganapathy *et al.*, 2019].

MmpL3, is a crucial mycobacterial transporter for the export of trehalose monomycolates from the periplasmic space to the mycobacteria cell wall. It is an important antitubercular drug target [Saxena and Singh, 2019]. The compounds PIPD1 (piperidinol based molecule) and 2-indole-carboxamides, although structurally distinct, target MmpL3

INTRODUCTION

transporter. PIPD1 and 2-indole carboxamides are bactericidal *in vitro* against *Mab* with good MIC of 0.0625–1 µg/mL (Figure 13) [Wu *et al.*, 2018].

Disulfiram is a repurposed drug from the treatment of alcohol dependence (Figure 15). Recently, disulfiram was found to be active *in vitro* and *ex vivo* against not only *Mab* in a time-dose dependent manner, but also against HIV [Das *et al.*, 2019].

The gaseous nitric oxide (NO) in the inhaled formulation is in phase II of clinical development for the treatment of *Mab* and other NTMs. NO is normally produced by the nitric oxide synthase from L-arginine; it is fundamental for a plethora of biological functions including also the defence mechanism against pathogens. CF patients are usually NO-deficient in the airways, which not only does not help getting rid of possible new infections, but contributes to the further impairment of lung function [Wu *et al.*, 2018; ClinicalTrials.gov]. Although the treatment with NO may not lead to a complete eradication of *Mab* infection, the bacterial load in the airways can be reduced by its use, meaning that there is space for improvements [Bentur *et al.*, 2020; Chiarelli *et al.*, 2020].

Amikacin liposome inhalation suspension (ALIS) is currently in Phase II clinical development [ClinicalTrials.gov]. ALIS is composed of small biocompatible, neutral liposomes of approximately 0.3 µm in diameter, encapsulated with amikacin. Once in the airways, liposomes can be directly absorbed by the pulmonary macrophages, allowing the intracellular acquisition of amikacin at high levels by cells infected with NTM [Olivier *et al.*, 2017]. Preliminary data show that this formulation has a reduced toxicity and improved efficacy in patients with *Mab* lung disease [Caimmi *et al.*, 2018].

Molgramostin, which is currently in phase 2 clinical trial, is an inhaled formulation of the Granulocyte-Macrophage Colony-Stimulating Factor (GM-CSF). GM-CSF is a protein naturally present in the human immune system, which plays an important role in activating the immune response against bacterial infections [ClinicalTrials.gov].

The lack of specific drugs against *Mab* is one of the main causes responsible for the spread of *Mab* clinical isolates among CF patients. More efforts in the development of the drug pipeline could help to find new specific drugs against this worrisome pathogen.

2.AIMS OF THE RESEARCH

Among mycobacterial species the most pathogen is *Mycobacterium tuberculosis*, which is the etiological agent of tuberculosis. Recently, the emergence of *Mycobacterium abscessus* as a new pathogen is worrying, in particular for cystic fibrosis patients.

In this work, our aim is to identify new strategies to contrast their spreading and to fill-in the drug pipelines for the development of more effective therapies against both mycobacterial species.

In order to characterize the mechanism of action of new drugs and novel cellular targets, this study was founded on two complementary approaches: the Drug-to-Target and the Target-to-Drug.

In the Drug-to-Target strategy, the aim is to find new, more powerful anti-mycobacterial drugs, and to characterize their mechanism of action. It could reduce the treatment time, but also hinder the spreading of Multi Drug Resistant (MDR) mycobacterial strains. This approach requires testing of hundreds of different molecules, some of which may have been described and used in clinical practice (Drug repurposing), while others are completely newly designed. This method of investigation requires time, but it is powerful, and potentially successful as it allows for large screening of different molecular classes.

For the second approach, the Target-to-Drug, the aim is to characterize already known drug targets and to find new inhibitors. Characterizing pharmacological targets is pivotal for drug development to have a better understanding of their behavior and resistance mechanism. In this regard, our focus was mainly on the *Mycobacterium tuberculosis* enzyme decaprenylphosphoryl-D-2-keto erythropentose reductase (DprE2), which works in association with the decaprenylphosphoryl- β -D-ribose 2'-oxidase (DprE1), which is a well-established drug target [Makarov *et al.*, 2009]. Our aim was to functionally characterize the putative DprE1-DprE2 complex to have a better understanding of its interaction, in order to develop new DprE1/DprE2 inhibitors.

3.MATERIALS AND METHODS

3.1 BACTERIAL STRAINS, MEDIA, AND GROWTH CONDITIONS

All bacterial strain used in this work are listed in table 5. For all cloning procedures *Escherichia coli* HST08 strain (Stellar Competent Cells) was used according to manufacture guidelines [Clontech Laboratories, Inc, Takara Bio]. For protein expression studies *Escherichia coli* BL21(DE3) strain was used. Mycobacterial strains were grown in Middlebrook 7H9 medium or on Middlebrook 7H11 agar, supplemented with 10% Oleic acid-Albumin-Dextrose-Catalase (OADC) Middlebrook Enrichment. For other bacterial strains, Luria-Bertani (LB) broth and agar were used. All bacteria were grown aerobically at 37°C. For each growth condition, when required, antibiotics or tested compounds were added to the media.

Table 5. Strains used in this study.

Strains	Features	Source
<i>M. tuberculosis</i> H37Rv	Wild-type	Laboratory collection
<i>M. tuberculosis</i> 53.3	(Rv2466c,W28S)	Laboratory collection
<i>M. tuberculosis</i> 53.8	(Rv0579, L240V)	Laboratory collection
<i>M. tuberculosis</i> NTB9	(DprE1, G387G)	Laboratory collection
<i>M. tuberculosis</i> NTB1	(DprE1, G387S)	Laboratory collection
<i>M. tuberculosis</i> DR1	(DmpL3, V681I)	Laboratory collection
<i>M. tuberculosis</i> Ty1	(Rv3405c, c190t)	Laboratory collection
<i>M. tuberculosis</i> 88.1	(CoaA, Q207R)	Laboratory collection
<i>M. tuberculosis</i> 88.7	(PyrG, V186G)	Laboratory collection
<i>M. tuberculosis</i> 81.10	(<i>ethA</i> , Δ1109-37)	Laboratory collection
<i>M. tuberculosis</i> IC1	(resistant to STR, INH, RIF, EMB)	Laboratory collection
<i>M. tuberculosis</i> IC2	(resistant to STR, INH, RIF, EMB, PYR, ETH, capreomycin)	Laboratory collection
<i>M. bovis</i> BCG Pasteur	Wild-type	Laboratory collection
<i>M. smegmatis</i> mc2155	Wild-type	Laboratory collection
<i>Escherichia coli</i> ATCC25922	Wild-type	Laboratory collection
<i>Bacillus subtilis</i> 168	Wild-type	Laboratory collection
<i>Salmonella thyphimurium</i> LT2	Wild-type	Laboratory collection
<i>Burkholderia cenocepacia</i> K56-2	Wild-type	Laboratory collection
<i>Escherichia coli</i> BL21(DE3)	F- ompT hsdSB (rB- mB-) dcm (DE3)	Laboratory collection

MATERIALS AND METHODS

<i>Escherichia coli</i> HST08	F ⁻ , endA1, supE44, thi-1, recA1, relA1, gyrA96, phoA, Φ 80d lacZ Δ M15, Δ (lacZYA - argF) U169, Δ (mrr - hsdRMS - mcrBC), Δ mcrA, λ -	Laboratory collection
<i>M. abscessus</i> ATCC19977	Wild-type	Laboratory collection (ST. Cole)
<i>M. bolletii</i> 1999-0888	Wild-type	Hôpital Raymond-Poincaré (Paris, France) (ST. Cole)
<i>M. massiliense</i> 2005-0524	Wild-type	Hôpital Raymond-Poincaré (Paris, France) (ST. Cole)
<i>M. abscessus</i> MDR clinical isolate 1	Resistant to amikacin, clarithromycin, doxycycline, bedaquiline, ciprofloxacin, erythromycin, meropenem, econazole, ethambutol, ethionamide, lansoprazole, pristinamycin, rifampicin, rifapentine, SQ109, sutezolid, thioacetazone.	Centre hospitalier universitaire vaudois (CHUV, Lausanne, Switzerland) (ST. Cole)
<i>M. abscessus</i> MDR clinical isolate 2 (from CF patient)	Resistant to amikacin, amoxicillin, clavulanic acid, cefepime, ceftazidime, ceftriaxone, ciprofloxacin, doxycycline, imipenem, linezolid, minocycline, moxifloxacin, tobramycin, trimethoprim/sulfam	Ospedale Pediatrico Bambino Gesù (Rome) (E.V. Fiscarelli)
<i>M. abscessus</i> clinical isolate n. 6	Resistant to clarithromycin, moxifloxacin, doxycycline, linezolid	ISS, Rome, Italy (L. Fattorini)
<i>M. abscessus</i> clinical isolate n. 7	Resistant to clarithromycin, amikacin, moxifloxacin, doxycycline (Intermediate sensitivity to linezolid)	ISS, Rome, Italy (L. Fattorini)
<i>M. abscessus</i> clinical isolate n. 8	Resistant to moxifloxacin, doxycycline	ISS, Rome, Italy (L. Fattorini)
<i>M. abscessus</i> clinical isolate n. 9	Resistant to clarithromycin, moxifloxacin, doxycycline	ISS, Rome, Italy (L. Fattorini)
<i>M. abscessus</i> clinical isolate n.10	Resistant to moxifloxacin, doxycycline	ISS, Rome, Italy (L. Fattorini)
<i>M. avium</i> subsp. <i>avium</i> Chester ATCC15769	Wild type	Laboratory collection (ST. Cole)
<i>M. avium</i> clinical isolate n.1	Resistant to linezolid (Intermediate sensitivity to Moxifloxacin)	ISS, Rome, Italy (L. Fattorini)
<i>M. avium</i> clinical isolate n.2	Resistant to linezolid (Intermediate sensitivity to Moxifloxacin)	ISS, Rome, Italy (L. Fattorini)
<i>M. avium</i> clinical isolate n.3	Resistant to linezolid (Intermediate sensitivity to Moxifloxacin)	ISS, Rome, Italy (L. Fattorini)
<i>M. avium</i> clinical isolate n.4	Resistant to linezolid and Moxifloxacin	ISS, Rome, Italy (L. Fattorini)
<i>M. kansasii</i> ATCC12478	Resistant to Streptomycin	Laboratory collection (J.A. Ainsa Claver)

MATERIALS AND METHODS

For heterologous expression of proteins in *Escherichia coli*, specific media were used as shown in table 6.

Table 6. Media used for protein expression trials.

	1 L Media					
	LB	Autoinducing (1x)	Autoinducing (2x)	Terrific	Super Broth	M9- glucose
Tryptone	10 g	10 g	20 g	12g	32 g	
Yeast Extract	10 g	5 g	10 g	24g	10 g	
(NH₄)₂SO₄		3,3 g	3,3 g			
KH₂PO₄		6,8 g	6,8 g	0,17M		3 g
Na₂HPO₄		7,1 g	7,1 g			6,78 g
Glycerol		5 g	10 g	5g		
Glucose		0,5 g	1 g			10 g
α-Lactose		2g	4 g			
MgSO₄		1 mM	1 mM			2 mM
K₂HPO₄				0,72M		
NaCl	5 g				5 g	0,5 g
NH₄Cl						1 g
CaCl₂						0,1 g

Bacteria were grown to exponential phase (OD_{600nm}: 0,6-0,7) and induced with 1 mM Isopropyl-β-D-1-thiogalattopiranoside (IPTG).

3.2 DETERMINATION OF THE MINIMAL INHIBITORY CONCENTRATION (MIC)

Two independent cultures were grown approximately to mid-log phase, diluted (as indicated in table 7) for REMA assay and were seeded in a 96-well black plate [Fluoronunc, Thermo Fisher] in presence of serial compound dilutions. A growth control containing no compound and a sterile control without inoculum were also included. The different conditions for MIC determination using the REMA assay are reported in table 7. At the end of the exposition time, resazurin was added at each well at a final concentration of 0.0025%. After further 1-day incubation, plates were read [Ex 544 nm, Em 590 nm, Fluoroskan ThermoScientific]. Bacterial viability was calculated as a percentage of resazurin turnover in the absence of compound.

MATERIALS AND METHODS

Table 7. REMA assay conditions for the bacteria used in this study.

Strains	OD _{600nm}	Temperature	Concentration assayed µg/mL	Drug exposure time in days	Control
<i>Mtb</i>	0,0005	37°C	32-16-8-4-2-1-0,5- 0,25	7	Streptomycin
<i>M. bovis</i> BCG	0,02			7	Streptomycin
N'TMs	0,02			3	Ciprofloxacin
<i>M. smegmatis</i>	0,02			3	Streptomycin
<i>E. coli</i>	0,0006		256-128-64-32- 16-8-4-2-1-0,5- 0,25	1	Kanamycin
<i>B. subtilis</i>	0,0006			1	Kanamycin
<i>S. typhimurium</i>	0,0006			1	Kanamycin
<i>B. cenocepacia</i>	0,0006			1	Ciprofloxacin

MIC determination for mycobacterial species was also performed onto solid medium. Briefly, dilutions of two independent cultures (about 10⁵-10⁶ CFU/mL) were streaked onto 7H11 solid medium containing a range of drug concentrations (in general 0.125 to 40 µg/mL), following the micro-dilution method. Plates were incubated at 37°C for the desired time (2 days for *M. smegmatis*, 3-4 days for *Mab*, 10 days for *Mav*, 15-18 days for *Mtb* and *M. bovis* BCG). The growth was visually evaluated; the lowest drug dilution at which visible growth failed to occur was taken as the MIC value. Results were expressed as the average of at least three independent determinations.

3.3 DNA PROCEDURES: CLONING, PLASMIDS, AND PRIMERS

DNA was manipulated following standard procedures [Sambrook and Russell, 2001]. DNA fragments were purified from agarose gel using the *Wizard SV Gel and PCR Clean-Up System* [Promega]. All genes were cloned using the *In-Fusion HD Cloning Plus Kit* [Takara Bio] following manufacturer's instructions. Plasmids used in this study are reported in table 8.

Table 8. Plasmids used in this study.

Vector	Features	Source
pETDuet™-1	Ampicillin resistant. Simultaneous expression of 2 genes	Novagen
pET-SUMO	Kanamycin resistant, pBR322	Invitrogen
pET-23b(+)	Ampicillin resistant; pBR322	Novagen

Stellar Competent Cells (*E. coli* HST08) were transformed with the desired plasmid following *In-Fusion HD Cloning Plus Kit* [Takara Bio] manufacturer's instructions. Plasmid isolation was performed using the *Plasmid Mini kit* [Qiagen]. To check the quality of the

MATERIALS AND METHODS

cloning, the plasmids were sequenced at Microsynth – AG (Switzerland). A list of all primers used in this study is reported in table 9.

Table 9. List of Primers.

Name	Sequence	Vector	Gene	Restriction Enzyme
DprE1Duet _FW	CACAGCCAGGATCCGCTGGAAG TTCTGTTCCAGGGGCCCTCTTTG ACGACGATGTTGAG	pETDuet TM -1	<i>Rp3790</i>	BamHI
DprE1Duet _RV	ATTATGCGGCCGCAAGCTTCATC TACAGCAGCTCCAA	pETDuet TM -1	<i>Rp3790</i>	HindIII
DprE2Duet _FW	GGAGATATACATATGGCTGCTG TAGATGGTTCTT	pETDuet TM -1	<i>Rp3790</i>	NdeI
DprE2Duet _FW_HYS	ATATGGCAGATCTCAATGCATCA CCATCATCACCACTGGAAGTTC TGTTCCAGGGGCCGTTCTTGA TGCCGTAGGA	pETDuet TM -1	<i>Rp3790</i>	NdeI
DprE2Duet _RV	GCAGCCTAGGTTAATTAAGCTC GGCATACTCAGATG	pETDuet TM -1	<i>Rp3790</i>	PacI
MSMEG_63 85FOR per Duet	AGAAGGAGATATAC ATAT TGCAGAAGATGGTGTTCGAC	pETDuet TM -1	<i>MSMEG_6385</i>	NdeI
MSMEG_63 82FOR per Duet	TCATCACACAGCCAGGATCCAC TGGAAGTTCTGTTCAGGGGCC CAACAGGTTGCGGGCAATG	pETDuet TM -1	<i>MSMEG_6382</i>	BamHI
MSMEG_63 82REV per Duet	ATGCGGCCGCAAGCTTCTGTCA GAGCAGTTGCAG	pETDuet TM -1	<i>MSMEG_6382</i>	HindIII
MSMEG_63 85FORH per Duet	ATATGAATGCATCACCATCATCA CCACCTGGAAGTTCTGTTCAG GGCCCCITGCAGAAGATGGTGT TCGAC	pETDuet TM -1	<i>MSMEG_6385</i>	NdeI
MSMEG_63 85REV per Duet	CAGCAGCCTAGGTTAATTAAGC ATCAGATGGGGAGCTT	pETDuet TM -1	<i>MSMEG_6385</i>	PacI
MSMEG_23 bFor	AGAAGGAGATATACATATTGCA GAAGATGGTGTTCGAC	pET-23b	<i>MSMEG_6385</i>	NdeI
MSMEG_23 bRev	GTGGTGGTGGTGACTCGAGGG CCCCTGGAACAGAACTTCCAGA AGGCAACAGATGGGGAGCTT	pET-23b	<i>MSMEG_6385</i>	XhoI
FOR_cis_ala	CGATCCCGGGCTGGAACGTGGC CGTGGACTTCCCGATCAAGG	pET-SUMO	<i>MSMEG_6382</i>	
FOR_cis_gli	CGATCCCGGGCTGGAACGTGGG CGTGGACTTCCCGATCAAG	pET-SUMO	<i>MSMEG_6382</i>	

MATERIALS AND METHODS

FOR_cis_ser	GATCCCGGGCTGGAACGTGTCC GTGGACTTCCCGATCAAGG	pET-SUMO	MSMEG_ 6382
REV_cis_ala	CCTTGATCGGGAAGTCCACGGC CACGTTCCAGCCCGGGATCG	pET-SUMO	MSMEG_ 6382
REV_cis_gli	CTTGATCGGGAAGTCCACGCC ACGTTCCAGCCCGGGATCG	pET-SUMO	MSMEG_ 6382
REV_cis_ser	CCTTGATCGGGAAGTCCACGGA CACGTTCCAGCCCGGGATC	pET-SUMO	MSMEG_ 6382

3.4 RNA-SEQ EXPERIMENTS

Triplicates of mycobacterial cultures grown to mid-exponential phase were exposed to high compound concentrations (10-fold and 30-fold MIC for *Mtb*; 10-fold and 20-fold MIC for *Mab*). Triplicate of not-treated cultures were included as control. After 4 hours (24 h for *Mtb*), cells were pelleted and stored at -80°C until use.

RNA was extracted using *Direct-zol*TM RNA Miniprep [Zymo Research] following manufacturer's instructions. DNase treatment was carried out twice using *TURBO DNA-free*TM Kit [Ambion] following the manufacturer's recommendations. RNA was stored at -80°C in RNase-free water. Amount and purity of RNA were determined spectrophotometrically; integrity of RNA was assessed on a 1% agarose gel.

RNA-Seq was performed by IGA Technology Service [<https://igatechnology.com/>, Udine, Italy] using the Illumina platform, after a ribosomal transcript depletion step. Libraries were then sequenced on single-end 75 bp mode on NextSeq 500 (Illumina, San Diego, CA). Reads were quality checked using FASTQC tool and pre-processed by Trimmomatic v0.38 to trim the adaptor sequences and remove low-quality sequences. The resulting clean reads were mapped to the mycobacterial reference genome using Bowtie2 v2.2.6. Gene expression estimates were made as raw read counts using featureCounts (v1.6.4) and summarized at CDS level.

Normalization of raw read counts and differential expression analysis was performed using DeSeq2 v1.24.0. Differentially expressed genes (DEG) were defined using the following criteria: $\log_2\text{FoldChange} > |2|$ (sample group/control) and FDR (false discovery rate) < 0.05 .

3.5 REAL-TIME PCR

Purified total RNA was reverse transcribed using QuantiTect[®] Reverse Transcription kit [Qiagen], following the manufacturer's recommendations. Real-Time PCR experiments were performed using QuantiTect SYBR Green PCR Master Mix

MATERIALS AND METHODS

[Qiagen] kit and the thermocycler "Rotor Gene 6000" [Corbett Life Science] to amplify and quantify a cDNA sequence of interest. All reactions were repeated in triplicate and the mean value was considered. *sigA* was used as internal gene control, since it is a housekeeping gene encoding σ A factor for both *Mab* and *Mtb*.

3.6 TIME-CONCENTRATION KILLING ASSAY

Two independent *Mtb* cultures were grown to exponential phase, diluted to 10^5 CFU/mL, and 10 mL were inoculated in 50 mL falcon tubes. In each tube Selamectin was added at the desired concentration: 0, 0.1, 0.5, 2, 8, 32 μ g/mL. At every time point (-3, 0, 1, 3, 7, 11, 14, 22 days) cultures were thoroughly mixed to disrupt clumps and were resuspended in sterile PBS 1X. Serial dilutions in PBS 1X were then plated onto Middlebrook 7H11 agar plates and incubated at 37°C for 3-4 weeks. Isoniazid was used as control at fixed concentrations (0,025 μ g/mL, 0.5-MIC).

Similarly, *Mab* was grown to mid-exponential phase and diluted to 10^6 CFU/mL. Two mL of cultures were transferred to each 15 mL Falcon tube. 11326083 was added to the respective tubes to achieve the final concentration of 3-, 30- or 150-fold their MIC. A drug-free control and Ciprofloxacin at its MIC value and 3-fold MIC were included as well. The cultures were incubated at 37°C for 5 days. At the indicated time-points, dilutions of each sample were plated onto Middlebrook 7H11 agar. The agar plates were incubated for 4 days at 37°C, and subsequently CFU value was determined by counting the colonies.

3.7 PRODUCTION AND CHARACTERIZATION OF DPRE1 MUTANTS

C394G, C394S and C394A mutant *M. smegmatis* DprE1 enzymes were generated using the pET-SUMO-*MSMEG_6382* recombinant vector and the *QuikChange site-directed mutagenesis kit* (Agilent), following manufacturer's recommendations with the primers reported in table 9. Wild-type and mutant enzymes were expressed and purified, and the enzyme activity assayed through a coupled Amplex Red/horseradish peroxidase reaction, as described before [Neres *et al.*, 2012]. Steady-state kinetic parameters were determined by assaying the enzyme at different concentrations of the DprE1 substrate analogue farnesyl-phosphoryl-D-ribofuranose (FPR) (12.5-800 μ M), and the kinetic constants K_m and k_{cat} determined by fitting the data to the Michaelis-Menten or the Hill equation, using Origin 8.0 software. For avermectins inhibition assays, the enzyme activity was determined in the presence of different compound concentrations (1.56-200 μ M). IC_{50} was determined according to the Equation 1, where $A[I]$ is the enzyme activity at inhibitor concentration $[I]$ and $A[0]$ is the enzyme activity without inhibitor.

$$A_{[I]} = A_{[0]} \times \left(1 - \frac{[I]}{[I] + IC_{50}} \right) \quad \text{Equation 1}$$

3.8 CO-EXPRESSION, PURIFICATION OF DPRE1-DPRE2 COMPLEX

E. Coli BL21 (DE3) competent cells were transformed by Heat shock with pET-SUMO-*MSMEG_6382* recombinant plasmid and selected onto LB-Kanamycin [50 µg/mL]. These cells were made competent and transformed with pET-23b-*MSMEG_6385* plasmid, selecting onto LB-Kanamycin [50 µg/mL]/Ampicillin [100 µg/mL] and used to co-express *M. smegmatis* DprE1 and DprE2.

Protein expression was achieved through induction with 1mM IPTG at 25°C, overnight. The day after, cells were harvested by centrifugation, resuspended in 50 mM potassium phosphate buffer pH 8.0, 500 mM KCl, (Buffer A), supplemented with 1 mM phenylmethylsulfonyl fluoride, lysed by sonication, and centrifuged at 50000 g for 20 minutes at 4°C. The cell-free extract was loaded on a 5mL HisTrap column equilibrated with Buffer A, the column washed with 30 mM imidazole in buffer A, then bound proteins were eluted with 500 mM of imidazole in Buffer A. The elution was monitored at 280 nm, and fractions showing absorbance were pooled, and dialyzed in Buffer B (50 mM potassium phosphate buffer pH 8.0, 150 mM KCl) overnight at 4°C, in the presence of SUMO-protease. The following day, the dialysed solution was loaded on a 1 mL HisTrap column equilibrated in Buffer B, and bound proteins eluted with 500 mM imidazole. The fractions that displayed absorbance at 280 nm and 414 nm were pooled, concentrated to 5 mL by ultrafiltration [Amicon® Ultra-10 mL, Millipore] and loaded on a HiLoad Superdex 75 16/60 column [Sigma-Aldrich] equilibrated in Buffer B. The column flowrate was maintained at 0.8 mL/min by an AKTA pump System [GE Healthcare Biosciences]. Fractions of 1.5 mL were collected and those that showed absorbance at 280 nm and 414 nm run on 1% SDS-PAGE. Fractions showing the two bands corresponding to DprE1 and DprE2 were pooled, flash frozen in liquid nitrogen and stored at -80°C until use. For the calibration of the HiLoad Superdex 75 16/60 column, the following proteins have been loaded: aldolase (158 kDa), albumin (67 kDa), ovalbumine (44 kDa), chymotrypsinogen A (25 kDa), Myoglobin (17 kDa) and ribonuclease (13.7 kDa).

The enzymatic activity of the purified DprE1-DprE2 complex was assayed following the decrease in absorbance of NADH. Indeed, DprE2 reduces the FPX produced by DprE1, oxidizing the NADH cofactor; this reaction can be monitored at 340 nm. Briefly, the standard reaction mixture contained 50 mM potassium phosphate buffer pH 8.0, 150 mM KCl, 0.2 mM NADH and about 2 µM of DprE1/DprE2 complex, and the reaction initiated by adding FPR solution at the desired concentration. Steady-state kinetic parameters were determined by assaying the enzyme at different concentrations of FPR (2.5-500 µM), and the kinetic constants K_m and k_{cat} determined by fitting the data to the Michaelis-Menten equation. The kinetic data obtained were compared to that achieved in the same conditions but using 2 µM of the two enzymes expressed and purified singularly.

4. RESULTS AND DISCUSSION

4.1 IN SEARCH FOR NEW DRUGS AND NOVEL CELLULAR TARGETS AGAINST TUBERCULOSIS

To this day Tuberculosis (TB) remains a leading cause of mortality worldwide [WHO, 2020]. Caused by *Mycobacterium tuberculosis*, the hurdles of its resolutions lay in the long, complex, and financially heavy therapy. To help achieve the EndTB strategy goals of 95% reduction in deaths and 90% reduction of new cases by 2035, new therapeutic strategies and a deeper understanding of TB drug development is urgently needed.

In our work we contributed to characterize the mechanism of action of new anti-TB drugs and novel cellular targets following different strategies:

1. Study of the mechanisms of resistance of Bedaquiline, a new antitubercular drug used in TB treatment [Degiacomi *et al.*, 2020].
2. Determination of the activity of new Triclosan macrocyclic derivatives against *Mtb* [Rodriguez *et al.*, 2020].
3. Identification and study of MtbI inhibitors [Chiarelli *et al.*, 2019].
4. Characterization of the mechanism of action of 11726172 (4-nitrobenzo[c][1,2,5]thiadiazol-5-yl thiazolidine-3-carbodithioate) anti-TB compound by global transcriptomic analysis.
5. Characterization of the mechanism of action of new DprE1 inhibitors [Liu *et al.*, 2020] and of selamectin, a repurposing drug which inhibits *Mtb* DprE1 enzyme.
6. Characterization of the DrpE1-DprE2 enzymatic complex.

4.1.1 Understanding the spread of bedaquiline resistance among *Mtb* clinical isolates

Among the newly introduced drugs in TB treatment, Bedaquiline, Delamanid and Pretomanid have proven to be efficient for the treatment of DR-TB [Migliori *et al.*, 2017; Keam *et al.*, 2019]; in particular, the use of bedaquiline is recommended for MDR and XDR-TB treatment [Ahmad *et al.*, 2018; Conradie *et al.*, 2020]. Despite its recent introduction in DR-TB therapy, *Mtb* bedaquiline resistant clinical isolates have already been reported [Vilellas, *et al.*, 2017; Ismail *et al.*, 2018; Zimenkov, *et al.*, 2017], harboring mutations in either *atpE* gene, encoding the target, or in *Rv0678*, coding for the repressor of the MmpS5-MmpL5 efflux pump.

To better understand the spreading of bedaquiline resistance in MDR- and XDR-TB, several *Mtb* resistant mutants were isolated starting from two MDR clinical isolates as parental cultures and miming what happens in clinical setting. The genomic DNAs of both isolates were subjected to Whole-Genome-Sequencing by Illumina, finding the mutations related to the MDR phenotype. [Degiacomi *et al.*, 2020]. Furthermore, both clinical isolates were bedaquiline sensitive and did not show mutations in the BDQ-resistance associated genes.

Exposing IC1 and IC2 strains to high concentration of bedaquiline (up to 20-fold MIC), spontaneous resistant mutants were isolated on solid medium at a frequency of 1.8×10^{-8} and 6×10^{-9} , respectively. The bedaquiline-resistant phenotype of 12 isolated mutants was confirmed by REMA assay, with MIC values ranging from 0,25 $\mu\text{g}/\text{mL}$ to 8 $\mu\text{g}/\text{mL}$, while the genotype was determined by Sanger sequencing of the *Rv0678*, *atpE* and *pepQ* genes after PCR amplification. None of 12 *Mtb* resistant mutants had mutation in *pepQ* gene, while different polymorphisms were found either in *atpE* or *Rv0678* genes (Table 10). Moreover, from a detailed search of the literature, all the already known mutations linked to bedaquiline resistance were collected in a data-set, including that found in our paper. This collection of bedaquiline mutations could be useful for the early detection of bedaquiline-resistance among *Mtb* clinical isolates.

RESULTS AND DISCUSSION

Table 10. Characterization of *Mtb* bedaquiline resistant mutants.

<i>Mtb</i> strains	MIC (µg/mL)	Mutation	Amino acid substitution
H37Rv	0.06	-	-
IC1	0.06	-	-
IC2	0.06	-	-
IC1 B	8	<i>atpE</i> : g187c	A63P
IC1 C	4	<i>atpE</i> : g187c	A63P
IC1 D	4	<i>atpE</i> : g187c	A63P
IC1 F	4	<i>atpE</i> : g187c	A63P
IC1 G	4	<i>atpE</i> : g187c	A63P
IC1 H	2	<i>atpE</i> : a83c	D28A
IC2 Q	0.5	<i>atpE</i> : a83g	D28G
IC1 L	0.5	<i>r0678</i> : c400t	R124Stop
IC1 M	0.5	<i>r0678</i> : g120c	L40F
IC1 N	0.5	<i>r0678</i> : a271c	T91P
IC1 O	0.5	<i>r0678</i> : g61t	E21Stop
IC2 P	0.25	<i>r0678</i> : g197a	G66E

4.1.2 Triclosan-based macrocyclic compounds as new direct InhA inhibitors

Our collaborators Prof. Christian Lherbet (Paul Sabatier-Toulouse III University, France) synthesized some triclosan macrocyclic derivatives as possible new direct InhA inhibitors. We tested their *in vitro* activity against *Mtb* growth, finding two compounds quite active (Table 11).

Table 11. Biological evaluation of macrocyclic triclosan macrocyclic derivatives.

Compound	% inhibition at 50 µM (IC50)	<i>Mtb</i> MIC (µg/mL)
Macrocycle 1 (M01)	52 %	20
Macrocycle 2 (M02)	93 % (4.7 ± 0.4 uM)	40
Triclosan (TCL)	100 % (58% at 0.5 uM)	20
Streptomycin		0.25

RESULTS AND DISCUSSION

MIC values for macrocycles M01 and M02 were found to be similar to that of TCL. M02 was able to inhibit InhA activity with an affinity (IC₅₀) in the micromolar range. Docking experiments showed that M02 binds the InhA active site. In conclusion, M02 compound is an important starting point for the development of new active triclosan macrocyclic derivatives that directly inhibit InhA.

4.1.3 Characterization of new inhibitors of Mg²⁺-dependent enzyme salicylate synthase (MbtI)

Mycobacterium tuberculosis salicylate synthase MbtI is a validated pharmacological target, involved in mycobactin-mediated iron acquisition pathway, that catalyses the two-step conversion of chorismate to salicylate [Meneghetti *et al.*, 2016]. Targeting this pathway is an interesting option for drug discovering as iron is fundamental for *Mtb* during infection, being also strictly correlated to the pathogen virulence.

In this context, an extended structure–activity relationships (SAR) study of a previously identified furan-based hit compound [Chiarelli *et al.*, 2018] was performed. The study of this hit optimization led to the disclosure of two new compounds **1h** and **10** (Figure 16), exhibiting a strong activity against MbtI (K_i=8.8 ± 0.7 μM and 4.2 ± 0.8 μM, respectively) and a moderate antitubercular activity with MIC of 250 μM. Moreover, through the Universal CAS liquid assay in iron-limiting conditions and quantification of the mycobactins, the antimycobacterial activity of the compounds was proven to be correlated with a reduction of siderophores production.

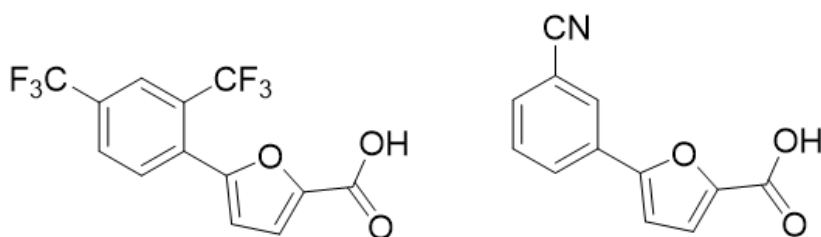


Figure 16: Structure of the new MbtI inhibitors **1h** and **10**.

4.1.4 Study of the mechanism of action of 11726172 by transcriptomic analysis

In collaboration with Dr. Vadim Makarov (Bach Institute of Biochemistry, Research Center of Biotechnology of the Russian Academy of Sciences, Russian

RESULTS AND DISCUSSION

Federation), we tested *in vitro* over 600 molecules against *Mtb* growth, of which only few showed to have a good minimal inhibitory concentration (Table 12).

Table 12. Screening of more than 600 compounds against *Mtb* growth.

MIC ($\mu\text{g}/\text{mL}$)	Number of Compounds	Compounds
0,25	1	11726172
0,5	14	11626056
1	5	-
2,5	10	-
5	12	-
10	19	-
20	41	-
> 20	547	-
Total	649	

Out of these compounds, two in particular were of great interest: 11626056 and 11726172 (Figure 17) because of their high activity. The characterization of the mechanism of action of 11626056 is described in Monakhova *et al.*, 2021.

11726172 (4-nitrobenzo[c][1,2,5]thiadiazol-5-yl thiazolidine-3-carbodithioate) compound is highly active against *Mtb* growth with an MIC of 0.25 $\mu\text{g}/\text{mL}$ (Figure 17). In order to study its mechanism of action, a panel of several *Mtb* mutants already available and harbouring different known mutations in genes encoding for drug targets (NTB1, DR1, 88.7), drug activators (53.3 and 81.10), or drug inactivator (Ty1) was used. Furthermore, its activity was also evaluated against two *Mtb* multi-drug resistant clinical isolates (Table 13). Interestingly, 11726172 was active against all *Mtb* strains tested, underlining that it could have a new mechanism of action being also active against MDR clinical isolates.

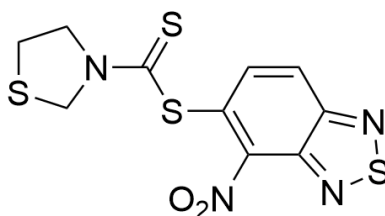


Figure 17. Molecular structure of 11726172 compound.

RESULTS AND DISCUSSION

Table 13. Activity of 11726172 against *Mtb* strains.

<i>Mtb</i> strains	MIC [$\mu\text{g}/\text{mL}$]		References
	11726172	Isoniazid	
H37Rv	0.25	0.05	-
IC1(res. to STR, INH, RIF, EMB)	0.25	> 2	Degiacomi <i>et al.</i> , 2020
IC2 (res. to STR, INH, RIF, EMB, PYR, ETH, CM)	0.25	> 2	Degiacomi <i>et al.</i> , 2020
53.3 (Rv2466c, W28S)	0.25	0.05	Albesa-Jove <i>et al.</i> , 2014
53.8 (Rv0579, L240V; Rv0158, V48A; <i>essxD</i> , M41R)	0.25	0.05	Mori <i>et al.</i> 2020
NTB1 (DprE1, G387S)	0.25	0.05	Makarov <i>et al.</i> , 2009
DR1 (MmpL3, V681I)	0.25	0.05	Poce <i>et al.</i> , 2013
Ty1 (Rv3405c, c190t)	0.25	0.05	Neres <i>et al.</i> , 2015
88.1 (CoaA, Q207R)	0.25	0.05	Chiarelli <i>et al.</i> , 2018
88.7 (PyrG, V186G)	0.25	0.05	Mori <i>et al.</i> , 2015
81.10 (EthA, D1109-37)	0.25	0.05	Mori <i>et al.</i> , 2015

To better understand the effect on *Mtb* growth after 11726172 exposure, a transcriptomic analysis by RNA-Seq was performed starting from *Mtb* cultures treated with different compound concentrations (10-fold and 30-fold MIC). The bioinformatic analysis was performed in collaboration with Prof. Davide Sassera (Department of Biology and Biotechnology, University of Pavia, Italy). Overall, in both conditions 88 genes were up-regulated, while 4 genes were repressed (Table 14, 15; Figures 18, 19).

Table 14. Commonly *Mtb* upregulated genes after 11726172 exposure.

Gene	log2FoldChange*	P-value*	Padj*	Functional category
<i>Arc</i>	4,518071112026	2,136640820154	3,76728624608	Cell wall and cell processes
	72	98E-22	235E-20	
<i>CtpG</i>	4,405768740882	1,137943784277	1,19299565924	Cell wall and cell processes
	99	28E-18	637E-16	
<i>Rv1972</i>	3,940447669889	7,760196208251	8,60051459765	Cell wall and cell processes
	25	24E-19	901E-17	
<i>Rv1671</i>	3,914358515859	1,680963465305	5,34463711632	Cell wall and cell processes
	31	89E-10	914E-09	
<i>LpqS</i>	3,774893372872	1,327632011047	6,43735571356	Cell wall and cell processes
	65	91E-12	855E-11	
<i>Rv2698</i>	3,646690146520	7,364780900647	7,14199627840	Cell wall and cell processes
	89	69E-18	31E-16	
<i>Rv0180c</i>	3,462145237535	2,043047002151	1,18283273452	Cell wall and cell processes
	26	1E-13	897E-11	

RESULTS AND DISCUSSION

<i>Rv2963</i>	3,440360890679	4,207245083703 66E-16	3,13844301532 432E-14	Cell wall and cell processes
<i>CfpV</i>	3,437960120024 17	1,377702261328 04E-16	1,11335563993 572E-14	Cell wall and cell processes
<i>Rv2025c</i>	3,298868064549 71	1,455503434772 09E-25	4,34299832575 456E-23	Cell wall and cell processes
<i>Rv3054c</i>	8,028457729429 43	1,207180315764 98E-42	1,17066311121 309E-39	Conserved hypotheticals
<i>Rv2641</i>	7,776595730696 59	2,215733455229 96E-48	2,86494335761 233E-45	Conserved hypotheticals
<i>Rv1673c</i>	7,170091046902 36	4,423372386785 92E-29	1,42985512402 855E-26	Conserved hypotheticals
<i>Rv3178</i>	6,622460020110 38	2,619609178893 81E-67	5,08073200246 455E-64	Conserved hypotheticals
<i>Rv0326</i>	6,484090413778 31	4,444686065666 2E-20	5,56159266087 716E-18	Conserved hypotheticals
<i>Rv3463</i>	5,717553236841 04	1,545763917305 06E-21	2,49674222267 307E-19	Conserved hypotheticals
<i>Rv0140</i>	5,643142981689 84	1,579476701553 33E-19	1,85660306828 041E-17	Conserved hypotheticals
<i>Rv1767</i>	4,495728779378 58	2,005391604093 37E-20	2,68238414906 144E-18	Conserved hypotheticals
<i>Rv0141c</i>	4,403819157356 52	1,469972884586 83E-15	9,83107727467 642E-14	Conserved hypotheticals
<i>Rv1993c</i>	4,357376583028 19	7,637251087081 15E-36	4,23212813811 254E-33	Conserved hypotheticals
<i>Rv2466c</i>	4,338320456252 87	7,411740159395 83E-12	3,05852554024 43E-10	Conserved hypotheticals
<i>Rv3353c</i>	4,069287458912 08	2,401515048973 18E-21	3,58287572114 115E-19	Conserved hypotheticals
<i>Rv0325</i>	3,872814578700 53	1,451198240347 18E-10	4,77050675788 703E-09	Conserved hypotheticals
<i>Rv2822c</i>	3,860987710074 15	1,318042033015 78E-11	5,06206440204 774E-10	Conserved hypotheticals
<i>Rv0740</i>	3,704388865759 98	3,945666206665 93E-12	1,71968979951 204E-10	Conserved hypotheticals
<i>Rv0142</i>	3,621254960783 95	9,374808575316 52E-17	7,87378095815 854E-15	Conserved hypotheticals
<i>Rv0990c</i>	3,326057377488 93	1,713401792075 04E-10	5,40348418817 812E-09	Conserved hypotheticals
<i>Rv0991c</i>	3,310931575403 72	4,712036070167 8E-07	6,94980529132 353E-06	Conserved hypotheticals
<i>Rv3222c</i>	3,101722955783 94	1,039151696024 49E-11	4,19882232174 896E-10	Conserved hypotheticals

RESULTS AND DISCUSSION

<i>Rv2699c</i>	3,010397266426 69	1,293209363338 21E-11	5,01635912038 892E-10	Conserved hypotheticals
<i>Rv3122</i>	3,008448456312 46	9,325531107987 78E-10	2,62128515709 309E-08	Conserved hypotheticals
<i>Rv1875</i>	3,005266221503 91	9,859917945037 31E-10	2,75155551861 869E-08	Conserved hypotheticals
<i>Rv2706c</i>	2,886802340047 65	6,722569454197 41E-08	1,23586952193 515E-06	Conserved hypotheticals
<i>Rv0329c</i>	2,820597345697 46	4,232560115045 52E-09	1,00110370038 18E-07	Conserved hypotheticals
<i>Rv0968</i>	2,803809861006 92	2,494176362621 61E-12	1,13822471889 52E-10	Conserved hypotheticals
<i>Rv0347</i>	2,799508287285 3	2,423299353501 85E-08	4,92145455090 768E-07	Conserved hypotheticals
<i>Rv1954c</i>	2,796090531634 95	3,587570857436 37E-05	0,00031342764 3153	Conserved hypotheticals
<i>Rv3269</i>	2,769717179610 91	3,052227517835 82E-09	7,46023329949 446E-08	Conserved hypotheticals
<i>Rv2823c</i>	2,584897258475 34	1,797601051818 78E-08	3,83126070329 947E-07	Conserved hypotheticals
<i>Rv1461</i>	2,532006046179 86	4,587393522792 21E-07	6,79179369271 412E-06	Conserved hypotheticals
<i>Rv2824c</i>	2,526551808519 57	1,237015493463 69E-07	2,10455399085 337E-06	Conserved hypotheticals
<i>RsbA</i>	3,442741193095 44	7,409533876109 96E-12	3,05852554024 43E-10	Information pathways
<i>Rv0560c</i>	7,213225531568 71	1,250298799986 09E-79	4,84990904514 605E-76	Intermediary metabolism and respiration
<i>Rv3174</i>	6,899626007486 82	1,625492929330 16E-36	1,05088117881 195E-33	Intermediary metabolism and respiration
<i>Cyp135 A1</i>	6,561143496376 98	1,609140385842 4E-21	2,49674222267 307E-19	Intermediary metabolism and respiration
<i>Rv1050</i>	5,988700049389 01	2,986336051810 53E-23	5,79199877248 653E-21	Intermediary metabolism and respiration
<i>TrxC</i>	5,483632925433 03	2,576993993783 84E-21	3,70228137106 945E-19	Intermediary metabolism and respiration
<i>TrxB2</i>	5,093034989220 02	1,727731730312 26E-20	2,39352549352 901E-18	Intermediary metabolism and respiration
<i>Rv3175</i>	5,067351390765 22	8,941192808753 66E-25	2,30509560835 626E-22	Intermediary metabolism and respiration
<i>Rv0331</i>	4,556868682745 44	5,585691375928 33E-14	3,49466078181 065E-12	Intermediary metabolism and respiration
<i>Rv2962c</i>	4,327218426158 55	6,032336172099 99E-23	1,11425866721 79E-20	Intermediary metabolism and respiration

RESULTS AND DISCUSSION

<i>TrxB1</i>	4,026790156288 08	1,058425051421 96E-12	5,33198801878 674E-11	Intermediary metabolism and respiration
<i>CysO</i>	3,951921630473 26	1,184573940063 75E-13	7,06917279001 119E-12	Intermediary metabolism and respiration
<i>Rv1334</i>	3,915688946123 82	1,393390516053 96E-12	6,67279236021 394E-11	Intermediary metabolism and respiration
<i>Rv0793</i>	3,837849181724 03	9,346057394138 23E-16	6,36023800558 986E-14	Intermediary metabolism and respiration
<i>MoeB1</i>	3,765327428407 73	2,145117770429 33E-14	1,36408390680 252E-12	Intermediary metabolism and respiration
<i>ThiX</i>	3,710388471189 11	1,751200347789 7E-16	1,38630737736 25E-14	Intermediary metabolism and respiration
<i>Rv0794c</i>	3,416868417769 77	2,406710243816 87E-13	1,37288662290 671E-11	Intermediary metabolism and respiration
<i>gysK2</i>	3,273069865279 09	5,592727433145 42E-13	2,97180681002 344E-11	Intermediary metabolism and respiration
<i>Rv0953c</i>	3,208001113035 96	3,097963250546 89E-11	1,14447613798 775E-09	Intermediary metabolism and respiration
<i>Rv0846c</i>	3,130370101055 61	1,280550126445 31E-11	5,01635912038 892E-10	Intermediary metabolism and respiration
<i>ClpC2</i>	3,007233048191 17	8,365751912685 78E-16	5,97592452201 721E-14	Intermediary metabolism and respiration
<i>PrpC</i>	2,959905942910 64	1,402363766071 81E-09	3,67551962742 741E-08	Intermediary metabolism and respiration
<i>CysM</i>	2,905616256217 53	1,206080287563 06E-09	3,27093358076 949E-08	Intermediary metabolism and respiration
<i>Rv2454c</i>	2,864321332186 28	2,636701501992 57E-08	5,27204387949 959E-07	Intermediary metabolism and respiration
<i>PrpD</i>	2,611847375400 5	3,770559634629 14E-07	5,71328157137 752E-06	Intermediary metabolism and respiration
<i>Rv1188</i>	2,562357693386 56	3,376577063877 57E-08	6,54887121539 054E-07	Intermediary metabolism and respiration
<i>MoaE1</i>	2,556977018001 02	1,436662447760 16E-07	2,39176550852 432E-06	Intermediary metabolism and respiration
<i>PapA4</i>	3,565702408480 13	4,511906483232 8E-12	1,94463169427 334E-10	Lipid metabolism
<i>PPE29</i>	3,502501932268 89	1,692567723887 62E-08	3,64748344497 783E-07	PE/PPE
<i>PPE15</i>	2,796729217259 86	1,222086377492 49E-09	3,27093358076 949E-08	PE/PPE
<i>Rv2642</i>	6,420973708699 84	2,068245394715 76E-39	1,60454477722 049E-36	Regulatory proteins
<i>Rv1674c</i>	6,373063975339 24	9,507999415751 52E-25	2,30509560835 626E-22	Regulatory proteins

RESULTS AND DISCUSSION

<i>Rv1049</i>	6,017140394968 06	1,122929834168 27E-23	2,41991379263 262E-21	Regulatory proteins
<i>CmiR</i>	5,676652872236 01	6,694074276106 46E-34	3,24578926462 712E-31	Regulatory proteins
<i>Rv2640c</i>	4,518659410636 52	1,547969190168 37E-18	1,58015065491 134E-16	Regulatory proteins
<i>CmiR</i>	4,353529367284 28	8,236415429992 18E-25	2,28207538949 569E-22	Regulatory proteins
<i>CsoR</i>	3,535498363718 23	2,030547452439 45E-13	1,18283273452 897E-11	Regulatory proteins
<i>Rv0328</i>	3,241144440789 63	3,597856378520 86E-10	1,09031913220 956E-08	Regulatory proteins
<i>Rv0196</i>	2,629325655061 23	6,163511523816 03E-07	8,82223660549 165E-06	Regulatory proteins
<i>Rv3177</i>	6,100366192352 43	4,519166200239 94E-30	1,94776063230 342E-27	Virulence, detoxification, adaptation
<i>MesT</i>	4,091595888502 92	1,191757473483 52E-17	1,10067315229 585E-15	Virulence, detoxification, adaptation
<i>ClpB</i>	4,039971344126 97	1,183975027506 11E-09	3,23425290964 522E-08	Virulence, detoxification, adaptation
<i>MymT</i>	3,871133181067 44	6,582380791823 28E-16	4,81755756443 066E-14	Virulence, detoxification, adaptation
<i>YrbE3A</i>	3,863750750475 15	2,397699690973 11E-16	1,82366217672 249E-14	Virulence, detoxification, adaptation
<i>KatG</i>	3,332098998530 15	1,458303370063 88E-12	6,89848630789 973E-11	Virulence, detoxification, adaptation
<i>YrbE3A</i>	2,889967879956 44	2,117315615649 35E-05	0,00019838326 7466	Virulence, detoxification, adaptation
<i>HigB</i>	2,687673125245 58	3,966818083215 78E-06	4,46008328834 609E-05	Virulence, detoxification, adaptation

* The values have been obtained after 11726172 treatment (30X MIC).

Table 15. Commonly *Mtb* down-regulated genes after 11726172 exposure.

Gene	log2FoldChange*	P-value*	Padj*	functional category
<i>MazE8</i>	-4,19354234562672	9,246259422498 07E-17	7,873780958158 54E-15	Virulence, detoxification, adaptation
<i>Rv0047c</i>	-2,84315170335902	1,657797356853 94E-08	3,592511702366 71E-07	Conserved hypotheticals
<i>Rv0430</i>	-2,70713443557783	2,839013466024 26E-08	5,618639405463 32E-07	Conserved hypotheticals
<i>Rv1632c</i>	-2,57419871980713	4,230498190814 7E-10	1,262315575551 56E-08	Conserved hypotheticals

* The values have been obtained after 11726172 treatment (30X MIC).

RESULTS AND DISCUSSION

Out of 11 functional categories defined for *Mtb* [Cole *et al.*, 1998], eight categories were represented amongst in induced genes in both conditions (Figures 18, 19). The most numerous ones are “Conserved hypotheticals” and “Intermediary metabolism and respiration”.

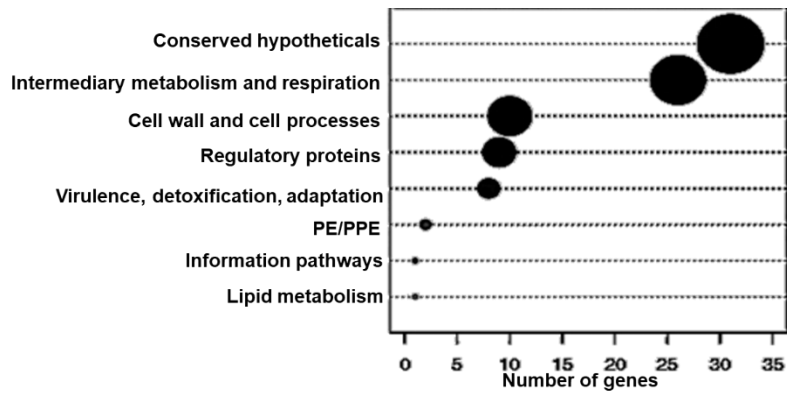


Figure 18. Genes induced in low treated samples and high treated samples amongst *Mtb* functional categories.

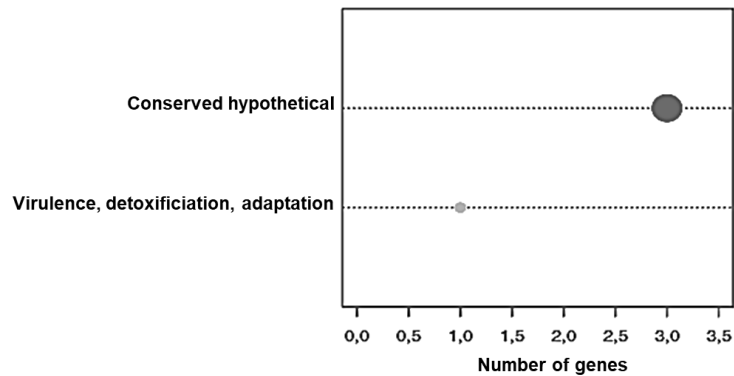


Figure 19. Genes repressed in low treated samples and high treated samples amongst *Mtb* functional categories.

Interestingly, several genes known to be induced by metals were up-regulated in response to 11726172 exposure, such as *cadI* (encoding a putative metal transporter), *furA* (encoding a Ferric uptake regulation protein), and *cysK2*. In particular, *cysK2* gene is involved

RESULTS AND DISCUSSION

in the biosynthesis of mycothiol that is a signalling molecule triggering responses upon exposure to reactive oxygen species. Metals-induced genes can be very important; since they can act as regulators of drug tolerance [Peterson *et al.*, 2016]. The gene coding for the cytochrome P450 Cyp135A1 was also up-regulated; cytochromes P450 are a group of heme-thiolate monooxygenases, which oxidize a variety of structurally unrelated compounds, including steroids, fatty acids, and xenobiotics. It could have an important role in response to external stress and it could be involved in the detoxification process correlated to 11726172. Another up-regulated gene was *Rv3914* which codes for a thioredoxin (TrxC) that is part of a thioredoxin system altogether with TrxA, TrxB and the reductase TrxR. TrxC is a disulfide reductase that catalyses the reduction of oxidized disulfide cysteines of different proteins. Then, the oxidated resulting thioredoxin can be reduced by the NADPH-dependant reductase TrxR. Moreover, another up-regulated gene is *rshA*, which codes for the anti-sigma factor for *sigH*. The sigma factor coded by *sigH* is involved in the response to heat and oxidative stresses, and it regulates the expression of other two sigma factor: SigE and SigB, which are also involved in stress response. In our case, the up-regulation of the anti-sigma factor encoded by *rshA* could limit the response to the stress induced by the drug exposure.

Among the down-regulated genes, the most repressed is *m2274A*, coding for the antitoxin MazE8. MazE8 is part of a Toxin-Antitoxin system (TA) in *Mtb* implicated in regulating adaptive responses to environmental stresses or xenobiotic. TA are present in a two-gene operon, generally induced during infection by hypoxia, oxidative stress, and low pH. Moreover, the MazE TA system seems to be implicated in the transition to the persistent state in *Mtb* and in producing a high inflammatory response in the host body [Slayden *et al.*, 2018]. The repression of the antitoxin MazE8 could help the compound in its toxic effect against *Mtb* cells.

To validate the expression profile obtained by RNA-Seq analysis, an experimental validation by Real-Time PCR was performed. To this aim, in both conditions of 11726172 treatment, three differentially expressed genes (two induced genes, *cyp135A1*, *trxC*, and one repressed, *mazE8*) were selected amongst the most up- or down-regulated genes and their level of expression was analysed. Housekeeping gene *sigA* was chosen as a reference gene, encoding σ^A factor of *M. tuberculosis*. Obtained results are reported in table 16. Expression profiles of the selected genes obtained by qPCR were consistent with the patterns of expression revealed by the RNA-Seq. The results were considered as technical validation of the differential expression gene analysis (Table 16).

RESULTS AND DISCUSSION

Table 16. Evaluation of expression levels of *cyp135A1*, *trxC*, and *mazE8* genes by qPCR.

Treatment of <i>Mtb</i> cultures	Expression levels					
	<i>cyp135A1</i>		<i>trxC</i>		<i>mazE8</i>	
	RT-PCR	RNA-Seq	RT-PCR	RNA-Seq	RT-PCR	RNA-Seq
10X MIC	8,86±0,39	7,41	10,65±0,60	5,22	0,22±1,48	-3,92
30X MIC	6,57±0,12	6,56	5,17±1,24	5,48	-4,55±1,97	-4,194

Taken together, these data suggest that 11726172 could have a pleiotropic effect on *Mtb* cells, triggering general stress responses. In particular, it seems to affect cell permeability; consequently, it perturbs metal homeostasis as well as the cytoplasmic redox potential.

In order to have further insights in the mechanism of action of 11726172, the study of the metabolome profile changes induced by 11726172 exposure is in progress in collaboration with Prof. Katarina Mikusová and Dr. Jana Kordulakova (Department of Biochemistry, Faculty of Natural Sciences, Comenius University, Bratislava, Slovakia).

4.1.5 Selamectin, a repurposing drug which inhibits *Mtb* DprE1 enzyme

Drug-repurposing consists in the transferring of routinely used drugs for a specific disease to a new one. This procedure can reduce the time necessary for the release of new drugs, thanks to the already known pharmaceutical kinetic of the compounds and plausible side effects on humans/animals.

In this regard, our collaborators, Prof. Josè Antonio Ainsa Claver and Dr. Santiago Ramon-Garçia (Department of Microbiology, Preventive Medicine and Public Health, University of Zaragoza, Spain) are working to repurpose members of the avermectin family (macrolides known for their anthelmintic activities) for TB treatment.

As showed in Lim *et al.* 2013, selamectin (altogether with other members of the avermectin family) is bactericidal against mycobacterial species, including multidrug-resistant and extensively drug-resistant *Mtb* clinical strains.

A panel of *Mtb* mutant strains harbouring different known mutations in genes encoding for drug targets (NTB1, DR1, 88.7), drug activators (53.3 and 81.10), or drug inactivator (Ty1) was used to investigate the possible mechanism of action of Selamectin. Furthermore, the activity of selamectin against 2 MDR *Mtb* clinical isolates was tested (Table 17). Surprisingly, NTB1 and NTB9 mutants showed a higher susceptibility to

RESULTS AND DISCUSSION

selamectin than the *Mtb* wild type strain. These mutants harbour a mutation in *Rv3790* gene coding for the decaprenylphosphoryl- β -D-ribose 2'-oxidase (DprE1), which is essential for *Mtb* growth and it is involved in the cell wall biosynthesis. DprE1 is the molecular target of Benzothiazinones (BTZs) [Makarov *et al.*, 2009] and other inhibitors [Degiacomi *et al.*, 2020]. The amino acidic change of the Cys387 in DprE1 in Gly or Ser seems to increase selamectin sensitivity. It is noteworthy that Cys387 is essential for the binding of BTZ to DprE1 [Makarov *et al.*, 2009]; consequently, it could be speculated a different mechanism of action of DprE1 for the selamectin (Table 17).

Table 17. Activity of Selamectin against a panel of *Mtb* strains.

<i>Mtb</i> strains	MIC [μ g/mL]			References
	selamectin	INH	BTZ043	
H37Rv	4-8	0.025	0.001	
53.3 (Rv2466c, W28S)	2-4	0.025		Albesa-Jove <i>et al.</i> , 2014
53.8 (Rv0579, L240V; Rv0158, V48A; esxD, M41R)	2-4	0.025		Mori <i>et al.</i> 2020
DR1 (Mmpl3, V681I)	2-4	0.025		Poce <i>et al.</i> , 2013
Ty1 (Rv3405c, c190t)	2-4	0.025		Neres <i>et al.</i> , 2015
88.1 (CoaA, Q207R)	2-4	0.025		Chiarelli <i>et al.</i> , 2018
88.7 (PyrG, V186G)	2-4	0.025		Mori <i>et al.</i> , 2015
81.10 (EthA, D1109-37)	4-8	0.025		Mori <i>et al.</i> , 2015
IC1(res. to STR, INH, RIF, EMB)	4-8	>0.2		Degiacomi <i>et al.</i> , 2020
IC2 (res. to STR, INH, RIF, EMB, PYR, ETH, CM)	4-8	>0.2		Degiacomi <i>et al.</i> , 2020
NTB1 (DprE1, G387S)	2	0.025	> 1	Makarov <i>et al.</i> , 2009
NTB9 (DprE1-C384G)	2	0.025	1	Makarov <i>et al.</i> , 2009

In order to confirm our result, a selamectin time-concentration killing assay was performed using *Mtb* H37Rv wild type and NTB1 strains. As shown in Figure 20A, selamectin is bactericidal against *Mtb* H37Rv strain at 32 μ g/mL, even if at 8 μ g/mL there was a high reduction of survival. On the other hand, selamectin bactericidal activity against NTB1 mutant was evident at concentration \geq 8 μ g/mL (from the time point t11) (Figure 20B). These data confirm the MIC results; NTB1 (and also NTB9) mutant is more sensitive to selamectin than the wild-type strain.

RESULTS AND DISCUSSION

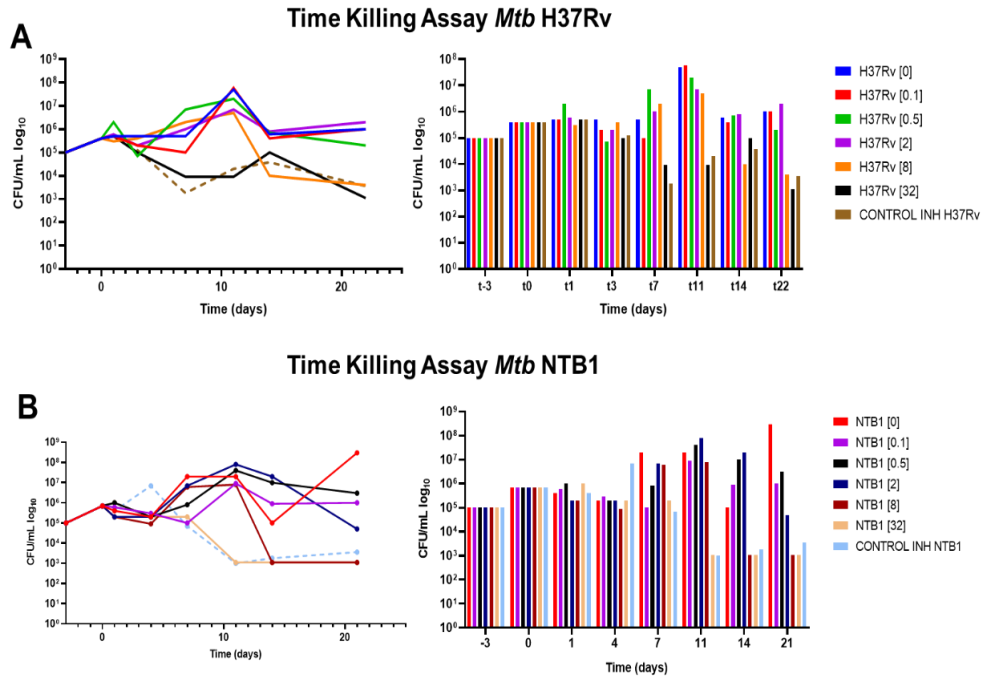


Figure 20. Time-Concentration killing Assay for *Mtb* wild type (A) and NTB1 (B) strains. The time-killing curve for selamectin against *Mtb* H37Rv and NTB1 strains (left) and their corresponding bar graph (right) for a clear comparison of the results were reported. Concentrations, expressed in µg/mL, of selamectin/INH used in the assay are reported in brackets.

Considering the achieved results, the activity of other avermectins was tested against both *Mtb* and NTB1 growth (Table 18). Two other avermectins (moxidectin and milbemycine oxime) were active against *Mtb* wild-type strain; no difference in their activity were evaluated in NTB1 mutant.

Table 18. Avermectins activity against *Mtb* strains.

Drugs	MIC µg/mL	
	H37Rv	NTB1
Selamectin	4-8	2-4
Ivermectin	>32	>32
Moxidectin	2	2
Molbemione Oxime	4	4

RESULTS AND DISCUSSION

In conclusion only selamectin showed to be more active against NTB1 mutant, harbouring a mutation in *dprE1* gene, than the wild-type strain. Consequently, we wanted to in depth study the reason of this behaviour and in particular if there is an interaction between selamectin and DprE1 enzyme. To this purpose, the effects of the compounds against the activity of DprE1 enzyme have been tested. All the compounds, initially assayed at 100 μM , were shown to strongly inhibit DprE1 activity; thus, the IC_{50} values have been determined (Figure 21; Table 19).

Table 19. IC_{50} values of avermectins against *M. smegmatis* DprE1.

	Moxidectin		Selamectin		Ivermectin		Milbemycine Oxime	
	value	SE	value	SE	value	SE	value	SE
Residual activity at 100 μM (%)	95.86	4.95	93.93	16.18	91.15	9.10	99.53	7.99
IC_{50} (μM)	6.13	0.91	2.61	1.10	13.23	3.27	25.54	5.54

As shown by these results, avermectins were confirmed to have an inhibitory effect on DprE1 activity; selamectin and moxidectin were the most active with IC_{50} values of 2.6 ± 1.1 and 6.1 ± 0.9 μM , respectively (Figure 21; Table 19).

RESULTS AND DISCUSSION

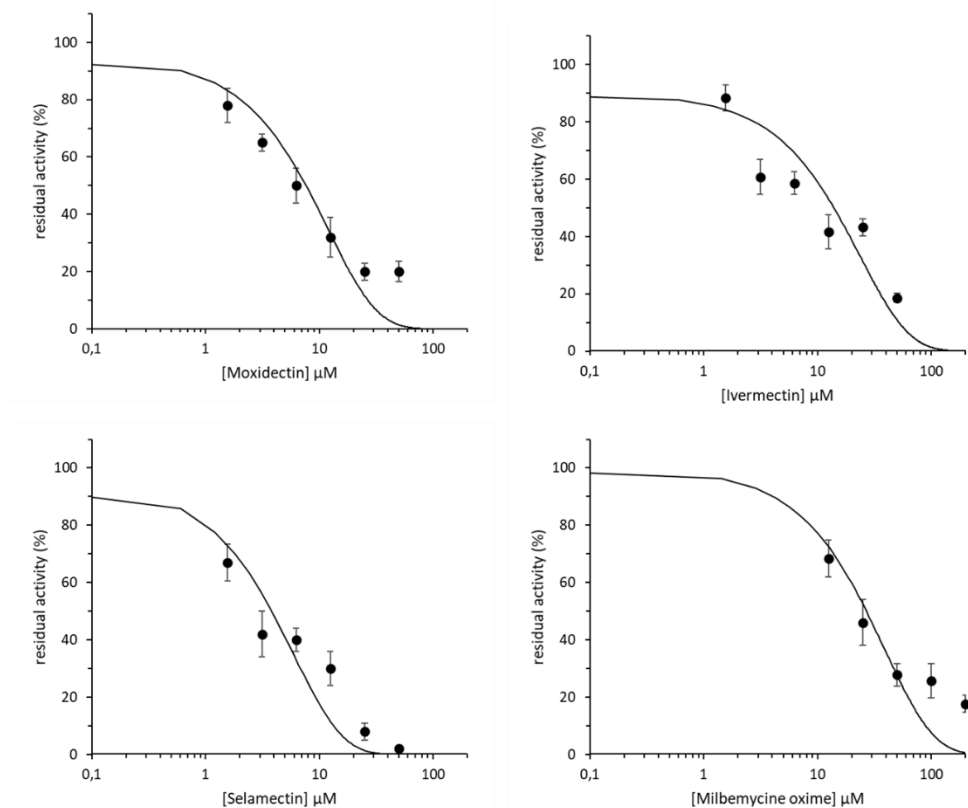


Figure 21. IC₅₀ determination of the different avermectins against *M. smegmatis* DprE1^{wt}.

Since in the NTB1 mutant the cysteine in position 387 (394 in *M. smegmatis*) of DprE1 is substituted with a serine, while in NTB9 it is substituted with a glycine, we produced the homologous *M. smegmatis* DprE1 mutant enzymes (C394S and C394G), through site-directed mutagenesis. At the same time, knowing that the presence of an alanine instead of a cysteine at this position confers natural resistance to BTZs [Makarov *et al.*, 2009], the C394A was also produced. These proteins were expressed and purified, as reported for the wild-type enzyme [Neres *et al.*, 2012]. Unfortunately, it was not possible to characterize the C394G mutant DprE1 as the *in vitro* activity of the purified protein was not detectable (data not shown). As the mutant proteins were not previously biochemically tested, to validate their *in vitro* activity, the steady state kinetic constants to the DprE1 substrate analogue farnesyl-phosphoryl-D-ribofuranose (FPR), were determined (Figure 22). The kinetic parameters of both mutant proteins resulted to be slightly impaired with

RESULTS AND DISCUSSION

respect to the wild type, in both V_{\max} and K_m values, leading to a significantly reduced catalytic efficiency (exemplified by their k_{cat}/K_m values) (Table 20).

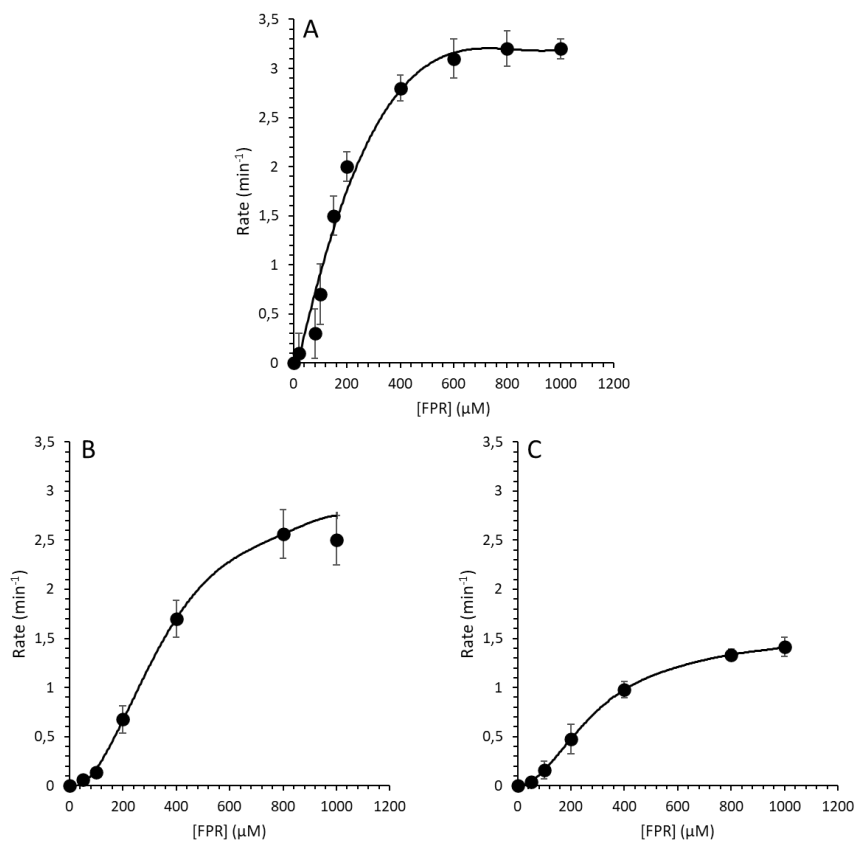


Figure 22. Steady-state kinetic analysis of the wild-type *M. smegmatis* DprE1 (A) and of the C394S (B) and C394A (C) mutant enzymes.

Table 20. Selamectin IC_{50} against *M. smegmatis* mutant DprE1.

	V_{\max} (min^{-1})	K_m (mM)	k_{cat}/K_m ($\text{min}^{-1} \text{mM}^{-1}$)
Wild Type	5.1 ± 0.4	0.190 ± 0.020	26.8 ± 3.2
C394A	2.8 ± 0.5	0.330 ± 0.022	8.5 ± 1.3
C394S	1.6 ± 0.3	0.310 ± 0.015	5.2 ± 1.1

RESULTS AND DISCUSSION

The enzymatic activity of the two active purified mutant enzymes was then assayed in the presence of selamectin. As shown in figure 23, the two mutant enzymes did not show a response to selamectin significantly different with respect to the wild type protein, with an IC_{50} of 3.9 ± 1.0 for C394A, while for the C394S mutant the IC_{50} was 12.1 ± 1.2 , thus even higher than that of the wild type (Figure 23). These results demonstrate that the position 394 in *M. smegmatis* DprE1 (corresponding to 387 in *Mtb*) is not directly involved in the binding of selamectin.

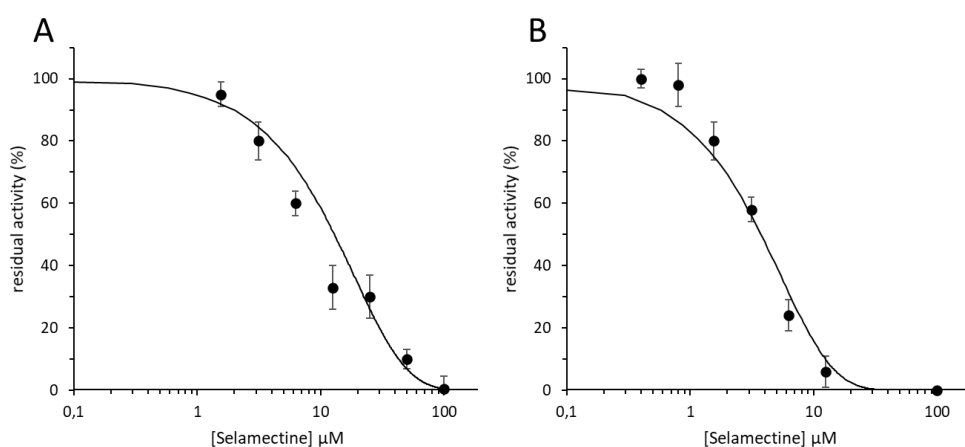


Figure 23. IC_{50} determination of Selamectin against the C394S (A) and C394A (B) mutant DprE1 enzymes.

The fact that NTB1 is more sensitive to this compound, could probably be due to the intrinsically low specific activity of the mutated enzyme, that is not longer able to support metabolic demands even at lower concentration of the inhibitor.

To investigate the possible binding site of selamectin to DprE1, our collaborator Prof. Fabrizio Manetti (Department of Biotechnology, Chemistry and Pharmacy, University of Siena, Italy) performed an *in silico* molecular docking, identifying the most plausible pose in correspondence to the leucine at position 275 in *Mtb* DprE1 structure. This amino acid is well conserved in *Mtb*, *M. smegmatis*, *Mab* and *M. bovis* BCG, while in *Mav* is substituted by a valine and in *Mycobacterium kansasii* (*Mkan*) by a phenylalanine. Interestingly, the activity of selamectin is higher against *Mkan* (Phe275 in DprE1) than *Mtb* (Leu275 in DprE1), while it is lower against *Mav* (Val275 in DprE1) [Dr. S. Ramon-Garcia, data not published]. According to the *in silico* model, the aromatic side chain of the phenylalanine 275 is accommodated in a region of space that contains a cage of additional aromatic residues. Such an aromatic machinery could be responsible for the stabilization of the selamectin-DprE1 interaction, enhancing the hydrophobic contacts to the binding site. Thus, the different sensitivity of the DprE1 enzymes bearing a Val or Leu residue could be

explained considering that the side chains are smaller and have lower lipophilicity than phenylalanine (in *Mkan*). To confirm this hypothesis the corresponding *M. smegmatis* mutant DprE1 enzymes (Phe275 and Val275) will be produced and characterized. Furthermore, in collaboration with Dr. Ramon-García (University of Zaragoza, Spain) the *M. smegmatis* strains carrying the Leu275Phe and Leu275Val will be produced, to have a better understanding of the effect of these mutations.

4.1.6 In-depth enzymatic study of DrpE1-DprE2 complex

Decaprenylphosphoryl- β -D-ribose 2'-oxidase (DprE1) works in association with decaprenylphosphoryl-D-2-keto erythropentose reductase (DprE2) for the epimerization of decaprenylphosphoryl- β -D ribose (DPR) into decaprenylphosphoryl arabinose (DPA) [Makarov *et al.*, 2009; Mikusová *et al.*, 2005], which is essential for the biosynthesis of arabinogalactan, a fundamental *Mtb* cell wall component. Even though DprE1 has been extensively studied, little is still known about DprE2. Indeed, several authors have suggested that the DprE1 and DprE2 could constitute a heterodimeric enzyme, and their direct interaction have been demonstrated through two hybrid system in *C. glutamicum* [Jankute *et al.*, 2014]. However, this complex has not been isolated and characterised yet.

In this regard, the goal was to in depth characterize DprE2 mechanism of action in association with DprE1, by meaning of co-expression in the same host, purification and biochemical analysis.

4.1.6.1 *Mtb* DprE1 and DprE2 co-expression and purification trials

A first attempt to express DprE1/DprE2 putative complex was performed using the pET-DUET-1 vector [Novagen, MerckMillipore, Germany] that allows for the simultaneous expression of both genes, in which *Rv3790* and *Rv3791* genes coding for DprE1 and DprE2, have been cloned. The recombinant vector was transformed in *E. coli* BL21(DE3) cells and the expression trials were performed with different media as well as different temperatures and times of induction (Table 21); each condition was then analysed in 15% SDS-PAGE (Figure 24). Only for the conditions showed in figure 24 it was possible to see an appreciable expression of both DprE1 and DprE2. These combinations were selected to attempt the scale-up to 1 litre of medium, which unfortunately was not successful (Figure 24).

RESULTS AND DISCUSSION

Table 21. Tested conditions for *Mtb* DprE1 and DprE2 co-expression.

Media	Temperatures (°C)					
	37/37	37/30	37/25	37/17	30/25	30/17
LB Broth	x	x	x	x	-	-
Terrific Broth	x	x	x	x	-	-
Terrific + Lactose	-	-	-	x	-	-
Autoinducing 1X	-	-	x	x	x	x
Autoinducing 2X	-	-	x	x	x	x
Super Broth	x	x	x	-	-	-
M9	x	x	x	-	-	-

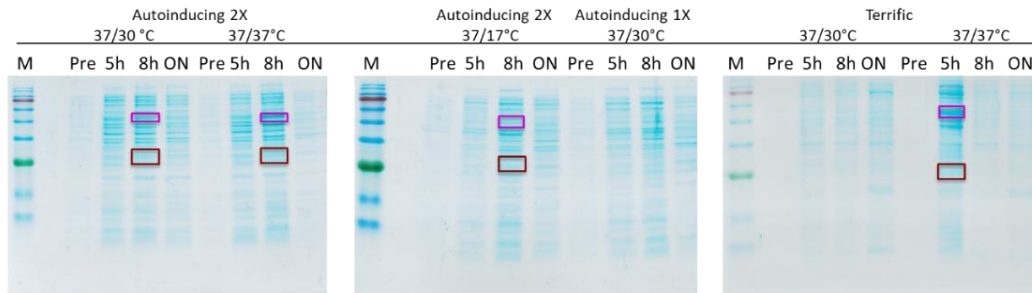


Figure 24. *Mtb* DprE1 and DprE2 co-expression trials. In figure are reported the expression trials of DprE1 (purple box) and DprE2 (red box) using the pET-DUET-1 expression system. At each time point (pre induction with IPTG, 5 hours post induction, 8 hours post induction and overnight post induction), samples were gathered and run on 15% SDS-PAGE.

4.1.6.2 Co-expression of *M. smegmatis* DprE1 and DprE2

Because the expression of *Mtb* DprE1 and DprE2 was not successful, a new attempt using the *Mycobacterium smegmatis* (*Msmeg*) homologue genes (*MSMEG_6382/dprE1-MSMEG_6385/dprE2*) was performed. A first expression trial was performed using the pET-DUET/*MSMEG_6382-MSMEG_6385* recombinant vector, but no significant expression of both proteins was detected (data not shown).

Due to the problems encountered in producing both proteins with the same expression vector, a co-expression was performed by cloning the two genes into separate expression vectors, respectively the pET-SUMO and the pET-23b plasmids. Then, *E. coli* BL21(DE3) cells were transformed with both recombinant vectors (pET-

RESULTS AND DISCUSSION

SUMO/*MSMEG_6382* and pET-23b/*MSMEG_6385*) and expression trials were performed. Among the tested conditions, an appreciable production of both enzymes was achieved upon 1 mM IPTG induction at 25°C overnight.

For the purification of the complex, a two-step immobilized metal affinity chromatography (IMAC) process has been applied. Indeed, the two enzymes have been cloned with a 6X-HisTag, but only in DprE1 the tag could be removed, upon digestion with SUMO-protease. The rationale behind this approach is that, if these two enzymes do in fact form a complex, once in IMAC fractionation they should be both retained in column, even if only one actually has the HisTag. Figure 25 presents the 15% SDS-PAGE of the fractions of IMAC purification. After the first chromatography two main bands, corresponding to DprE1 and DprE2, were eluted with 500 mM imidazole. This fraction was then dialysed in the presence of SUMO-protease, to remove the tag from DprE1, then loaded on another IMAC column. In this case the excess of DprE1 was directly eluted with the flow through (Figure 25, lane 3). However, some DprE1 was retained in the column, together with DprE2, strongly suggesting that the two proteins interact, as the former lack the His-tag (Figure 25, lane 4).

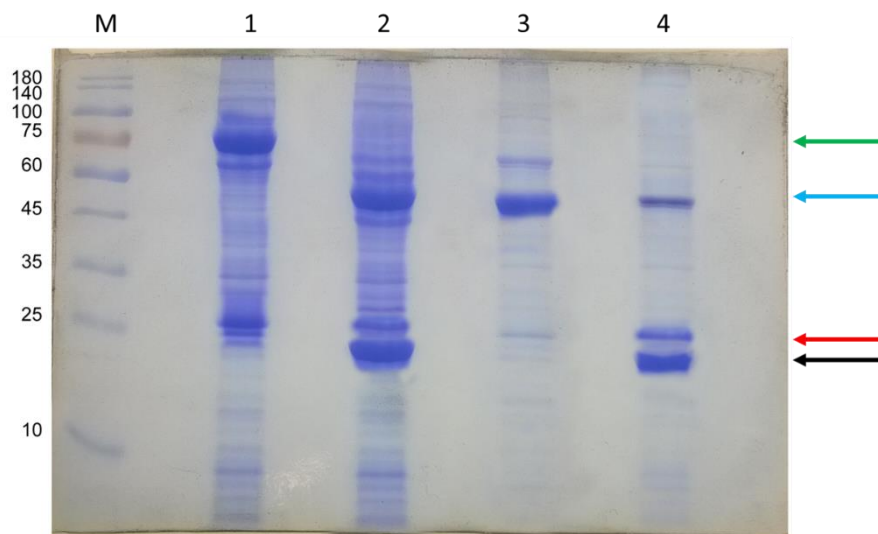


Figure 25. Purification of *Msmeg* DprE1/DprE2 complex. 15% SDS-PAGE of the fractions from the IMAC chromatographies. Lane 1: the products of the first IMAC eluted in 500mM Imidazole; lane 2: the products of the first IMAC after overnight dialysis in presence of the SUMO-protease to remove the SUMO-tag on the DprE1 fused protein; lane 3: flow-through of the second IMAC; lane 4: the first IMAC eluted in 500 mM Imidazole. Green arrow indicates DprE1 before Sumo-protease cleavage, blue arrow cleaved DprE1, red arrow DprE2, black arrow SUMO-tag.

RESULTS AND DISCUSSION

To further purify the obtained complex, removing the SUMO-tag that have been co-eluted during the second IMAC, a size exclusion chromatography has been performed on a column HiLoad Superdex 75 16/60, and elution monitored at 280 nm. The chromatogram is shown in figure 26. The fraction showing absorbance have been analysed in SDS-PAGE (Figure 27).

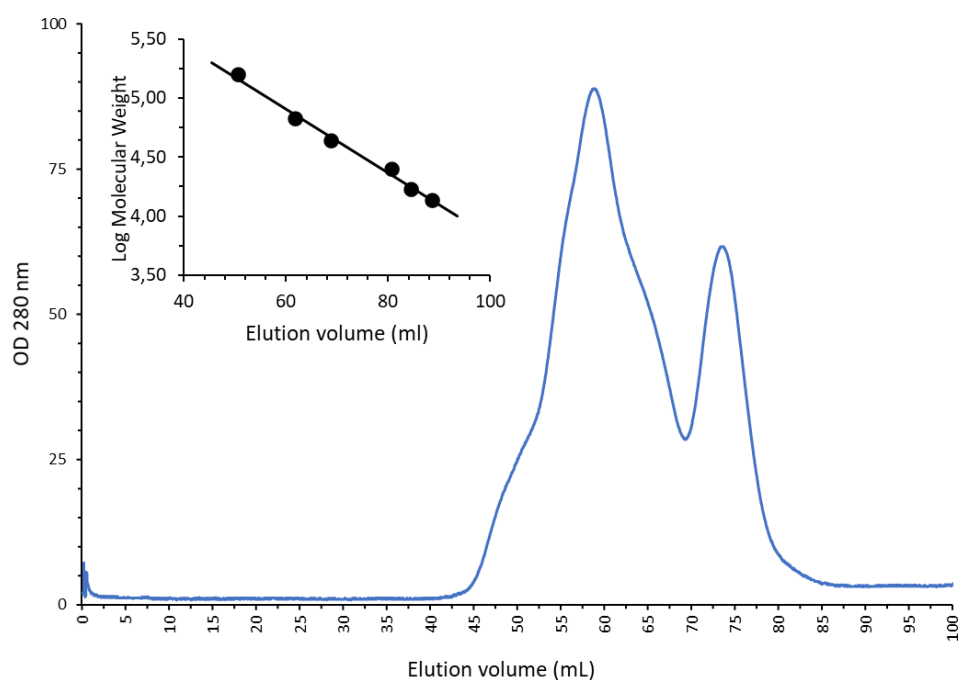


Figure 26. Elution profile of the size-exclusion protein Chromatography. Each fraction is spectrophotometrically monitored at an absorbance of $\lambda=280$ nm, indicative of the protein content and of $\lambda=414$ nm (not shown), proportional to the concentration of the FAD cofactor, and consequently of DprE1. The insert shows the calibration curve of the column, performed as described in “Material and Methods”.

As it is evident in Figure 26, two main discrete peaks appear. In particular, the first peak had an elution volume of 59 mL, corresponding to a molecular weight of about 77 kDa, as calculated from the calibration curve. This value is close to the expected molecular weight of the hypothetical DprE1/DprE2 complex, being 77.5 kDa. This is consistent with the fact that this macromolecule also absorbs at $\lambda = 414$ nm, proving the presence of a flavoprotein, such as DprE1 in these fractions.

The SDS-PAGE analysis displayed the presence of both DprE1 and DprE2 bands (Figure 27). These evidences confirmed that recombinant DprE1 and DprE2 when co-

RESULTS AND DISCUSSION

expressed are able to form a stable complex in solution. The second peak, with a molecular weight of about 27 kDa, corresponds to the SUMO-tag.

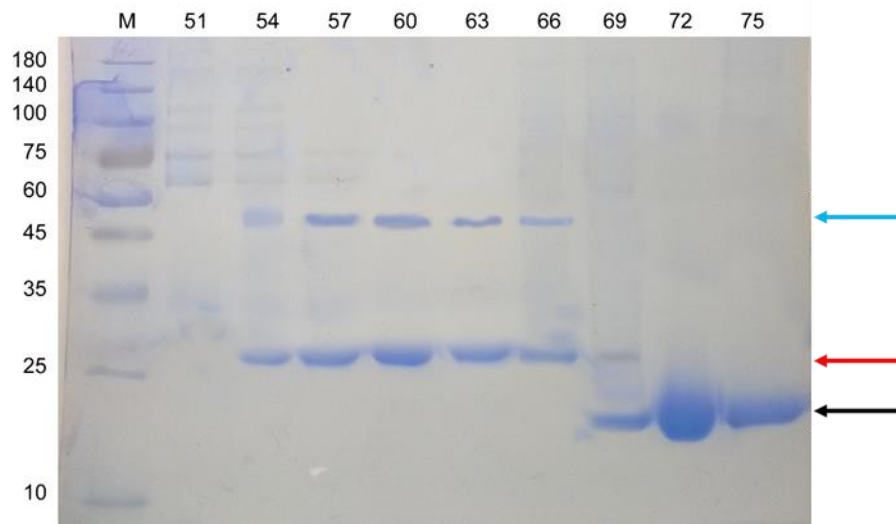


Figure 27. SDS-PAGE of the fractions corresponding to the first and second peaks. Each lane represents an eluted fraction, from 50 to 65 are the fractions of the first peak, while the fractions 72 to 75 are representative of the second peak. Blue arrow indicates DprE1, red arrow DprE2, black arrow SUMO-tag.

These fractions were then pooled together, concentrated, and subjected to enzyme activity assay, demonstrating that this complex is catalytically active. The steady-state kinetic analysis of the complex as a function of FPR was performed (Figure 28), determining the Michaelis-Menten constants. These results were compared with those obtained using *Msmeg* DprE1 and DprE2 expressed and purified separately.

RESULTS AND DISCUSSION

The co-expressed complex showed a V_{\max} value similar to that obtained with the two enzymes singularly expressed and purified, then mixed together in the assay mixture. By contrast, the affinity was significantly higher (Table 22).

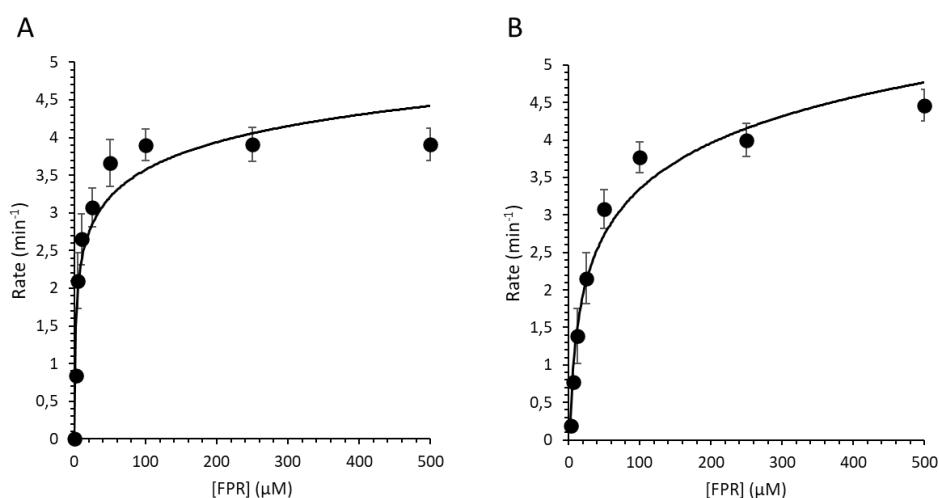


Figure 28. Steady state kinetic analysis of DprE1/DprE2 complex co-expressed (A) and of the components singularly expressed and purified (B).

Table 22. Steady state kinetic analysis values of DprE1/DprE2 complex co-expressed or mixed together.

	V_{\max} (min ⁻¹)	K_m (mM)	k_{cat}/K_m (min ⁻¹ mM ⁻¹)
Mixed enzymes	5.1 ± 0.3	0.044 ± 0.003	115 ± 5
Co-expressed Complex	5.1 ± 0.5	0.005 ± 0.0004	1020 ± 8.6

These results demonstrate that the co-expressed complex is biochemically active and it shows a better affinity for the substrate than the proteins expressed individually. This suggests that the optimal conformation of the active site is reached only when the two proteins are synthesized simultaneously, so they can fold together. Moreover, the fact that the complex is more efficient in catalysing the reaction, with a k_{cat}/K_m value about 10-fold higher, indicates that the conversion of DPR to DPA is not merely the sum of two distinct reactions, but it is achieved through the reaction of a single heterodimeric enzyme.

4.2 FIGHTING *Mycobacterium abscessus* IN CYSTIC FIBROSIS PATIENTS

Among the NTM that affect CF patients, *Mab* is the most represented worldwide and the one with the lowest cure rate (25–58%). New more specific and effective drugs in NTM management are urgently needed, especially against *Mab*. For this aim we followed two different approaches, that are described below.

4.2.1 Identification of 11326083 as anti-*Mab* compound

Out of more than 700 compounds tested until now synthesized by Dr. Makarov, only 1 molecule, named 11326083, was active against *Mab* growth (CUT-OFF: MIC \leq 8 $\mu\text{g}/\text{mL}$) (Figure 29) with an MIC of 1 $\mu\text{g}/\text{mL}$. 11326083 is an ethyl 6-((N-(5-fluoro-2-methylphenyl)carbamimidoyl)thio)-1-hydroxy-1,2-dihydropyridine-3-carboxylate, belonging to the hydroxypyridine class. The activity of 11326083 was also tested against other NTM species, NTM MDR clinical isolates, other mycobacterial species, Gram-positive and Gram-negative bacteria (Table 23). 11326083 is active also against *Mab* MDR strains, other NTM as well as *Mav* wild type and MDR isolates. Interestingly, its activity seems to be specific against mycobacterial species.

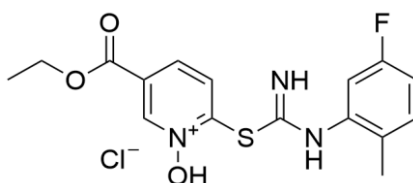


Figure 29. Structure of 11326083.

Table 23. Activity of 11326083 against bacterial species.

Strains	Genotype/Drug resistance	11326083 MIC [$\mu\text{g}/\text{mL}$]
<i>M. abscessus</i> ATCC 19977	Wild-type	1-2
<i>M. bolletii</i> 1999-0888	Wild-type	1-2
<i>M. massiliense</i> 2005-0524	Wild-type	1-2
<i>M. abscessus</i> MDR clinical isolate 1	Resistant to amikacin, clarithromycin, doxycycline, bedaquiline, ciprofloxacin, erythromycin, meropenem, econazole, ethambutol, ethionamide, lansoprazole, pristinamycin, rifampicin, rifapentine, SQ109, sutezolid, thioacetazone.	1-2

RESULTS AND DISCUSSION

<i>M. abscessus</i> MDR clinical isolate 2 (from CF patient)	Resistant to amikacin, amoxicillin, clavulanic acid, cefepime, ceftazidime, ceftriaxone, ciprofloxacin, doxycycline, imipenem, linezolid, minocycline, moxifloxacin, tobramycin, trimethoprim/sulfam	1
<i>M. abscessus</i> clinical isolate n. 6	Resistant to clarithromycin, moxifloxacin, doxycycline, linezolid	2
<i>M. abscessus</i> clinical isolate n. 7	Resistant to clarithromycin, amikacin, moxifloxacin, doxycycline (Intermediate sensitivity to linezolid)	1-2
<i>M. abscessus</i> clinical isolate n. 8	Resistant to moxifloxacin, doxycycline	2
<i>M. abscessus</i> clinical isolate n. 9	Resistant to clarithromycin, moxifloxacin, doxycycline	2
<i>M. abscessus</i> clinical isolate n.10	Resistant to moxifloxacin, doxycycline	2
<i>M. avium</i> subsp. <i>avium</i> Chester ATCC15769	Wild-type	1-2
<i>M. avium</i> clinical isolate n.1	Resistant to linezolid (Intermediate sensitivity to Moxifloxacin)	1-2
<i>M. avium</i> clinical isolate n.2	Resistant to linezolid (Intermediate sensitivity to Moxifloxacin)	1-2
<i>M. avium</i> clinical isolate n.3	Resistant to linezolid (Intermediate sensitivity to Moxifloxacin)	1-2
<i>M. avium</i> clinical isolate n.4	Resistant to linezolid and Moxifloxacin	2
<i>M. kansasii</i> ATCC12478	Resistant to Streptomycin	<0,25
<i>M. tuberculosis</i> H37Rv	Wild-type	0.0625
<i>M. bovis</i> BCG Pasteur	Wild-type	0.125
<i>M. smegmatis</i> mc2155	Wild-type	2.5
<i>Escherichia coli</i> ATCC25922	Wild-type	32
<i>Bacillus subtilis</i> 168	Wild-type	16
<i>Salmonella</i> <i>thyphimurium</i> LT2	Wild-type	32
<i>Burkholderia cenocepacia</i> K56-2	Wild-type	> 256

RESULTS AND DISCUSSION

Because of the majority of antibiotic used in *Mab* therapy is bacteriostatic, the survival of *Mab* upon drug exposure for 4 days at concentrations ranging from 3- to 150-fold MIC was evaluated through TKA assay (Figure 30). 11326083 effectively reduced bacterial growth at concentration up to 30-fold MIC, with values comparable to ciprofloxacin (bacteriostatic); *Mab* growth was completely suppressed at 150-fold MIC. Consequently, 11326083 is bactericidal at high concentrations, making this a bimodal dose-dependent compound and an even more promising hit than before.

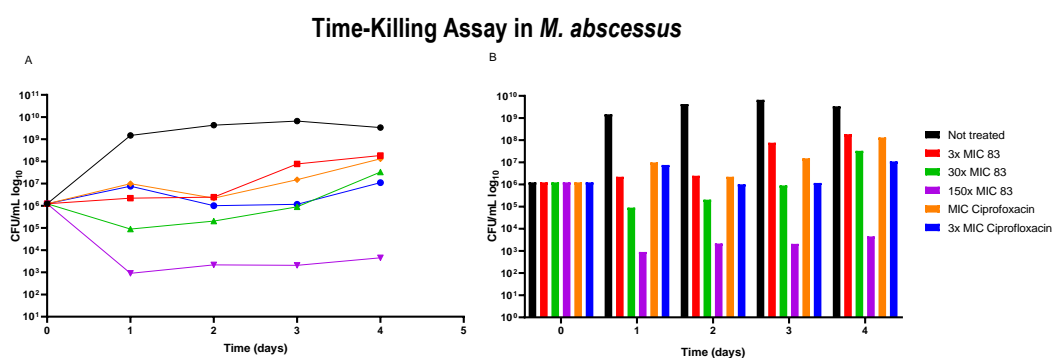


Figure 30. Time-Killing kinetic assay of 11326083 against *Mab* growth. 11326083 effectively reduced bacterial growth at 3- and 30-fold MIC. 11326083 bactericidal activity is comparable to ciprofloxacin at 3- and 30-fold MIC, while *Mab* growth was completely suppressed at 150-fold 83 MIC.

4.2.2. Study of 11326083 mechanism of action

It is known that mutations in the gene encoding the target confer drug-resistance, thus, to determine the target of 11326083, we attempted to isolate *Mab* spontaneous resistant mutants without success. *Mab* spontaneous mutants resistant to 11326083 were isolated by plating wild type cultures at exponential growth phase onto solid medium in the presence of high concentrations of the compound (10-20X the MIC for the wild-type strain). The plates were then incubated at 37°C for 7 days. Even though we were able to isolate single colonies onto solid medium, it was not possible to confirm the resistant phenotype by MIC determination (both onto solid medium and by REMA assay). It was hypothesized that the 11326083 target could be highly essential for *Mab* growth; consequently also single SNPs could be not vital for the pathogen.

For this reason, to better understand the effect on *Mab* growth after 11326083 exposure, the global transcriptional profile was evaluated by RNA-Seq. Triplicates of *Mab* cultures were exposed to 11326083 at concentration equal to 10- and 20-fold MIC (Table 24). Untreated cultures were also included. Total RNA was extracted from these cultures and subjected to RNA-Seq. The bioinformatic analysis was performed in collaboration with Prof. Davide Sassera. DEGs were defined using the following criteria: log₂FoldChange >

RESULTS AND DISCUSSION

|2| (sample group/control) and FDR (false discovery rate) < 0.05 (Table 24). We analysed differences in the enrichment of Mycobrowser categories (<https://mycobrowser.epfl.ch>) for the DEGs (Table 24). Most of the over-expressed and down-regulated genes fell into two main functional categories: hypothetical conserved proteins, whose function is still unknown, and intermediate metabolism and cellular respiration (Figure 31; Table 25).

Table 24. Differentially expressed genes in *Mab* after exposure to 11326083.

Treatment of <i>Mab</i> cultures	Up-regulated (log2FC > 2.5)	Down-regulated (log2FC < 2.5)
10-fold MIC	475	172
20-fold MIC	439	234
Common genes	363	129

Table 25. Top-20 deregulated genes in *Mab* after exposure to 11326083 (20X MIC).

		Up-regulated genes			
	Product	Functional category	Functional subcategory	log2Fold Change	padj
<i>MAB_4663</i>	Hypothetical protein	Hypothetical conserved protein	-	9,438495024	6,89E-251
<i>MAB_0448c</i>	Hypothetical protein	Hypothetical conserved protein	-	9,382848473	1,20E-227
<i>MAB_1044c</i>	Glyoxylase / protein associated with bleomycin resistance	Hypothetical conserved protein	Metabolism of metals	9,262713489	2,42E-137
<i>MAB_0512</i>	Aminotransferase / cysteine-desulfurase	Intermediate metabolism and cellular respiration	Nitrogen and sulfur metabolism	8,923449893	1,92E-209
<i>MAB_3055c</i>	Aminotransferase / cysteine-desulfurase	Intermediate metabolism and cellular respiration	Nitrogen and sulfur metabolism	8,574786795	1,83E-213
<i>MAB_4664</i>	Hypothetical protein	Hypothetical conserved protein	-	8,485444808	1,67E-290
<i>MAB_0470c</i>	Putative hydrolase	Hypothetical conserved protein	-	8,299087141	1,13E-272

RESULTS AND DISCUSSION

<i>MAB_2567</i>	Arsenic transporter, ArsC	Cell wall and cell processes	Metabolism of metals	7,864110652	6,95E-274
<i>MAB_3016c</i>	Hypothetical protein	Hypothetical conserved protein	-	7,748450127	5,68E-148
<i>MAB_4736</i>	Serin/threonine Kinase-PknE	Hypothetical conserved protein	Cellular stress	7,654447785	1,85E-219
<i>MAB_1270</i>	Hypothetical protein	Hypothetical conserved protein	-	7,516943452	4,17E-197
<i>MAB_0351</i>	Catalase	Hypothetical conserved protein	Cellular stress	7,442769359	1,23E-192
<i>MAB_1043c</i>	Putative oxidoreductase	Intermediate metabolism and cellular respiration	-	7,419796069	4,21E-116
<i>MAB_1224</i>	Hypothetical protein	Hypothetical conserved protein	-	7,417149245	1,37E-232
<i>MAB_2459</i>	Hypothetical protein	Hypothetical conserved protein	-	7,393843311	3,73E-92
<i>MAB_2604c</i>	Transcriptional regulator, ArsR	Regulatory proteins	Metabolism of metals	7,387174553	7,76E-163
<i>MAB_0827</i>	Hypothetical dehydrogenase	Intermediate metabolism and cellular respiration	-	7,386301377	1,42E-190
<i>MAB_4143c</i>	Anti-factor sigma ECF, ChrR	Information relating to cellular pathways	Transcription-associated enzymes	7,278599399	1,38E-93
<i>MAB_2603c</i>	Putative membrane protein	Cell wall and cell processes	Membrane protein	7,254254687	5,24E-197
<i>MAB_0485</i>	Putative oxidoreductase	Intermediate metabolism and cellular respiration	-	7,238249503	1,89E-133
Down-regulated genes					
<i>MAB_3999</i>	Hypothetical protein	Conserved hypothetical proteins	-	5,566388838	3,85E-59

RESULTS AND DISCUSSION

<i>MAB_2362</i>	Hypothetical protein	Conserved hypothetical proteins	-	- 5,355994849	2,39E- 121
<i>MAB_2363</i>	Hypothetical protein	Conserved hypothetical proteins	-	- 5,323498555	1,53E- 137
<i>MAB_2322</i>	Ribosomal protein 50S, L35, RpmI	Cellular pathways	Protein synthesis	-5,31967408	1,84E- 82
<i>MAB_2323</i>	Ribosomal protein 50S, L20, RplT	Cellular pathways	Protein synthesis	- 5,167787119	6,69E- 80
<i>MAB_2009</i>	Cell division protein, FtsZ	Cell wall and cell processes	Cell division and septal formation	- 4,659460164	2,38E- 80
<i>MAB_3834c</i>	L-lactate dehydrogenase, LldD1	Intermediate metabolism and cellular respiration	Biosynthesis of ATP, cytochromes, quinolones	- 4,658916216	3,21E- 34
<i>MAB_1008c</i>	Protein belonging to the MCE family	Virulence, detoxification and adaptation	MCE proteins	- 4,527600924	1,50E- 43
<i>MAB_1450</i>	ATP-synthetase delta chain AtpFH	Intermediate metabolism and cellular respiration	Biosynthesis of ATP, cytochromes, quinolones	-4,4426458	8,22E- 98
<i>MAB_2012</i>	Hypothetical protein	Conserved hypothetical proteins	-	- 4,362405395	7,99E- 53
<i>MAB_3998</i>	Hypothetical protein	Conserved hypothetical proteins	-	- 4,294324421	3,15E- 142
<i>MAB_3223c</i>	Signalling peptidase I, LepB	Cell wall and cell processes	-	- 4,046643445	4,21E- 58
<i>MAB_1452</i>	ATP-synthetase gamma subunit AtpG	Intermediate metabolism and cellular respiration	Biosynthesis of ATP, cytochromes, quinolones	-3,99627465	4,01E- 81
<i>MAB_3794c</i>	Ribosomal protein 50S, L30, RpmD	Information relating to cellular pathways	Protein synthesis	- 3,987528115	1,46E- 08
<i>MAB_1453</i>	ATP synthetase beta subunit AtpD	Intermediate metabolism and cellular respiration	Biosynthesis of ATP, cytochromes, quinolones	-3,97531526	5,57E- 120

RESULTS AND DISCUSSION

<i>MAB_3835c</i>	Protein E responsible to the synthesis of the coenzyme PQQ	Intermediate metabolism and cellular respiration	Biosynthesis of ATP, cytochromes, quinolones	- 3,901268901	1,14E- 20
<i>MAB_1142c</i>	Peptidil-tRNA hydrolase (PTH)	Intermediate metabolism and cellular respiration	-	- 3,878715004	9,00E- 26
<i>MAB_0191c</i>	Short-chain dehydrogenase / reductase	Intermediate metabolism and cellular respiration	-	-3,86406847	5,30E- 49
<i>MAB_1451</i>	ATP-synthetase alfa chain, AtpA	Intermediate metabolism and cellular respiration	Biosynthesis of ATP, cytochromes, quinolones	- 3,824667043	8,77E- 90
<i>MAB_2854c</i>	Hypothetical protein	Conserved hypothetical proteins	-	- 3,820736319	8,87E- 77

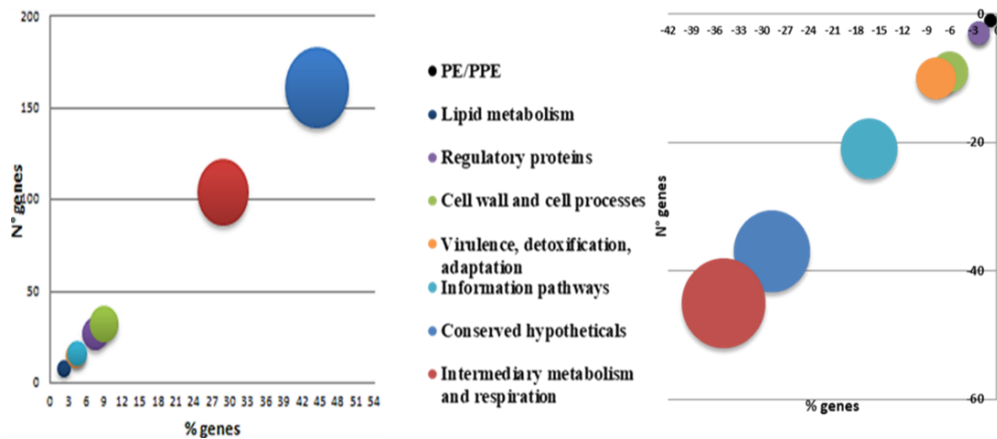


Figure 31. Functional categories related to up-regulated (on the left) and down-regulated (on the right) genes in common in both treatments.

To understand which metabolic pathways was influenced by treatment with 11326083, an accurate analysis was carried out to identify the functional sub-categories associated with DGEs which are in common for both treatments (Figure 32).

RESULTS AND DISCUSSION

Regarding the up-regulated genes, most of them were included in the following sub-categories:

- cellular stress, such as carbonic anhydrases, alternative sigma factors, etc.;
- metal metabolism, e.g. metal transporter (ArsC) or transcriptional regulators (ArsR), which respond to the presence of metals;
- nitrogen and sulphur metabolism, genes coding for enzymes involved in detoxification process;
- chaperonins and heat shock proteins, which are up-regulated in presence of cellular stress;
- membrane proteins, such as hypothetical efflux pumps induced by the presence of the compound (Figure 29).

The most representative functional sub-categories for down-regulated genes were:

- protein synthesis;
- transcription, e.g. genes coding for RNA polymerase, Rho factors, etc.;
- ATP biosynthesis, cytochromes, as well as the quinones components of the respiratory chain;
- MCE family, genes encoding factors which promote pathogen entry in macrophages (Figure 32).

These data highlight how the exposure to 11326083 inhibits fundamental metabolic pathways such as protein synthesis, ATP synthesis, respiration, and transcription. Moreover, using this compound could also have an anti-virulence effect by blocking the MCE family proteins which are implicated in promoting the entry of pathogenic mycobacteria into the macrophage [Sassi and Drancourt, 2014].

These results were technically validated by quantitative-PCR (Table 26).

RESULTS AND DISCUSSION

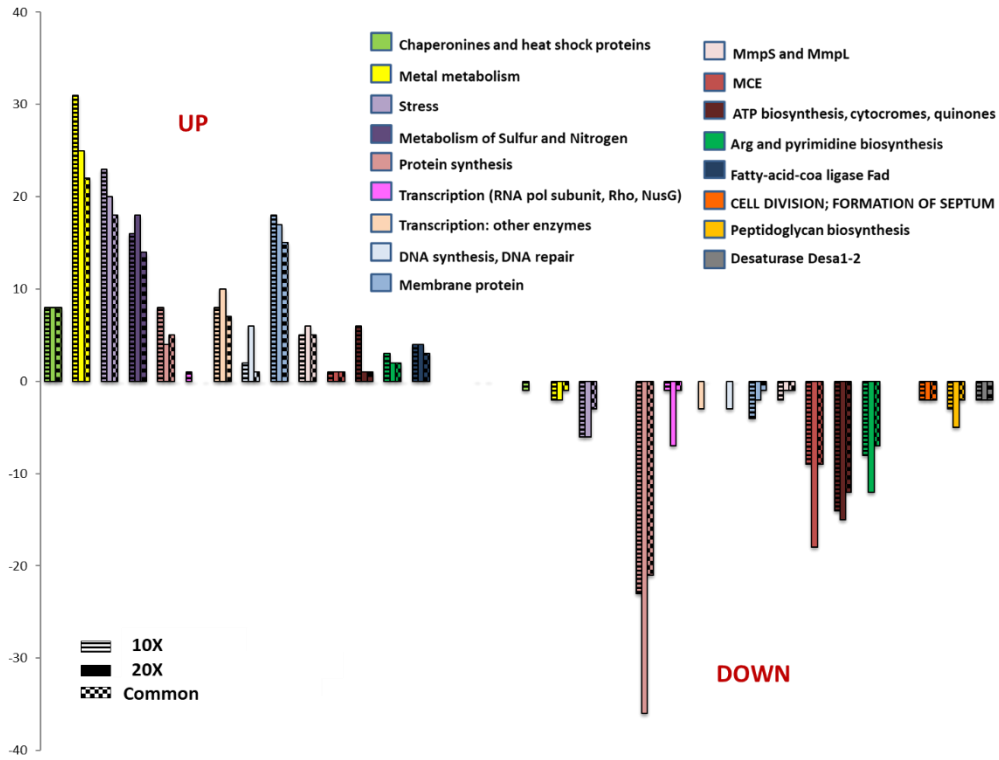


Figure 32. Functional subcategories associated with *Mab* genes differentially expressed in both treatments.

Table 26. Evaluation of expression levels of over-expressed and down-regulated genes by qPCR.

<i>Mab</i> cultures	Expression levels					
	<i>MAB_3211c</i>		<i>MAB_2245</i>		<i>MAB_3998</i>	
	RT-PCR	RNA-Seq	RT-PCR	RNA-Seq	RT-PCR	RNA-Seq
Not treated	1±0.37	-	1±0.20	-	1±0.15	-
10X 083 MIC	1117.97 ± 0.34	6.24	595.66 ± 0.48	5.66	0.39±0.11	-4.41
20X 083 MIC	564.83 ± 0.31	5.96	73.18 ± 0.25	2.86	0.31±0.09	-4.29

4.2.3. Structure-activity relationship (SAR) of 11326083 structure

In order to understand the structure-activity relationship (SAR) of the compound, we tested the activity of 24 new derivatives and 6 possible metabolites. No derivative was more active than the hit compound; only the putative metabolite 11226084 was found to be more active than 11326083, showing a MIC value of 0.25 $\mu\text{g}/\text{mL}$ (Figure 33). The studies on SAR will be further examined by means of mass spectrometry; furthermore, the synthesis of new 11226084 derivatives is ongoing. We decided to focus on 11226084, which is also active against other NTM species and MDR clinical isolates.

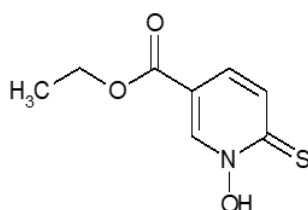


Figure 33. Structure of 11326084.

We have already demonstrated that also 11326084 is bactericidal at high concentrations as previously shown with 11326083 (Figure 34). The characterization of the mechanism of action of 11326084 is in progress as well as toxicity studies. Furthermore, its activity will be also evaluated in a *Mab* infected murine model.

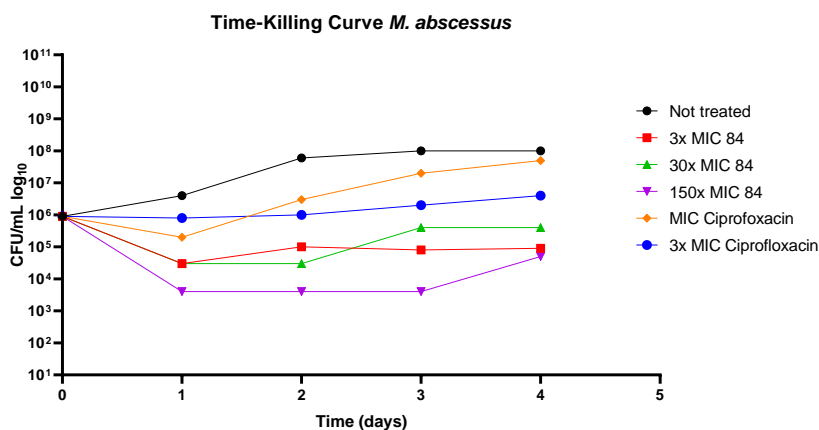


Figure 34. Time-Killing kinetic assay of 11326084 against *Mab* growth. 11326084 effectively reduced bacterial growth at 3- and 30-fold MIC. 11326084 bactericidal activity is higher than ciprofloxacin already at 3-fold MIC. *Mab* growth was completely suppressed at 150-fold 84 MIC.

4.2.4 MmpL3 inhibitors active against *Mycobacterium abscessus*

MmpL3 has been recently described as a new, promising drug target in *Mab* [Li *et al.*, 2018]. Recently, the crystal structure of *Mycobacterium smegmatis* MmpL3 has been determined alone and in complex with 4 anti-TB drugs [Zhang *et al.*, 2019]. Taking advantage of this, our collaborator Prof. Fabrizio Manetti (Department of Biotechnology, Chemistry and Pharmacy, University of Siena, Italy) performed an *in silico* virtual screening by means of pharmacophore modelling and docking simulations on compound libraries (more than 276.000 molecules) against the *Mab* virtual structure of MmpL3 (54.18% homology with *M. smegmatis* structure). Among the tested molecules, there are already licensed anticancer drugs or molecules used for other diseases in preclinical or clinical trials, etc. Interestingly, 48 possible MmpL3 inhibitors were found that we tested against *Mab* growth (Table 27). Their screening led to 3 active compounds: CAY3 (Mefluoquine), which is a well-known approved antimalarial compound, 135792 (benzoimidazole analogue), and 120330 (derivative of arylurea).

Table 27. *In silico* screening of MmpL3 inhibitors.

Compound libraries	Library size	MmpL3 inhibitors selected <i>in silico</i>	MIC in <i>Mab</i> ($\mu\text{g/mL}$)
Drug Bank (Canada)	~ 10.000	10	CAY3: ~ 16
NCI library (USA)	~ 265.000	28	120330 and 135792: ~ 16
Library from Prof. Corelli (University of Siena)	~ 1.000	6	-
New compounds	-	4	-
Total	~ 276.000	48 selected	3 active compounds

Hoping to find more active compounds, different analogues of the selected hit active compounds were tested without success (Table 28). Only two analogues showed an activity similar as mefluoquine.

Table 28. Overview of the MIC values for the analogues of the hit compounds.

	n° of compounds	MIC \leq 16 $\mu\text{g/mL}$
Mefluoquine analogues	14	2 (NSC4377 = 16; NSC13480 = 16)
Arylurea analogues	8	0
Benzoimidazole analogues	28	0

Following Prof. Manetti's suggestion, we decided to not further characterize the 120330 compound for its possible toxicity issue. Finally, Mefluoquine and 135792 were tested to be active also against other NTM species and MDR clinical isolates (Table 29).

RESULTS AND DISCUSSION

Table 29. Activity of CAY3 and 1235792 against bacterial species.

Strains	Genotype	MIC (µg/mL)	
		CAY3	1235792
<i>M. abscessus</i> ATCC 19977	Wild-type	16-32	16-32
<i>M. bolletii</i> 1999-0888	Wild-type	32	32
<i>M. massiliense</i> 2005-0524	Wild-type	32	32
<i>M. abscessus</i> MDR clinical isolate 1	Resistant to amikacin, clarithromycin, doxycycline, bedaquiline, ciprofloxacin, erythromycin, meropenem, econazole, ethambutol, ethionamide, lansoprazole, pristinamycin, rifampicin, rifapentine, SQ109, sutezolid, thiacetazone.	32	32
<i>M. abscessus</i> MDR clinical isolate 2 (from CF patient)	Resistant to amikacin, amoxicillin, clavulanic acid, cefepime, ceftazidime, ceftriaxone, ciprofloxacin, doxycycline, imipenem, linezolid, minocycline, moxifloxacin, tobramycin, trimethoprim/sulfam	32	32
<i>M. abscessus</i> clinical isolate n. 6	Resistant to clarithromycin, moxifloxacin, doxycycline, linezolid	32	32
<i>M. abscessus</i> clinical isolate n. 7	Resistant to clarithromycin, amikacin, moxifloxacin, doxycycline (Intermediate sensitivity to linezolid)	32	32
<i>M. abscessus</i> clinical isolate n. 8	Resistant to moxifloxacin, doxycycline	32	32
<i>M. abscessus</i> clinical isolate n. 9	Resistant to clarithromycin, moxifloxacin, doxycycline	32	32
<i>M. abscessus</i> clinical isolate n.10	Resistant to moxifloxacin, doxycycline	32	32
<i>M. avium</i> subsp. <i>avium</i> Chester ATCC15769	Wild-type	64	64
<i>M. avium</i> clinical isolate n.1	Resistant to linezolid (Intermediate sensitivity to Moxifloxacin)	64	64
<i>M. avium</i> clinical isolate n.2	Resistant to linezolid (Intermediate sensitivity to Moxifloxacin)	64	64
<i>M. avium</i> clinical isolate n.3	Resistant to linezolid (Intermediate sensitivity to Moxifloxacin)	64	64
<i>M. avium</i> clinical isolate n.4	Resistant to linezolid and Moxifloxacin	64	64
<i>M. smegmatis</i> mc2155	Wild-type	16	128

To validate MmpL3 as the target of these inhibitors, a biochemical assay in which we can appreciate the possible inhibition of MmpL3 activity [Degiacomi *et al.*, 2017] is in progress

5.CONCLUSIONS

Mycobacterial infections are a heavy burden worldwide, with the deadliest pathogen *Mycobacterium tuberculosis* (*Mtb*) and the emerging Nontuberculous mycobacteria (NTM). Furthermore, pharmacological treatments against these mycobacterial infections can be proven unsuccessful, due to the development of drug-resistant strains, treatment drop-out, and their peculiar cell wall, which is the main cause for both their drug-resistance and their virulence.

To help contrasting these issues, this research work aimed at identifying new promising anti-mycobacterial molecules and at characterizing already known pharmacological targets.

Among the pharmacological targets, we focused on DprE1 BTZ molecular target [Makarov *et al.*, 2009], to better understand how this enzyme works, and particularly its association with DprE2, by characterizing their interaction as a heterodimer and their biochemical activity as a complex. To this purpose, we attempted to achieve the co-expression of both *Mtb* enzymes, but unsuccessfully, despite the several approaches used. To overcome this issue, we moved to *Mycobacterium smegmatis* DprE1 and DprE2, that were successfully co-expressed and purified in *Escherichia coli*, by using two different recombinant vectors. Through size exclusion chromatography, it was demonstrated that DprE1 and DprE2 form strong interactions, behaving as a heterodimer in the elution profile. Furthermore, the complex was catalytically active, and the kinetic analysis demonstrated that this complex is significantly more efficient than the two enzymes produced separately. These results further strengthened our hypothesis that DprE1-DprE2 form a heterocomplex. We are in-depth validating DprE1-DprE2 biochemical activity and working to obtain a crystallographic structure of the complex (Manuscript in preparation). Ultimately, our study on the DprE1-DprE2 complex lays the foundations for the development of new inhibitors directed against both enzymes following the concept of multitargeting drug development [Stelitano *et al.*, 2020].

We also focused our work on the study of the mechanism of action of either new compounds or repurposing drugs active against *Mtb* and *Mycobacterium abscessus* (*Mab*).

CONCLUSIONS

We studied the mechanism of action of 11726172, which is a novel compound synthesized by Dr. V. Makarov. This compound showed to have good activity against *Mtb* wild type strain and MDR clinical isolates *in vitro*. To have more insights in its mechanism of action, we performed a transcriptomic analysis. Our findings suggested that 11726172 may have a pleiotropic effect on *Mtb* growth, triggering general stress responses. In particular, it seems to affect cell permeability; consequently, it perturbs metal homeostasis as well as the cytoplasmic redox potential. Furthermore, the repression of the antitoxin MazE8 could increase the toxic effect on *Mtb* cells upon drug exposure. Thus, for a better understanding of its mechanism of action, in collaboration with Dr. Katarina Mikusová (Department of Biochemistry, Faculty of Natural Sciences, Comenius University, Bratislava, Slovakia), the study of the metabolome profile changes induced by 11726172 exposure is ongoing.

As the process of drug development may require long period of time and resources, the drug repurposing strategy has gained the attention of the scientific community. Avermectins are a family of macrolides with antiparasitic activity which was repurposed against different mycobacteria species (e.g.: *Mtb*, *Mycobacterium ulcerans*) [Lim *et al.*, 2013; Scherr *et al.*, 2015]. In this work, we identified the mechanism of action of selamectin, belonging to avermectin class, in mycobacteria. We found that selamectin was more active against NTB1 and NTB9 mutants than against the wild-type strain. These mutants harbour the BTZs-resistance mutations C387S and C387G in DprE1, respectively [Makarov *et al.*, 2009]. We further confirmed this finding by Time-Concentration Killing assay. These results suggested that DprE1 is involved in selamectin mechanism of action and that this residue should be investigated to understand its role. Using a biochemical approach, we demonstrated that selamectin interacts with DprE1, having an inhibitory effect on its activity, but that the Cys387 residue (Cys394 in *M. smegmatis*) is not involved in the binding with avermectins. Consequently, selamectin could bind DprE1 differently than BTZs. Thanks to the collaboration with Prof. F. Manetti we hypothesize through molecular docking, that DprE1 Leu275 residue could be responsible for the selamectin binding site. To validate this hypothesis, we would like to test the activity of mutated enzymes harbouring some substitution in Leu275 (Val and Phe), and to produce *M. smegmatis* strains carrying these mutations. These experiments are in progress; in this way, we are able to carefully elucidate the mechanism of action of selamectin in mycobacteria.

To better understand the reason of the spreading of bedaquiline resistance among MDR- and XDR *Mtb* clinical isolates, we generated *Mtb* mutants resistant to bedaquiline starting from two MDR clinical isolates and mimicking what happens in clinical settings. As expected, these mutants harbored mutations in both *atpE* and *Rv0678* genes. The growth curves of bedaquiline resistant mutants were also evaluated, showing that *Rv0678* mutations could give an advantage in the growth rate, explaining their spread in clinical settings also prior to bedaquiline treatment [Degiacomi *et al.*, 2020]. Moreover, all the

CONCLUSIONS

mutations associated with bedaquiline resistance were collected in a data-set, hoping that it could be useful for the early detection of bedaquiline-resistance in MDR/XDR clinical isolates.

In this work, we also found a good candidate against *Mab* infections affecting in particular CF patients [Degiacomi *et al.*, 2020]. 11326083 showed good activity, not only against *Mab* growth, but also against other NTM and drug-resistant clinical isolates. Thanks to transcriptomic analysis, we discovered that several metabolic pathways are affected after 11326083 exposure, such as protein synthesis, ATP synthesis, respiration, and transcription. A putative more active metabolite, named 11226084, was also detected. The characterization of the mechanism of action of 11326083 and its metabolite as well as their toxicity studies are ongoing. Furthermore, the activity of these compounds will be also evaluated in a *Mab* infected murine model.

Finally, 3 putative Mmpl3 inhibitors (repurposing compounds) active against *Mab* growth were identified. We are validating MmpL3 as cellular target of these compounds. It is important to underline that among these 3 compounds there is mefloquine, which is a well-known antimalarial that is repurposed to fight *Mab* infections.

In conclusion, with our work we contributed to better understand the mechanisms underlying the onset of drug resistant mycobacterial strains, but we also provided the scientific community with information for the development of new therapeutical approaches hoping for a safer, shorter, and more responsive treatment for the patient affected by mycobacterial infections.

REFERENCES

- Albesa-Jové, D., Chiarelli, L. R., Makarov, V., Pasca, M. R., Urresti, S., Mori, G., Salina, E., Vocat, A., Comino, N., Mohorko, E., Ryabova, S., Pfeiffer, B., Lopes Ribeiro, A. L., Rodrigo-Unzueta, A., Tera, M., Zanoni, G., Buroni, S., Altmann, K. H., Hartkoorn, R. C., Glockshuber, R., ... Guerin, M. E. (2014). Rv2466c mediates the activation of TP053 to kill replicating and non-replicating *Mycobacterium tuberculosis*. *ACS chemical biology*, 9(7), 1567–1575. <https://doi.org/10.1021/cb500149m>
- Alderwick, L. J., Harrison, J., Lloyd, G. S., & Birch, H. L. (2015). The Mycobacterial Cell Wall-Peptidoglycan and Arabinogalactan. *Cold Spring Harbor perspectives in medicine*, 5(8), a021113. <https://doi.org/10.1101/cshperspect.a021113>
- Alexandrova, L., Zicari, S., Matyugina, E., Khandzhinskaya, A., Smirnova, T., Andreevskaya, S., Chernousova, L., Vanpouille, C., Kochetkov, S., & Margolis, L. (2017). Dual-targeted anti-TB/anti-HIV heterodimers. *Antiviral research*, 145, 175–183. <https://doi.org/10.1016/j.antiviral.2017.07.011>
- Andries, K., Verhasselt, P., Guillemont, J., Göhlmann, H. W., Neefs, J. M., Winkler, H., Van Gestel, J., Timmerman, P., Zhu, M., Lee, E., Williams, P., de Chaffoy, D., Huitric, E., Hoffner, S., Cambau, E., Truffot-Pernot, C., Lounis, N., & Jarlier, V. (2005). A diarylquinoline drug active on the ATP synthase of *Mycobacterium tuberculosis*. *Science (New York, N.Y.)*, 307(5707), 223–227. <https://doi.org/10.1126/science.1106753>
- Auguste, P., Tsertsvadze, A., Pink, J., Court, R., McCarthy, N., Sutcliffe, P., & Clarke, A. (2017). Comparing interferon-gamma release assays with tuberculin skin test for identifying latent tuberculosis infection that progresses to active tuberculosis: systematic review and meta-analysis. *BMC infectious diseases*, 17(1), 200. <https://doi.org/10.1186/s12879-017-2301-4>
- Aygun, D., Akcakaya, N., Cokugras, H., & Camcioglu, Y. (2019). Evaluation of Clinical and Laboratory Characteristics of Children with Pulmonary and Extrapulmonary Tuberculosis. *Medicina (Kaunas, Lithuania)*, 55(8), 428. <https://doi.org/10.3390/medicina55080428>
- Aziz, D. B., Low, J. L., Wu, M. L., Gengenbacher, M., Teo, J., Dartois, V., & Dick, T. (2017). Rifabutin Is Active against *Mycobacterium abscessus* Complex. *Antimicrobial agents and chemotherapy*, 61(6), e00155-17. <https://doi.org/10.1128/AAC.00155-17>
- Bahuguna, A., & Rawat, D. S. (2020). An overview of new antitubercular drugs, drug candidates, and their targets. *Medicinal research reviews*, 40(1), 263–292. <https://doi.org/10.1002/med.21602>
- Bald, D., Villellas, C., Lu, P., & Koul, A. (2017). Targeting Energy Metabolism in *Mycobacterium tuberculosis*, a New Paradigm in Antimycobacterial Drug Discovery. *mBio*, 8(2), e00272-17. <https://doi.org/10.1128/mBio.00272-17>

REFERENCES

- Bañuls, A. L., Sanou, A., Van Anh, N. T., & Godreuil, S. (2015). *Mycobacterium tuberculosis*: ecology and evolution of a human bacterium. *Journal of medical microbiology*, 64(11), 1261–1269. <https://doi.org/10.1099/jmm.0.000171>
- Baranowski, C., Rego, E. H., & Rubin, E. J. (2019). The Dream of a *Mycobacterium*. *Microbiology spectrum*, 7(2), 10.1128/microbiolspec.GPP3-0008-2018. <https://doi.org/10.1128/microbiolspec.GPP3-0008-2018>
- Barberis, I., Bragazzi, N. L., Galluzzo, L., & Martini, M. (2017). The history of tuberculosis: from the first historical records to the isolation of Koch's bacillus. *Journal of preventive medicine and hygiene*, 58(1), E9–E12.
- Batt, S. M., Jabeen, T., Bhowruth, V., Quill, L., Lund, P. A., Eggeling, L., Alderwick, L. J., Fütterer, K., & Besra, G. S. (2012). Structural basis of inhibition of *Mycobacterium tuberculosis* DprE1 by benzothiazinone inhibitors. *Proceedings of the National Academy of Sciences of the United States of America*, 109(28), 11354–11359. <https://doi.org/10.1073/pnas.1205735109>
- Bentur, L., Gur, M., Ashkenazi, M., Livnat-Levanon, G., Mizrahi, M., Tal, A., Ghaffari, A., Geffen, Y., Aviram, M., & Efrati, O. (2020). Pilot study to test inhaled nitric oxide in cystic fibrosis patients with refractory *Mycobacterium abscessus* lung infection. *Journal of cystic fibrosis : official journal of the European Cystic Fibrosis Society*, 19(2), 225–231. <https://doi.org/10.1016/j.jcf.2019.05.002>
- Bernut, A., Viljoen, A., Dupont, C., Sapriel, G., Blaise, M., Bouchier, C., Brosch, R., de Chastellier, C., Herrmann, J. L., & Kremer, L. (2016). Insights into the smooth-to-rough transitioning in *Mycobacterium boletii* unravels a functional Tyr residue conserved in all mycobacterial MmpL family members. *Molecular microbiology*, 99(5), 866–883. <https://doi.org/10.1111/mmi.13283>
- Bhat, Z. S., Rather, M. A., Maqbool, M., Lah, H. U., Yousuf, S. K., & Ahmad, Z. (2017). Cell wall: A versatile fountain of drug targets in *Mycobacterium tuberculosis*. *Biomedicine & pharmacotherapy = Biomedicine & pharmacotherapie*, 95, 1520–1534. <https://doi.org/10.1016/j.biopha.2017.09.036>
- Bhutani, I., Loharch, S., Gupta, P., Madathil, R., & Parkesh, R. (2015). Structure, dynamics, and interaction of *Mycobacterium tuberculosis* (Mtb) DprE1 and DprE2 examined by molecular modeling, simulation, and electrostatic studies. *PLoS one*, 10(3), e0119771. <https://doi.org/10.1371/journal.pone.0119771>
- Bishop, B. F., Bruce, C. I., Evans, N. A., Goudie, A. C., Gratton, K. A., Gibson, S. P., Pacey, M. S., Perry, D. A., Walshe, N. D., & Witty, M. J. (2000). Selamectin: a novel broad-spectrum endectocide for dogs and cats. *Veterinary parasitology*, 91(3-4), 163–176. [https://doi.org/10.1016/s0304-4017\(00\)00289-2](https://doi.org/10.1016/s0304-4017(00)00289-2)
- Bottai, D., Stinear, T. P., Supply, P., & Brosch, R. (2014). Mycobacterial Pathogenomics and Evolution. *Microbiology spectrum*, 2(1), MGM2–2013. <https://doi.org/10.1128/microbiolspec.MGM2-0025-2013>
- Brites, D., & Gagneux, S. (2017). The Nature and Evolution of Genomic Diversity in the *Mycobacterium tuberculosis* Complex. *Advances in experimental medicine and biology*, 1019, 1–26. https://doi.org/10.1007/978-3-319-64371-7_1

REFERENCES

- Bruchfeld, J., Correia-Neves, M., & Källenius, G. (2015). Tuberculosis and HIV Coinfection. *Cold Spring Harbor perspectives in medicine*, 5(7), a017871. <https://doi.org/10.1101/cshperspect.a017871>
- Bryant, J. M., Grogono, D. M., Rodriguez-Rincon, D., Everall, I., Brown, K. P., Moreno, P., Verma, D., Hill, E., Drijkoningen, J., Gilligan, P., Esther, C. R., Noone, P. G., Giddings, O., Bell, S. C., Thomson, R., Wainwright, C. E., Coulter, C., Pandey, S., Wood, M. E., Stockwell, R. E., ... Floto, R. A. (2016). Emergence and spread of a human-transmissible multidrug-resistant nontuberculous mycobacterium. *Science (New York, N.Y.)*, 354(6313), 751–757. <https://doi.org/10.1126/science.aaf8156>
- Cadena, A. M., Fortune, S. M., & Flynn, J. L. (2017). Heterogeneity in tuberculosis. *Nature reviews. Immunology*, 17(11), 691–702. <https://doi.org/10.1038/nri.2017.69>
- Caimmi, D., Martocq, N., Trioleyre, D., Guinet, C., Godreuil, S., Daniel, T., & Chiron, R. (2018). Positive Effect of Liposomal Amikacin for Inhalation on *Mycobacterium abscessus* in Cystic Fibrosis Patients. *Open forum infectious diseases*, 5(3), ofy034. <https://doi.org/10.1093/ofid/ofy034>
- Calmette A. (1931). Preventive Vaccination Against Tuberculosis with BCG. *Proceedings of the Royal Society of Medicine*, 24(11), 1481–1490.
- Caly, L., Druce, J. D., Catton, M. G., Jans, D. A., & Wagstaff, K. M. (2020). The FDA-approved drug ivermectin inhibits the replication of SARS-CoV-2 in vitro. *Antiviral research*, 178, 104787. <https://doi.org/10.1016/j.antiviral.2020.104787>
- Cambier, C. J., Takaki, K. K., Larson, R. P., Hernandez, R. E., Tobin, D. M., Urdahl, K. B., Cosma, C. L., & Ramakrishnan, L. (2014). Mycobacteria manipulate macrophage recruitment through coordinated use of membrane lipids. *Nature*, 505(7482), 218–222. <https://doi.org/10.1038/nature12799>
- Chakaya, J. M., Harries, A. D., & Marks, G. B. (2020). Ending tuberculosis by 2030-Pipe dream or reality?. *International journal of infectious diseases : IJID : official publication of the International Society for Infectious Diseases*, 92S, S51–S54. <https://doi.org/10.1016/j.ijid.2020.02.021>
- Cheng, A., Tsai, Y. T., Chang, S. Y., Sun, H. Y., Wu, U. I., Sheng, W. H., Chen, Y. C., & Chang, S. C. (2019). *In Vitro* Synergism of Rifabutin with Clarithromycin, Imipenem, and Tigecycline against the *Mycobacterium abscessus* Complex. *Antimicrobial agents and chemotherapy*, 63(4), e02234-18. <https://doi.org/10.1128/AAC.02234-18>
- Chiarelli, L. R., Degiacomi, G., Egorova, A., Makarov, V., & Pasca, M. R. (2020). Nitric oxide-releasing compounds for the treatment of lung infections. *Drug discovery today*, S1359-6446(20)30463-3. Advance online publication. <https://doi.org/10.1016/j.drudis.2020.10.027>
- Chiarelli, L. R., Mori, G., Orena, B. S., Esposito, M., Lane, T., de Jesus Lopes Ribeiro, A. L., Degiacomi, G., Zemanová, J., Szádocka, S., Huszár, S., Palčeková, Z., Manfredi, M., Gosetti, F., Lelièvre, J., Ballell, L., Kazakova, E., Makarov, V., Marengo, E., Mikusova, K., Cole, S. T., ... Pasca, M. R. (2018). A multitarget approach to drug discovery inhibiting *Mycobacterium tuberculosis* PyrG and PanK. *Scientific reports*, 8(1), 3187. <https://doi.org/10.1038/s41598-018-21614-4>
- Choo, S. W., Wee, W. Y., Ngeow, Y. F., Mitchell, W., Tan, J. L., Wong, G. J., Zhao, Y., & Xiao, J. (2014). Genomic reconnaissance of clinical isolates of emerging human pathogen

REFERENCES

- Mycobacterium abscessus* reveals high evolutionary potential. *Scientific reports*, 4, 4061. <https://doi.org/10.1038/srep04061>
- Chopra, S., Matsuyama, K., Hutson, C., & Madrid, P. (2011). Identification of antimicrobial activity among FDA-approved drugs for combating *Mycobacterium abscessus* and *Mycobacterium chelonae*. *The Journal of antimicrobial chemotherapy*, 66(7), 1533–1536. <https://doi.org/10.1093/jac/dkr154>
- Christophe, T., Jackson, M., Jeon, H. K., Fenistein, D., Contreras-Dominguez, M., Kim, J., Genovesio, A., Carralot, J. P., Ewann, F., Kim, E. H., Lee, S. Y., Kang, S., Seo, M. J., Park, E. J., Skovierová, H., Pham, H., Riccardi, G., Nam, J. Y., Marsollier, L., Kempf, M., ... Brodin, P. (2009). High content screening identifies decaprenyl-phosphoribose 2' epimerase as a target for intracellular antimycobacterial inhibitors. *PLoS pathogens*, 5(10), e1000645. <https://doi.org/10.1371/journal.ppat.1000645>
- Cohen, K., & Maartens, G. (2019). A safety evaluation of bedaquiline for the treatment of multi-drug resistant tuberculosis. *Expert opinion on drug safety*, 18(10), 875–882. <https://doi.org/10.1080/14740338.2019.1648429>
- Cole, S. T., Brosch, R., Parkhill, J., Garnier, T., Churcher, C., Harris, D., Gordon, S. V., Eiglmeier, K., Gas, S., Barry, C. E., 3rd, Tekaiia, F., Badcock, K., Basham, D., Brown, D., Chillingworth, T., Connor, R., Davies, R., Devlin, K., Feltwell, T., Gentles, S., ... Barrell, B. G. (1998). Deciphering the biology of *Mycobacterium tuberculosis* from the complete genome sequence. *Nature*, 393(6685), 537–544. <https://doi.org/10.1038/31159>
- Collaborative Group for the Meta-Analysis of Individual Patient Data in MDR-TB treatment–2017, Ahmad, N., Ahuja, S. D., Akkerman, O. W., Alffenaar, J. C., Anderson, L. F., Baghaei, P., Bang, D., Barry, P. M., Bastos, M. L., Behera, D., Benedetti, A., Bisson, G. P., Boeree, M. J., Bonnet, M., Brode, S. K., Brust, J., Cai, Y., Caumes, E., Cegielski, J. P., ... Menzies, D. (2018). Treatment correlates of successful outcomes in pulmonary multidrug-resistant tuberculosis: an individual patient data meta-analysis. *Lancet (London, England)*, 392(10150), 821–834. [https://doi.org/10.1016/S0140-6736\(18\)31644-1](https://doi.org/10.1016/S0140-6736(18)31644-1)
- Conradie, F., Diacon, A. H., Ngubane, N., Howell, P., Everitt, D., Crook, A. M., Mendel, C. M., Egizi, E., Moreira, J., Timm, J., McHugh, T. D., Wills, G. H., Bateson, A., Hunt, R., Van Niekerk, C., Li, M., Oluhosi, M., Spigelman, M., & Nix-TB Trial Team (2020). Treatment of Highly Drug-Resistant Pulmonary Tuberculosis. *The New England journal of medicine*, 382(10), 893–902. <https://doi.org/10.1056/NEJMoa1901814>
- Correa-Macedo, W., Cambri, G., & Schurr, E. (2019). The Interplay of Human and *Mycobacterium Tuberculosis* Genomic Variability. *Frontiers in genetics*, 10, 865. <https://doi.org/10.3389/fgene.2019.00865>
- Coscolla, M., & Gagneux, S. (2014). Consequences of genomic diversity in *Mycobacterium tuberculosis*. *Seminars in immunology*, 26(6), 431–444. <https://doi.org/10.1016/j.smim.2014.09.012>
- Cosma, C. L., Sherman, D. R., & Ramakrishnan, L. (2003). The secret lives of the pathogenic mycobacteria. *Annual review of microbiology*, 57, 641–676. <https://doi.org/10.1146/annurev.micro.57.030502.091033>

REFERENCES

- Daffé, M., & Marrakchi, H. (2019). Unraveling the Structure of the Mycobacterial Envelope. *Microbiology spectrum*, 7(4), 10.1128/microbiolspec.GPP3-0027-2018. <https://doi.org/10.1128/microbiolspec.GPP3-0027-2018>
- Das, S., Garg, T., Chopra, S., & Dasgupta, A. (2019). Repurposing disulfiram to target infections caused by non-tuberculous mycobacteria. *The Journal of antimicrobial chemotherapy*, 74(5), 1317–1322. <https://doi.org/10.1093/jac/dkz018>
- Degiacomi, G., Belardinelli, J. M., Pasca, M. R., De Rossi, E., Riccardi, G., & Chiarelli, L. R. (2020). Promiscuous targets for antitubercular drug discovery: The paradigm of DprE1 and MmpL3. *Applied Sciences*, 10(2), 623.
- Degiacomi, G., Benjak, A., Madacki, J., Boldrin, F., Provvedi, R., Palù, G., Kordulakova, J., Cole, S. T., & Manganeli, R. (2017). Essentiality of *mmpL3* and impact of its silencing on *Mycobacterium tuberculosis* gene expression. *Scientific reports*, 7, 43495. <https://doi.org/10.1038/srep43495>
- Degiacomi, G., Sammartino, J. C., Chiarelli, L. R., Riabova, O., Makarov, V., & Pasca, M. R. (2019). *Mycobacterium abscessus*, an Emerging and Worrisome Pathogen among Cystic Fibrosis Patients. *International journal of molecular sciences*, 20(23), 5868. <https://doi.org/10.3390/ijms20235868>
- Degiacomi, G., Sammartino, J. C., Sinigiani, V., Marra, P., Urbani, A., & Pasca, M. R. (2020). *In vitro* Study of Bedaquiline Resistance in *Mycobacterium tuberculosis* Multi-Drug Resistant Clinical Isolates. *Frontiers in microbiology*, 11, 559469. <https://doi.org/10.3389/fmicb.2020.559469>
- Desta, Z., Soukhova, N. V., & Flockhart, D. A. (2001). Inhibition of cytochrome P450 (CYP450) isoforms by isoniazid: potent inhibition of CYP2C19 and CYP3A. *Antimicrobial agents and chemotherapy*, 45(2), 382–392. <https://doi.org/10.1128/AAC.45.2.382-392.2001>
- Dookie, N., Rambaran, S., Padayatchi, N., Mahomed, S., & Naidoo, K. (2018). Evolution of drug resistance in *Mycobacterium tuberculosis*: a review on the molecular determinants of resistance and implications for personalized care. *The Journal of antimicrobial chemotherapy*, 73(5), 1138–1151. <https://doi.org/10.1093/jac/dkx506>
- Duarte, R., Lönnroth, K., Carvalho, C., Lima, F., Carvalho, A., Muñoz-Torrico, M., & Centis, R. (2018). Tuberculosis, social determinants and co-morbidities (including HIV). *Pulmonology*, 24(2), 115–119. <https://doi.org/10.1016/j.rppnen.2017.11.003>
- Dubée, V., Bernut, A., Cortes, M., Lesne, T., Dorchene, D., Lefebvre, A. L., Hugonnet, J. E., Gutmann, L., Mainardi, J. L., Herrmann, J. L., Gaillard, J. L., Kremer, L., & Arthur, M. (2015). β -Lactamase inhibition by avibactam in *Mycobacterium abscessus*. *The Journal of antimicrobial chemotherapy*, 70(4), 1051–1058. <https://doi.org/10.1093/jac/dku510>
- Dubuisson, T., Bogatcheva, E., Krishnan, M. Y., Collins, M. T., Einck, L., Nacy, C. A., & Reddy, V. M. (2010). *In vitro* antimicrobial activities of capuramycin analogues against non-tuberculous mycobacteria. *The Journal of antimicrobial chemotherapy*, 65(12), 2590–2597. <https://doi.org/10.1093/jac/dkq372>
- Dulberger, C. L., Rubin, E. J., & Boutte, C. C. (2020). The mycobacterial cell envelope - a moving target. *Nature reviews. Microbiology*, 18(1), 47–59. <https://doi.org/10.1038/s41579-019-0273-7>

REFERENCES

- Egan M. E. (2016). Genetics of Cystic Fibrosis: Clinical Implications. *Clinics in chest medicine*, 37(1), 9–16. <https://doi.org/10.1016/j.ccm.2015.11.002>
- Ernst J. D. (2018). Mechanisms of *M. tuberculosis* Immune Evasion as Challenges to TB Vaccine Design. *Cell host & microbe*, 24(1), 34–42. <https://doi.org/10.1016/j.chom.2018.06.004>
- Esteban, J., & García-Coca, M. (2018). *Mycobacterium* Biofilms. *Frontiers in microbiology*, 8, 2651. <https://doi.org/10.3389/fmicb.2017.02651>
- European Centre for Disease Prevention and Control (2018). Handbook on tuberculosis laboratory diagnostic methods in the European Union – Updated 2018. Stockholm: ECDC.
- Fan, H. H., Wang, L. Q., Liu, W. L., An, X. P., Liu, Z. D., He, X. Q., Song, L. H., & Tong, Y. G. (2020). Repurposing of clinically approved drugs for treatment of coronavirus disease 2019 in a 2019-novel coronavirus-related coronavirus model. *Chinese medical journal*, 133(9), 1051–1056. <https://doi.org/10.1097/CM9.0000000000000797>
- Floto, R. A., Olivier, K. N., Saiman, L., Daley, C. L., Herrmann, J. L., Nick, J. A., Noone, P. G., Bilton, D., Corris, P., Gibson, R. L., Hempstead, S. E., Koetz, K., Sabadosa, K. A., Sermet-Gaudelus, I., Smyth, A. R., van Ingen, J., Wallace, R. J., Winthrop, K. L., Marshall, B. C., & Haworth, C. S. (2016). US Cystic Fibrosis Foundation and European Cystic Fibrosis Society consensus recommendations for the management of non-tuberculous mycobacteria in individuals with cystic fibrosis: executive summary. *Thorax*, 71(1), 88–90. <https://doi.org/10.1136/thoraxjnl-2015-207983>
- Forbes B. A. (2017). Mycobacterial Taxonomy. *Journal of clinical microbiology*, 55(2), 380–383. <https://doi.org/10.1128/JCM.01287-16>
- Ganapathy, U. S., Dartois, V., & Dick, T. (2019). Repositioning rifamycins for *Mycobacterium abscessus* lung disease. *Expert opinion on drug discovery*, 14(9), 867–878. <https://doi.org/10.1080/17460441.2019.1629414>
- Garg, K., Saini, V., Dhillon, R., & Agarwal, P. (2019). Isoniazid mono-resistant tuberculosis: Time to take it seriously. *The Indian journal of tuberculosis*, 66(2), 247–252. <https://doi.org/10.1016/j.ijtb.2019.04.001>
- GBD 2015 Mortality and Causes of Death Collaborators (2016). Global, regional, and national life expectancy, all-cause mortality, and cause-specific mortality for 249 causes of death, 1980–2015: a systematic analysis for the Global Burden of Disease Study 2015. *Lancet (London, England)*, 388(10053), 1459–1544. [https://doi.org/10.1016/S0140-6736\(16\)31012-1](https://doi.org/10.1016/S0140-6736(16)31012-1)
- Giannetti, L., Giorgi, A., Necci, F., Ferretti, G., Buiarelli, F., & Neri, B. (2011). Validation study on avermectine residues in foodstuffs. *Analytica chimica acta*, 700(1-2), 11–15. <https://doi.org/10.1016/j.aca.2010.12.035>
- Gns, H. S., Gr, S., Murahari, M., & Krishnamurthy, M. (2019). An update on Drug Repurposing: Re-written saga of the drug's fate. *Biomedicine & pharmacotherapy = Biomedecine & pharmacotherapie*, 110, 700–716. <https://doi.org/10.1016/j.biopha.2018.11.127>
- Gori, A., Bandera, A., Marchetti, G., Degli Esposti, A., Catozzi, L., Nardi, G. P., Gazzola, L., Ferrario, G., van Embden, J. D., van Soolingen, D., Moroni, M., & Franzetti, F. (2005). Spoligotyping and *Mycobacterium tuberculosis*. *Emerging infectious diseases*, 11(8), 1242–1248. <https://doi.org/10.3201/eid1108.040982>

REFERENCES

- Griffin, J., Fletcher, N., Clemence, R., Blanchflower, S., & Brayden, D. J. (2005). Selamectin is a potent substrate and inhibitor of human and canine P-glycoprotein. *Journal of veterinary pharmacology and therapeutics*, 28(3), 257–265. <https://doi.org/10.1111/j.1365-2885.2005.00655.x>
- Grobbelaar, M., Louw, G. E., Sampson, S. L., van Helden, P. D., Donald, P. R., & Warren, R. M. (2019). Evolution of rifampicin treatment for tuberculosis. *Infection, genetics and evolution : journal of molecular epidemiology and evolutionary genetics in infectious diseases*, 74, 103937. <https://doi.org/10.1016/j.meegid.2019.103937>
- Guillemin, I., Jarlier, V., & Cambau, E. (1998). Correlation between quinolone susceptibility patterns and sequences in the A and B subunits of DNA gyrase in mycobacteria. *Antimicrobial agents and chemotherapy*, 42(8), 2084–2088. <https://doi.org/10.1128/AAC.42.8.2084>
- Gutiérrez, A. V., Viljoen, A., Ghigo, E., Herrmann, J. L., & Kremer, L. (2018). Glycopeptidolipids, a Double-Edged Sword of the *Mycobacterium abscessus* Complex. *Frontiers in microbiology*, 9, 1145. <https://doi.org/10.3389/fmicb.2018.01145>
- Hameed, H., Islam, M. M., Chhotaray, C., Wang, C., Liu, Y., Tan, Y., Li, X., Tan, S., Delorme, V., Yew, W. W., Liu, J., & Zhang, T. (2018). Molecular Targets Related Drug Resistance Mechanisms in MDR-, XDR-, and TDR-*Mycobacterium tuberculosis* Strains. *Frontiers in cellular and infection microbiology*, 8, 114. <https://doi.org/10.3389/fcimb.2018.00114>
- Hansen, J. L., Ippolito, J. A., Ban, N., Nissen, P., Moore, P. B., & Steitz, T. A. (2002). The structures of four macrolide antibiotics bound to the large ribosomal subunit. *Molecular cell*, 10(1), 117–128. [https://doi.org/10.1016/s1097-2765\(02\)00570-1](https://doi.org/10.1016/s1097-2765(02)00570-1)
- Hartkoorn, R. C., Uplekar, S., & Cole, S. T. (2014). Cross-resistance between clofazimine and bedaquiline through upregulation of MmpL5 in *Mycobacterium tuberculosis*. *Antimicrobial agents and chemotherapy*, 58(5), 2979–2981. <https://doi.org/10.1128/AAC.00037-14>
- Henkle, E., & Winthrop, K. L. (2015). Nontuberculous mycobacteria infections in immunosuppressed hosts. *Clinics in chest medicine*, 36(1), 91–99. <https://doi.org/10.1016/j.ccm.2014.11.002>
- Howard, S. T., Rhoades, E., Recht, J., Pang, X., Alsup, A., Kolter, R., Lyons, C. R., & Byrd, T. F. (2006). Spontaneous reversion of *Mycobacterium abscessus* from a smooth to a rough morphotype is associated with reduced expression of glycopeptidolipid and reacquisition of an invasive phenotype. *Microbiology (Reading, England)*, 152(Pt 6), 1581–1590. <https://doi.org/10.1099/mic.0.28625-0>
- Huang, H., Berg, S., Spencer, J. S., Vereecke, D., D'Haeze, W., Holsters, M., & McNeil, M. R. (2008). Identification of amino acids and domains required for catalytic activity of DPPR synthase, a cell wall biosynthetic enzyme of *Mycobacterium tuberculosis*. *Microbiology (Reading, England)*, 154(Pt 3), 736–743. <https://doi.org/10.1099/mic.0.2007/013532-0>
- Huang, L., Nazarova, E. V., & Russell, D. G. (2019). *Mycobacterium tuberculosis*: Bacterial Fitness within the Host Macrophage. *Microbiology spectrum*, 7(2), 10.1128/microbiolspec.BAI-0001-2019. <https://doi.org/10.1128/microbiolspec.BAI-0001-2019>
- Hunt-Serracin, A. C., Parks, B. J., Boll, J., & Boutte, C. C. (2019). *Mycobacterium abscessus* Cells Have Altered Antibiotic Tolerance and Surface Glycolipids in Artificial Cystic Fibrosis Sputum

REFERENCES

- Medium. *Antimicrobial agents and chemotherapy*, 63(7), e02488-18. <https://doi.org/10.1128/AAC.02488-18>
- Hurst-Hess, K., Rudra, P., & Ghosh, P. (2017). *Mycobacterium abscessus* WhiB7 Regulates a Species-Specific Repertoire of Genes To Confer Extreme Antibiotic Resistance. *Antimicrobial agents and chemotherapy*, 61(11), e01347-17. <https://doi.org/10.1128/AAC.01347-17>
- Ieven, M., Coenen, S., Loens, K., Lammens, C., Coenjaerts, F., Vanderstraeten, A., Henriques-Normark, B., Crook, D., Huygen, K., Butler, C. C., Verheij, T., Little, P., Zlateva, K., van Loon, A., Claas, E., Goossens, H., & GRACE consortium (2018). Aetiology of lower respiratory tract infection in adults in primary care: a prospective study in 11 European countries. *Clinical microbiology and infection : the official publication of the European Society of Clinical Microbiology and Infectious Diseases*, 24(11), 1158–1163. <https://doi.org/10.1016/j.cmi.2018.02.004>
- Ismail, N. A., Omar, S. V., Joseph, L., Govender, N., Blows, L., Ismail, F., Koornhof, H., Dreyer, A. W., Kaniga, K., & Ndjeka, N. (2018). Defining Bedaquiline Susceptibility, Resistance, Cross-Resistance and Associated Genetic Determinants: A Retrospective Cohort Study. *EBioMedicine*, 28, 136–142. <https://doi.org/10.1016/j.ebiom.2018.01.005>
- Jankute, M., Byng, C. V., Alderwick, L. J., & Besra, G. S. (2014). Elucidation of a protein-protein interaction network involved in *Corynebacterium glutamicum* cell wall biosynthesis as determined by bacterial two-hybrid analysis. *Glycoconjugate journal*, 31(6-7), 475–483. <https://doi.org/10.1007/s10719-014-9549-3>
- Ji, Z., Jian, M., Chen, T., Luo, L., Li, L., Dai, X., Bai, R., Ding, Z., Bi, Y., Wen, S., Zhou, G., Abi, M. E., Liu, A., & Bao, F. (2019). Immunogenicity and Safety of the M72/AS01E Candidate Vaccine Against Tuberculosis: A Meta-Analysis. *Frontiers in immunology*, 10, 2089. <https://doi.org/10.3389/fimmu.2019.02089>
- Johansen, M. D., Herrmann, J. L., & Kremer, L. (2020). Non-tuberculous mycobacteria and the rise of *Mycobacterium abscessus*. *Nature reviews. Microbiology*, 18(7), 392–407. <https://doi.org/10.1038/s41579-020-0331-1>
- Jungmann, N. A., Lang, D., Saleh, S., Van Der Mey, D., & Gerisch, M. (2019). *In vitro-in vivo* correlation of the drug-drug interaction potential of antiretroviral HIV treatment regimens on CYP1A1 substrate riociguat. *Expert opinion on drug metabolism & toxicology*, 15(11), 975–984. <https://doi.org/10.1080/17425255.2019.1681968>
- Khosravi, A. D., Hashemzadeh, M., Hashemi Shahraki, A., & Teimoori, A. (2017). Differential Identification of Mycobacterial Species Using High-Resolution Melting Analysis. *Frontiers in microbiology*, 8, 2045. <https://doi.org/10.3389/fmicb.2017.02045>
- Kim, S. Y., Jhun, B. W., Moon, S. M., Shin, S. H., Jeon, K., Kwon, O. J., Yoo, I. Y., Huh, H. J., Ki, C. S., Lee, N. Y., Shin, S. J., Daley, C. L., Suh, G. Y., & Koh, W. J. (2018). Mutations in *gyrA* and *gyrB* in Moxifloxacin-Resistant *Mycobacterium avium* Complex and *Mycobacterium abscessus* Complex Clinical Isolates. *Antimicrobial agents and chemotherapy*, 62(9), e00527-18. <https://doi.org/10.1128/AAC.00527-18>
- Kim, T. S., Choe, J. H., Kim, Y. J., Yang, C. S., Kwon, H. J., Jeong, J., Kim, G., Park, D. E., Jo, E. K., Cho, Y. L., & Jang, J. (2017). Activity of LCB01-0371, a Novel Oxazolidinone, against *Mycobacterium abscessus*. *Antimicrobial agents and chemotherapy*, 61(9), e02752-16. <https://doi.org/10.1128/AAC.02752-16>

REFERENCES

- King, J., Brunel, S. F., & Warris, A. (2016). *Aspergillus* infections in cystic fibrosis. *The Journal of infection*, 72 Suppl, S50–S55. <https://doi.org/10.1016/j.jinf.2016.04.022>
- Koh W. J. (2017). Nontuberculous Mycobacteria-Overview. *Microbiology spectrum*, 5(1), 10.1128/microbiolspec.TNMI7-0024-2016. <https://doi.org/10.1128/microbiolspec.TNMI7-0024-2016>
- Kolly, G. S., Boldrin, F., Sala, C., Dhar, N., Hartkoorn, R. C., Ventura, M., Serafini, A., McKinney, J. D., Manganelli, R., & Cole, S. T. (2014). Assessing the essentiality of the decaprenyl-phospho-d-arabinofuranose pathway in *Mycobacterium tuberculosis* using conditional mutants. *Molecular microbiology*, 92(1), 194–211. <https://doi.org/10.1111/mmi.12546>
- Laing, R., Gillan, V., & Devaney, E. (2017). Ivermectin - Old Drug, New Tricks?. *Trends in parasitology*, 33(6), 463–472. <https://doi.org/10.1016/j.pt.2017.02.004>
- Lee, A., Xie, Y. L., Barry, C. E., & Chen, R. Y. (2020). Current and future treatments for tuberculosis. *BMJ (Clinical research ed.)*, 368, m216. <https://doi.org/10.1136/bmj.m216>
- Lee, M. R., Sheng, W. H., Hung, C. C., Yu, C. J., Lee, L. N., & Hsueh, P. R. (2015). *Mycobacterium abscessus* Complex Infections in Humans. *Emerging infectious diseases*, 21(9), 1638–1646. <https://doi.org/10.3201/2109.141634>
- Lerat, I., Cambau, E., Roth Dit Bettoni, R., Gaillard, J. L., Jarlier, V., Truffot, C., & Veziris, N. (2014). *In vivo* evaluation of antibiotic activity against *Mycobacterium abscessus*. *The Journal of infectious diseases*, 209(6), 905–912. <https://doi.org/10.1093/infdis/jit614>
- Li, W., Yazidi, A., Pandya, A. N., Hegde, P., Tong, W., Calado Nogueira de Moura, V., North, E. J., Sygusch, J., & Jackson, M. (2018). MmpL3 as a Target for the Treatment of Drug-Resistant Nontuberculous Mycobacterial Infections. *Frontiers in microbiology*, 9, 1547. <https://doi.org/10.3389/fmicb.2018.01547>
- Li, Y., Sun, F., & Zhang, W. (2019). Bedaquiline and delamanid in the treatment of multidrug-resistant tuberculosis: Promising but challenging. *Drug development research*, 80(1), 98–105. <https://doi.org/10.1002/ddr.21498>
- Lim, L. E., Vilchèze, C., Ng, C., Jacobs, W. R., Jr, Ramón-García, S., & Thompson, C. J. (2013). Anthelmintic avermectins kill *Mycobacterium tuberculosis*, including multidrug-resistant clinical strains. *Antimicrobial agents and chemotherapy*, 57(2), 1040–1046. <https://doi.org/10.1128/AAC.01696-12>
- Liu, K., Li, F., Lu, J., Liu, S., Dorko, K., Xie, W., & Ma, X. (2014). Bedaquiline metabolism: enzymes and novel metabolites. *Drug metabolism and disposition: the biological fate of chemicals*, 42(5), 863–866. <https://doi.org/10.1124/dmd.113.056119>
- Liu, L., Kong, C., Fumagalli, M., Savková, K., Xu, Y., Huszár, S., Sammartino, J. C., Fan, D., Chiarelli, L. R., Mikušová, K., Sun, Z., & Qiao, C. (2020). Design, synthesis and evaluation of covalent inhibitors of DprE1 as antitubercular agents. *European journal of medicinal chemistry*, 208, 112773. <https://doi.org/10.1016/j.ejmech.2020.112773>
- Lopeman, R. C., Harrison, J., Desai, M., & Cox, J. (2019). *Mycobacterium abscessus*: Environmental Bacterium Turned Clinical Nightmare. *Microorganisms*, 7(3), 90. <https://doi.org/10.3390/microorganisms7030090>

REFERENCES

- Lu, P., Asseri, A. H., Kremer, M., Maaskant, J., Ummels, R., Lill, H., & Bald, D. (2018). The anti-mycobacterial activity of the cytochrome bcc inhibitor Q203 can be enhanced by small-molecule inhibition of cytochrome bd. *Scientific reports*, 8(1), 2625. <https://doi.org/10.1038/s41598-018-20989-8>
- Luthra, S., Rominski, A., & Sander, P. (2018). The Role of Antibiotic-Target-Modifying and Antibiotic-Modifying Enzymes in *Mycobacterium abscessus* Drug Resistance. *Frontiers in microbiology*, 9, 2179. <https://doi.org/10.3389/fmicb.2018.02179>
- Makarov, V., Lechartier, B., Zhang, M., Neres, J., van der Sar, A. M., Raadsen, S. A., Hartkoorn, R. C., Ryabova, O. B., Vocat, A., Decosterd, L. A., Widmer, N., Buclin, T., Bitter, W., Andries, K., Pojer, F., Dyson, P. J., & Cole, S. T. (2014). Towards a new combination therapy for tuberculosis with next generation benzothiazinones. *EMBO molecular medicine*, 6(3), 372–383. <https://doi.org/10.1002/emmm.201303575>
- Makarov, V., Manina, G., Mikusova, K., Möllmann, U., Ryabova, O., Saint-Joanis, B., Dhar, N., Pasca, M. R., Buroni, S., Lucarelli, A. P., Milano, A., De Rossi, E., Belanova, M., Bobovska, A., Dianiskova, P., Kordulakova, J., Sala, C., Fullam, E., Schneider, P., McKinney, J. D., ... Cole, S. T. (2009). Benzothiazinones kill *Mycobacterium tuberculosis* by blocking arabinan synthesis. *Science (New York, N.Y.)*, 324(5928), 801–804. <https://doi.org/10.1126/science.1171583>
- Malone, K. M., & Gordon, S. V. (2017). *Mycobacterium tuberculosis* Complex Members Adapted to Wild and Domestic Animals. *Advances in experimental medicine and biology*, 1019, 135–154. https://doi.org/10.1007/978-3-319-64371-7_7
- Marrakchi, H., Lanéelle, M. A., & Daffé, M. (2014). Mycolic acids: structures, biosynthesis, and beyond. *Chemistry & biology*, 21(1), 67–85. <https://doi.org/10.1016/j.chembiol.2013.11.011>
- Martiniano, S. L., Nick, J. A., & Daley, C. L. (2019). Nontuberculous Mycobacterial Infections in Cystic Fibrosis. *Thoracic surgery clinics*, 29(1), 95–108. <https://doi.org/10.1016/j.thorsurg.2018.09.008>
- McEuen, K., Borlak, J., Tong, W., & Chen, M. (2017). Associations of Drug Lipophilicity and Extent of Metabolism with Drug-Induced Liver Injury. *International journal of molecular sciences*, 18(7), 1335. <https://doi.org/10.3390/ijms18071335>
- Merola, V. M., & Eubig, P. A. (2018). Toxicology of Avermectins and Milbemycins (Macrocyclic Lactones) and the Role of P-Glycoprotein in Dogs and Cats. *The Veterinary clinics of North America. Small animal practice*, 48(6), 991–1012. <https://doi.org/10.1016/j.cvsm.2018.07.002>
- Migliori, G. B., De Iaco, G., Besozzi, G., Centis, R., & Cirillo, D. M. (2007). First tuberculosis cases in Italy resistant to all tested drugs. *Euro surveillance : bulletin Européen sur les maladies transmissibles = European communicable disease bulletin*, 12(5), E070517.1. <https://doi.org/10.2807/esw.12.20.03194-en>
- Mikusová, K., Huang, H., Yagi, T., Holsters, M., Vereecke, D., D'Haese, W., Scherman, M. S., Brennan, P. J., McNeil, M. R., & Crick, D. C. (2005). Decaprenylphosphoryl arabinofuranose, the donor of the D-arabinofuranosyl residues of mycobacterial arabinan, is formed via a two-step epimerization of decaprenylphosphoryl ribose. *Journal of bacteriology*, 187(23), 8020–8025. <https://doi.org/10.1128/JB.187.23.8020-8025.2005>

REFERENCES

- Mirnejad, R., Asadi, A., Khoshnood, S., Mirzaei, H., Heidary, M., Fattorini, L., Ghodousi, A., & Darban-Sarokhalil, D. (2018). Clofazimine: A useful antibiotic for drug-resistant tuberculosis. *Biomedicine & pharmacotherapy = Biomedecine & pharmacotherapie*, *105*, 1353–1359. <https://doi.org/10.1016/j.biopha.2018.06.023>
- Mogashoa, T., Melamu, P., Derendinger, B., Ley, S. D., Streicher, E. M., Iketleng, T., Mupfumi, L., Mokomane, M., Kgwaadira, B., Rankgoane-Pono, G., Tsholofelo, T. T., Kasvosve, I., Moyo, S., Warren, R. M., & Gaseitsiwe, S. (2019). Detection of Second Line Drug Resistance among Drug Resistant *Mycobacterium Tuberculosis* Isolates in Botswana. *Pathogens (Basel, Switzerland)*, *8*(4), 208. <https://doi.org/10.3390/pathogens8040208>
- Monakhova, N., Korduláková, J., Vocat, A., Egorova, A., Lepioshkin, A., Salina, E. G., Nosek, J., Repková, E., Zemanová, J., Jurdáková, H., Górová, R., Roh, J., Degiacomi, G., Sammartino, J. C., Pasca, M. R., Cole, S. T., Mikušová, K., & Makarov, V. (2021). Design and Synthesis of Pyrano[3,2-*b*]indolones Showing Antimycobacterial Activity. *ACS infectious diseases*, *7*(1), 88–100. <https://doi.org/10.1021/acsinfectdis.0c00622>
- Mondino, S., Gago, G., & Gramajo, H. (2013). Transcriptional regulation of fatty acid biosynthesis in mycobacteria. *Molecular microbiology*, *89*(2), 372–387. <https://doi.org/10.1111/mmi.12282>
- Mori, G., Chiarelli, L. R., Esposito, M., Makarov, V., Bellinzoni, M., Hartkoorn, R. C., Degiacomi, G., Boldrin, F., Ekins, S., de Jesus Lopes Ribeiro, A. L., Marino, L. B., Centárová, I., Svetlíková, Z., Blaško, J., Kazakova, E., Lepioshkin, A., Barilone, N., Zanon, G., Porta, A., Fondi, M., ... Pasca, M. R. (2015). Thiophenecarboxamide Derivatives Activated by EthA Kill *Mycobacterium tuberculosis* by Inhibiting the CTP Synthetase PyrG. *Chemistry & biology*, *22*(7), 917–927. <https://doi.org/10.1016/j.chembiol.2015.05.016>
- Mori, G., Orena, B. S., Chiarelli, L. R., Degiacomi, G., Riabova, O., Sammartino, J. C., Makarov, V., Riccardi, G., & Pasca, M. R. (2020). Rv0579 Is Involved in the Resistance to the TP053 Antitubercular Prodrug. *Frontiers in microbiology*, *11*, 292. <https://doi.org/10.3389/fmicb.2020.00292>
- Mori, M., Stelitano, G., Gelain, A., Pini, E., Chiarelli, L. R., Sammartino, J. C., Poli, G., Tuccinardi, T., Beretta, G., Porta, A., Bellinzoni, M., Villa, S., & Meneghetti, F. (2020). Shedding X-ray Light on the Role of Magnesium in the Activity of *Mycobacterium tuberculosis* Salicylate Synthase (MbtI) for Drug Design. *Journal of medicinal chemistry*, *63*(13), 7066–7080. <https://doi.org/10.1021/acs.jmedchem.0c00373>
- Murdoch, D. R., & Howie, S. (2018). The global burden of lower respiratory infections: making progress, but we need to do better. *The Lancet. Infectious diseases*, *18*(11), 1162–1163. [https://doi.org/10.1016/S1473-3099\(18\)30407-9](https://doi.org/10.1016/S1473-3099(18)30407-9)
- Nahid, P., Mase, S. R., Migliori, G. B., Sotgiu, G., Bothamley, G. H., Brozek, J. L., Cattamanchi, A., Cegielski, J. P., Chen, L., Daley, C. L., Dalton, T. L., Duarte, R., Fregonese, F., Horsburgh, C. R., Jr, Ahmad Khan, F., Kheir, F., Lan, Z., Lardizabal, A., Lauzardo, M., Mangan, J. M., ... Seaworth, B. (2019). Treatment of Drug-Resistant Tuberculosis. An Official ATS/CDC/ERS/IDSA Clinical Practice Guideline. *American journal of respiratory and critical care medicine*, *200*(10), e93–e142. <https://doi.org/10.1164/rccm.201909-1874ST>

REFERENCES

- Naidoo, A., Naidoo, K., McIlleron, H., Essack, S., & Padayatchi, N. (2017). A Review of Moxifloxacin for the Treatment of Drug-Susceptible Tuberculosis. *Journal of clinical pharmacology*, 57(11), 1369–1386. <https://doi.org/10.1002/jcph.968>
- Nash, K. A., Brown-Elliott, B. A., & Wallace, R. J., Jr (2009). A novel gene, erm(41), confers inducible macrolide resistance to clinical isolates of *Mycobacterium abscessus* but is absent from *Mycobacterium chelonae*. *Antimicrobial agents and chemotherapy*, 53(4), 1367–1376. <https://doi.org/10.1128/AAC.01275-08>
- Neres, J., Hartkoorn, R. C., Chiarelli, L. R., Gadupudi, R., Pasca, M. R., Mori, G., Venturelli, A., Savina, S., Makarov, V., Kolly, G. S., Molteni, E., Binda, C., Dhar, N., Ferrari, S., Brodin, P., Delorme, V., Landry, V., de Jesus Lopes Ribeiro, A. L., Farina, D., Saxena, P., ... Cole, S. T. (2015). 2-Carboxyquinoxalines kill *Mycobacterium tuberculosis* through noncovalent inhibition of DprE1. *ACS chemical biology*, 10(3), 705–714. <https://doi.org/10.1021/cb5007163>
- Neres, J., Pojer, F., Molteni, E., Chiarelli, L. R., Dhar, N., Boy-Röttger, S., Buroni, S., Fullam, E., Degiacomi, G., Lucarelli, A. P., Read, R. J., Zanoni, G., Edmondson, D. E., De Rossi, E., Pasca, M. R., McKinney, J. D., Dyson, P. J., Riccardi, G., Mattevi, A., Cole, S. T., ... Binda, C. (2012). Structural basis for benzothiazinone-mediated killing of *Mycobacterium tuberculosis*. *Science translational medicine*, 4(150), 150ra121. <https://doi.org/10.1126/scitranslmed.3004395>
- Nessar, R., Reyrat, J. M., Murray, A., & Gicquel, B. (2011). Genetic analysis of new 16S rRNA mutations conferring aminoglycoside resistance in *Mycobacterium abscessus*. *The Journal of antimicrobial chemotherapy*, 66(8), 1719–1724. <https://doi.org/10.1093/jac/dkr209>
- Nguyen, T., Anthony, R. M., Bañuls, A. L., Nguyen, T., Vu, D. H., & Alffenaar, J. C. (2018). Bedaquiline Resistance: Its Emergence, Mechanism, and Prevention. *Clinical infectious diseases : an official publication of the Infectious Diseases Society of America*, 66(10), 1625–1630. <https://doi.org/10.1093/cid/cix992>
- Nieto Ramirez, L. M., Quintero Vargas, K., & Diaz, G. (2020). Whole Genome Sequencing for the Analysis of Drug Resistant Strains of *Mycobacterium tuberculosis*: A Systematic Review for Bedaquiline and Delamanid. *Antibiotics (Basel, Switzerland)*, 9(3), 133. <https://doi.org/10.3390/antibiotics9030133>
- Nobre, A., Alarico, S., Maranhã, A., Mendes, V., & Empadinhas, N. (2014). The molecular biology of mycobacterial trehalose in the quest for advanced tuberculosis therapies. *Microbiology (Reading, England)*, 160(Pt 8), 1547–1570. <https://doi.org/10.1099/mic.0.075895-0>
- Obregón-Henao, A., Arnett, K. A., Henao-Tamayo, M., Massoudi, L., Creissen, E., Andries, K., Lenaerts, A. J., & Ordway, D. J. (2015). Susceptibility of *Mycobacterium abscessus* to antimycobacterial drugs in preclinical models. *Antimicrobial agents and chemotherapy*, 59(11), 6904–6912. <https://doi.org/10.1128/AAC.00459-15>
- Olivier, K. N., Griffith, D. E., Eagle, G., McGinnis, J. P., 2nd, Micioni, L., Liu, K., Daley, C. L., Winthrop, K. L., Ruoss, S., Addrizzo-Harris, D. J., Flume, P. A., Dorgan, D., Salathe, M., Brown-Elliott, B. A., Gupta, R., & Wallace, R. J., Jr (2017). Randomized Trial of Liposomal Amikacin for Inhalation in Nontuberculous Mycobacterial Lung Disease. *American journal of respiratory and critical care medicine*, 195(6), 814–823. <https://doi.org/10.1164/rccm.201604-0700OC>

REFERENCES

- Omansen, T. F., Porter, J. L., Johnson, P. D., van der Werf, T. S., Stienstra, Y., & Stinear, T. P. (2015). *In-vitro* activity of avermectins against *Mycobacterium ulcerans*. *PLoS neglected tropical diseases*, 9(3), e0003549. <https://doi.org/10.1371/journal.pntd.0003549>
- Patel, H., Pawara, R., Pawara, K., Ahmed, F., Shirkhedkar, A., & Surana, S. (2019). A structural insight of bedaquiline for the cardiotoxicity and hepatotoxicity. *Tuberculosis (Edinburgh, Scotland)*, 117, 79–84. <https://doi.org/10.1016/j.tube.2019.06.005>
- Peterson, E., Ma, S., Sherman, D. R., & Baliga, N. S. (2016). Network analysis identifies Rv0324 and Rv0880 as regulators of bedaquiline tolerance in *Mycobacterium tuberculosis*. *Nature microbiology*, 1(8), 16078. <https://doi.org/10.1038/nmicrobiol.2016.78>
- Pfyyffer, G. E. (2015). *Mycobacterium*: general characteristics, laboratory detection, and staining procedures. *Manual of clinical microbiology*, 536-569.
- Poce, G., Bates, R. H., Alfonso, S., Coccozza, M., Porretta, G. C., Ballell, L., Rullas, J., Ortega, F., De Logu, A., Agus, E., La Rosa, V., Pasca, M. R., De Rossi, E., Wac, B., Franzblau, S. G., Manetti, F., Botta, M., & Biava, M. (2013). Improved BM212 MmpL3 inhibitor analogue shows efficacy in acute murine model of tuberculosis infection. *PloS one*, 8(2), e56980. <https://doi.org/10.1371/journal.pone.0056980>
- Podder, V., & Sadiq, N. M. (2020). Levofloxacin. In *StatPearls*. StatPearls Publishing.
- Prammananan, T., Sander, P., Brown, B. A., Frischkorn, K., Onyi, G. O., Zhang, Y., Böttger, E. C., & Wallace, R. J., Jr (1998). A single 16S ribosomal RNA substitution is responsible for resistance to amikacin and other 2-deoxystreptomine aminoglycosides in *Mycobacterium abscessus* and *Mycobacterium chelonae*. *The Journal of infectious diseases*, 177(6), 1573–1581. <https://doi.org/10.1086/515328>
- Ramsey, B. W., Downey, G. P., & Goss, C. H. (2019). Update in Cystic Fibrosis 2018. *American journal of respiratory and critical care medicine*, 199(10), 1188–1194. <https://doi.org/10.1164/rccm.201902-0310UP>
- Ravimohan, S., Kornfeld, H., Weissman, D., & Bisson, G. P. (2018). Tuberculosis and lung damage: from epidemiology to pathophysiology. *European respiratory review : an official journal of the European Respiratory Society*, 27(147), 170077. <https://doi.org/10.1183/16000617.0077-2017>
- Riccardi, G., & Pasca, M. R. (2014). Trends in discovery of new drugs for tuberculosis therapy. *The Journal of antibiotics*, 67(9), 655–659. <https://doi.org/10.1038/ja.2014.109>
- Richard, M., Gutiérrez, A. V., Viljoen, A., Rodriguez-Rincon, D., Roquet-Baneres, F., Blaise, M., Overall, I., Parkhill, J., Floto, R. A., & Kremer, L. (2018). Mutations in the MAB_2299c TetR Regulator Confer Cross-Resistance to Clofazimine and Bedaquiline in *Mycobacterium abscessus*. *Antimicrobial agents and chemotherapy*, 63(1), e01316-18. <https://doi.org/10.1128/AAC.01316-18>
- Rodriguez, F., Saffon, N., Sammartino, J. C., Degiacomi, G., Pasca, M. R., & Lherbet, C. (2020). First triclosan-based macrocyclic inhibitors of InhA enzyme. *Bioorganic chemistry*, 95, 103498. <https://doi.org/10.1016/j.bioorg.2019.103498>
- Rudra, P., Hurst-Hess, K., Lappierre, P., & Ghosh, P. (2018). High Levels of Intrinsic Tetracycline Resistance in *Mycobacterium abscessus* Are Conferred by a Tetracycline-Modifying Monooxygenase. *Antimicrobial agents and chemotherapy*, 62(6), e00119-18. <https://doi.org/10.1128/AAC.00119-18>

REFERENCES

- Ruopp, M., Chiswell, K., Thaden, J. T., Merchant, K., & Tsalik, E. L. (2015). Respiratory Tract Infection Clinical Trials from 2007 to 2012. A Systematic Review of ClinicalTrials.gov. *Annals of the American Thoracic Society*, 12(12), 1852–1863. <https://doi.org/10.1513/AnnalsATS.201505-291OC>
- Salzman, V., Mondino, S., Sala, C., Cole, S. T., Gago, G., & Gramajo, H. (2010). Transcriptional regulation of lipid homeostasis in mycobacteria. *Molecular microbiology*, 78(1), 64–77. <https://doi.org/10.1111/j.1365-2958.2010.07313.x>
- Sambrook, J., & Russell, D. W. (2001). *Molecular cloning: A laboratory manual*, the third edition.
- Sangana, R., Gu, H., Chun, D. Y., & Einolf, H. J. (2018). Evaluation of Clinical Drug Interaction Potential of Clofazimine Using Static and Dynamic Modeling Approaches. *Drug metabolism and disposition: the biological fate of chemicals*, 46(1), 26–32. <https://doi.org/10.1124/dmd.117.077834>
- Sassi, M., & Drancourt, M. (2014). Genome analysis reveals three genomospecies in *Mycobacterium abscessus*. *BMC genomics*, 15(1), 359. <https://doi.org/10.1186/1471-2164-15-359>
- Saxena, A. K., & Singh, A. (2019). Mycobacterial tuberculosis Enzyme Targets and their Inhibitors. *Current topics in medicinal chemistry*, 19(5), 337–355. <https://doi.org/10.2174/1568026619666190219105722>
- Scherr, N., Pluschke, G., Thompson, C. J., & Ramón-García, S. (2015). Selamectin Is the Avermectin with the Best Potential for Buruli Ulcer Treatment. *PLoS neglected tropical diseases*, 9(8), e0003996. <https://doi.org/10.1371/journal.pntd.0003996>
- Scoffone, V. C., Trespidi, G., Chiarelli, L. R., Barbieri, G., & Buroni, S. (2019). Quorum Sensing as Antivirulence Target in Cystic Fibrosis Pathogens. *International journal of molecular sciences*, 20(8), 1838. <https://doi.org/10.3390/ijms20081838>
- Shah, I., Poojari, V., & Meshram, H. (2020). Multi-Drug Resistant and Extensively-Drug Resistant Tuberculosis. *Indian journal of pediatrics*, 87(10), 833–839. <https://doi.org/10.1007/s12098-020-03230-1>
- Sia, J. K., & Rengarajan, J. (2019). Immunology of *Mycobacterium tuberculosis* Infections. *Microbiology spectrum*, 7(4), 10.1128/microbiolspec.GPP3-0022-2018. <https://doi.org/10.1128/microbiolspec.GPP3-0022-2018>
- Simeone, R., Sayes, F., Song, O., Gröschel, M. I., Brodin, P., Brosch, R., & Majlessi, L. (2015). Cytosolic access of *Mycobacterium tuberculosis*: critical impact of phagosomal acidification control and demonstration of occurrence in vivo. *PLoS pathogens*, 11(2), e1004650. <https://doi.org/10.1371/journal.ppat.1004650>
- Simner, P. J., Woods, G. L., & Wengenack, N. L. (2016). Mycobacteria. *Microbiology spectrum*, 4(4), 10.1128/microbiolspec.DMIH2-0016-2015. <https://doi.org/10.1128/microbiolspec.DMIH2-0016-2015>
- Singh, B., Cocker, D., Ryan, H., & Sloan, D. J. (2019). Linezolid for drug-resistant pulmonary tuberculosis. *The Cochrane database of systematic reviews*, 3(3), CD012836. <https://doi.org/10.1002/14651858.CD012836.pub2>
- Skolnik, K., Kirkpatrick, G., & Quon, B. S. (2016). Nontuberculous Mycobacteria in Cystic Fibrosis. *Current treatment options in infectious diseases*, 8(4), 259–274. <https://doi.org/10.1007/s40506-016-0092-6>

REFERENCES

- Slayden, R. A., Dawson, C. C., & Cummings, J. E. (2018). Toxin-antitoxin systems and regulatory mechanisms in *Mycobacterium tuberculosis*. *Pathogens and disease*, 76(4), 10.1093/femspd/fty039. <https://doi.org/10.1093/femspd/fty039>
- Sonawane, A. A., Shastri, J., & Bavdekar, S. B. (2019). Respiratory Pathogens in Infants Diagnosed with Acute Lower Respiratory Tract Infection in a Tertiary Care Hospital of Western India Using Multiplex Real Time PCR. *Indian journal of pediatrics*, 86(5), 433–438. <https://doi.org/10.1007/s12098-018-2840-8>
- Soroka, D., Dubée, V., Soulier-Escrihuela, O., Cuinet, G., Hugonnet, J. E., Gutmann, L., Mainardi, J. L., & Arthur, M. (2014). Characterization of broad-spectrum *Mycobacterium abscessus* class A β -lactamase. *The Journal of antimicrobial chemotherapy*, 69(3), 691–696. <https://doi.org/10.1093/jac/dkt410>
- Stelitano, G., Sammartino, J. C., & Chiarelli, L. R. (2020). Multitargeting Compounds: A Promising Strategy to Overcome Multi-Drug Resistant Tuberculosis. *Molecules (Basel, Switzerland)*, 25(5), 1239. <https://doi.org/10.3390/molecules25051239>
- Stephenson, D., Perry, A., Appleby, M. R., Lee, D., Davison, J., Johnston, A., Jones, A. L., Nelson, A., Bourke, S. J., Thomas, M. F., De Soya, A., Lordan, J. L., Lumb, J., Robb, A. E., Samuel, J. R., Walton, K. E., & Perry, J. D. (2019). An evaluation of methods for the isolation of nontuberculous mycobacteria from patients with cystic fibrosis, bronchiectasis and patients assessed for lung transplantation. *BMC pulmonary medicine*, 19(1), 19. <https://doi.org/10.1186/s12890-019-0781-2>
- Story-Roller, E., Maggioncalda, E. C., Cohen, K. A., & Lamichhane, G. (2018). *Mycobacterium abscessus* and β -Lactams: Emerging Insights and Potential Opportunities. *Frontiers in microbiology*, 9, 2273. <https://doi.org/10.3389/fmicb.2018.02273>
- Sunnetcioglu, A., Sunnetcioglu, M., Binici, I., Baran, A. I., Karahocagil, M. K., & Saydan, M. R. (2015). Comparative analysis of pulmonary and extrapulmonary tuberculosis of 411 cases. *Annals of clinical microbiology and antimicrobials*, 14, 34. <https://doi.org/10.1186/s12941-015-0092-2>
- Tahlan, K., Wilson, R., Kastrinsky, D. B., Arora, K., Nair, V., Fischer, E., Barnes, S. W., Walker, J. R., Alland, D., Barry, C. E., 3rd, & Boshoff, H. I. (2012). SQ109 targets MmpL3, a membrane transporter of trehalose monomycolate involved in mycolic acid donation to the cell wall core of *Mycobacterium tuberculosis*. *Antimicrobial agents and chemotherapy*, 56(4), 1797–1809. <https://doi.org/10.1128/AAC.05708-11>
- Thijs, E., Wierckx, K., Vandecasteele, S., & Van den Bruel, A. (2019). Adrenal insufficiency, be aware of drug interactions!. *Endocrinology, diabetes & metabolism case reports*, 2019, 19-0062. Advance online publication. <https://doi.org/10.1530/EDM-19-0062>
- Tiberi, S., du Plessis, N., Walzl, G., Vjecha, M. J., Rao, M., Ntoumi, F., Mfinanga, S., Kapata, N., Mwaba, P., McHugh, T. D., Ippolito, G., Migliori, G. B., Maeurer, M. J., & Zumla, A. (2018). Tuberculosis: progress and advances in development of new drugs, treatment regimens, and host-directed therapies. *The Lancet. Infectious diseases*, 18(7), e183–e198. [https://doi.org/10.1016/S1473-3099\(18\)30110-5](https://doi.org/10.1016/S1473-3099(18)30110-5)
- Tiberi, S., Scardigli, A., Centis, R., D'Ambrosio, L., Muñoz-Torrico, M., Salazar-Lezama, M. A., Spanevello, A., Visca, D., Zumla, A., Migliori, G. B., & Caminero Luna, J. A. (2017). Classifying new anti-tuberculosis drugs: rationale and future perspectives. *International*

REFERENCES

- journal of infectious diseases : IJID : official publication of the International Society for Infectious Diseases*, 56, 181–184. <https://doi.org/10.1016/j.ijid.2016.10.026>
- Trefzer, C., Škovierová, H., Buroni, S., Bobovská, A., Nenci, S., Molteni, E., Pojer, F., Pasca, M. R., Makarov, V., Cole, S. T., Riccardi, G., Mikušová, K., & Johnsson, K. (2012). Benzothiazinones are suicide inhibitors of mycobacterial decaprenylphosphoryl-β-D-ribofuranose 2'-oxidase DprE1. *Journal of the American Chemical Society*, 134(2), 912–915. <https://doi.org/10.1021/ja211042r>
- Turenne C. Y. (2019). Nontuberculous mycobacteria: Insights on taxonomy and evolution. *Infection, genetics and evolution : journal of molecular epidemiology and evolutionary genetics in infectious diseases*, 72, 159–168. <https://doi.org/10.1016/j.meegid.2019.01.017>
- Udwadia, Z. F., Amale, R. A., Ajbani, K. K., & Rodrigues, C. (2012). Totally drug-resistant tuberculosis in India. *Clinical infectious diseases: an official publication of the Infectious Diseases Society of America*, 54(4), 579–581. <https://doi.org/10.1093/cid/cir889>
- Unissa, A. N., Subbian, S., Hanna, L. E., & Selvakumar, N. (2016). Overview on mechanisms of isoniazid action and resistance in *Mycobacterium tuberculosis*. *Infection, genetics and evolution : journal of molecular epidemiology and evolutionary genetics in infectious diseases*, 45, 474–492. <https://doi.org/10.1016/j.meegid.2016.09.004>
- Unubol, N., Kizilkaya, I. T., Okullu, S. O., Koksalan, K., & Kocagoz, T. (2019). Simple Identification of Mycobacterial Species by Sequence-Specific Multiple Polymerase Chain Reactions. *Current microbiology*, 76(7), 791–798. <https://doi.org/10.1007/s00284-019-01661-4>
- van Dorn A. (2017). Multidrug-resistant *Mycobacterium abscessus* threatens patients with cystic fibrosis. *The Lancet. Respiratory medicine*, 5(1), 15. [https://doi.org/10.1016/S2213-2600\(16\)30444-1](https://doi.org/10.1016/S2213-2600(16)30444-1)
- van Meel, E. R., den Dekker, H. T., Elbert, N. J., Jansen, P. W., Moll, H. A., Reiss, I. K., de Jongste, J. C., Jaddoe, V., & Duijts, L. (2018). A population-based prospective cohort study examining the influence of early-life respiratory tract infections on school-age lung function and asthma. *Thorax*, 73(2), 167–173. <https://doi.org/10.1136/thoraxjnl-2017-210149>
- Velayati, A. A., Masjedi, M. R., Farnia, P., Tabarsi, P., Ghanavi, J., ZiaZarifi, A. H., & Hoffner, S. E. (2009). Emergence of new forms of totally drug-resistant tuberculosis bacilli: super extensively drug-resistant tuberculosis or totally drug-resistant strains in iran. *Chest*, 136(2), 420–425. <https://doi.org/10.1378/chest.08-2427>
- Veziris, N., Bernard, C., Guglielmetti, L., Le Du, D., Marigot-Outtandy, D., Jaspard, M., Caumes, E., Lerat, I., Rioux, C., Yazdanpanah, Y., Tiotiu, A., Lemaitre, N., Brossier, F., Jarlier, V., Robert, J., Sougakoff, W., Aubry, A., CNR MyRMA and the Tuberculosis Consilium of the CNR MyRMA, & CNR MyRMA and Tuberculosis Consilium of the CNR MyRMA (2017). Rapid emergence of *Mycobacterium tuberculosis* bedaquiline resistance: lessons to avoid repeating past errors. *The European respiratory journal*, 49(3), 1601719. <https://doi.org/10.1183/13993003.01719-2016>
- Viljoen, A., Raynaud, C., Johansen, M. D., Roquet-Banères, F., Herrmann, J. L., Daher, W., & Kremer, L. (2019). Verapamil Improves the Activity of Bedaquiline against *Mycobacterium abscessus* *In Vitro* and in Macrophages. *Antimicrobial agents and chemotherapy*, 63(9), e00705-19. <https://doi.org/10.1128/AAC.00705-19>

REFERENCES

- Villellas, C., Coeck, N., Meehan, C. J., Lounis, N., de Jong, B., Rigouts, L., & Andries, K. (2017). Unexpected high prevalence of resistance-associated Rv0678 variants in MDR-TB patients without documented prior use of clofazimine or bedaquiline. *The Journal of antimicrobial chemotherapy*, 72(3), 684–690. <https://doi.org/10.1093/jac/dkw502>
- Vosátka, R., Krátký, M., & Vinšová, J. (2018). Triclosan and its derivatives as antimycobacterial active agents. *European journal of pharmaceutical sciences : official journal of the European Federation for Pharmaceutical Sciences*, 114, 318–331. <https://doi.org/10.1016/j.ejps.2017.12.013>
- Wallace, R. J., Jr, Dukart, G., Brown-Elliott, B. A., Griffith, D. E., Scerpella, E. G., & Marshall, B. (2014). Clinical experience in 52 patients with tigecycline-containing regimens for salvage treatment of *Mycobacterium abscessus* and *Mycobacterium chelonae* infections. *The Journal of antimicrobial chemotherapy*, 69(7), 1945–1953. <https://doi.org/10.1093/jac/dku062>
- Wallis, R. S., Dawson, R., Friedrich, S. O., Venter, A., Paige, D., Zhu, T., Silvia, A., Gobey, J., Ellery, C., Zhang, Y., Eisenach, K., Miller, P., & Diacon, A. H. (2014). Mycobactericidal activity of sutezolid (PNU-100480) in sputum (EBA) and blood (WBA) of patients with pulmonary tuberculosis. *PLoS one*, 9(4), e94462. <https://doi.org/10.1371/journal.pone.0094462>
- WHO (2017). Forum of International Respiratory Societies. The Global Impact of Respiratory Disease – Second Edition. Sheffield, European Respiratory Society, 2017
- WHO consolidated guidelines on drug-resistant tuberculosis treatment (2019). Geneva: World Health Organization. Licence: CC BY-NC-SA 3.0 IGO.
- WHO methods and data sources for global burden of disease estimates 2000-2016 (June 2018). Department of Information, Evidence and Research WHO, Geneva.
- World Health Organization (2016-2020). Global tuberculosis reports 2016-2020. https://www.who.int/tb/publications/global_report/en/
- Wu, M. L., & Dick, T. (2015). Metabolic flexibility and morphological plasticity in mycobacteria. *Future microbiology*, 10(4), 449–452. <https://doi.org/10.2217/fmb.14.151>
- Wu, M. L., Aziz, D. B., Dartois, V., & Dick, T. (2018). NTM drug discovery: status, gaps and the way forward. *Drug discovery today*, 23(8), 1502–1519. <https://doi.org/10.1016/j.drudis.2018.04.001>
- Xu, J., Li, S. Y., Almeida, D. V., Tasneen, R., Barnes-Boyle, K., Converse, P. J., Upton, A. M., Mdluli, K., Fotouhi, N., & Nuermberger, E. L. (2019). Contribution of Pretomanid to Novel Regimens Containing Bedaquiline with either Linezolid or Moxifloxacin and Pyrazinamide in Murine Models of Tuberculosis. *Antimicrobial agents and chemotherapy*, 63(5), e00021-19. <https://doi.org/10.1128/AAC.00021-19>
- Yan, J., Kevat, A., Martinez, E., Teese, N., Johnson, K., Ranganathan, S., Harrison, J., Massie, J., & Daley, A. (2020). Investigating transmission of *Mycobacterium abscessus* amongst children in an Australian cystic fibrosis centre. *Journal of cystic fibrosis : official journal of the European Cystic Fibrosis Society*, 19(2), 219–224. <https://doi.org/10.1016/j.jcf.2019.02.011>
- Ye, M., Xu, L., Zou, Y., Li, B., Guo, Q., Zhang, Y., Zhan, M., Xu, B., Yu, F., Zhang, Z., & Chu, H. (2019). Molecular Analysis of Linezolid-Resistant Clinical Isolates of *Mycobacterium abscessus*. *Antimicrobial agents and chemotherapy*, 63(2), e01842-18. <https://doi.org/10.1128/AAC.01842-18>

REFERENCES

- Zhang, B., Li, J., Yang, X., Wu, L., Zhang, J., Yang, Y., Zhao, Y., Zhang, L., Yang, X., Yang, X., Cheng, X., Liu, Z., Jiang, B., Jiang, H., Guddat, L. W., Yang, H., & Rao, Z. (2019). Crystal Structures of Membrane Transporter MmpL3, an Anti-TB Drug Target. *Cell*, 176(3), 636–648.e13. <https://doi.org/10.1016/j.cell.2019.01.003>
- Zhang, L., Zhao, Y., Gao, Y., Wu, L., Gao, R., Zhang, Q., Wang, Y., Wu, C., Wu, F., Gurcha, S. S., Veerapen, N., Batt, S. M., Zhao, W., Qin, L., Yang, X., Wang, M., Zhu, Y., Zhang, B., Bi, L., Zhang, X., ... Rao, Z. (2020). Structures of cell wall arabinosyltransferases with the anti-tuberculosis drug ethambutol. *Science (New York, N.Y.)*, 368(6496), 1211–1219. <https://doi.org/10.1126/science.aba9102>
- Zimenkov, D. V., Nosova, E. Y., Kulagina, E. V., Antonova, O. V., Arslanbaeva, L. R., Isakova, A. I., Krylova, L. Y., Peretokina, I. V., Makarova, M. V., Safonova, S. G., Borisov, S. E., & Gryadunov, D. A. (2017). Examination of bedaquiline- and linezolid-resistant *Mycobacterium tuberculosis* isolates from the Moscow region. *The Journal of antimicrobial chemotherapy*, 72(7), 1901–1906. <https://doi.org/10.1093/jac/dkx094>
- Zong, Z., Jing, W., Shi, J., Wen, S., Zhang, T., Huo, F., Shang, Y., Liang, Q., Huang, H., & Pang, Y. (2018). Comparison of *In Vitro* Activity and MIC Distributions between the Novel Oxazolidinone Delpazolid and Linezolid against Multidrug-Resistant and Extensively Drug-Resistant *Mycobacterium tuberculosis* in China. *Antimicrobial agents and chemotherapy*, 62(8), e00165-18. <https://doi.org/10.1128/AAC.00165-18>

LIST OF ORIGINAL WORKS

Papers that are part of this research line

- Degiacomi, G., **Sammartino, J. C.**, Sinigiani, V., Marra, P., Urbani, A., & Pasca, M. R. (2020). *In vitro* Study of Bedaquiline Resistance in *Mycobacterium tuberculosis* Multi-Drug Resistant Clinical Isolates. *Frontiers in microbiology*, *11*, 559469. <https://doi.org/10.3389/fmicb.2020.559469> (IF=4.926).
- Liu, L., Kong, C., Fumagalli, M., Savková, K., Xu, Y., Huszár, S., **Sammartino, J. C.**, Fan, D., Chiarelli, L. R., Mikušová, K., Sun, Z., & Qiao, C. (2020). Design, synthesis and evaluation of covalent inhibitors of DprE1 as antitubercular agents. *European journal of medicinal chemistry*, *208*, 112773. <https://doi.org/10.1016/j.ejmech.2020.112773> (IF=5.207).
- Rodriguez, F., Saffon, N., **Sammartino, J. C.**, Degiacomi, G., Pasca, M. R., & Lherbet, C. (2020). First triclosan-based macrocyclic inhibitors of InhA enzyme. *Bioorganic chemistry*, *95*, 103498. <https://doi.org/10.1016/j.bioorg.2019.103498> (IF=4.567).
- Degiacomi, G.*, **Sammartino, J. C.***, Chiarelli, L. R., Riabova, O., Makarov, V., & Pasca, M. R. (2019). *Mycobacterium abscessus*, an Emerging and Worrisome Pathogen among Cystic Fibrosis Patients. *International journal of molecular sciences*, *20*(23), 5868. <https://doi.org/10.3390/ijms20235868> *Equal contribution (IF=4.653).
- Chiarelli, L. R., Mori, M., Beretta, G., Gelain, A., Pini, E., **Sammartino, J. C.**, Stelitano, G., Barlocco, D., Costantino, L., Lapillo, M., Poli, G., Caligiuri, I., Rizzolio, F., Bellinzoni, M., Tuccinardi, T., Villa, S., & Meneghetti, F. (2019). New insight into structure-activity of furan-based salicylate synthase (MbtI) inhibitors as potential antitubercular agents. *Journal of enzyme inhibition and medicinal chemistry*, *34*(1), 823–828. <https://doi.org/10.1080/14756366.2019.1589462> (IF=3.719).
- Sammartino, J. C.**, Stelitano, G., Degiacomi, G., Riccardi, G., Chiarelli, L. R. Functional characterization of the antitubercular drug target Decaprenylphosphoryl- β -D-ribose epimerase (DprE1/DprE2) complex. **Manuscript in preparation.**

Papers in collaboration with other research lines

- Monakhova, N., Korduláková, J., Vocat, A., Egorova, A., Lepioshkin, A., Salina, E. G., Nosek, J., Repková, E., Zemanová, J., Jurdáková, H., Górová, R., Roh, J., Degiacomi, G., **Sammartino, J. C.**, Pasca, M. R., Cole, S. T., Mikušová, K., & Makarov, V. (2021). Design and Synthesis of Pyrano[3,2-*b*]indolones Showing Antimycobacterial Activity. *ACS infectious diseases*, *7*(1), 88–100. <https://doi.org/10.1021/acsinfecdis.0c00622> (IF=4.970).
- Mori, M., Stelitano, G., Gelain, A., Pini, E., Chiarelli, L. R., **Sammartino, J. C.**, Poli, G., Tuccinardi, T., Beretta, G., Porta, A., Bellinzoni, M., Villa, S., & Meneghetti, F. (2020). Shedding X-ray Light on the Role of Magnesium in the Activity of *Mycobacterium tuberculosis* Salicylate Synthase

LIST OF ORIGINAL WORKS

- (MbtI) for Drug Design. *Journal of medicinal chemistry*, 63(13), 7066–7080. <https://doi.org/10.1021/acs.jmedchem.0c00373> (IF=6.521).
- Stelitano, G., **Sammartino, J. C.**, & Chiarelli, L. R. (2020). Multitargeting Compounds: A Promising Strategy to Overcome Multi-Drug Resistant Tuberculosis. *Molecules (Basel, Switzerland)*, 25(5), 1239. <https://doi.org/10.3390/molecules25051239> (IF= 3.589).
- Mori, G., Orena, B. S., Chiarelli, L. R., Degiacomi, G., Riabova, O., **Sammartino, J. C.**, Makarov, V., Riccardi, G., & Pasca, M. R. (2020). Rv0579 Is Involved in the Resistance to the TP053 Antitubercular Prodrug. *Frontiers in microbiology*, 11, 292. <https://doi.org/10.3389/fmicb.2020.00292> (IF= 4.926).
- Chiarelli, L. R., Salina, E. G., Mori, G., Azhikina, T., Riabova, O., Lepioshkin, A., Grigorov, A., Forbak, M., Madacki, J., Orena, B. S., Manfredi, M., Gosetti, F., Buzzi, A., Degiacomi, G., **Sammartino, J. C.**, Marengo, E., Korduláková, J., Riccardi, G., Mikušová, K., Makarov, V., ... Pasca, M. R. (2020). New Insights into the Mechanism of Action of the Thienopyrimidine Antitubercular Prodrug TP053. *ACS infectious diseases*, 6(2), 313–323. <https://doi.org/10.1021/acsinfecdis.9b00388> (IF=4.970).
- Mori, M., **Sammartino, J. C.**, Costantino, L., Gelain, A., Meneghetti, F., Villa, S., & Chiarelli, L. R. (2019). An Overview on the Potential Antimycobacterial Agents Targeting Serine/Threonine Protein Kinases from *Mycobacterium tuberculosis*. *Current topics in medicinal chemistry*, 19(9), 646–661. <https://doi.org/10.2174/1568026619666190227182701> (IF=3.335).

Posters

- Sammartino J. C.**, Degiacomi G., Urbani A., Muñoz Muñoz L., Chiarelli L.R., Makarov V., Ramon-García S., Pasca M.R. Fighting *Mycobacterium abscessus* infection in Cystic Fibrosis patients. IX International Conference BIFI 2020, Saragozza, Spain, 03-05/02/2020.
- Sammartino J. C.**, Degiacomi G., Chiarelli L.R., Urbani A., Makarov V., Pasca M.R. New weapons against *Mycobacterium abscessus* and other Non-Tuberculous Mycobacteria. XVII Convention of FFC investigators in cystic fibrosis, Verona (Italy), 14-16 November 2019.
- Ezquerria J.M., Lucía A., Millán A.C., Blázquez J., Pasca M.R., Degiacomi G., **Sammartino J. C.**, Vilcheze C., Aínsa J.A., Ramón-García S. Mode of action elucidation studies of the avermectins against mycobacteria. Myco Porto, Oporto (Portugal), 19-20/09/2019.
- Repková E., Zemanová J., Nosek J., Vocat A., Degiacomi G., **Sammartino J. C.**, Salina E., Pasca M.R., Cole S., Mikušová K., Makarov V., Korduláková J. Mechanism of resistance of a novel pyranoidole derivative. Gordon Research Conference, Castelldefels (Spain), 7-12/07/2019.
- Sammartino J. C.**, Degiacomi G., Makarov V., Chiarelli L.R., Pasca M.R. Fighting *Mycobacterium abscessus* infection in Cystic Fibrosis patients. SIMGBM 33rd Congress, Firenze (Italy), 19-22/06/2019.
- Degiacomi G., **Sammartino J. C.**, Postiglione U., Sasserà D., Korduláková J., Salina E., Mikusova K., Makarov V., Riccardi G., Pasca M.R. Dissecting the mechanisms of action of new promising classes of compounds active against *Mycobacterium tuberculosis*. SIMGBM 33rd Congress, Firenze (Italy), 19-22/06/2019.

LIST OF ORIGINAL WORKS

- Chiarelli L.R., **Sammartino J. C.**, Degiacomi G., Korduláková J., Lherbet C., Pasca M.R. Coumarin-thiacetazone: a novel antitubercular compound as a new tool for *Mycobacterium tuberculosis* fluorescent labelling. SIMGBM 33rd Congress, Firenze (Italy), 19-22/06/2019.
- Stelitano G., Mori M., **Sammartino J. C.**, Gelain A., Tuccinardi T., Villa S., Meneghetti F, Chiarelli L.R. Targeting iron uptake pathway for the development of novel antitubercular drugs. SIMGBM 33rd Congress, Firenze (Italy), 19-22/06/2019.
- Degiacomi G., **Sammartino J. C.**, Chiarelli L.R., Makarov V., Pasca M.R. New weapons against *Mycobacterium abscessus* and other nontuberculous Mycobacteria. 16th Convention of FFC investigators in cystic fibrosis, Verona (Italy), 22-24/11/2018.

Talks

- Sammartino J. C.**, invited speaker. La riemergenza della tubercolosi orale: aspetti genetici ed epidemiologici. Emocomponenti e Terapie Cellulari: dal Laboratorio all'Outcome Clinico, International Non transfusional Hemocomponents academy, intHEMA, Napoli (Italy), 6-7 December 2019

New insight into structure-activity of furan-based salicylate synthase (MbtI) inhibitors as potential antitubercular agents

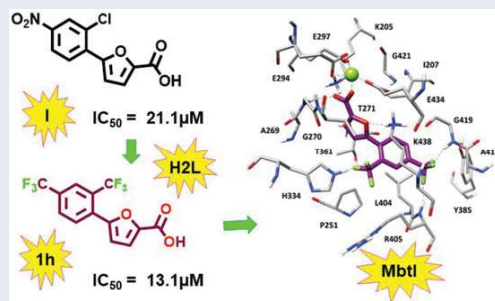
Laurent R. Chiarelli^{a*}, Matteo Mori^{b*}, Giangiacomo Beretta^c, Arianna Gelain^b, Elena Pini^b,
Josè Camilla Sammartino^a, Giovanni Stelitano^a, Daniela Barlocco^b, Luca Costantino^d,
Margherita Lapillo^e, Giulio Poli^e, Isabella Caligiuri^f, Flavio Rizzolio^{f,g}, Marco Bellinzoni^h,
Tiziano Tuccinardi^e, Stefania Villa^b and Fiorella Meneghetti^b

^aDepartment of Biology and Biotechnology “L. Spallanzani”, University of Pavia, Pavia, Italy; ^bDepartment of Pharmaceutical Sciences, University of Milano, Milano, Italy; ^cDepartment of Environmental Science and Policy, University of Milano, Milano, Italy; ^dDepartment of Life Sciences, University of Modena e Reggio Emilia, Modena, Italy; ^eDepartment of Pharmacy, University of Pisa, Pisa, Italy; ^fPathology Unit, Department of Molecular Biology and Translational Research, National Cancer Institute and Center for Molecular Biomedicine, Aviano, Italy; ^gDepartment of Molecular Science and Nanosystems, Ca’ Foscari University of Venezia, Venezia-Mestre, Italy; ^hInstitut Pasteur, Paris, France

ABSTRACT

Starting from the analysis of the hypothetical binding mode of our previous furan-based hit (**1**), we successfully achieved our objective to replace the nitro moiety, leading to the disclosure of a new lead exhibiting a strong activity against MbtI. Our best candidate **1h** displayed a K_i of 8.8 μM and its antimycobacterial activity ($\text{MIC}^{99} = 250 \mu\text{M}$) is conceivably related to mycobactin biosynthesis inhibition. These results support the hypothesis that 5-phenylfuran-2-carboxylic derivatives are a promising class of MbtI inhibitors.

GRAPHICAL ABSTRACT



ARTICLE HISTORY

Received 11 February 2019
Revised 22 February 2019
Accepted 25 February 2019

KEYWORDS

Tuberculosis; siderophores; mycobactins; drug design; antimycobacterial agent; molecular modelling

Introduction

Tuberculosis (TB) is an infectious disease caused by an obligate aerobic bacterium, known as *Mycobacterium tuberculosis* (Mtb). When the bacilli are inhaled, they reach the alveolar spaces of the lungs and are mainly ingested by macrophages. As a consequence, TB primarily affects the lungs, but at later stages it can also spread to other vital organs. Despite significant improvements with respect to diagnosis, treatment, and preventive measures have been successfully implemented in many healthcare

systems around the world, this disease still remains the world's biggest threat to human health causing 54 million deaths between 2000 and 2017¹. Standard therapeutic regimens have remained substantially unchanged over the past 60 years with outdated drugs and very long therapies that are still used for the treatment of new and relapse cases. In addition to the length of the cure, other hurdles related to the management of TB infections include interactions with drugs used in comorbid conditions, especially HIV, and severe side effects. All these issues contribute

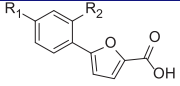
CONTACT Stefania Villa stefania.villa@unimi.it Dipartimento di Scienze Farmaceutiche, Università degli Studi di Milano, Via L. Mangiagalli 25, Milano 20133, Italy

*These authors contributed equally to this work.

Supplemental data for this article can be accessed [here](#).

© 2019 The Author(s). Published by Informa UK Limited, trading as Taylor & Francis Group.

This is an Open Access article distributed under the terms of the Creative Commons Attribution-NonCommercial License (<http://creativecommons.org/licenses/by-nc/4.0/>), which permits unrestricted non-commercial use, distribution, and reproduction in any medium, provided the original work is properly cited.

Table 1. *In vitro* activity of compounds 1a–p.


1a–i R ₁ =CF ₃				1j–p R ₁ =NO ₂			
Code	R ₂	Residual activity at 100 μM (%)	Mbtl IC ₅₀ (μM)*	Code	R ₂	Residual activity at 100 μM (%)	Mbtl IC ₅₀ (μM)*
1a	Cl	6.1 ± 2.5	28.5 ± 2.6	1j**	Cl	11.3 ± 4.2	17.9 ± 3.2
1b	F	6.1 ± 1.1	27.6 ± 7.3	1j	F	32.1 ± 2.4	–
1c	Br	38.0 ± 3.7	–	1k	Br	26.4 ± 4.8	–
1d	OH	16.8 ± 2.7	35.9 ± 10.3	1l	OH	13.9 ± 4.0	29.8 ± 4.2
1e	CH ₃	19.3 ± 2.2	31.5 ± 9.6	1m	CH ₃	13.2 ± 5.8	28.5 ± 1.5
1f	NH ₂	13.1 ± 2.4	34.6 ± 10.9	1n	NH ₂	13.5 ± 3.8	24.2 ± 5.4
1g	CN	5.7 ± 1.5	18.5 ± 3.2	1o	CN	5.0 ± 1.9	24.4 ± 5.9
1h	CF ₃	3.9 ± 1.7	13.1 ± 2.0	1p	CF ₃	25.1 ± 3.7	41.8 ± 5.3
1i	<i>m</i> -CF ₃	64.3 ± 4.5	–	–	–	–	–

*Only for compounds with residual activity ≤25%; **new fluorimetric assay value determined for the sake of comparison.

to determine a poor patient compliance that, together with the improper use of TB antibiotics, has led to the insurgence of multi-drug-resistant (MDR) and extensively drug-resistant (XDR) bacterial strains^{2–4}. As confirmed by the latest WHO report, drug resistance is becoming a real emergency; therefore, there is a growing interest in the development of novel anti-TB compounds^{5–8}. A few of them reached clinical trials and two drugs, delamanid and bedaquiline, have been recently approved; however, more information on their effectiveness, safety, and tolerability are still required because severe side effects have been reported^{9,10}. In this scenario, the research of many more TB drug candidates to sustain an effective and productive drug pipeline is pivotal. Targeting Mtb iron uptake systems is now a validated strategy for the development of antimycobacterial compounds, because iron is essential for Mtb survival in the host and its acquisition is strongly correlated with virulence¹¹. Among the four different iron acquisition pathways used by Mtb, the most thoroughly characterised one is based on the production of two types of siderophores: carboxymycobactins, which acquire iron extracellularly and transport it into the cytoplasm of the bacteria, and mycobactins, which facilitate the transport of iron through the cell wall into the cytoplasm. Notably, targeting this biosynthetic process is an attractive strategy, because its impairment lowers the pathogen virulence and survival without causing toxicity issues. Indeed, as this pathway is absent in humans, the risk of off-target effects is minimal; moreover, being an unexplored biological process for the development of drugs, there is no known resistance mechanism. The first step of the biosynthesis of these siderophores is catalysed by the Mg²⁺-dependent enzyme salicylate synthase (MbtI), a validated pharmacological target^{12–15}, whose crystal structure has been recently solved¹⁶.

In this context, the aim of our project is the identification of new MbtI inhibitors as potential antitubercular agents. Our previous computational studies generated a pharmacophore model, that allowed the identification of the interesting hit compound **1** (Table 1). Then, a structure–activity relationship study on monosubstituted derivatives underlined the importance of the nitro moiety for potency¹⁴. However, the nitro group is considered a structural alert for the development of a potential drug, since drugs containing nitro groups have been extensively associated with mutagenicity and genotoxicity¹⁷. On these bases, in the present work, we designed additional analogs (compounds **1a–p**, Table 1) exploring other hitherto unconsidered pharmacophoric features and evaluating the possibility of replacing the nitro group.

Materials and methods

Chemistry

Compounds **1a,b,d–i,l–n,p** were synthesised by a Suzuki–Miyaura reaction¹⁸, followed by a base-catalysed hydrolysis of the ester function¹⁹. Compounds **1c,j,k,o** were synthesised by a Sandmeyer reaction²⁰, starting from 2-furan carboxylic acid methyl ester and the diazonium salts of the appropriate amines; the ester function was then hydrolysed in basic conditions²¹. The general procedures, the synthetic pathways (Supplementary Schemes 1 and 2), the details concerning the specific synthetic steps and the analytical data are provided in the Supplementary Material.

Mbtl enzymatic assays

Recombinant *M. tuberculosis* MbtI was produced and purified as previously reported¹⁴. Enzyme activity was determined measuring the production of salicylic acid by a fluorimetric assay slightly modified from Vasani et al.¹² Briefly, assays were performed at 37 °C in a final volume of 400 μL of 50 mM HEPES pH 7.5, 5 mM MgCl₂, using 1–2 μM MbtI and the reactions were started by the addition of chorismic acid and monitored using a Perkin-Elmer LS3 fluorimeter (Ex. λ = 305 nm, Em. λ = 420 nm). Inhibition assays were performed in the presence of the compound at 100 μM (stock solution 20 mM in DMSO), at 50 μM chorismic acid. For significantly active compounds, IC₅₀ and K_i values were determined. To verify that the compounds were not PAINS, their ability to inhibit MbtI activity was tested in the presence of 0.1 mg/mL of bovine serum albumin (BSA) or in the presence of 0.01% (v/v) Triton X-100 to confirm that they did not act as aggregate, and in the presence of 100 mM of 1,4-dithio-DL-threitol (DTT) to exclude an enzyme inhibition due to reaction with cysteines²².

Minimal inhibitory concentration determinations and siderophore production assay

The MIC⁹⁹ values of active compounds against *M. bovis* BCG were determined in low-iron Chelated Sauton's medium²³, using the resazurin reduction assay (REMA)²⁴. Siderophore activity in the culture was tested in *M. bovis* BCG using the Universal CAS liquid assay. To this purpose, *M. bovis* was grown in 7H9 medium, subcultured in chelated Sauton's medium and then diluted to an

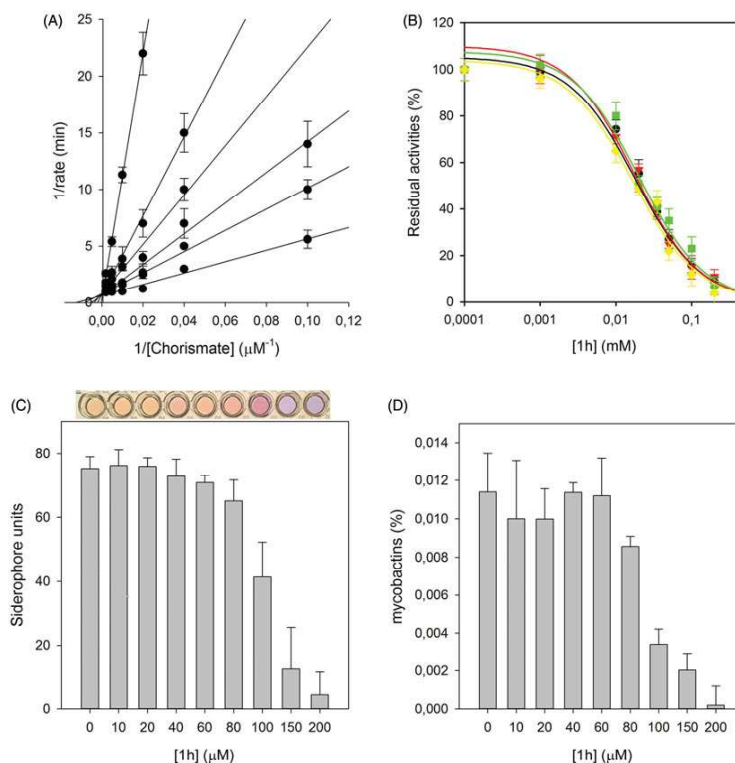


Figure 1. Biological characterisation of **1h**. The global reciprocal plot of data from MbtI steady-state kinetics analysis towards chorismic acid, in the presence of different concentrations of **1h** (A), highlights the competitive behaviour of the inhibitor. IC_{50} plots of **1h** in the presence of BSA (green squares), Triton X-100 (red triangles) and DTT (yellow diamonds) (B) confirm that the compound is not a PAI-N. The Universal CAS assay performed on culture media of *M. bovis* BCG cells grown in the presence of **1h** (C), together with the determination of the mycobactins in the above-mentioned cells (D), confirm that the antimycobacterial activity is related to iron uptake inhibition. All data are mean \pm SD of three replicates.

OD_{600} of 0.01 in chelated Sauton's containing different concentrations of the test compound. After 15 days of incubation at 37 °C, cells were harvested, supernatants were used to perform CAS assay and cell pellets were used for the determination of mycobactins. For CAS assay, an aliquot of 100 μ L of supernatant was mixed with 100 μ L of CAS assay liquid solution in a 96-well plate, incubated for 10 min at room temperature, and the absorbance was measured at 630 nm. For mycobactin determination, cell pellets were extracted in ethanol overnight, then 0.1 M $FeCl_3$ in ethanol was added until no color change was observed. The mixture was incubated at room temperature for 1 h, then mycobactins were extracted in chloroform, washed with water, evaporated and the residue was dissolved in methanol. The concentration of mycobactins was determined measuring the absorbance at 450 nm (1% solution of mycobactins gives an absorbance of 42.8).

Cell viability assay

MRC5 human fibroblast lung cells were maintained at 37 °C in a humidified atmosphere containing 5% CO_2 , according to the

supplier's indications. Cells (10^4) were plated in 96-well culture plates. The day after seeding, vehicle or compounds were added at different concentrations to the medium. Compounds were added to the cell culture at a concentration ranging from 200 to 0.01 μ M. Cell viability was measured after 96 h according to the supplier's instructions (Promega, cat. n° G7571) with a Tecan M1000 PRO instrument. IC_{50} values were calculated from logistic dose-response curves.

Docking studies

All the compounds were docked into the minimised average structure of MbtI complexed with the lead compound **1**¹⁴. The software Gold with the four fitness functions implemented (i.e. GoldScore, ChemScore, Astex Statistical Potential, and ChemPLP) and plants were employed in this study as previously reported^{14,25}, since they have been already used showing good results in the previous virtual screening study on MbtI inhibitors performed in our laboratory¹⁵. The docking site was defined as the region comprising all residues that stayed within 10 Å from

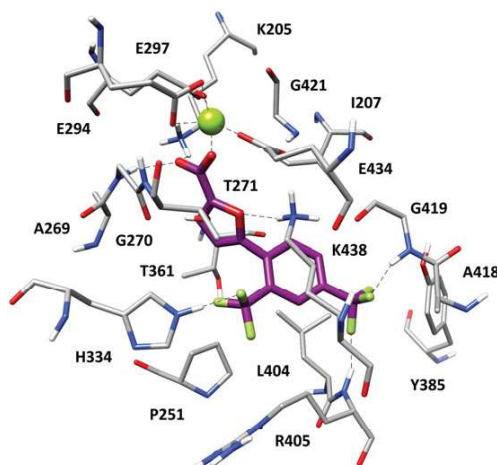


Figure 2. Minimised average structure of 1h within MbtI binding site.

the reference compound **1**. By applying the five docking methods, five different binding dispositions (best-scored docking pose) resulted from the docking of each ligand into the protein binding site. The RMSD of these docking poses against the remaining four was evaluated by using the *rms_analysis* software of the Gold suite. On this basis, for each ligand docked into the protein binding site, a 5×5 matrix was generated reporting the RMSD results. By using an in-house programme, these results were clustered, so that among the five results, all of the similar docking poses were grouped together.²⁶ We selected an RMSD clustering threshold of 2.0 Å; therefore, the so-obtained clusters contained the group of poses that were less than 2.0 Å away from all others poses belonging to the same cluster. For each compound, the binding mode belonging to the most populated cluster identified by the consensus docking evaluation was taken into consideration and subjected to MD simulations.

MD simulations

All simulations were performed using AMBER 16²⁷. General amber force field (GAFF) parameters were assigned to the ligands, whereas partial charges were determined using the AM1-BCC method as implemented in the Antechamber suite of AMBER16. MD simulations were carried out employing the ff14SB force field at 300 K. Magnesium ion was inserted considering its disposition and interaction into the 2FN1 PDB code. Ligand-protein complexes were placed in a rectangular parallelepiped water-box and solvated with a 20 Å water cap by using the TIP3P explicit solvent model. Sodium ions were added as counterions in order to neutralise the system. Before MD simulations, two steps of minimisation were performed; in the first stage, a position constraint of 500 kcal/(mol·Å²) was applied to keep the protein fixed thus minimising only water molecules. In the second stage, the whole system was energy minimised through 5000 steps of steepest descent followed by conjugate gradient (CG), until a convergence of 0.05 kcal/(mol·Å²) and imposing a harmonic potential of 10 kcal/(mol·Å²) to the protein α carbon. Particle mesh Ewald (PME) electrostatics and periodic boundary conditions were used

in the simulations. The time step of the simulations was 2 fs with a cutoff of 10 Å for the non-bonded interactions, while the SHAKE algorithm was applied to keep all bonds involving hydrogen atoms fixed. Constant-volume periodic boundary MD simulation was carried out for the first 0.5 ns, during which the temperature of the system was raised from 0 to 300 K. Then 19.5 ns of constant-pressure periodic boundary MD was performed at 300 K, using the Langevin thermostat in order to maintain constant the temperature of the system. A harmonic force constraint of 10 kcal/(mol·Å²) was applied to the protein α carbons during the first 3.5 ns, whereas in the last 16.5 ns no restraints were applied to the system. All the obtained MD trajectories were analyzed using the Cpptraj programme implemented in AMBER 16.

Result and discussion

In order to further develop our library of furan-based candidates, we examined the substitution pattern at the *para* and *ortho* positions of the phenyl ring. Herein, we disclose additional SAR data; firstly, we synthesised a phenyl di-substituted analog of **1**, characterised by the presence of the trifluoromethyl group (**1a**), because we knew that the more druggable *p*-CF₃ in place of the *p*-NO₂ group was still able to inhibit MbtI⁴. Compound **1a** displayed encouraging inhibiting properties (residual enzyme activity at 100 μM, as % RA, of 6.1 ± 2.5, IC₅₀ = 28.5 ± 2.6 μM). Therefore, we took into account this compound as a new hit and we focussed on the effects of a variety of electron donating/withdrawing or hydrophilic groups in the *ortho* position of the phenyl ring, keeping the CF₃ group in *para* position (**1b–l**). Then, the effects of the previously analysed substituents in *ortho* position were evaluated in the second series of derivatives **1j–p**, bearing the original *p*-NO₂ group (Table 1).

The activity of all compounds (**1a–p**) was tested against the recombinant MbtI, prepared and assayed as previously reported¹⁴. The substitution of the chlorine atom with the fluorine in **1b** did not affect the activity, while the introduction of the bromine atom in **1c** diminished the inhibitory effect of the compound (% RA 38.0 ± 3.7), due to the low capability of bromine to act as

hydrogen bond acceptor together with its higher atomic radius determining a negative steric constraint. The presence of the electron donating groups in **1d**, **1e**, and **1f** did not lead to an improvement of the biological effects. When an electron withdrawing moiety was introduced in the *ortho* position, as in **1g**, we detected an increased activity. This outcome was confirmed by the introduction of an *o*-CF₃ moiety that led to the disclosure of **1h**, having an IC₅₀ value comparable to that of the most active inhibitor (**1**), previously identified. Derivative **1i** was then prepared and tested to assess the importance of having the electron withdrawing moiety in *ortho* position of the phenyl ring; interestingly, moving the CF₃ to the *meta* position significantly decreased the inhibitory activity of the compound. A parallel trend of biological results was obtained for the *p*-NO₂ derivatives **1j–p**. These compounds were prepared and tested to compare the impact of the CF₃ and NO₂ groups on the activity and to better understand their role in the interaction with the target. The outcomes reflected the similar biological behaviour observed for this series (**1j–p**) with respect to the previous one (**1a–i**), confirming the ability of CF₃ to act as a bioisostere of the nitro moiety, according to the bioisosterism between fluorine and carbonyl functionality²⁸. Of note, the presence of two CF₃ substituents in **1h** synergically contributed to enhance the activity, as shown by the comparison of the IC₅₀ value of **1h** and the respective derivative **1p** belonging to the *para*-nitro series (13.1 vs. 41.8 μM).

For the most active compound, **1h**, an accurate biological analysis was thus performed (Figure 1). Kinetic analysis allowed the determination of the *K_i* value 8.8 ± 0.7 μM, allowing the classification of this compound as competitive inhibitor of Mbtl. Then, additional tests were performed to verify that **1h** was not a PAIN compound. The addition of BSA and Triton X-100 did not influence its IC₅₀, proving that the compound did not form aggregates with the target. Similarly, the addition of DTT did not impact on **1h** activity, showing that the ligand did not interact with the cysteine residues of the protein. To evaluate the antimycobacterial activity of **1h** we used the nonpathogenic *M. bovis* BCG, whose siderophores closely resemble Mtb mycobactins^{29,30}. The minimal inhibitory concentration (MIC₉₉) value, determined in iron-limiting conditions in chelated Sauton's medium, was similar to that of hit **1** (250 μM versus 500 μM). Moreover, to assess if the antitubercular activity was indeed related to iron uptake inhibition, the effects of the compound on siderophore production were evaluated by means of the Universal CAS liquid assay³⁰. Firstly, the level of siderophore activity in the medium was measured and the colorimetric assay revealed that the removal of iron was inversely related to the concentration of the compound. Similarly, the quantification of mycobactins isolated from the cell pellet evidenced that the concentration of mycobactins decreased at higher **1h** concentrations. All these outcomes suggested that the inhibitory effect towards Mtb growth was due to mycobactin biosynthesis inhibition. Finally, compounds **1**, **1h** and **1p** were selected for evaluating their antiproliferative activity against human MRC-5 fibroblasts. The biological results showed that the three compounds did not affect the growth of these normal cells (MRC-5, IC₅₀ > 100 μM), thus indicating the potentially low level of toxicity of this class of compounds.

With the aim of elucidating the binding mode of this class of derivatives, molecular modelling studies were performed on the most active compound of the series. Compound **1h** was subjected to a consensus docking protocol and the result was refined through 20 ns of MD simulation with explicit water molecules (see Supplementary Material for details). Figure 2 shows the minimised average structure of **1h** bound to the catalytic site of Mbtl. The

two aromatic rings of the ligand lay on the hydrophobic wall constituted by I207, P251, T361, and L404, thus forming lipophilic interactions with these residues. On the other side of the binding site, the ligand core moiety shows multiple interactions with K438: a hydrogen bond formed by the furan oxygen and a cation-π interaction established through the phenyl ring, which also forms additional hydrophobic contacts with the side chain of the residue. The carboxylic group of **1h** coordinates the Mg²⁺ ion and also forms H-bonds with the backbone nitrogen of G270 and the side chain of K205 that contribute to anchor the ligand to the Mbtl binding site. According to the experimental results, the *p*-CF₃ group of the ligand replaces the *p*-NO₂ group of the parent compound **1** by forming two H-bonds with the backbone nitrogen of R405 and G419, while the *o*-CF₃ substituent of **1h** shows an additional hydrogen bond with the side chain of H334. The same consensus docking and MD protocols were then applied on compounds **1a** and **1q** to gain a better interpretation of the obtained SAR. In agreement with the experimental data, the binding mode predicted for **1a** confirmed the importance of the *o*-CF₃ substituent of **1h**. In fact, the *o*-chlorine atom of **1a** does not show any hydrogen bond with H334. Moreover, although the ligand perfectly chelates the Mg²⁺ ion, the presence of the chlorine atom determines a small shift in the binding orientation that hampers the formation of H-bonds with G270 and K205 predicted for **1h** (Figure S1). Nevertheless, the presence of an *o*-CF₃ moiety was found to be detrimental when associated with the *p*-NO₂ group originally present in **1**, as observed for compound **1p**. Interestingly, MD simulations suggested that **1p** is not able to form the H-bond and cation-π interactions with K438 (Figure S2). In order to establish the H-bond network among its *p*-NO₂ group, the backbone nitrogen of R405 and the side chain of Y385, **1p** moves toward these residues and slightly rotates toward K438, which thus moves away from the ligand to avoid steric clashes. Due to its orientation within Mbtl binding site, **1p** cannot even interact with H334 through the *o*-CF₃ as predicted for **1h**.

To conclude, starting from the analysis of the hypothetical binding mode of our previous furan-based hit **1**, we successfully performed the bioisosteric replacement of the nitro group. Our preliminary hit optimisation study led to the disclosure of a new compound (**1h**) exhibiting a strong activity against Mbtl, comparable to the most potent competitive inhibitor reported so far¹⁴. Our best candidate **1h**, characterised by the presence of two CF₃ substituents in the *ortho* and *para* positions of its phenyl ring, displayed an IC₅₀ value of 13.1 ± 2.0 μM (*K_i* = 8.8 ± 0.7 μM) and the antimycobacterial activity showed by this compound (MIC₉₉ = 250 μM) is conceivably related to mycobactin biosynthesis inhibition. Moreover, preliminary assays against noncancerous human fibroblast lung cells did not reveal cytotoxicity issues. These results support the hypothesis that 5-phenylfuran-2-carboxylic derivatives are a promising class of Mbtl inhibitors and allowed us to gather new information for a further optimisation of this class of compounds.

Disclosure statement

No potential conflict of interest was reported by the authors.

Funding

This work was funded by University of Milan (Linea B), and the Italian Ministry of Education, University and Research (MIUR): Dipartimenti di Eccellenza Programme (2018–2022) - Dept. of Biology and Biotechnology "L. Spallanzani", University of Pavia.

ORCID

Laurent R. Chiarelli  <http://orcid.org/0000-0003-0348-9764>
 Matteo Mori  <http://orcid.org/0000-0002-7491-1494>
 Giangiacomo Beretta  <http://orcid.org/0000-0003-0987-0857>
 Arianna Gelain  <http://orcid.org/0000-0001-9104-732X>
 Elena Pini  <http://orcid.org/0000-0003-0554-566X>
 José Camilla Sammartino  <http://orcid.org/0000-0003-3707-3118>
 Giovanni Stelitano  <http://orcid.org/0000-0002-5219-4770>
 Daniela Barlocco  <http://orcid.org/0000-0002-8593-1853>
 Luca Costantino  <http://orcid.org/0000-0001-5334-8084>
 Giulio Poli  <http://orcid.org/0000-0002-8061-5632>
 Isabella Caligiuri  <http://orcid.org/0000-0002-4355-5597>
 Flavio Rizzolio  <http://orcid.org/0000-0002-3400-4363>
 Marco Bellinzoni  <http://orcid.org/0000-0002-8887-6917>
 Tiziano Tuccinardi  <http://orcid.org/0000-0002-6205-4069>
 Stefania Villa  <http://orcid.org/0000-0001-6616-1163>
 Fiorella Meneghetti  <http://orcid.org/0000-0002-6511-7360>

References

- Glaziou P, Floyd K, Ravignone MC. Global epidemiology of tuberculosis. *Semin Respir Crit Care Med* 2018;39:271–85.
- Zhang Y, Yew W. Mechanisms of drug resistance in *Mycobacterium tuberculosis*. *Int J Tuberc Lung Dis* 2009;13:1320–30.
- Gandhi NR, Nunn P, Dheda K, et al. Multidrug-resistant and extensively drug-resistant tuberculosis: a threat to global control of tuberculosis. *Lancet* 2010;375:1830–43.
- Falzon D, Gandhi N, Migliori GB, et al. Resistance to fluoroquinolones and second-line injectable drugs: impact on multidrug-resistant TB outcomes. *Eur Respir J* 2013;42:156–68.
- Koul A, Arnoult E, Lounis N, et al. The challenge of new drug discovery for tuberculosis. *Nature* 2011;469:483–90.
- Zumla A, Nahid P, Cole ST. Advances in the development of new tuberculosis drugs and treatment regimens. *Nat Rev Drug Discov* 2013;12:388–404.
- Fanzani L, Porta F, Meneghetti F, et al. *Mycobacterium tuberculosis* low molecular weight phosphatases (MPtpA and MPtpB): from biological insight to inhibitors. *Curr Med Chem* 2015;22:3110–32.
- Meneghetti F, Villa S, Gelain A, et al. Iron acquisition pathways as targets for antitubercular drugs. *Curr Med Chem* 2016;23:4009–26.
- Borisov SE, Dheda K, Enwerem M, et al. Effectiveness and safety of bedaquiline-containing regimens in the treatment of MDR- and XDR-TB: a multicentre study. *Eur Respir J* 2017;49:1700387.
- D'Ambrosio L, Centis R, Tiberi S, et al. Delamanid and bedaquiline to treat multidrug-resistant and extensively drug-resistant tuberculosis in children: a systematic review. *J Thorac Dis* 2017;9:2093–101.
- De Voss JJ, Rutter K, Schroeder BG, et al. The salicylate-derived mycobactin siderophores of *Mycobacterium tuberculosis* are essential for growth in macrophages. *Proc Natl Acad Sci USA* 2000;97:1252–7.
- Vasan M, Neres J, Williams J, et al. Inhibitors of the salicylate synthase (MbtI) from *Mycobacterium tuberculosis* discovered by high-throughput screening. *ChemMedChem* 2010;5:2079–87.
- Manos-Turvey A, Cergol KM, Salam NK, et al. Synthesis and evaluation of *M. tuberculosis* salicylate synthase (MbtI) inhibitors designed to probe plasticity in the active site. *Org Biomol Chem* 2012;10:9223.
- Chiarelli LR, Mori M, Barlocco D, et al. Discovery and development of novel salicylate synthase (MbtI) furanic inhibitors as antitubercular agents. *Eur J Med Chem* 2018;155:754–63.
- Pini E, Poli G, Tuccinardi T, et al. New chromane-based derivatives as inhibitors of *Mycobacterium tuberculosis* salicylate synthase (MbtI): preliminary biological evaluation and molecular modeling studies. *Molecules* 2018;23:1506.
- Harrison AJ, Yu M, Gardenborg T, et al. The structure of MbtI from *Mycobacterium tuberculosis*, the first enzyme in the biosynthesis of the *Siderophore mycobactin*, reveals it to be a salicylate synthase. *J Bacteriol* 2006;188:6081–91.
- Nepali K, Lee H-Y, Liou J-P. Nitro-group-containing drugs. *J Med Chem* 2018. [Epub ahead of print]. doi:10.1021/acs.jmedchem.8b00147
- Porta F, Gelain A, Barlocco D, et al. A field-based disparity analysis of new 1,2,5-oxadiazole derivatives endowed with antiproliferative activity. *Chem Biol Drug Des* 2017;90:820–39.
- Masciocchi D, Gelain A, Porta F, et al. Synthesis, structure–activity relationships and stereochemical investigations of new tricyclic pyridazinone derivatives as potential STAT3 inhibitors. *Medchemcomm* 2013;4:1181.
- Gorak YI, Obushak ND, Matiichuk VS, Lytvyn RZ. Synthesis of heterocycles from arylation products of unsaturated compounds: XVIII. 5-Arylfuran-2-carboxylic acids and their application in the synthesis of 1,2,4-thiadiazole, 1,3,4-oxadiazole, and [1,2,4]triazolo[3,4-b][1,3,4]thiadiazole derivatives. *Russ J Org Chem* 2009;45:541–50.
- Cattò C, Grazioso G, Dell'Orto S, et al. The response of *Escherichia coli* biofilm to salicylic acid. *Biofouling* 2017;33:235–51.
- Dahlin JL, Nissink JWM, Strasser JM, et al. PAINS in the assay: chemical mechanisms of assay interference and promiscuous enzymatic inhibition observed during a sulfhydryl-scavenging HTS. *J Med Chem* 2015;58:2091–113.
- Siegrist MS, Unnikrishnan M, McConnell MJ, et al. Mycobacterial Esx-3 is required for mycobactin-mediated iron acquisition. *Proc Natl Acad Sci USA* 2009;106:18792–7.
- Palomino J-C, Martin A, Camacho M, et al. Resazurin microtiter assay plate: simple and inexpensive method for detection of drug resistance in *Mycobacterium tuberculosis*. *Antimicrob Agents Chemother* 2002;46:2720–2.
- Tuccinardi T, Poli G, Dell'Agnello M, et al. Receptor-based virtual screening evaluation for the identification of estrogen receptor β ligands. *J Enzyme Inhib Med Chem* 2015;30:662–70.
- Poli G, Martinelli A, Tuccinardi T. Reliability analysis and optimization of the consensus docking approach for the development of virtual screening studies. *J Enzyme Inhib Med Chem* 2016;31:167–73.
- Case DA, Berryman JT, Betz RM, Cerutti DS, Cheatham III TE, Darden TA, Duke RE, Giese TJ, Gohlke H, Goetz AW, et al. 2015. AMBER, Version 14. San Francisco, CA: University of California.
- Meanwell NA. Fluorine and fluorinated motifs in the design and application of bioisosteres for drug design. *J Med Chem* 2018;61:5822–80.
- Brosch R, Philipp WJ, Stavropoulos E, et al. Genomic analysis reveals variation between *Mycobacterium tuberculosis* H37Rv and the attenuated *M. tuberculosis* H37Ra strain. *Infect Immun* 1999;67:5768–74.
- Schwyn B, Neilands JB. Universal chemical assay for the detection and determination of siderophores. *Anal Biochem* 1987;160:47–56.



Review

Mycobacterium abscessus, an Emerging and Worrisome Pathogen among Cystic Fibrosis Patients

Giulia Degiacomi ^{1,†}, José Camilla Sammartino ^{1,2,†} , Laurent Roberto Chiarelli ¹ ,
Olga Riabova ³, Vadim Makarov ³ and Maria Rosalia Pasca ^{1,*}

¹ Department of Biology and Biotechnology “Lazzaro Spallanzani”, University of Pavia, 27100 Pavia, Italy; giulia.degiacomi@unipv.it (G.D.); jose.sammartino@iusspavia.it (J.C.S.); laurent.chiarelli@unipv.it (L.R.C.)

² IUSS—University School for Advanced Studies, 27100 Pavia, Italy

³ Bach Institute of Biochemistry, Research Center of Biotechnology of the Russian Academy of Sciences, 119071 Moscow, Russia; obr1973@mail.ru (O.R.); makar-cl@ropnet.ru (V.M.)

* Correspondence: mariarosalia.pasca@unipv.it; Tel.: +39-0382-985576

† These authors contributed equally to this work.

Received: 7 October 2019; Accepted: 20 November 2019; Published: 22 November 2019



Abstract: Nontuberculous mycobacteria (NTM) have recently emerged as important pathogens among cystic fibrosis (CF) patients worldwide. *Mycobacterium abscessus* is becoming the most worrisome NTM in this cohort of patients and recent findings clarified why this pathogen is so prone to this disease. *M. abscessus* drug therapy takes up to 2 years and its failure causes an accelerated lung function decline. The *M. abscessus* colonization of lung alveoli begins with smooth strains producing glycopeptidolipids and biofilm, whilst in the invasive infection, “rough” mutants are responsible for the production of trehalose dimycolate, and consequently, cording formation. Human-to-human *M. abscessus* transmission was demonstrated among geographically separated CF patients by whole-genome sequencing of clinical isolates worldwide. Using a *M. abscessus* infected CF zebrafish model, it was demonstrated that *CFTR* (cystic fibrosis transmembrane conductance regulator) dysfunction seems to have a specific role in the immune control of *M. abscessus* infections only. This pathogen is also intrinsically resistant to many drugs, thanks to its physiology and to the acquisition of new mechanisms of drug resistance. Few new compounds or drug formulations active against *M. abscessus* are present in preclinical and clinical development, but recently alternative strategies have been investigated, such as phage therapy and the use of β -lactamase inhibitors.

Keywords: *Mycobacterium abscessus*; cystic fibrosis; drug resistance; nontuberculous mycobacteria

1. Introduction

Cystic fibrosis (CF) is an autosomal recessive disease characterized by the involvement of respiratory, gastrointestinal, and male reproductive tracts, even if most of the morbidity and mortality arises from CF lung disease [1,2]. In particular, thick airway secretions impair the mucociliary clearance, which increases bacterial colonization and infection [3].

In this context, nontuberculous mycobacteria (NTM) have recently emerged as important pathogens in CF lung disease worldwide [2–4]. Over the last two decades, the incidence of NTM infections among CF patients has raised from 3.3% to 22.6%, increasing morbidity and mortality associated with these pathogens [4–6]. At the same time, for other CF pathogens, such as *Pseudomonas aeruginosa* and *Burkholderia cepacia*, the incidence has significantly decreased [7,8]. Additionally, the NTM incidence is underestimated because of misdiagnosis of NTM infections such as tuberculosis (TB) is common in developing countries; moreover, data from several countries are missing [7,8].

The most commonly identified NTM species in CF individuals are the slow growing *Mycobacterium avium* complex (MAC) and the rapidly growing *Mycobacterium abscessus* complex (MABSC) (95% of CF cases) [2–4]. MABSC is more common in European CF populations and its incidence is globally increasing; moreover, it is frequently found in younger CF patients (including children) and in those with more severe lung disease [4,9,10]. MABSC includes the following *M. abscessus* subspecies: *Mycobacterium abscessus* subsp. *abscessus* (*Mab*), *Mycobacterium abscessus* subsp. *bolletii* (*M. bolletii*), and *Mycobacterium abscessus* subsp. *massiliense* (*M. massiliense*). The MAC predominantly consists of *Mycobacterium avium* subsp. *avium* (*Mav*) and *Mycobacterium avium* subsp. *intracellulare* [2–6].

Among NTM subspecies, *Mab* is becoming the most prominent and worrisome pathogen in hospitals and CF centers around the world [4,7,10,11]. It is the major NTM causing respiratory infections worldwide (up to 80%), most often in immunocompromised patients, such as those with CF and HIV-positive status, and in patients with chronic obstructive pulmonary disease (COPD) and bronchiectasis [4,7,10–16].

Mab drug therapy takes up to 2 years (see below), with only about 30% of patients experiencing successful treatment outcomes [11,17]. *Mab* treatment is also challenging, since failed eradication leads to an accelerated lung function decline. *Mab*-infected CF patients are even excluded from lung transplant lists in some countries. Consequently, in this cohort of patients, preventing *Mab* infection is essential. Room cleaning protocols have recently been changed and *Mab*-infected CF patients are now hospitalized in specialized CF centers, where there are 15 independent air changes per hour in the rooms to remove potentially infectious aerosol, thus preventing transmission [12].

Mab's success in becoming an emerging CF pathogen is due to several reasons, including:

1. Possible direct person-to-person transmission;
2. Biofilm and drug resistance;
3. Association between *CFTR* (cystic fibrosis transmembrane conductance regulator) mutations and formation of granuloma in the presence of *Mab* infection;
4. Lack of active drugs (in particular with bactericidal activity) (Figure 1).

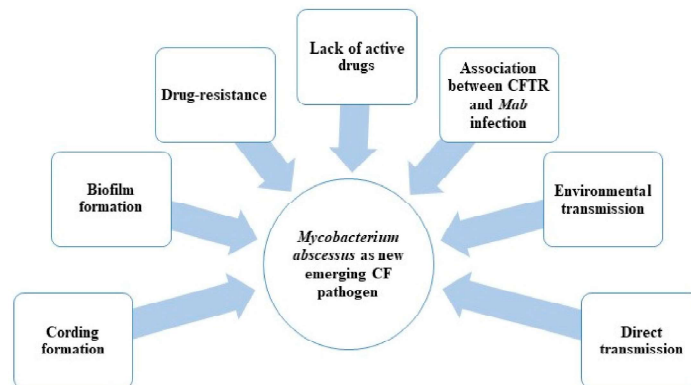


Figure 1. Factors contributing to the spread of *M. abscessus* (*Mab*) as an emerging pathogen among cystic fibrosis (CF) patients. CFTR: cystic fibrosis transmembrane conductance regulator.

In this review, we will focus on analyzing all of these aspects in order to find a possible “Achilles’ heel” to fight this emerging pathogen.

2. Possible *M. abscessus* Direct Transmission among CF Patients

Mab, similar to other NTM subspecies, is ubiquitous in the environment, such as in soil and drinking water, and remains viable even after water treatment. Therefore, this pathogen can survive in environments near to human populations, particularly in human water sources, including hospital and domestic water supplies [16]. *Mab* and other NTM subspecies are also commonly found in urban water plumbing and water systems, sometimes in symbiosis with Amoebae [18–27]. Moreover, *Mab* has been isolated from fish [28–33] and animals [34–40], who could also represent reservoirs for human infections. This makes exposure common and disinfection difficult, which is very problematic in healthcare settings [7,15,16,19,23].

However, in sporadic and epidemic *Mab* infections, the pathogen is almost never isolated from the closest environment [7].

Until recently, it was believed that among CF patients, the majority of *Mab* infections were acquired by individuals through exposure to soil, household dust, or water, potentially via fomites and aerosols [41]. The mode of *Mab* transmission is still under investigation, and only recently was human-to-human *Mab* transmission demonstrated using whole-genome sequencing (WGS) [11,14,42].

In fact, Bryant et al. (2016) [14], using WGS of prominent worldwide *Mab* clinical isolates, showed that the majority of infections were acquired through direct transmission, potentially via fomites and aerosols. In particular, they generated WGS of 1080 *Mab* clinical isolates from 517 patients, obtained from CF centers from Europe, the United States, and Australia. They also identified that 74% of isolates were clustered in three dominant circulating clones: *Mab* clusters 1 and 2 and *M. massiliense* cluster 1. These 3 clusters were present in all CF centers, indicating transcontinental spreading of these strains by a possible human-to-human transmission within the global CF patient community. The clustered strains presented less than 20 single-nucleotide polymorphisms (SNPs), indicating a high level of human-to-human transmission among geographically separated CF patients [14]. Interestingly, these clustered *Mab* isolates were associated with bad clinical outcomes and presented increased virulence *in vivo*, thus representing an urgent international challenge [14].

According to the previous study, Yan et al. (2019) performed WGS of *Mab* isolates from 22 CF patients [43]. WGS identified a cluster of three CF patients infected by *Mab* isolates that differed by < 7 SNPs, suggesting a possible direct transmission among them. Several hospital attendances were found in common for these 3 patients, even if they were hospitalized in separate single rooms and there were no known social links between them [43]. The genomes of these *Mab* isolates are very similar to those previously described, confirming the presence of global circulating *Mab* clones in CF centers [14].

An additional study evaluated the transmission of *Mab* isolates in 4 Italian CF centers using the WGS of clinical isolates [44]. They found 7 possible person-to-person transmissions (SNP difference cut-off of < 30); only three CF patients were hospitalized in the same CF center at the same time [44]. Moreover, one of the *Mab* clusters identified in this study is the same as cluster 1 detected by Bryant and collaborators [14,44], again highlighting the presence of circulating virulent *Mab* strains worldwide in CF centers.

These last studies [14,43,44] show how it is possible to monitor human-to-human *Mab* transmission by WGS approach only, and to ascertain if different patients, even if geographically separated, share the same strain. *Mab* and *M. massiliense* belong to the same complex (MABSC) [2]; at this point, it is important to underline that the possibility of direct transmission for *M. massiliense* subspecies was also shown by genomic approach [14]. How human-to-human direct *Mab* transmission occurs is still under investigation.

Moreover, the human-to-human transmission helped *Mab* evolution from an environmental bacterium to a transmissible human pathogen. This evolution also affected the strategies used in CF centers to contain *Mab* infections. Before this last discovery, effective sterilizing techniques and other hygiene practices were performed to reduce the risk of environmental *Mab* transmission. Now, the *Mab* infection control recommendations include general infection control measures (e.g., hand

washing) and advise the segregation of infected CF patients from the other ones in order to avoid direct transmission [12].

3. Pathogenesis of *M. abscessus*

The most common *Mab* infection sites are the respiratory tract, the skin, and soft tissue [4].

It is well known that predisposing factors for *Mab* pulmonary infections are chronic bronchiectasis and CF disease, as in these conditions the pathogen can firstly develop a biofilm, colonizing the host, and later progress into an invasive disease [45–47]. The progress of *Mab* infection in the CF lung is still under investigation [47], but a recent study showed that *Mab* aggregates form a biofilm around lung alveoli [48]. It is noteworthy that mycobacteria growing in biofilms are more tolerant to antibiotics, contributing to their drug resistance [49].

Moreover, the *Mab* cell wall contributes largely to its drug resistance and to its pathogenicity, thanks to the large presence of complex lipids, among which are five major glycopeptidolipids (GPLs) that differ in location or number of acetyl and sugar moieties [49–53].

Because of its peculiar cell wall, *Mab* shows smooth (S) or rough (R) colony morphologies, associated with distinct in vitro and in vivo features. In particular, the wild-type S strains produce abundant GPLs and minimal trehalose dimycolate (TDM), whilst R mutants have genetic lesions in the GPL loci, producing little or no GPLs and higher levels of TDM [49,50,53,54]. TDM, contributing also to the *Mycobacterium tuberculosis* virulence, was found on the surface of *Mab* R strains [53,54]. In fact, TDM is responsible for the cording phenotype, a key factor in increasing *Mab* virulence, causing invasive infection [53]. The lack of cording in the S variant may be due to the presence of GPLs masking other cell surface molecules (e.g., TDM) that activate innate immunity, causing inhibition of the macrophage apoptotic response, reduced production of radical oxygen species (ROS), and limitation of the spread of *Mab* among macrophages [49–55]. Furthermore, the high presence of GPLs in S strains is responsible for the formation of a robust biofilm during the infection [48,49].

The *gpl* locus is highly conserved in *Mycobacterium smegmatis*, *Mab*, and *Mav* [50]. This locus contains *mmpS4*, *mmpL4a*, and *mmpL4b* genes, which encode membrane proteins essential for the GPL biosynthesis and transport across the plasma membrane [50,56,57]. The transition from high-GPL (S strains) to low-GPL producers (R strains) is linked to mutations in genes involved in GPL biosynthesis and transport, similar to in the crucial Tyr/Asp couples in *MmpL4a*/*MmpL4b*. In fact, it was shown that point mutations in *MmpL4a* at Tyr842 or *MmpL4b* at Tyr854 caused loss of GPL production, suggesting that no functional redundancy exists between *MmpL4a* and *MmpL4b* [56]; moreover, the disruption of *mmpL4b* in *Mab* S strain inhibits GPL production, causing an R morphotype [58]. Then, the *Mab* S-to-R transition leads to the following events:

- Arrest of lipid transport;
- Production of serpentine cords;
- Growth as extracellular cords, allowing escape from the innate immune defenses;
- Induction of a strong humoral response that contributes to acute and severe infections [51,53–55,58].

The high virulence of *Mab* R mutants was confirmed in in vivo infection models, such as with zebrafish, where the transition to the R morphotype is characterized by an increased virulence because of the cording formation, which is responsible for invasive infection and larval death [55,56,59,60]. Moreover, it was found in a zebrafish model that the inactivation of *MAB_4780*, encoding a dehydratase required for cording formation, strongly affects *Mab* R pathogenicity; this attenuation causes both cord deficiency and intracellular growth impairment [60]. Furthermore, the *Mab* R strains induce more aggressive and invasive pulmonary disease, particularly in CF patients; in fact, these mutants are more frequently isolated after a long persistent infection and are associated with increased lung function decline [48,53,61–64].

Consequently, the possibility of transition between S and R morphotypes is very relevant in *Mab* pulmonary infection in CF patients [59,61,62]. These patients are particularly susceptible to

colonization by biofilm-forming bacteria because of their altered lung physiology. In these conditions, *Mab* S strains expressing GPL may be favored [65]. A rough cord-forming variant could emerge from CF patients chronically colonized with an S strain, giving a more aggressive, invasive pulmonary infection [60–63].

The presence of the two morphotypes in *Mab* is also fundamental to its escape from the innate immune system. In particular, the innate immune response to pulmonary pathogens is mediated by the expression of TLR2 and then of IL-8 and human b-defensin 2 (HbD2) from the respiratory epithelial cells. It was shown that only *Mab* R strain stimulates the expression of IL-8 and HbD2, while *Mab* S variant is able to “mask” the bioactive cell wall lipids with GPLs. Because S variants are predominant during the first phases of infection, *Mab* is then able to avoid the innate immune system [51].

Another *Mab* peculiarity is that although it is a rapid grower, it persists in lungs associated with granulomatous lesions, a landmark of *M. tuberculosis* infection. Recently, Dubois et al. (2018) showed that an *mmpL8* deletion mutant presented a decreased intracellular viability in a zebrafish model and a diminished propensity to induce granuloma formation [66]; moreover, this mutant had impaired adhesion to macrophages. In fact, *MmpL8* is also required for the production of a glycolipid (glycosyl diacylated nonadecyl diol alcohol (GDND)), which is derived from a combination of oleic and stearic acids. In *mmpL8* knock-out (KO) mutant, the reduced GDND production could be the cause of the modified interaction between bacteria and macrophages, resulting in a decreased virulence [66].

Finally, Laencina and collaborators (2018) [67] demonstrated that genes belonging to *Mab* ESX-4 locus are essential for its intracellular survival inside amoebae and macrophages. Interestingly, a *Mab* mutant with a deletion in *eccB4* gene, coding for a structural key ESX component, was attenuated. In fact, it was less efficient at blocking phagosomal acidification and failed to damage phagosomes. The authors speculated that because *Mab* lacks ESX-1, ESX-4 could be a surrogate of *M. tuberculosis* ESX-1 [67].

CFTR Mutations Specialize M. abscessus as CF Pathogen

Recently, steps were taken to decipher why CF patients are so predisposed to *Mab* infections. Using zebrafish model, Bernut and collaborators (2016) showed that both macrophages and neutrophils are required to control *Mab* infection; moreover, impaired TNF signaling produced aberrant granulomas, and subsequent larval death [68].

In 2019, the same research group demonstrated that *CFTR* participates in neutrophil chemotaxis to the infected *Mab* sites, stimulating the oxidative host defenses [69]. In fact, in a zebrafish model, *Mab* infection was characterized by the recruitment of the bacilli by macrophages; in particular, the activation of macrophages resulted in neutrophil chemotaxis leading to granuloma formation, and ROS production by NOX2, which led to intracellular *Mab* death. In these conditions, the granuloma sequestered *Mab*, containing the infection [69]. Otherwise, *Mab*-infected, *CFTR*-depleted zebrafish were rapidly infected; in this case, the *CFTR* dysfunction reduced both macrophage bactericidal activity and neutrophil recruitment to form the protective granulomas [69]. Interestingly, these findings are only observed with *Mab* and not with other mycobacteria; consequently, *CFTR* seems to have a specific role in the immune control of only *Mab* infections [68,69].

These findings clarified the increasing emergence of *Mab* as a CF pathogen. Therefore, *Mab*'s intrinsic drug resistance often results in long therapies and poor clinical outcomes in CF patients [17,70,71], accelerating lung function decline at a greater rate than other bacteria, including *Pseudomonas aeruginosa* and *Burkholderia cepacia* [8,63,65].

Mab is often called the “incurable nightmare” because the cure rate among CF patients with *Mab* pulmonary infection is only 25%–58% [8,64,65]. CF patients with *Mab* infection are more likely to require transplant or to die despite adequate treatment [65,71,72]. However, CF patients with pre-transplant *Mab* infection could develop post-transplant invasive *Mab* disease. In selected CF patients, surgical resection of infected lung tissue could be beneficial. Consequently, progressive *Mab*

disease, despite antibiotic therapy, is considered as a contraindication for lung transplantation by several CF centers, and is associated with treatment failure and increased mortality [65,70–72].

Recently, the U.S. Food and Drug Administration (FDA) approved Trikafta (elexacaftor/tezacaftor/ivacaftor) for the treatment of CF in people aged 12 years and older who have at least one F508del mutation in the *CFTR* gene. The approval of Trikafta was supported by positive results of two global Phase 3 studies [73,74].

If the association among *CFTR* mutation and *Mab* infection is validated, indirectly, Trikafta could also protect CF patients from this pathogen. For this reason, it is mandatory to investigate this topic further, in particular for CF patients.

4. Current Therapy against *M. abscessus* Infections

Unfortunately, antitubercular drug use is limited in the management of *Mab* infections, since this bacterium possesses extremely high intrinsic and acquired antibiotic resistance, making its eradication more difficult. *Mab* drug treatment in CF is even more challenging because thick mucus secretions cause an increased renal drug clearance and a possible decreased gastrointestinal absorption [17,71].

In 2016, the recommendations for NTM management in CF were published [17,71]. The treatment duration was 1 year following culture conversion (the time of conversion starts from the date of the first of three consecutive negative cultures) [17,71]. *Mab* treatment consists of an intensive phase of therapy followed by a continuation phase. The intensive phase should include daily oral macrolide treatment (preferably azithromycin) in conjunction with 3–12 weeks of intravenous (IV) amikacin and one or more of the following antibiotics: IV tigecycline, imipenem, or ceftazidime. The duration of the intensive phase of therapy depends on the type of infection and the tolerability of the treatment [71]. The continuation phase includes the following drugs: inhaled amikacin and a quotidian oral macrolide (preferably azithromycin), in addition to 2–3 oral antibiotics (to be chosen from minocycline, clofazimine, moxifloxacin, and linezolid) [71] (Figure 2).

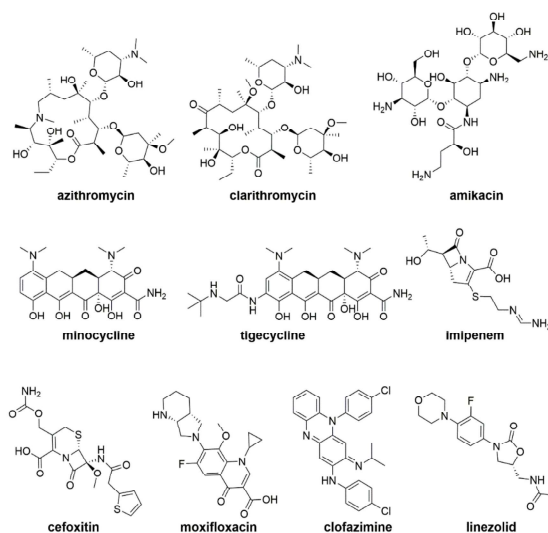


Figure 2. Drugs currently used in *Mab* therapy.

Moreover, in agreement with the current American Thoracic Society guidelines, in order to prevent the emergence of macrolide resistance, clarithromycin and azithromycin must be prescribed in combination with other drugs [17,71]. Lastly, the interactions with other chronic medications could affect the tolerance and efficacy of the antibiotic therapy [2].

Mechanisms of Resistance to Drugs Used in Therapy

As mentioned above, *Mab* is intrinsically resistant to many drugs, including several antitubercular drugs, because of its physiology. At the same time, this pathogen acquired new mechanisms of drug resistance through genomic mutations. In fact, the long drug treatment contributed to the spreading of drug-resistant strains caused by development of mutations either in the target or in other related genes [8,11,75,76]. In this way, drug efficacy is seriously compromised. Several factors contribute to its intrinsic and acquired drug resistance, such as target gene mutations, drug efflux, an impermeable cell wall, and antibiotic-modifying or -inactivating enzymes [11,75,76]. Moreover, particularly among CF patients, respiratory habitats where *Mab* is very close to other pathogens (for example, *P. aeruginosa*) could represent reservoirs for transfer of novel drug resistance or virulence genes [75].

The most important and common mechanisms of acquired resistance to drugs used in *Mab* therapy are reported below (Table 1).

Table 1. Mechanisms of resistance to current drugs used against *Mab* infections.

Drugs	Targets	Mechanism of Resistance	Enzymes/Proteins Related to Mechanism of Resistance	References
Macrolides	23S rRNA	Mutations in target gene	Rrl (<i>MAB_r5052</i>)	[77,78]
		Modification of target	Erm(41) (<i>MAB_2297</i>)	[77]
		Induction of WhiB7 activator	Activation of <i>Erm(41)</i> (<i>MAB_2297</i>)	[8,79]
Aminoglycosides	30S subunit of ribosome	Mutations in target genes	16S rRNA (<i>rrs</i> , <i>MAB_r5051</i>) RpsL (<i>MAB_3851c</i>)	[80,81]
		Enzymatic drug modification	AAC(2') (<i>MAB_4395</i>) Eis2 (<i>MAB_4532c</i>)	[75]
		Induction of WhiB7 activator	Activation of <i>eis2</i> (<i>MAB_4532c</i>)	[8,79]
β -lactams	Penicillin-binding protein	Enzymatic drug modification	Bla_Mab (<i>MAB_2875</i>)	[82]
Tetracyclines	30S subunit of ribosome	Enzymatic drug modification	Mab1ctX (<i>MAB_1496c</i>)	[83]
Clofazimine		Mutations in the repressor → Over-expression of an efflux pump	MAB_2299c	[84]
Fluoroquinolones	A subunit of DNA gyrase	Mutations in target gene	GyrA (<i>MAB_0019</i>)	[85,86]
		Other mechanisms?	not detected	[86]
Linezolid	23S rRNA	Mutations in target gene	Rrl (<i>MAB_r5052</i>)	[87]
		Efflux pumps?	LmrS and MmpL9?	

The macrolides, which are used in *Mab* therapy, bind in the peptide exit tunnel of the ribosome, preventing the growth of the peptide chain and consequently inhibiting protein synthesis [88]. In fact, in several *Mab* isolates, high levels of macrolide resistance are linked to mutations in the peptidyltransferase-binding region of the 23S rRNA gene [77,88]. Critical mutations in nucleotides 2058 and 2059, which are involved in the binding of macrolides to ribosomes, are a frequent cause of constitutive macrolide resistance in *Mab* [78]. In fact, the acquisition of 23S rRNA gene mutations during therapy with macrolides has been reported for several NTM species, in particular for *Mab* [77,89].

Mab erm(41) gene encodes a methyl-transferase that modifies the clarithromycin ribosomal binding site, causing resistance [77]. In particular, the inactivating enzyme Erm(41) methylates A2058 in the peptidyltransferase region of the 23S rRNA (the drug target), preventing the binding with macrolides [8,77,88]. The T28C polymorphism in *erm(41)* sequence is responsible for the inducible

macrolide resistance in *Mab* [78,79]. The long duration of *Mab* macrolide therapy could be the major cause of the spreading of constitutively macrolide-resistant isolates [77,78,88,89]. This mechanism of drug resistance is not present in *M. massiliense*, since it harbors a deletion in the *erm(41)* gene [77,89].

The mechanism of resistance to aminoglycosides in *Mab* is mainly based on the modification of the 30S subunit of the ribosome (the drug target); in fact, the 16S rRNA (*rrs*) and *rpsL* genes are mutated in the 90% of cases of aminoglycoside resistance. In particular, mutations at position 1408 of the *rrs* gene in *Mab* clinical isolates are associated with aminoglycoside resistance [8,80]. In addition, other *Mab* mutations related to high level of aminoglycoside resistance were isolated *in vitro* in the *rrs* gene at position 1406, 1409, and 1491 [81].

Furthermore, the enzymatic drug modification could be the cause of *Mab* aminoglycoside resistance. The *Mab* 20-N-acetyltransferase (AAC(2')), encoded by *MAB_4395* gene, is able to acetylate several aminoglycosides. In fact, a *Mab* strain harboring a deletion of *MAB_4395* is more sensitive to aminoglycosides (4–64 fold reduction in the Minimum Inhibitory Concentration (MIC)) [75]. Moreover, another N-acetyltransferase, named Eis2 (coded by *MAB_4532c*), is able to modify aminoglycosides, conferring resistance in *Mab* strains [75].

Cefoxitin (cephalosporin) and imipenem (carbapenem) are the only two β -lactams used in therapy against *Mab*. Regrettably, this pathogen produces a strong, constitutive class A β -lactamase (Bla_ *Mab*, encoded by *MAB_2875*) responsible for β -lactam resistance [82]. Imipenem and cefoxitin are hydrolyzed at a very slow rate by Bla_ *Mab*, contributing to their clinical activity.

Tetracycline affects bacterial protein synthesis by binding the 30S ribosomal subunit and interfering with the delivery of aminoacylated tRNA to the A-site. *Mab* resistance to tetracycline is conferred by the tetracycline inactivating monooxygenase MabTetX (coded by *MAB_1496c*) [83]. Sublethal concentrations of tetracycline confer a strong induction of MabTetX; a strain with a deletion in *MAB_1496c* is highly sensitive to this drug. However, tigecycline, a glycylcycline tetracycline, is a poor substrate of MabTetX and is not able to induce the expression of MabTetX [83].

Clofazimine and bedaquiline are two drugs used for TB treatment; recently, clofazimine was introduced in *Mab* therapy, whilst bedaquiline is under preclinical evaluation. Both drugs have a common mechanism of resistance in both *M. tuberculosis* and *Mab* [84,90], consisting of mutations in the gene coding for the repressor of the efflux pump MmpS5-MmpL5 (*Rv0678* in *M. tuberculosis* and *MAB_2299c* in *Mab*) [84,90].

Mutations in *gyrA*, which codes for the fluoroquinolone target DNA gyrase, have been related to resistance in *Mab* [85,86]. However, in a recent study, in which 105 MAC or MABC clinical isolates were analyzed, including 72 resistant to moxifloxacin, no clear correlation was found between mutations in *gyrA* and *gyrB* genes and fluoroquinolone resistance, indicating that other new mechanisms of resistance should be involved [86].

Linezolid, belonging to the oxazolidinone class, is active against *Mab* growth. The main mechanism of resistance involves mutations in 23S rRNA (coded by *rrl- MAB_r5052*), the drug target, and in ribosomal proteins (L3, L4, and L22) [87]. Currently, the contribution of some efflux pumps to linezolid resistance is being also investigated [87].

The WhiB7 regulator, encoded by *MAB_3508c*, is a multi-drug inducible transcriptional regulator that activates the expression of genes, conferring aminoglycoside and macrolide resistance (*eis2* and *erm(41)*, respectively) in *Mab* [8,79]. WhiB7 is strongly induced when exposed to antibiotics that target the ribosome, such as erythromycin, clarithromycin, amikacin, tetracycline, and spectinomycin. The strong induction of WhiB7 confers amikacin and clarithromycin resistance; deletion of *MAB_3508c* gene renders *Mab* more susceptible to amikacin and clarithromycin [8,79].

5. New Drugs and New Treatments in Preclinical and Clinical Trials

As reported above, the acquired mechanisms of resistance to drugs used in therapy limit the efficacy of the current *Mab* treatment; for this reason, new active compounds with a novel mechanism of action are needed.

Choo et al. (2014) [91] demonstrated that the *Mab* genome shares considerable sequence similarity with that of *M. tuberculosis*. Consequently, the already generated data in TB drug discovery could also be used to identify new compounds active against *Mab* and other NTM [91]. Unfortunately, only a few antitubercular drugs, such as bedaquiline, are active against *Mab* growth, and are currently under evaluation for their use in therapy.

The *Mab* drug discovery is considered very challenging because of the typical lack of bactericidal activity, both in the currently recommended *Mab* treatment and in new tested compounds; it could be the reason for the poor therapeutic success in *Mab* infection [92]. For example, among the drugs currently used in *Mab* treatment, tigecycline and imipenem are bacteriostatic, while clarithromycin presents only a weak bactericidal activity at high concentrations [92]. The antitubercular bedaquiline is active against *Mab* growth, but it is also bacteriostatic (see below) [8]. The bacteriostatic activity could depend on the presence of several chromosomally encoded drug-modifying enzymes, the typical mycobacterial cell wall, or the presence of GLPs.

The new drugs that are active against *Mab* should, therefore, be bactericidal in order to be more effective. Moreover, new drug combinations, as well as repurposed compounds, are being tested against this pathogen.

Despite some active compounds being in preclinical development, only a few compounds are present in clinical trials (Table 2). It is noteworthy that several clinical trials include CF patients, highlighting the emerging role of *Mab* in this cohort of patients. Some drugs active against *Mab* growth, which are currently both in preclinical and in clinical trials, are described below (Table 2; Figure 3).

Table 2. Compounds in preclinical and clinical development against *Mab* infections.

Drugs	Development Phase	Target	Mechanism of Resistance	References
Bedaquiline	Preclinical studies	ATP synthase	MmpS5-MmpL5 efflux pump	[84,93–98]
Tedizolid	Preclinical studies	50S ribosome	-	[99]
Delpazolid	Preclinical studies	50S ribosome	-	[100]
Indole-2-carboxamides	Preclinical studies	MmpL3	-	[101–103]
PIPDI	Preclinical studies	MmpL3	-	[104]
SQ641	Preclinical studies	Translocase-1	-	[105]
Rifabutin	Preclinical studies	RNA polymerase	-	[106,107]
Disulfiram	Preclinical studies	-	-	[108]
β-lactams (combinations)	Preclinical studies	Penicillin-binding protein	Bla_Mab	[82,109–112]
Tigecycline	Phase II	30S subunit of ribosome	-	[83,113,114]
Nitric oxide	Phase II	-	-	[113,115,116]
Liposomal Amikacin for Inhalation	Phase II	23S rRNA	-	[113,116,117]
Inhaled Molgramostim	Phase II	-	-	[113,116]

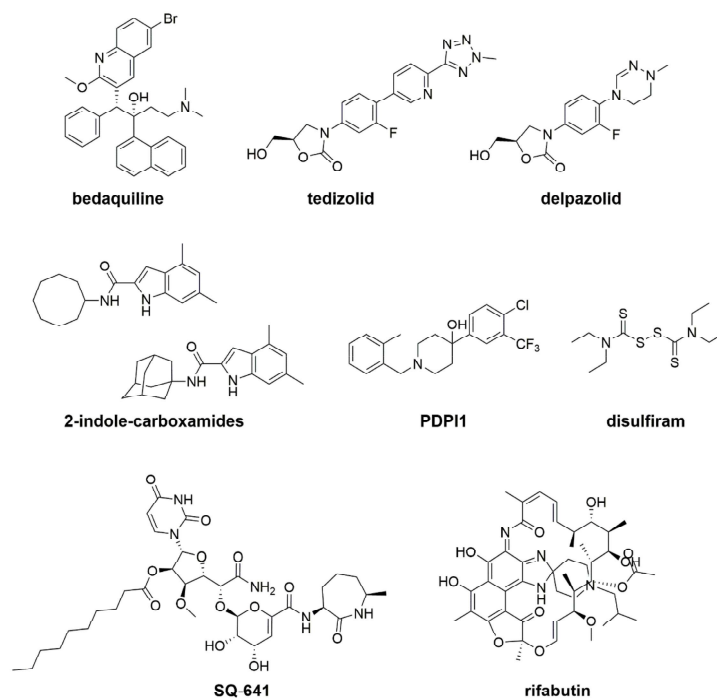


Figure 3. Anti-Mab drugs in preclinical and clinical studies.

5.1. Bedaquiline

Bedaquiline (BED), an antitubercular drug belonging to diarylquinoline class, was approved by the U.S. Food and Drug Administration (FDA) in 2012 for the treatment of patients affected by pulmonary MDR- and XDR-TB only [118–120]. BED targets the mycobacterial ATP synthase (subunit c encoded by *atpE*) [120]. Another mechanism of resistance is linked to mutations in the *M. tuberculosis Rv0678* gene, which codes for the transcriptional repressor of the MmpS5-MmpL5 efflux system, causing cross-resistance between clofazimine and BED [90]. BED is also active against MAC and MABSC species, and its possible use is under evaluation because it lacks bactericidal activity, as previously described [93]. Moreover, *Mab* shares the same mechanism of BED resistance as *M. tuberculosis*; in fact, Mab_4383/Mab_4382 and Mab_4384 in *Mab* are homologous to MmpS5/MmpL5 and Rv0678 in *M. tuberculosis* [84,90]. Several BED-resistant *Mab* strains harbored mutations in the Mab_4384 gene, and consequently an over-expression of MmpS5-MmpL5 efflux pump as a mechanism of resistance [84,94]. Recently, it was shown that verapamil, an efflux inhibitor, improved the BED activity against *Mab* clinical isolates, both in vitro and *ex vivo* [95].

Conflicting results were found when BED was tested in vivo, possibly because of its bacteriostatic activity; in a mouse model the BED treatment seemed to reduce the bacterial load [96], while in another murine model BED did not present any activity [97]. Interestingly, BED was highly effective in a zebrafish model of *Mab* infection; in particular, a short BED treatment was able to protect the *Mab*-infected larvae [98].

Overall, more studies are needed in order to understand if BED could be used against *Mab* infections, overtaking the problem related to its bacteriostatic activity and its mechanism of resistance. Different approaches could be performed, such as the use of BED in combination with an efflux inhibitor or the synthesis of new more effective BED derivatives.

5.2. New Oxazolidinone Derivatives: Tedizolid and Delpazolid

Linezolid, belonging to the oxazolidinone class, is administrated in NTM treatment, including *Mab* infections, but its clinical use is often related to adverse events. Recently, two other oxazolidinones were found to be more active against NTM than linezolid: tedizolid and delpazolid [99,100].

Currently, the most promising anti-*Mab* oxazolidinone is delpazolid, which is in phase II trials for TB treatment; it is active against *Mab* both in vitro and in vivo, likely without adverse effects [100].

5.3. MmpL3 Inhibitors: Indole-2-Carboxamides and PIPD1

Recently, MmpL3 inhibitors were found to be very effective against both *M. tuberculosis* and *Mab* [101–104,121].

Two lead compounds belonging to indole-2-carboxamides showed a potent bactericidal activity against *Mab* in vitro (MIC = 0.125 µg/mL) and *ex vivo*. Moreover, they were also active against a panel of *Mab* clinical isolates. It was shown that their cellular target is the mycolic acid transporter MmpL3. In particular, the indole-2-carboxamides strongly inhibited the transport of trehalose monomycolate, causing the loss of trehalose dimycolate production and abrogating mycolylation of arabinogalactan [101]. Moreover, these compounds showed minimal in vitro cytotoxicity and good selectivity indices [102]. Finally, in 2019 Pandya and collaborators tested the two lead compounds in vivo using a *Mab*-infected mouse model. Oral administration of the MmpL3 inhibitors showed a statistically significant reduction in bacterial load in the lungs and spleens of *Mab*-infected mice [103]. This last study confirms that indole-2-carboxamides are very promising anti-*Mab* compounds.

Dupont and collaborators (2016) performed a screening of a library of 177 anti-TB compounds against *Mab* growth. A new piperidinol-based molecule, PIPD1, was identified and characterized as having a potent bactericidal activity against *Mab*. Thanks to the isolation and characterization of some resistant *Mab* mutants, MmpL3 was identified as a cellular target [104]. Moreover, the treatment with PIPD1 in the *Mab*-infected zebrafish model decreased bacterial load and improved survival of the infected embryos [8].

MmpL3 represents the only new *Mab* drug target; moreover, the bactericidal activity of MmpL3 inhibitors indicates this target as one of the most druggable ones for this pathogen.

5.4. Capuramycin SQ641

Capuramycins are a novel class of nucleoside antibiotics targeting translocase-1, which is essential for peptidoglycan synthesis. SQ641 is the most active capuramycin against *Mab* growth (MIC = 0.25–1 µg/mL) and it is bactericidal. Furthermore, SQ641 showed synergy with rifabutin and streptomycin against *Mab* [105].

5.5. Repurposing and Repositioning Drugs: Rifabutin, Disulfiram, and β -Lactams

One of the strategies of discovery for new antimicrobial drugs is to reposition or to repurpose existing antibiotics, thus reducing the cost and time of their clinical development.

Following this aim, Aziz et al. (2017) identified rifabutin as a hit against *Mab* growth, starting from a screening of 2700 FDA-approved drugs [106]. Moreover, this drug is bactericidal against *Mab* and also effective *ex vivo*, even if other rifamycins are not active against this pathogen. Rifabutin has synergistic activity in several drug combinations, such as with amikacin, cefoxitin, linezolid, clarithromycin (in triple combination with tigecycline), and azithromycin [107].

Disulfiram is a drug used in the treatment of alcoholism. It was demonstrated that it has an antimicrobial activity against several microorganisms, and clinical trials for its use in treatment of a

spectrum of diseases, such as HIV infection, are in progress. Surprisingly, disulfiram is active *in vitro* and *ex vivo* against *Mab*, showing time- and concentration-dependent killing, similar to amikacin [108]. It also synergized with moxifloxacin, ciprofloxacin, vancomycin, teicoplanin, and amikacin. In a murine model infected with *Mycobacterium fortuitum*, disulfiram significantly reduced bacterial counts in kidneys; consequently, it could also be active *in vivo* against *Mab* [108].

Currently, in the guidelines for treatment of *Mab* infections, only the two β -lactams ceftazidime and imipenem are included [109]. BlaMab is a very active β -lactamase encoded by a chromosomal gene [82], and it is responsible for the poor efficacy of β -lactams against *Mab*, as previously indicated. Interestingly, avibactam is a β -lactamase inhibitor, approved by the FDA in 2014, able to efficiently inhibit the β -lactamase BlaMab [110]. Recently, 206 paired combinations of antibiotics (β -lactams, β -lactamase inhibitors, rifamycins) were tested for *in vitro* synergy against *Mab* growth. Only 24 combinations exhibited synergy. Of these, 13 combinations included two β -lactams; 5 a β -lactam and avibactam; 6 included a β -lactam and a rifamycin. In the 5 combinations with avibactam, the MICs of three β -lactams (cefuroxime, imipenem, and biapenem) were reduced to below therapeutic breakpoints [111].

Pandey and collaborators (2019) discovered that the combinations of ceftazidime with either ceftaroline or imipenem were synergistic and had clinically relevant activities against clinical MABC isolates. Interestingly, these last β -lactams combinations were also active against THP-1 human macrophages infected with three different *Mab* clinical isolates [112].

Furthermore, the evaluation of these repositioning drugs (rifabutin and disulfiram, combinations of β -lactams) for their use in therapy against *Mab* is an interesting field of research and could complement the lack of new compounds against this pathogen. Even if more studies are needed, the recent findings of the inhibitory effect of avibactam against *Mab* β -lactamase support this research field.

5.6. Tigecycline

Tigecycline is a glycylyccline tetracycline in phase II of clinical development [83,113]. In this clinical trial, data were collected from 52 patients (58.3% with CF). Interestingly, in >60% of patients with *Mab* infections, including those with CF, an improvement was found when tigecycline was added to a multidrug treatment for ≥ 1 month [113,114].

5.7. Inhaled Formulation Nitric Oxide

An inhaled formulation of Nitric oxide (NO) is in phase II of clinical development for the treatment of *Mab* and the other NTMs [113].

NO is physiologically formed from L-arginine by NO synthase, and it plays an essential role in a variety of biological processes in the lung, including host defense against pathogens. Unfortunately, the airways of CF patients are NO-deficient, contributing to impaired lung function. Consequently, the increase of airway NO level is related to an improvement in lung function.

For this reason, NO is considered to be very promising against NTM infections. Bentur et al. (2019) evaluated the efficacy, safety, and tolerability of the intermittent inhaled NO in 9 CF patients with refractory *Mab* lung infection through a prospective, open labeled, multi-center, pilot study [115]. The treatment did not result in a *Mab* culture conversion (defined as 3 consecutive monthly negative culture of sputum samples), but caused a reduction in airway bacterial load. The main limitation of this study was the small number of CF-treated patients; additional clinical studies, for example with the use of larger cohorts of CF patients as well as an increase in the duration of NO therapy, are needed to understand the potential of this treatment [115].

5.8. Liposomal Amikacin for Inhalation

Liposomal amikacin for inhalation (LAI) is an inhaled drug in phase II of clinical development [113,116]. It is a novel formulation of amikacin, characterized by reduced toxicity and consequently an improved effectiveness in patients with refractory *Mab* lung disease. Caimmi and collaborators (2018) prescribed LAI to 5 CF patients with *Mab* infection at the Montpellier CF Center. Interestingly, 3 patients completed the treatment and did not have any respiratory exacerbation, showing negative cultures for *Mab* in their sputum [117].

Currently, another study is in progress, including 30 CF patients and the efficacy, safety, and tolerability of once-daily dosing of LAI 590 mg for 12 months [116].

5.9. Inhaled Molgramostim

Inhaled molgramostim is a formulation of granulocyte macrophage-colony-stimulating factor. It is a protein naturally occurring in the human immune system that plays an important role in activating the immune system to kill bacteria such as NTM. A phase 2 study is currently underway to test the effectiveness of inhaled mogramostim against NTM (including *Mab*) in adults with CF [113,116].

6. Conclusions and Future Perspectives

Mab is becoming one of the most frightening CF pathogens, as previously underlined. Clinical isolate sequencing has demonstrated that human-to-human *Mab* transmission is possible, further threatening CF patient health and contributing to its spread [14,43,44]. *Mab* virulence among CF patients is related to three important factors: (1) the transition from the S variant, important for colonization, to the R strain, fundamental for cell invasion [53]; (2) the GLPs of S strains, which are able to masquerade TDM and other lipids responsible for the activation of the innate immune system [51]; (3) the role of *CFTR* mutations in promoting *Mab* infections, as *CFTR* seems to have a specific role in the immune control of only this pathogen [69].

A key challenge for *Mab* infection treatment is to develop new strategies for its eradication, since, current therapy is poorly effective and no new drugs are on the horizon.

Alternative strategies, such as phage therapy, have already been investigated. Recently, after bilateral lung transplantation, a 15-year-old girl with CF and a disseminated *Mab* infection was successfully treated with a phage therapy [122,123]. This was the first therapeutic use of phages for a human mycobacterial infection, which was also well tolerated and without adverse reactions. This amazing result opens the possibility to use phage therapy against *Mab* infections in CF patients, even if accurate clinical trials are needed.

The finding of the β -lactamase inhibitor avibactam that effectively blocked Bla_*Mab* provides a new chance for the use of old antibiotics, such as β -lactams. Le Run and collaborators (2019) showed that the addition of avibactam improved the activity of the imipenem–tedizolid combination [124]. Interestingly, Lefebvre et al. (2017) demonstrated that the inhibition of Bla_*Mab* by avibactam improved the efficacy of imipenem against *Mab* *in vitro*, in macrophages and in zebrafish models [125], indicating that it should be clinically evaluated. It is noteworthy that the aztreonam–avibactam and ceftazidime–avibactam combinations are in phase I of clinical development for Gram-negative infections [113].

Among the possible new approaches, an interesting anti-virulence strategy could be exploited for inhibiting MAB_4780, the dehydratase required for cording formation [62], which is essential for *Mab* pathogenicity. This alternative approach to standard chemotherapy may represent an attractive way to attenuate cording, and consequently to control invasive and acute *Mab* infections, even among CF patients.

Another possible method for fighting drug-resistant *Mab* infections could be the design of Whib7 inhibitors that could be used in combination with the current therapy [79]. The inhibition of the

activation of genes conferring aminoglycoside and macrolide resistance (*eis2* and *erm(41)*), respectively) in *Mab* could improve the efficacy of the current *Mab* treatment.

As described before, inhaled formulation or drugs or NO are also very promising in the fight against *Mab* infections. A further evaluation of efficacy and safety is needed prior to effective clinical use.

The emergence of *Mab* as a CF pathogen has left patients unprepared in the fight against this pathogen, which is intrinsically resistant to several classes of antibiotics already in use. Overall, a better understanding of *Mab* pathogenicity and more efforts in drug development pipeline could help to pave the way for next-generation antimicrobials that are effective in *Mab* treatment, in order to save more infected people.

Author Contributions: All the authors reviewed the literature and wrote the manuscript.

Funding: This research was funded by the Italian Cystic Fibrosis Foundation, grant number FFC#19/2018 (adopted by Delegazione FFC di Brindisi Torre, Delegazione FFC di Ascoli Piceno, Delegazione FFC di Novara). This research was also supported by the Italian Ministry of Education, Universities, and Research (MIUR): Dipartimenti di Eccellenza Program (2018–2022)—Department of Biology and Biotechnology “L. Spallanzani”, University of Pavia (to G.D., J.C.S., L.R.C., and M.R.P.).

Acknowledgments: This review is dedicated to Ludovica, a little girl affected by cystic fibrosis with the hope of a future with an effective therapy.

Conflicts of Interest: The authors declare no conflict of interest.

References

1. Pranke, I.; Golec, A.; Hinzpeter, A.; Edelman, A.; Sermet-Gaudelus, I. Emerging Therapeutic Approaches for Cystic Fibrosis. From Gene Editing to Personalized Medicine. *Front. Pharmacol.* **2019**, *10*, 121. [[CrossRef](#)] [[PubMed](#)]
2. Skolnik, K.; Kirkpatrick, G.; Quon, B.S. Nontuberculous Mycobacteria in Cystic Fibrosis. *Curr. Treat. Options Infect. Dis.* **2016**, *8*, 259–274. [[CrossRef](#)] [[PubMed](#)]
3. Viviani, L.; Harrison, M.J.; Zolin, A.; Haworth, C.S.; Floto, R.A. Epidemiology of nontuberculous mycobacteria (NTM) amongst individuals with cystic fibrosis (CF). *J. Cyst. Fibros.* **2016**, *15*, 619–623. [[CrossRef](#)] [[PubMed](#)]
4. Martiniano, S.L.; Nick, J.A.; Daley, C.L. Nontuberculous Mycobacterial Infections in Cystic Fibrosis. *Thorac. Surg. Clin.* **2019**, *29*, 95–108. [[CrossRef](#)] [[PubMed](#)]
5. Daniel-Wayman, S.; Abate, G.; Barber, D.L.; Bermudez, L.E.; Coler, R.N.; Cynamon, M.H.; Daley, C.L.; Davidson, R.M.; Dick, T.; Floto, R.A.; et al. Advancing Translational Science for Pulmonary Nontuberculous Mycobacterial Infections. A Road Map for Research. *Am. J. Respir. Crit. Care Med.* **2019**, *199*, 947–951. [[CrossRef](#)]
6. Salsgiver, E.L.; Fink, A.K.; Knapp, E.A.; LiPuma, J.J.; Olivier, K.N.; Marshall, B.C.; Saiman, L. Changing Epidemiology of the Respiratory Bacteriology of Patients with Cystic Fibrosis. *Chest* **2016**, *149*, 390–400. [[CrossRef](#)]
7. Mougari, F.; Guglielmetti, L.; Raskine, L.; Sermet-Gaudelus, I.; Veziris, N.; Cambau, E. Infections caused by *Mycobacterium abscessus*: Epidemiology, diagnostic tools and treatment. *Expert Rev. Anti-Infect. Ther.* **2016**, *14*, 1139–1154. [[CrossRef](#)]
8. Wu, M.L.; Aziz, D.B.; Dartois, V.; Dick, T. NTM drug discovery: Status, gaps and the way forward. *Drug Discov. Today* **2018**, *23*, 1502–1519. [[CrossRef](#)]
9. Qvist, T.; Pressler, T.; Høiby, N.; Katzenstein, T.L. Shifting paradigms of nontuberculous mycobacteria in cystic fibrosis. *Respir. Res.* **2014**, *15*, 41. [[CrossRef](#)]
10. Andrew, E.C.; Connell, T.; Robinson, P.; Curtis, N.; Massie, J.; Robertson, C.; Harrison, J.; Shanthikumar, S.; Bryant, P.A.; Starr, M.; et al. Pulmonary *Mycobacterium abscessus* complex in children with cystic fibrosis: A practical management guideline. *J. Paediatr. Child Health* **2019**, *55*, 502–511. [[CrossRef](#)]
11. van Dorn, A. Multidrug-resistant *Mycobacterium abscessus* threatens patients with cystic fibrosis. *Lancet Respir. Med.* **2017**, *5*, 15. [[CrossRef](#)]

12. Stephenson, D.; Perry, A.; Appleby, M.R.; Lee, D.; Davison, J.; Johnston, A.; Jones, A.L.; Nelson, A.; Bourke, S.J.; Thomas, M.F.; et al. An evaluation of methods for the isolation of nontuberculous mycobacteria from patients with cystic fibrosis, bronchiectasis and patients assessed for lung transplantation. *BMC Pulm. Med.* **2019**, *19*, 19. [[CrossRef](#)] [[PubMed](#)]
13. Davidson, R.M. A Closer Look at the Genomic Variation of Geographically Diverse *Mycobacterium abscessus* Clones That Cause Human Infection and Disease. *Front. Microbiol.* **2018**, *9*, 2988. [[CrossRef](#)] [[PubMed](#)]
14. Bryant, J.M.; Grogono, D.M.; Rodriguez-Rincon, D.; Everall, I.; Brown, K.P.; Moreno, P.; Verma, D.; Hill, E.; Drijkoningen, J.; Gilligan, P.; et al. Emergence and spread of a human-transmissible multidrug-resistant nontuberculous mycobacterium. *Science* **2016**, *354*, 751–757. [[CrossRef](#)]
15. Lopeman, R.C.; Harrison, J.; Desai, M.; Cox, J.A.G. *Mycobacterium abscessus*: Environmental Bacterium Turned Clinical Nightmare. *Microorganisms* **2019**, *7*, 90. [[CrossRef](#)]
16. Thomson, R.; Tolson, C.; Sidjabat, H.; Huygens, F.; Hargreaves, M. *Mycobacterium abscessus* isolated from municipal water—A potential source of human infection. *BMC Infect. Dis.* **2013**, *13*, 241. [[CrossRef](#)]
17. Floto, R.A.; Olivier, K.N.; Saiman, L.; Daley, C.L.; Herrmann, J.L.; Nick, J.A.; Noone, P.G.; Bilton, D.; Corris, P.; Gibson, R.L.; et al. US Cystic Fibrosis Foundation and European Cystic Fibrosis Society consensus recommendations for the management of non-tuberculous mycobacteria in individuals with cystic fibrosis. *Thorax* **2016**, *71* (Suppl. 1), i1–i22. [[CrossRef](#)]
18. Sood, G.; Parrish, N. Outbreaks of nontuberculous mycobacteria. *Curr. Opin. Infect. Dis.* **2017**, *30*, 404–409. [[CrossRef](#)]
19. King, D.N.; Donohue, M.J.; Vesper, S.J.; Villegas, E.N.; Ware, M.W.; Vogel, M.E.; Furlong, E.F.; Kolpin, D.W.; Glassmeyer, S.T.; Pfaller, S. Microbial pathogens in source and treated waters from drinking water treatment plants in the United States and implications for human health. *Sci. Total Environ.* **2016**, *562*, 987–995. [[CrossRef](#)]
20. Thomson, R.; Tolson, C.; Carter, R.; Coulter, C.; Huygens, F.; Hargreaves, M. Isolation of nontuberculous mycobacteria (NTM) from household water and shower aerosols in patients with pulmonary disease caused by NTM. *J. Clin. Microbiol.* **2013**, *51*, 3006–3011. [[CrossRef](#)]
21. Torvinen, E.; Suomalainen, S.; Paulin, L.; Kusnetsov, J. Mycobacteria in Finnish cooling tower waters. *Appl. Microbiol.* **2014**, *122*, 353–358. [[CrossRef](#)] [[PubMed](#)]
22. Alqumber, M.A. Prevalence of mycobacteria in water reservoirs of Albaha, Saudi Arabia. *Saudi Med. J.* **2014**, *35*, 466–471. [[PubMed](#)]
23. Williams, M.M.; Chen, T.H.; Keane, T.; Toney, N.; Toney, S.; Armbruster, C.R.; Butler, W.R.; Arduino, M.J. Point-of-use membrane filtration and hyperchlorination to prevent patient exposure to rapidly growing mycobacteria in the potable water supply of a skilled nursing facility. *Infect. Control Hosp. Epidemiol.* **2011**, *32*, 837–844. [[CrossRef](#)] [[PubMed](#)]
24. Honda, J.R.; Hasan, N.A.; Davidson, R.M.; Williams, M.D.; Epperson, L.E.; Reynolds, P.R.; Smith, T.; Iakhiaeva, E.; Bankowski, M.J.; Wallace, R.J., Jr.; et al. Environmental Nontuberculous Mycobacteria in the Hawaiian Islands. *PLoS Negl. Trop. Dis.* **2016**, *10*, e0005068. [[CrossRef](#)] [[PubMed](#)]
25. Liu, R.; Yu, Z.; Zhang, H.; Yang, M.; Shi, B.; Liu, X. Diversity of bacteria and mycobacteria in biofilms of two urban drinking water distribution systems. *Can. J. Microbiol.* **2012**, *58*, 261–270. [[CrossRef](#)] [[PubMed](#)]
26. Delafont, V.; Mougari, F.; Cambau, E.; Joyeux, M.; Bouchon, D.; Héchard, Y.; Moulin, L. First evidence of amoebae-mycobacteria association in drinking water network. *Environ. Sci. Technol.* **2014**, *48*, 11872–11882. [[CrossRef](#)]
27. Donohue, M.J.; Mistry, J.H.; Donohue, J.M.; O'Connell, K.; King, D.; Byran, J.; Covert, T.; Pfaller, S. Increased Frequency of Nontuberculous Mycobacteria Detection at Potable Water Taps within the United States. *Environ. Sci. Technol.* **2015**, *49*, 6127–6133. [[CrossRef](#)]
28. Puk, K.; Banach, T.; Wawrzyniak, A.; Adaszek, L.; Ziętek, J.; Winiarczyk, S.; Guz, L. Detection of *Mycobacterium marinum*, *M. peregrinum*, *M. fortuitum* and *M. abscessus* in aquarium fish. *J. Fish Dis.* **2018**, *41*, 153–156. [[CrossRef](#)]
29. Schets, F.M.; van den Berg, H.H.; de Zwaan, R.; van Soelingen, D.; de Roda Husman, A.M. The microbiological quality of water in fish spas with Garra rufa fish, the Netherlands, October to November 2012. *Euro Surveill.* **2015**, *20*, 2–8. [[CrossRef](#)]

30. Varello, K.; Prearo, M.; Serracca, L.; Meloni, D.; Rossini, I.; Righetti, M.; Pezzolato, M.; Fioravanti, M.L.; Ercolini, C.; Bozzetta, E. Granulomatous lesions in a wild mullet population from the eastern Ligurian Sea (Italy): Mycobacteriosis vs. pseudotuberculosis. *J. Fish Dis.* **2014**, *37*, 553–558. [[CrossRef](#)]
31. Favaro, L.; Scanzio, T.; Varello, K.; Caffara, M.; Righetti, M.; Bozzetta, E.; Prearo, M. Mixed mycobacterial infection in an adult koi carp *Cyprinus carpio* L. *J. Fish Dis.* **2014**, *37*, 753–755. [[CrossRef](#)] [[PubMed](#)]
32. Zaroni, R.G.; Florio, D.; Fioravanti, M.L.; Rossi, M.; Prearo, M. Occurrence of *Mycobacterium* spp. in ornamental fish in Italy. *J. Fish Dis.* **2008**, *31*, 433–441. [[PubMed](#)]
33. Chang, T.C.; Hsieh, C.Y.; Chang, C.D.; Shen, Y.L.; Huang, K.C.; Tu, C.; Chen, L.C.; Wu, Z.B.; Tsai, S.S. Pathological and molecular studies on mycobacteriosis of milkfish *Chanos chanos* in Taiwan. *Dis. Aquat. Org.* **2006**, *72*, 147–151. [[CrossRef](#)] [[PubMed](#)]
34. Reisfeld, L.; Ikuta, C.Y.; Ippolito, L.; Silvatti, B.; Ferreira Neto, J.S.; Catão-Dias, J.L.; Rosas, F.C.W.; Neto, J.A.; da Silva, V.M.F. Cutaneous mycobacteriosis in a captive Amazonian manatee *Trichechus inunguis*. *Dis. Aquat. Org.* **2018**, *127*, 231–236. [[CrossRef](#)]
35. Katale, B.Z.; Mbugi, E.V.; Botha, L.; Keyyu, J.D.; Kendall, S.; Dockrell, H.M.; Michel, A.L.; Kazwala, R.R.; Rweyemamu, M.M.; van Helden, P.; et al. Species diversity of non-tuberculous mycobacteria isolated from humans, livestock and wildlife in the Serengeti ecosystem, Tanzania. *BMC Infect. Dis.* **2014**, *14*, 616. [[CrossRef](#)]
36. Clayton, L.A.; Stamper, M.A.; Whitaker, B.R.; Hadfield, C.A.; Simons, B.; Mankowski, J.L. *Mycobacterium abscessus* pneumonia in an Atlantic bottlenose dolphin (*Tursiops truncatus*). *J. Zoo Wildl. Med.* **2012**, *43*, 961–965. [[CrossRef](#)]
37. Jassies-van der Lee, A.; Houwers, D.J.; Meertens, N.; van der Zanden, A.G.; Willemse, T. Localised pyogranulomatous dermatitis due to *Mycobacterium abscessus* in a cat: A case report. *Vet. J.* **2009**, *179*, 304–306. [[CrossRef](#)]
38. Lunn, J.A.; Martin, P.; Zaki, S.; Malik, R. Pneumonia due to *Mycobacterium abscessus* in two domestic ferrets (*Mustelo putorius furo*). *Aust. Vet. J.* **2005**, *83*, 542–546. [[CrossRef](#)]
39. Karlson, A.G.; Seibold, H.R.; Wolf, R.H. *Mycobacterium abscessus* infection in an owl monkey (*Aotus trivirgatus*). *Pathol. Vet.* **1970**, *7*, 448–454.
40. Jang, S.S.; Hirsh, D.C. Rapidly growing members of the genus *Mycobacterium* affecting dogs and cats. *J. Am. Anim. Hosp. Assoc.* **2002**, *38*, 217–220. [[CrossRef](#)]
41. Falkinham, J.O., 3rd. Nontuberculous mycobacteria from household plumbing of patients with nontuberculous mycobacteria disease. *Emerg. Infect. Dis.* **2011**, *17*, 419–424. [[CrossRef](#)] [[PubMed](#)]
42. Bryant, J.M.; Grogono, D.M.; Greaves, D.; Foweraker, J.; Roddick, L.; Inns, T.; Reacher, M.; Haworth, C.S.; Curran, M.D.; Harris, S.R.; et al. Whole-genome sequencing to identify transmission of *Mycobacterium abscessus* between patients with cystic fibrosis: A retrospective cohort study. *Lancet* **2013**, *381*, 1551–1560. [[CrossRef](#)]
43. Yan, J.; Kevat, A.; Martinez, E.; Teese, N.; Johnson, K.; Ranganathan, S.; Harrison, J.; Massie, J.; Daley, A. Investigating transmission of *Mycobacterium abscessus* amongst children in an Australian cystic fibrosis centre. *J. Cyst. Fibros.* **2019**, in press. [[CrossRef](#)]
44. Tortoli, E.; Kohl, T.A.; Trovato, A.; Baldan, R.; Campana, S.; Cariani, L.; Colombo, C.; Costa, D.; Cristadoro, S.; Di Serio, M.C.; et al. *Mycobacterium abscessus* in patients with cystic fibrosis: Low impact of inter-human transmission in Italy. *Eur. Respir. J.* **2017**, *50*, 1602525. [[CrossRef](#)] [[PubMed](#)]
45. Esteban, J.; García-Coca, M. *Mycobacterium* Biofilms. *Front. Microbiol.* **2018**, *8*, 2651. [[CrossRef](#)] [[PubMed](#)]
46. Benwill, J.L.; Wallace, R.J., Jr. *Mycobacterium abscessus*: Challenges in diagnosis and treatment. *Curr. Opin. Infect. Dis.* **2014**, *27*, 506–510. [[CrossRef](#)]
47. Qvist, T.; Eickhardt, S.; Kragh, K.N.; Andersen, C.B.; Iversen, M.; Hoiby, N.; Bjarnsholt, T. Chronic pulmonary disease with *Mycobacterium abscessus* complex is a biofilm infection. *Eur. Respir. J.* **2015**, *46*, 1823–1826. [[CrossRef](#)]
48. Fennelly, K.P.; Ojano-Dirain, C.; Yang, Q.; Liu, L.; Lu, L.; Proguilske-Fox, A.; Wang, G.P.; Antonelli, P.; Schultz, G. Biofilm Formation by *Mycobacterium abscessus* in a Lung Cavity. *Am. J. Respir. Crit. Care Med.* **2016**, *193*, 692–693. [[CrossRef](#)]
49. Hunt-Serracin, A.C.; Parks, B.J.; Boll, J.; Boutte, C. Biofilm-associated *Mycobacterium abscessus* cells have altered antibiotic tolerance and surface glycolipids in Artificial Cystic Fibrosis Sputum Media. *Antimicrob. Agents Chemother.* **2019**, *63*, e02488-18. [[CrossRef](#)]

50. Gutiérrez, A.V.; Viljoen, A.; Ghigo, E.; Herrmann, J.L.; Kremer, L. Glycopeptidolipids, a Double-Edged Sword of the *Mycobacterium abscessus* Complex. *Front. Microbiol.* **2018**, *9*, 1145. [[CrossRef](#)]
51. Davidson, L.B.; Nessar, R.; Kempaiah, P.; Perkins, D.J.; Byrd, T.F. *Mycobacterium abscessus* glycopeptidolipid prevents respiratory epithelial TLR2 signaling as measured by H β D2 gene expression and IL-8 release. *PLoS ONE* **2011**, *6*, e29148. [[CrossRef](#)] [[PubMed](#)]
52. Schorey, J.S.; Sweet, L. The mycobacterial glycopeptidolipids: Structure, function, and their role in pathogenesis. *Glycobiology* **2008**, *18*, 832–841. [[CrossRef](#)] [[PubMed](#)]
53. Howard, S.T.; Rhoades, E.; Recht, J.; Pang, X.; Alsup, A.; Kolter, R.; Lyons, C.R.; Byrd, T.F. Spontaneous reversion of *Mycobacterium abscessus* from a smooth to a rough morphotype is associated with reduced expression of glycopeptidolipid and reacquisition of an invasive phenotype. *Microbiology* **2006**, *152*, 1581–1590. [[CrossRef](#)] [[PubMed](#)]
54. Rüger, K.; Hampel, A.; Billig, S.; Rücker, N.; Suerbaum, S.; Bange, F.C. Characterization of rough and smooth morphotypes of *Mycobacterium abscessus* isolates from clinical specimens. *J. Clin. Microbiol.* **2014**, *52*, 244–250. [[CrossRef](#)]
55. Bernut, A.; Herrmann, J.L.; Kissa, K.; Dubremetz, J.F.; Gaillard, J.L.; Lutfalla, G.; Kremer, L. *Mycobacterium abscessus* cording prevents phagocytosis and promotes abscess formation. *Proc. Natl. Acad. Sci. USA* **2014**, *111*, E943–E952. [[CrossRef](#)]
56. Bernut, A.; Viljoen, A.; Dupont, C.; Sapriel, G.; Blaise, M.; Bouchier, C.; Brosch, R.; de Chastellier, C.; Herrmann, J.L.; Kremer, L. Insights into the smooth-to-rough transitioning in *Mycobacterium boletii* unravels a functional Tyr residue conserved in all mycobacterial MmpL family members. *Mol. Microbiol.* **2016**, *99*, 866–883. [[CrossRef](#)]
57. Medjahed, H.; Reytrat, J.M. Construction of *Mycobacterium abscessus* defined glycopeptidolipid mutants: Comparison of genetic tools. *Appl. Environ. Microbiol.* **2009**, *75*, 1331–1338. [[CrossRef](#)]
58. Nessar, R.; Reytrat, J.M.; Davidson, L.B.; Byrd, T.F. Deletion of the *mmpL4b* gene in the *Mycobacterium abscessus* glycopeptidolipid biosynthetic pathway results in loss of surface colonization capability, but enhanced ability to replicate in human macrophages and stimulate their innate immune response. *Microbiology* **2011**, *157*, 1187–1195. [[CrossRef](#)]
59. Bernut, A.; Herrmann, J.L.; Ordway, D.; Kremer, L. The diverse cellular and animal models to decipher the physiopathological traits of *Mycobacterium abscessus* infection. *Front. Cell Infect. Microbiol.* **2017**, *7*, 100. [[CrossRef](#)]
60. Halloum, I.; Carrère-Kremer, S.; Blaise, M.; Viljoen, A.; Bernut, A.; Le Moigne, V.; Vilchèze, C.; Guérardel, Y.; Lutfalla, G.; Herrmann, J.L.; et al. Deletion of a dehydratase important for intracellular growth and cording renders rough *Mycobacterium abscessus* avirulent. *Proc. Natl. Acad. Sci. USA* **2016**, *113*, E4228–E4237. [[CrossRef](#)]
61. Koh, W.J.; Jeong, B.H.; Kim, S.Y.; Jeon, K.; Park, K.U.; Jhun, B.W.; Lee, H.; Park, H.Y.; Kim, D.H.; Huh, H.J.; et al. Mycobacterial Characteristics and Treatment Outcomes in *Mycobacterium abscessus* Lung Disease. *Clin. Infect. Dis.* **2017**, *64*, 309–316. [[CrossRef](#)] [[PubMed](#)]
62. Esther, C.R., Jr.; Esserman, D.A.; Gilligan, P.; Kerr, A.; Noone, P.G. Chronic *Mycobacterium abscessus* infection and lung function decline in cystic fibrosis. *J. Cyst. Fibros.* **2010**, *9*, 117–123. [[CrossRef](#)] [[PubMed](#)]
63. Sanguinetti, M.; Ardito, F.; Fiscarelli, E.; La Sorda, M.; D'Argenio, P.; Ricciotti, G.; Fadda, G. Fatal pulmonary infection due to multidrug-resistant *Mycobacterium abscessus* in a patient with cystic fibrosis. *J. Clin. Microbiol.* **2001**, *39*, 816–819. [[CrossRef](#)] [[PubMed](#)]
64. Jönsson, B.E.; Gilljam, M.; Lindblad, A.; Ridell, M.; Wold, A.E.; Welinder Olsson, C. Molecular epidemiology of *Mycobacterium abscessus*, with focus on cystic fibrosis. *J. Clin. Microbiol.* **2007**, *45*, 1497–1504. [[CrossRef](#)]
65. Qvist, T.; Taylor-Robinson, D.; Waldmann, E.; Olesen, H.V.; Hansen, C.R.; Mathiesen, I.H.; Høiby, N.; Katzenstein, T.L.; Smyth, R.L.; Diggle, P.J.; et al. Comparing the harmful effects of nontuberculous mycobacteria and Gram negative bacteria on lung function in patients with cystic fibrosis. *J. Cyst. Fibros.* **2016**, *15*, 380–385. [[CrossRef](#)]
66. Dubois, V.; Viljoen, A.; Laencina, L.; Le Moigne, V.; Bernut, A.; Dubar, F.; Blaise, M.; Gaillard, J.L.; Guérardel, Y.; Kremer, L.; et al. MmpL8(MAB) controls *Mycobacterium abscessus* virulence and production of a previously unknown glycolipid family. *Proc. Natl. Acad. Sci. USA* **2018**, *115*, E10147–E10156. [[CrossRef](#)]

67. Laencina, L.; Dubois, V.; Le Moigne, V.; Viljoen, A.; Majlessi, L.; Pritchard, J.; Bernut, A.; Piel, L.; Roux, A.L.; Gaillard, J.L.; et al. Identification of genes required for *Mycobacterium abscessus* growth in vivo with a prominent role of the ESX-4 locus. *Proc. Natl. Acad. Sci. USA* **2018**, *115*, E1002–E1011. [[CrossRef](#)]
68. Bernut, A.; Nguyen-Chi, M.; Halloum, I.; Herrmann, J.L.; Lutfalla, G.; Kremer, L. *Mycobacterium abscessus*-Induced Granuloma Formation Is Strictly Dependent on TNF Signaling and Neutrophil Trafficking. *PLoS Pathog.* **2016**, *12*, e1005986. [[CrossRef](#)]
69. Bernut, A.; Dupont, C.; Ogryzko, N.V.; Neyret, A.; Herrmann, J.L.; Floto, R.A.; Renshaw, S.A.; Kremer, L. CFTR Protects against *Mycobacterium abscessus* Infection by Fine-Tuning Host Oxidative Defenses. *Cell Rep.* **2019**, *26*, 1828–1840.e4. [[CrossRef](#)]
70. Leung, J.M.; Olivier, K.N. Nontuberculous mycobacteria: The changing epidemiology and treatment challenges in cystic fibrosis. *Curr. Opin. Pulm. Med.* **2013**, *19*, 662–669. [[CrossRef](#)]
71. Floto, R.A.; Olivier, K.N.; Saiman, L.; Daley, C.L.; Herrmann, J.L.; Nick, J.A.; Noone, P.G.; Bilton, D.; Corris, P.; Gibson, R.L.; et al. US Cystic Fibrosis Foundation and European Cystic Fibrosis Society consensus recommendations for the management of non-tuberculous mycobacteria in individuals with cystic fibrosis: Executive summary. *Thorax* **2016**, *71*, 88–90. [[CrossRef](#)] [[PubMed](#)]
72. Lobo, L.J.; Chang, L.C.; Esther, C.R., Jr.; Gilligan, P.H.; Tulu, Z.; Noone, P.G. Lung transplant outcomes in cystic fibrosis patients with pre-operative *Mycobacterium abscessus* respiratory infections. *Clin. Transplant.* **2013**, *27*, 523–529. [[CrossRef](#)] [[PubMed](#)]
73. Heijerman, H.G.M.; McKone, E.F.; Downey, D.G.; Van Braeckel, E.; Rowe, S.M.; Tullis, E.; Mall, M.A.; Welter, J.J.; Ramsey, B.W.; McKee, C.M.; et al. Efficacy and safety of the elexacaftor plus tezacaftor plus ivacaftor combination regimen in people with cystic fibrosis homozygous for the F508del mutation: A double-blind, randomised, phase 3 trial. *Lancet* **2019**, in press. [[CrossRef](#)]
74. Middleton, P.G.; Mall, M.A.; Dřevínek, P.; Lands, L.C.; McKone, E.F.; Polineni, D.; Ramsey, B.W.; Taylor-Cousar, J.L.; Tullis, E.; Vermeulen, F.; et al. Elexacaftor-Tezacaftor-Ivacaftor for Cystic Fibrosis with a Single Phe508del Allele. *N. Engl. J. Med.* **2019**, *381*, 1809–1819. [[CrossRef](#)] [[PubMed](#)]
75. Luthra, S.; Rominski, A.; Sander, P. The Role of Antibiotic-Target-Modifying and Antibiotic-Modifying Enzymes in *Mycobacterium abscessus* Drug Resistance. *Front. Microbiol.* **2018**, *9*, 2179. [[CrossRef](#)]
76. Brown-Elliott, B.A.; Nash, K.A.; Wallace, R.J., Jr. Antimicrobial susceptibility testing, drug resistance mechanisms, and therapy of infections with nontuberculous mycobacteria. *Clin. Microbiol. Rev.* **2012**, *25*, 545–582. [[CrossRef](#)]
77. Nash, K.A.; Brown-Elliott, B.A.; Wallace, R.J., Jr. A novel gene, *erm(41)*, confers inducible macrolide resistance to clinical isolates of *Mycobacterium abscessus* but is absent from *Mycobacterium chelonae*. *Antimicrob. Agents Chemother.* **2009**, *53*, 1367–1376. [[CrossRef](#)]
78. Pfister, P.; Jenni, S.; Poehlsgaard, J.; Thomas, A.; Douthwaite, S.; Ban, N.; Böttger, E.C. The structural basis of macrolide-ribosome binding assessed using mutagenesis of 23S rRNA positions 2058 and 2059. *J. Mol. Biol.* **2004**, *342*, 1569–1581. [[CrossRef](#)]
79. Hurst-Hess, K.; Rudra, P.; Ghosh, P. *Mycobacterium abscessus* WhiB7 Regulates a Species-Specific Repertoire of Genes to Confer Extreme Antibiotic Resistance. *Antimicrob. Agents Chemother.* **2017**, *61*, e01347-17. [[CrossRef](#)]
80. Prammananan, T.; Sander, P.; Brown, B.A.; Frischkorn, K.; Onyi, G.O.; Zhang, Y.; Böttger, E.C.; Wallace, R.J., Jr. A single 16S ribosomal RNA substitution is responsible for resistance to amikacin and other 2-deoxystreptamine aminoglycosides in *Mycobacterium abscessus* and *Mycobacterium chelonae*. *J. Infect. Dis.* **1998**, *177*, 1573–1581. [[CrossRef](#)]
81. Nessar, R.; Reytrat, J.M.; Murray, A.; Gicquel, B. Genetic analysis of new 16S rRNA mutations conferring aminoglycoside resistance in *Mycobacterium abscessus*. *J. Antimicrob. Chemother.* **2011**, *66*, 1719–1724. [[CrossRef](#)] [[PubMed](#)]
82. Soroka, D.; Dubée, V.; Soulier-Escrihuela, O.; Cuinet, G.; Hugonnet, J.E.; Gutmann, L.; Mainardi, J.L.; Arthur, M. Characterization of broad-spectrum *Mycobacterium abscessus* class A β -lactamase. *J. Antimicrob. Chemother.* **2014**, *69*, 691–696. [[CrossRef](#)] [[PubMed](#)]
83. Rudra, P.; Hurst-Hess, K.; Lappierre, P.; Ghosh, P. High Levels of Intrinsic Tetracycline Resistance in *Mycobacterium abscessus* Are Conferred by a Tetracycline-Modifying Monooxygenase. *Antimicrob. Agents Chemother.* **2018**, *62*, e00119-18. [[CrossRef](#)] [[PubMed](#)]

84. Richard, M.; Gutiérrez, A.V.; Viljoen, A.; Rodriguez-Rincon, D.; Roquet-Baneres, F.; Blaise, M.; Everall, I.; Parkhill, J.; Floto, R.A.; Kremer, L. Mutations in the MAB_2299c TetR Regulator Confer Cross-Resistance to Clofazimine and Bedaquiline in *Mycobacterium abscessus*. *Antimicrob. Agents Chemother.* **2018**, *63*, e01316-18. [[CrossRef](#)]
85. Guillemain, I.; Jarlier, V.; Cambau, E. Correlation between quinolone susceptibility patterns and sequences in the A and B subunits of DNA gyrase in mycobacteria. *Antimicrob. Agents Chemother.* **1998**, *42*, 2084–2088. [[CrossRef](#)]
86. Kim, S.Y.; Jhun, B.W.; Moon, S.M.; Shin, S.H.; Jeon, K.; Kwon, O.J.; Yoo, I.Y.; Huh, H.J.; Ki, C.S.; Lee, N.Y.; et al. Mutations in *gyrA* and *gyrB* in Moxifloxacin-Resistant *Mycobacterium avium* Complex and *Mycobacterium abscessus* Complex Clinical Isolates. *Antimicrob. Agents Chemother.* **2018**, *62*, e00527-18. [[CrossRef](#)]
87. Ye, M.; Xu, L.; Zou, Y.; Li, B.; Guo, Q.; Zhang, Y.; Zhan, M.; Xu, B.; Yu, F.; Zhang, Z.; et al. Molecular Analysis of Linezolid-Resistant Clinical Isolates of *Mycobacterium abscessus*. *Antimicrob. Agents Chemother.* **2019**, *63*, e01842-18. [[CrossRef](#)]
88. Hansen, J.L.; Ippolito, J.A.; Ban, N.; Nissen, P.; Moore, P.B.; Steitz, T.A. The structures of four macrolide antibiotics bound to the large ribosomal subunit. *Mol. Cell* **2002**, *10*, 117–128. [[CrossRef](#)]
89. Nessar, R.; Cambau, E.; Reytrat, J.M.; Murray, A.; Gicquel, B. *Mycobacterium abscessus*: A new antibiotic nightmare. *J. Antimicrob. Chemother.* **2012**, *67*, 810–818. [[CrossRef](#)]
90. Hartkoorn, R.C.; Uplekar, S.; Cole, S.T. Cross-resistance between clofazimine and bedaquiline through upregulation of MmpL5 in *Mycobacterium tuberculosis*. *Antimicrob. Agents Chemother.* **2014**, *58*, 2979–2981. [[CrossRef](#)]
91. Choo, S.W.; Wee, W.Y.; Ngeow, Y.F.; Mitchell, W.; Tan, J.L.; Wong, G.J.; Zhao, Y.; Xiao, J. Genomic reconnaissance of clinical isolates of emerging human pathogen *Mycobacterium abscessus* reveals high evolutionary potential. *Sci. Rep.* **2014**, *4*, 4061. [[CrossRef](#)] [[PubMed](#)]
92. Maurer, F.P.; Bruderer, V.L.; Ritter, C.; Castelberg, C.; Bloemberg, G.V.; Böttger, E.C. Lack of antimicrobial bactericidal activity in *Mycobacterium abscessus*. *Antimicrob. Agents Chemother.* **2014**, *58*, 3828–3836. [[CrossRef](#)] [[PubMed](#)]
93. Phillely, J.V.; Wallace, R.J., Jr.; Benwill, J.L.; Taskar, V.; Brown-Elliott, B.A.; Thakkar, F.; Aksamit, T.R.; Griffith, D.E. Preliminary Results of Bedaquiline as Salvage Therapy for Patients with Nontuberculous Mycobacterial Lung Disease. *Chest* **2015**, *148*, 499–506. [[CrossRef](#)] [[PubMed](#)]
94. Li, B.; Ye, M.; Guo, Q.; Zhang, Z.; Yang, S.; Ma, W.; Yu, F.; Chu, H. Determination of MIC Distribution and Mechanisms of Decreased Susceptibility to Bedaquiline among Clinical Isolates of *Mycobacterium abscessus*. *Antimicrob. Agents Chemother.* **2018**, *62*, e00175-18. [[CrossRef](#)]
95. Viljoen, A.; Raynaud, C.; Johansen, M.D.; Roquet-Banères, F.; Herrmann, J.L.; Daher, W.; Kremer, L. Improved activity of bedaquiline by verapamil against *Mycobacterium abscessus* in vitro and in macrophages. *Antimicrob. Agents Chemother.* **2019**, *63*, e00705-19. [[CrossRef](#)]
96. Obregón-Henao, A.; Arnett, K.A.; Henao-Tamayo, M.; Massoudi, L.; Creissen, E.; Andries, K.; Lenaerts, A.J.; Ordway, D.J. Susceptibility of *Mycobacterium abscessus* to antimycobacterial drugs in preclinical models. *Antimicrob. Agents Chemother.* **2015**, *59*, 6904–6912. [[CrossRef](#)]
97. Lerat, I.; Cambau, E.; Roth Dit Bettoni, R.; Gaillard, J.L.; Jarlier, V.; Truffot, C.; Veziris, N. In Vivo evaluation of antibiotic activity against *Mycobacterium abscessus*. *J. Infect. Dis.* **2014**, *209*, 905–912. [[CrossRef](#)]
98. Dupont, C.; Viljoen, A.; Thomas, S.; Roquet-Banères, F.; Herrmann, J.L.; Pethe, K.; Kremer, L. Bedaquiline inhibits the ATP Synthase in *Mycobacterium abscessus* and Is Effective in Infected Zebrafish. *Antimicrob. Agents Chemother.* **2017**, *61*, e01225-17. [[CrossRef](#)]
99. Brown-Elliott, B.A.; Wallace, R.J., Jr. In Vitro Susceptibility Testing of Tedizolid against Nontuberculous Mycobacteria. *J. Clin. Microbiol.* **2017**, *55*, 1747–1754. [[CrossRef](#)]
100. Kim, T.S.; Choe, J.H.; Kim, Y.J.; Yang, C.S.; Kwon, H.J.; Jeong, J.; Kim, G.; Park, D.E.; Jo, E.K.; Cho, Y.L.; et al. Activity of LCB01-0371, a Novel Oxazolidinone, against *Mycobacterium abscessus*. *Antimicrob. Agents Chemother.* **2017**, *61*, e02752-16. [[CrossRef](#)]
101. Kozikowski, A.P.; Onajole, O.K.; Stec, J.; Dupont, C.; Viljoen, A.; Richard, M.; Chaira, T.; Lun, S.; Bishai, W.; Raj, V.S.; et al. Targeting Mycolic Acid Transport by Indole-2-carboxamides for the Treatment of *Mycobacterium abscessus* Infections. *J. Med. Chem.* **2017**, *60*, 5876–5888. [[CrossRef](#)] [[PubMed](#)]

102. Franz, N.D.; Belardinelli, J.M.; Kaminski, M.A.; Dunn, L.C.; Calado Nogueira de Moura, V.; Blaha, M.A.; Truong, D.D.; Li, W.; Jackson, M.; North, E.J. Design, synthesis and evaluation of indole-2-carboxamides with pan anti-mycobacterial activity. *Bioorg. Med. Chem.* **2017**, *25*, 3746–3755. [CrossRef] [PubMed]
103. Pandya, A.N.; Prathipati, P.K.; Hegde, P.; Li, W.; Graham, K.F.; Mandal, S.; Drescher, K.M.; Destache, C.J.; Ordway, D.; Jackson, M.; et al. Indole-2-Carboxamides Are Active against *Mycobacterium abscessus* in a Mouse Model of Acute Infection. *Antimicrob. Agents Chemother.* **2019**, *63*, e02245-18. [CrossRef] [PubMed]
104. Dupont, C.; Viljoen, A.; Dubar, F.; Blaise, M.; Bernut, A.; Pawlik, A.; Bouchier, C.; Brosch, R.; Guérardel, Y.; Lelièvre, J.; et al. A new piperidinol derivative targeting mycolic acid transport in *Mycobacterium abscessus*. *Mol. Microbiol.* **2016**, *101*, 515–529. [CrossRef] [PubMed]
105. Dubuisson, T.; Bogatcheva, E.; Krishnan, M.Y.; Collins, M.T.; Einck, L.; Nacy, C.A.; Reddy, V.M. In vitro antimicrobial activities of capuramycin analogues against non-tuberculous mycobacteria. *J. Antimicrob. Chemother.* **2010**, *65*, 2590–2597. [CrossRef]
106. Aziz, D.B.; Low, J.L.; Wu, M.L.; Gengenbacher, M.; Teo, J.W.P.; Dartois, V.; Dick, T. Rifabutin Is Active against *Mycobacterium abscessus* Complex. *Antimicrob. Agents Chemother.* **2017**, *61*, e00155-17. [CrossRef]
107. Ganapathy, U.S.; Dartois, V.; Dick, T. Repositioning rifamycins for *Mycobacterium abscessus* lung disease. *Expert Opin. Drug Discov.* **2019**, *14*, 867–878. [CrossRef]
108. Das, S.; Garg, T.; Chopra, S.; Dasgupta, A. Repurposing disulfiram to target infections caused by non-tuberculous mycobacteria. *J. Antimicrob. Chemother.* **2019**, *74*, 1317–1322. [CrossRef]
109. Story-Roller, E.; Maggioncalda, E.C.; Cohen, K.A.; Lamichhane, G. *Mycobacterium abscessus* and β -Lactams: Emerging Insights and Potential Opportunities. *Front. Microbiol.* **2018**, *9*, 2273. [CrossRef]
110. Dubev, V.; Bernut, A.; Cortes, M.; Lesne, T.; Dorchene, D.; Lefebvre, A.-L.; Hugonnet, J.E.; Gutmann, L.; Mainardi, J.L.; Herrmann, J.L.; et al. β -Lactamase inhibition by avibactam in *Mycobacterium abscessus*. *J. Antimicrob. Chemother.* **2015**, *70*, 1051–1058. [CrossRef]
111. Story-Roller, E.; Maggioncalda, E.C.; Lamichhane, G. Select β -Lactam Combinations Exhibit Synergy against *Mycobacterium abscessus* In Vitro. *Antimicrob. Agents Chemother.* **2019**, *63*, e02613-18. [CrossRef] [PubMed]
112. Pandey, R.; Chen, L.; Manca, C.; Jenkins, S.; Glaser, L.; Vinnard, C.; Stone, G.; Lee, J.; Mathema, B.; Nuermberger, E.L.; et al. Dual β -Lactam Combinations Highly Active against *Mycobacterium abscessus* Complex In Vitro. *MBio* **2019**, *10*, e02895-18. [CrossRef] [PubMed]
113. ClinicalTrials.gov. Available online: <https://clinicaltrials.gov/> (accessed on 1 October 2019).
114. Wallace, R.J., Jr.; Dukart, G.; Brown-Elliott, B.A.; Griffith, D.E.; Scerpella, E.G.; Marshall, B. Clinical experience in 52 patients with tigecycline-containing regimens for salvage treatment of *Mycobacterium abscessus* and *Mycobacterium chelonae* infections. *J. Antimicrob. Chemother.* **2014**, *69*, 1945–1953. [CrossRef] [PubMed]
115. Bentur, L.; Gur, M.; Ashkenazi, M.; Livnat-Levanon, G.; Mizrahi, M.; Tal, A.; Ghaffari, A.; Gefen, Y.; Aviram, M.; Efrati, O. Pilot study to test inhaled nitric oxide in cystic fibrosis patients with refractory *Mycobacterium abscessus* lung infection. *J. Cyst. Fibros.* **2019**, in press. [CrossRef] [PubMed]
116. Drug Development Pipeline. Available online: <https://www.cff.org/Trials/Pipeline/> (accessed on 1 October 2019).
117. Caimmi, D.; Martocq, N.; Trioleyre, D.; Guinet, C.; Godreuil, S.; Daniel, T.; Chiron, R. Positive Effect of Liposomal Amikacin for Inhalation on *Mycobacterium abscessus* in Cystic Fibrosis Patients. *Open Forum Infect. Dis.* **2018**, *5*, ofy034. [CrossRef]
118. Diacon, A.H.; Pym, A.; Grobusch, M.P.; de los Rios, J.M.; Gotuzzo, E.; Vasilyeva, I.; Leimane, V.; Andries, K.; Bakare, N.; De Marez, T.; et al. Multidrug-resistant tuberculosis and culture conversion with bedaquiline. *N. Engl. J. Med.* **2014**, *371*, 723–732. [CrossRef]
119. Guglielmetti, L.; Jaspard, M.; Le Dú, D.; Lachâtre, M.; Marigot-Outtandy, D.; Bernard, C.; Veziris, N.; Robert, J.; Yazdanpanah, Y.; Caumes, E.; et al. Long-term outcome and safety of prolonged bedaquiline treatment for multidrug-resistant tuberculosis. *Eur. Respir. J.* **2017**, *49*, 1601799. [CrossRef]
120. Andries, K.; Verhasselt, P.; Guillemont, J.; Göhlmann, H.W.; Neefs, J.M.; Winkler, H.; Van Gestel, J.; Timmerman, P.; Zhu, M.; Lee, E.; et al. A diarylquinoline drug active on the ATP synthase of *Mycobacterium tuberculosis*. *Science* **2005**, *307*, 223–227. [CrossRef]
121. Saxena, A.K.; Singh, A. Mycobacterial tuberculosis Enzyme Targets and their Inhibitors. *Curr. Top. Med. Chem.* **2019**, *19*, 337–355. [CrossRef]
122. Fox, A. Engineered phages stymie drug-resistant infection. *Science* **2019**, *364*, 518–519. [CrossRef]

123. Dedrick, R.M.; Guerrero-Bustamante, C.A.; Garland, R.A.; Russell, D.A.; Ford, K.; Harris, K.; Gilmour, K.C.; Soothill, J.; Jacobs-Sera, D.; Schooley, R.T.; et al. Engineered bacteriophages for treatment of a patient with a disseminated drug-resistant *Mycobacterium abscessus*. *Nat. Med.* **2019**, *25*, 730–733. [[CrossRef](#)]
124. Le Run, E.; Arthur, M.; Mainardi, J.L. In Vitro and Intracellular Activity of Imipenem Combined with Tedizolid, Rifabutin, and Avibactam against *Mycobacterium abscessus*. *Antimicrob. Agents Chemother.* **2019**, *63*, e01915-18. [[CrossRef](#)]
125. Lefebvre, A.L.; Le Moigne, V.; Bernut, A.; Veckerlé, C.; Compain, F.; Herrmann, J.L.; Kremer, L.; Arthur, M.; Mainardi, J.L. Inhibition of the β -Lactamase Bla(*Mab*) by Avibactam Improves the In Vitro and In Vivo Efficacy of Imipenem against *Mycobacterium abscessus*. *Antimicrob. Agents Chemother.* **2017**, *61*, e02440-16. [[CrossRef](#)] [[PubMed](#)]



© 2019 by the authors. Licensee MDPI, Basel, Switzerland. This article is an open access article distributed under the terms and conditions of the Creative Commons Attribution (CC BY) license (<http://creativecommons.org/licenses/by/4.0/>).



ELSEVIER

Contents lists available at ScienceDirect

European Journal of Medicinal Chemistry

journal homepage: <http://www.elsevier.com/locate/ejmech>

Research paper

Design, synthesis and evaluation of covalent inhibitors of DprE1 as antitubercular agents

Lingfeng Liu^a, Chengcheng Kong^b, Marco Fumagalli^c, Karin Savková^d, Yiwen Xu^a, Stanislav Huszár^d, José C. Sammartino^{c,e}, Dongguang Fan^a, Laurent R. Chiarelli^{c,****}, Katarína Mikušová^{d,***}, Zhaogang Sun^{b,**}, Chunhua Qiao^{a,*}^a College of Pharmaceutical Sciences, Soochow University, 199 Renai Road, Suzhou, 215123, PR China^b Beijing Key Laboratory of Drug Resistance Tuberculosis Research, Department of Pharmacology, Beijing Tuberculosis and Thoracic Tumor Research Institute, Beijing Chest Hospital, Capital Medical University, 97 Ma Chang Street, Beijing, 101149, PR China^c Department of Biology and Biotechnology, University of Pavia, Via Ferrata 9, 27100, Pavia, Italy^d Department of Biochemistry, Faculty of Natural Sciences, Comenius University in Bratislava, Mlynská dolina, Ilkovicova 6, 842 15, Bratislava, Slovakia^e University School for Advanced Studies – IUSS Pavia, Piazza Della Vittoria 15, 27100, Pavia, Italy

ARTICLE INFO

Article history:

Received 24 June 2020

Received in revised form

5 August 2020

Accepted 17 August 2020

Available online 30 August 2020

Keywords:

Anti-tuberculosis

DprE1

1,3-Benzothiazin-4-one scaffold

Covalent inhibitors

ABSTRACT

Decaprenylphosphoryl- β -D-ribose 2'-oxidoreductase (DprE1) is a promising drug target for the development of novel anti-tubercular agents, and inhibitors of DprE1 are being investigated extensively. Among them, the 1,3-benzothiazinone compounds such as BTZ043, and its closer congener, PBTZ169, are undergoing clinical studies. It has been shown that both BTZ compounds are prodrugs, the nitro group is reduced to nitroso first, to which an adjacent Cys387 in the DprE1 binding pocket is covalently bound and results in suicide enzyme inhibition. We figured that replacement of the nitro with an electrophilic warhead would still achieve covalent interaction with nucleophilic Cys387, while the required reductive activation could be circumvented. To test this hypothesis, a number of covalent inhibitors of DprE1 were designed and prepared. The compounds inhibitory potency against DprE1 and anti-tubercular activity were investigated, their chemical reactivity, formation of covalent adduct between the warhead and the enzyme was demonstrated by mass spectrometry.

© 2020 Elsevier Masson SAS. All rights reserved.

Tuberculosis (TB), the disease caused primarily by *Mycobacterium tuberculosis* bacillus, has been torturing mankind since the ancient times. With the invention of isoniazid, pyrazinamide, rifamycin and ethambutol in the 1950s and 1960s, the disease was considered curable. Although the number of TB cases has been decreasing globally during the last 20 years, the last report by World Health Organization still estimates 10 million new cases and 1.45 million deaths in 2018 [1]. In addition, surveillance data emphasize the ongoing problem of multidrug resistant TB [1], related to poor adherence to the professional prescription, or co-

morbidities resulting in the compromised immune response. The occurrence of drug resistance and the need to make the long and demanding TB treatment more efficient, leads to continuous efforts to develop novel drugs against TB.

One of the most promising targets for the development of new antituberculosis agents is decaprenylphosphoryl-D-ribose 2'-oxidoreductase (DprE1) [2]. DprE1 is a highly conserved FAD-containing enzyme, which, along with its downstream NADH-dependent reductase DprE2, catalyzes the conversion of decaprenylphosphoryl- β -D-ribofuranose (DPR) to decaprenylphosphoryl- β -D-arabinofuranose (DPA). DPA is essential for the synthesis of the mycobacterial cell wall component arabinan [3], and the sole donor substrate for a series of membrane-embedded arabinosyltransferases including the ethambutol targets EmbA, EmbB, and EmbC [4]. Recently, the periplasmic localization of DprE1 was confirmed, which further substantiates the vulnerability of DprE1 as a promising antitubercular drug target [5].

The first identified class of DprE1 inhibitors were nitro-

* Corresponding author.

** Corresponding author.

*** Corresponding author.

**** Corresponding author.

E-mail addresses: laurent.chiarelli@unipv.it (L.R. Chiarelli), katarina.mikusova@uniba.sk (K. Mikušová), sunzg75@163.com (Z. Sun), qiaochunhua@suda.edu.cn (C. Qiao).

benzothiazinones (BTZs), with compound BTZ043 (Fig. 1) [2] as the lead. The minimal inhibitory concentration (MIC) value, for the next generation nitro-benzothiazinone, PBTZ 169 (Fig. 1), is as low as 1 ng/mL against *Mycobacterium tuberculosis* [6]. This value is 20 folds lower than that of the well known first line drug isoniazid. Structure-activity relationship study confirmed that the 8-nitro group is critical for both enzymatic and cellular activity. Upon binding to DprE1, the nitro group is reduced to a nitroso and that specifically forms a covalent adduct with the Cys387 residue in the active site of DprE1 [7,8].

Recently, a boost to develop covalent drugs has occurred, examples of purposely designed covalent inhibitors are currently approved or at advanced stage of clinical trials [9]. Compared to the non-covalent counterparts, covalent drugs show strong and long acting interaction property that allows better pharmacologic response at a lower concentration [10]. To engineer a covalent drug, the protein/inhibitor interacting pocket features the existence of a nucleophilic residue, such as Ser/Thr, Lys, Met or Cys. Accordingly, the inhibitor molecule bears an electrophilic warhead, or a moiety that could be metabolically activated to the electrophilic part. Typical warhead was observed as a Michael addition acceptor [11], or a cyano group [12]. In DprE1, the presence of Cys387 in the proximity of the BTZ binding site provides the opportunity to achieve selectivity by covalent targeting with electrophilic inhibitors [13]. In this study, we investigated three types (A, B, and C) of BTZ derived compounds, with nitro group replaced by electrophilic warheads (Fig. 2). Compared to the reported prodrug PBTZ169, our designed compounds were expected to inhibit DprE1 through formation of covalent adduct without going through the reductive activation step.

1. Results and discussion

1.1. Chemistry

The designed type A and type C compounds were synthesized following the synthetic route shown in Scheme 1.

PBTZ169 (**1**) was prepared according to the published procedure [6]. Next, reduction of the nitro group to amino was achieved using iron and ammonium chloride. The following Sandmeyer reaction proceeded successfully using *tert*-butyl nitrite/NaNO₂ in combination with copper halides, and converted the aromatic amino group to the corresponding halides (**C01**, **C02** and **C03**). Compound **C03** further served as a common intermediate for the preparation of compounds **C04** and **A01-A07**. Specifically, reaction of **C03** with zinc cyanide using tetrakis (triphenylphosphine)palladium (0) as catalyst gave compound **C04**. Reaction of **C03** with methyl acrylate, acrylamide, *N*-methacrylamide, *N,N*-dimethyl acrylamide, acrylonitrile, methyl propiolate, 2-vinylpyridine provided **A01-A07**, accordingly. Hydrogenation of **A01**, **A05** and **A02** using Pd/C as catalyst furnished **D01**, **D02** and **D03**. All double bond configuration was assigned as *trans*-based on the coupling constant in the ¹H NMR [14].

The designed type B compounds were prepared following the route shown in Scheme 2.

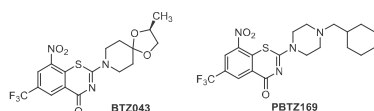


Fig. 1. Reported 1,3-benzothiazinone type DprE1 inhibitors BTZ043 and PBTZ169.

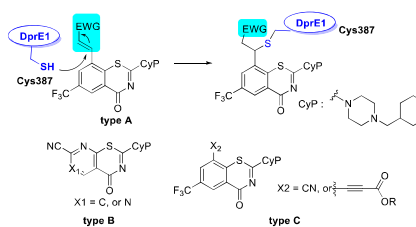


Fig. 2. Design rationale for covalent inhibitors of DprE1.

As shown in Scheme 2, The cyano containing compounds **B01**, **B02** and **B03** were prepared from commercial available starting material 2,6-dichloronicotinic acid or 2,4-dichloropyrimidine-5-carboxylic acid. The carboxylic acid was first transformed using oxalyl chloride to acyl chloride **3a/3b**, which was treated with ammonium thiocyanate to provide isothiocyanate **4a/4b**. Compound **B02** was successfully prepared through one more step reaction between **4b** and 1-(cyclohexylmethyl)piperazine. While reaction of **4a** with 1-(cyclohexylmethyl)piperazine gave intermediate **5** instead of the desired cyclization product, further treatment of **5** with triethylamine in toluene under reflux condition provided intermediate **6**. Finally, compound **B01** was prepared through reaction of **6** with zinc cyanide using palladium catalyst.

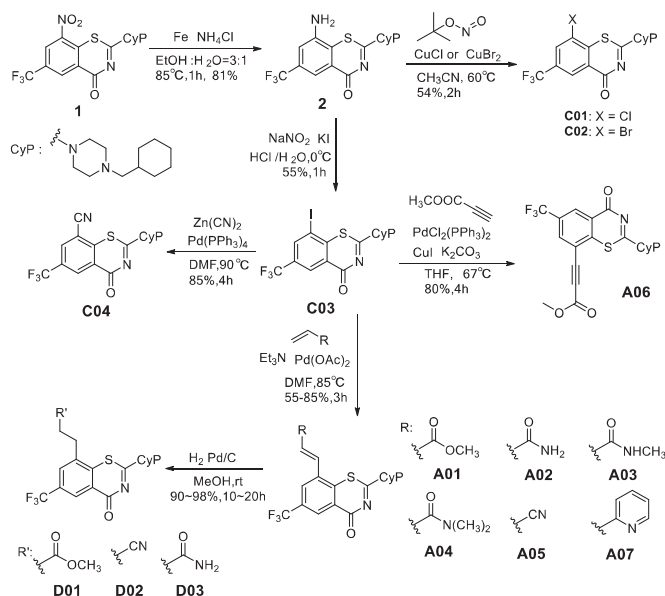
1.2. Biological evaluation and chemical stability study

The prepared compounds were evaluated for their inhibitory activity against both DprE1 and *M. tuberculosis* H37Rv (ATCC 25618). The results are shown in Table 1.

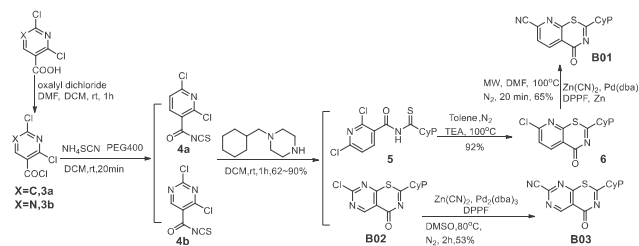
Overall, five out of seven type A compounds displayed good DprE1 inhibitory activity, with **A02**, **A03** and **A06**, in which nitro group replaced by acrylamide, *N*-methacrylamide and methyl propiolate exhibited IC₅₀ less than 0.4 μM; and **A01** and **A04** (methyl acrylate and *N,N*-dimethyl acrylamide, respectively) displayed similar IC₅₀ 1.25 μM against DprE1. It was noted that low activity is observed for compound **A07** (no inhibitory activity at concentration up to 20 μM), considering this compound bears more bulky pyridyl (**A07**), the result may suggest that the binding pocket for the BTZ scaffold at 8-position is space restricted, consistent with previously reported study [15]. It is surprising to notice compound **A05**, with cyano group as warhead, showed dramatic loss of enzyme inhibition activity. Subsequent chemical reactivity study with methyl thioglycolate and stability investigation in PBS buffer revealed **A05** decomposition in the assay solution, explaining the observed low biological activity.

Inconsistent with the enzyme activity, compounds with high inhibitory potency against DprE1 did not display good cellular activity. As shown in Table 1, all type A compounds displayed low *anti*-Mtb H37Rv activity, with MIC values mostly higher than 20 μM. This result suggested the compound poor ability to penetrate the mycomembrane and implement the inhibitory ability.

To validate the covalent inhibitor design rationale, we investigated the compound reactivity toward a nucleophile like methyl thioglycolate (MT) [16]. The result is shown in Table 2. Indeed, except **A03** and **A07**, all other tested compounds show reactivity with electrophile, and covalent adducts with MT were detected as subjecting to mass analysis. The most reactive **A05** had a half life 0.2 h. Further stability study in pH7.4 PBS buffer recorded a half life about 25 min, suggesting the possible decomposition process in the assay solution, which also explains the observed lack of DprE1 and



Scheme 1. Synthetic route for compounds A01-A07, C01-C04 and D01-D03.



Scheme 2. Synthetic route for compound B01, B02 and B03.

anti-mycobacterial activity. By comparison, compound **A06** (methyl propiolate), **A01** (methyl acrylate), **A02** (acrylamide), **A04** (*N,N*-dimethyl acrylamide) displayed stability improvement, half life between 1.0 h and 24 h in the presence of MT. Although **A07** displayed low chemical reactivity toward MT, its weak DprE1 inhibitory activity was more likely due to the intolerance of the bulky pyridyl group in the enzyme binding pocket. Additionally, our detected MT adduct peak for each compound correlates well with the calculated mass (supporting information).

With the 7-cyano warhead, compounds **B01** and **B03** were expected to act as covalent DprE1 inhibitors. Unfortunately, both compounds lost DprE1 activity. Compound **B02**, prepared as the reaction intermediate for **B03**, also shown low DprE1 activity. Taking together, the results suggest only phenyl other than other hetero aromatic rings could be accommodated in the binding

pocket, which is in agreement with the previously reported study [2]. Alternatively, it could be possible that 7-substitution on the phenyl ring was deleterious for enzyme activity. With low DprE1 inhibition capability, the type **B** compounds demonstrated weak (**B03**, MIC 6.7 μ M) or no (**B02**, MIC > 20 μ M) antibacterial activity (Table 1). We confirmed that **B02** could form covalent adduct with MT, and the half life is about 4 h.

During the process of preparation type **A** compounds, the halogen substituted **C01**, **C02** and **C03** were readily obtained. Although these compounds would not act through a covalent inhibition manner as PBTZ169 does, it was interesting to justify how well the 1,3-benzothiazin-4-one scaffold exerts its enzymatic inhibition activity in a non-covalent binding mode. Thus, compounds **C01-C03** were examined for their DprE1 inhibition activity, and micromolar IC₅₀s were recorded (Table 1), which confirmed the

Table 1
Inhibition of DprE1 by prepared compounds and their activity against *M. tuberculosis* H37Rv strain.

Compd	core	R(X)		
		IC ₅₀ , DprE1 (μM)	MIC(μM, <i>Mtb</i> H37Rv)	
A01	A		1.24 (±0.30)	>20.00
A02	A		0.20 (±0.04)	20.00 (±1.4)
A03	A		0.39 (±0.11)	20.00 (±1.56)
A04	A		1.25 (±0.20)	>20.00
A05	A		a	>20.00
A06	A		0.14 (±0.02)	10.00 (±0.26)
A07	A		a	>20.00
B01	B		7.72 (±0.75)	>12.00
B02	B		>20.00	>20.00
B03	B		>20.00	6.73 (±0.44)
C01	C		0.92 (±0.13)	0.03 (±0.01)
C02	C		1.84 (±0.30)	0.16 (±0.02)
C03	C		2.35 (±0.25)	0.63 (±0.04)
C04	C		1.70 (±0.84)	0.16 (±0.10)
D01	C		5.40 (±0.77)	>9.00
D02	C		13.2 (±1.77)	>9.00
D03	C		16.7 (±1.95)	>9.00
1 (PBTZ169)			0.01 (±0.001)	0.011 (±0.02)

^a:"a":compound shows less than 70% inhibitory activity at 20 μM.

significance of the nitro group for DprE1 activity in PBTZ169. The cyano is an apparent covalent warhead and drugs incorporated cyano were discovered in several precedents [17], thus, compound **C04** was prepared and studied. It was found that **C04** displayed IC₅₀ 1.7 μM for the enzyme. However, all type C compounds did retain significant *M. tuberculosis* potency, with MIC 0.03 μM for **C01**, 0.16 μM for **C02** and 0.63 μM for **C03**. Compared to PBTZ169 (MIC 0.01 μM), the antibacterial activity decrease for **C01** was not as pronounced as the enzyme inhibition activity loss. Particularly, it was worthy to say that the antibacterial potency of type C

compounds were superior to the current first-line drug isoniazid (INH, MIC 2.5 μM).

1.3. Type A compounds bind covalently to DprE1

To confirm the designed type A compounds could covalently bind to DprE1, **A01** and **A02** were selected as representative and co-incubated with the enzyme. As a control, DprE1 was incubated with only the solvent DMSO. The mixture was then dialyzed and subjected for mass analysis. As shown in Fig. 3, DprE1 protein

Table 2
Compound reactivity toward methyl thioglycolate (MT).

Compd	core	R(X)	Reactivity with MT (TLC monitor)	Half life $t_{1/2}$ (h)	Calculated covalent adduct mass/detected adduct peak
A05	A			0.2	568.7/568.6
A01	A			1.0	601.7/601.6
A06	A			1.2	599.7/599.6
B02	B			4	449.6/449.7
A02	A			10	586.7/586.6
C04	C			12	542.6/542.6
A04	A			>48	614.7/614.6
A03	A				no
A07	A				no

incubated with DMSO showed a MW of 50,940 Da. By contrast, the protein showed a MW of 51,430 Da after incubation with **A01**, and 51,390 Da when incubated with **A02**, thus an increase in molecular weight of 490 ± 20 or 460 ± 20 Da, respectively, was observed, which supports the covalent adduct formation between DprE1 and the compounds.

Next, to confirm that the covalent bond is formed with the Cys387, the modified protein was subjected to trypsin digestion, and the peptide fragments were analyzed. The LC-MS profile of the protein incubated with **A01** showed a peak with a retention time of 43.27 min, that was absent in profile of the DprE1 alone (Fig. S1, panel B, supporting information). The fragmentation of the peptide showed a sequence compatible with 387 -CVDFP- 391 , with the compound forming an adduct with Cys387 (Fig. S2, top panel). Similarly, the LC-MS profile of the protein incubated with **A02** showed an additional peak with a retention time of 29.33 min (Fig. S1, panel C, supporting information) with the peptide compatible with the sequence 385 -NICVDFPIK- 393 , with the compound bound to the Cys387 (Fig. S2, bottom panel). Thus, the data confirm that the compounds react with the Cys387 of DprE1, forming a covalent adduct.

To further examine the covalent inhibitor design rationale, the double bond in the warhead in the A-type of compounds **A01**, **A05** and **A02** was reduced to single bond and three type **D** compounds (**D01-D03**) were obtained. Compared to the corresponding double bond counterparts, **D01** lost its inhibitory activity about 5 times, **D02** increased its inhibitory activity and **D03** displayed dramatic loss of activity against DprE1 enzyme. Our efforts to identify the covalent adduct between **D01** and DprE1 enzyme failed, which suggests that covalent bond was not formed in this case, as expected.

1.4. Metabolic labeling of *M. tuberculosis* indicates inhibition of DprE1 by the target compounds in the cells

Despite promising inhibitory activities of the selected

compounds from A-series against DprE1 enzyme, their MIC values for *M. tuberculosis* H37Rv were rather high (Table 1). Therefore, we were interested if these molecules target DprE1 in the cells. For this experiment we chose compounds **A01**, **A02**, **A03** and **A06** and examined their effects in *M. tuberculosis* H37Rv by metabolic labeling, as described [18]. The cultures were radiolabeled in three different conditions: (i) for 24 h with ^{14}C acetate added along with the drugs at $100 \times$ MICs, (ii) for 24 h with ^{14}C acetate added along with the drugs at $10 \times$ MICs, (iii) for 24 h at $10 \times$ MICs with ^{14}C acetate added after 24 h of pre-treatment with the drug. The compound **A01**, for which MIC was found to be $> 20.00 \mu\text{M}$ was tested at 0.2 mM and 2 mM concentration. The lipids were extracted from the radiolabeled cells and analyzed by thin-layer chromatography (TLC). As shown in Fig. 4, addition of the control inhibitors, BTZ043 and PBTZ169 caused accumulation of trehalose dimycolates (TDM) and trehalose monomycolates (TMM) in comparison with the control cells. Inhibition of DprE1 by these drugs results in restriction of synthesis of arabinan chains available for the attachment of mycolic acids. Under these conditions, TMM, the donor of mycolic acids for their deposition on arabinogalactan, serves as an acceptor of surplus mycolic acids and TDM is produced. Consequently, increased amounts of TMM and TDM can be considered as a "signature" for inhibitors targeting arabinogalactan portion of mAGP. This phenotype was clearly produced by the control drugs BTZ043 and PBTZ169 at $100 \times$ MIC, while the effects of the tested compounds from A-series were not so profound. For compound **A06** we observed just overall decrease in ^{14}C acetate incorporation into lipids under these conditions. However, at $10 \times$ MIC and longer incubation in the presence of the tested compounds, we can see the expected phenotype, particularly for the compounds **A01**, **A02** and **A06**. The results of this experiment suggest that these compounds target DprE1 in *M. tuberculosis* H37Rv. Likewise, compounds **C01** and **C02**, which were examined by the same approach, appear to target DprE1 based on the lipid profiles obtained from the radiolabeled cells, although covalent binding is not expected in this case.

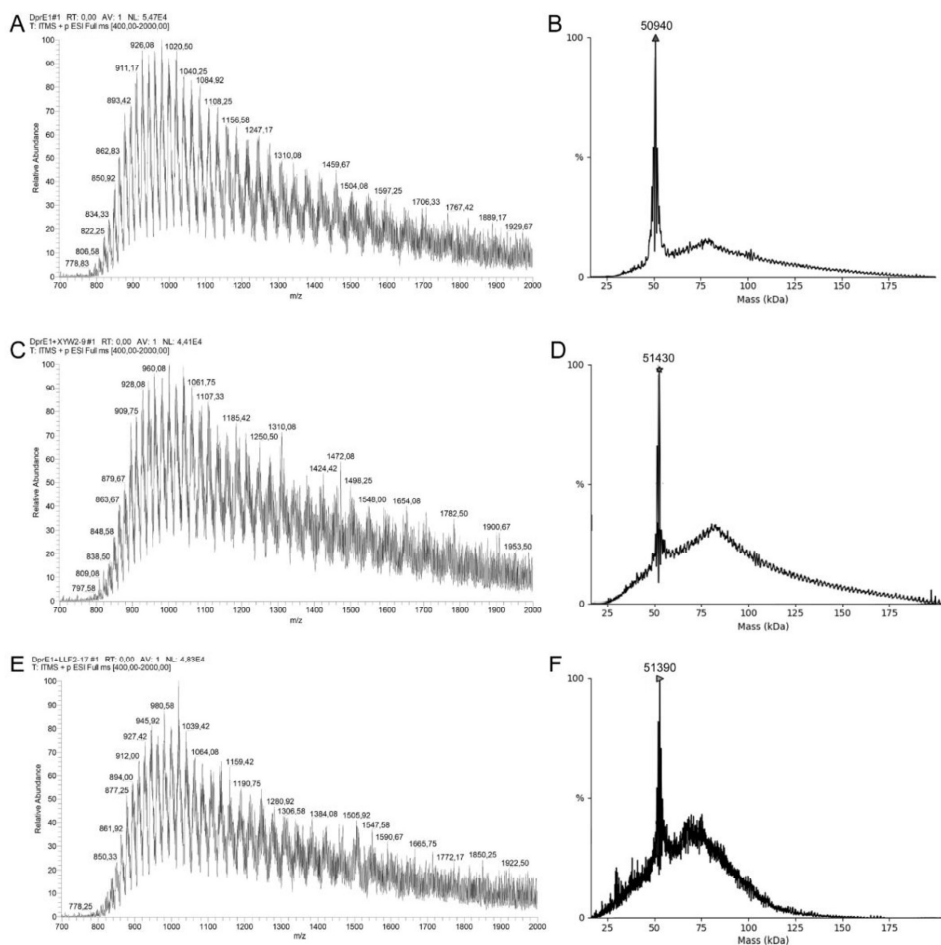


Fig. 3. Mass spectrometry analysis of DprE1 and DprE1-A01/DprE1-A02 complexes demonstrates the formation of a covalent adduct between the protein and the compound. A) ESI-MS profile of DprE1; B) deconvolution of the spectrum in panel A; C) ESI-MS profile of DprE1 after incubation with A01; D) deconvolution of the spectrum in panel C. E) ESI-MS profile of DprE1 after incubation with A02; F) deconvolution of the spectrum in panel E.

2. Conclusion

In summary, we have designed and prepared a number of covalent inhibitors of DprE1. Biochemical evaluation of these compounds was performed. We validated the concept of selective targeting of the cysteine of the DprE1 active site through incorporation of a warhead at the 8 position of 1,3-benzothiazin-4-one scaffold. Compared to the reported nitro BTZ inhibitors, our designed covalent inhibitors circumvent the required reductive activation step. Nonetheless, delicate balance for the compound stability and reactivity towards a nucleophile is critical for practical application of these covalent inhibitors.

3. Experimental section

All commercially available reagents and solvents were used as received. All reactions were monitored by thin layer chromatography (TLC). Compounds were detected by ultraviolet light (UV) absorption at either 254 or 365 nm. TLC was performed on silica HSGF254 plates. All final products were characterized by ^1H NMR, ^{13}C NMR and MS analyses. ^1H NMR and ^{13}C NMR spectra were measured on an INOVA-400 MHz or Agilent DD2-600 MHz spectrometer and referenced to TMS. Analysis of sample purity was performed on SHIMADZU LC-20AD high performance liquid chromatography (HPLC) system. HPLC conditions were as follows:

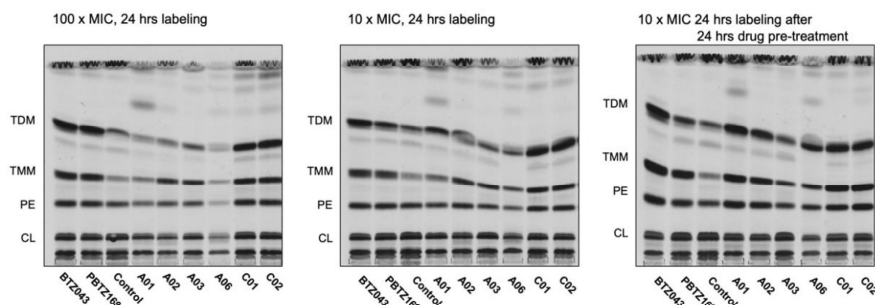


Fig. 4. Evaluation of the effects of the prepared compounds by metabolic radiolabeling. TLC analysis of the lipids from radiolabeled *M. tuberculosis* H37Rv. Mycobacteria were incubated with [^{14}C]-acetate and BTZ043, PBTZ169 or compounds **A01**, **A02**, **A03**, **A06**, **C01** and **C02** at $100 \times \text{MIC}$ (left panel) or $10 \times \text{MIC}$ concentration for 24 h (middle panel). Inhibitors were added along with the label (left and middle panels) or 24 h prior to label addition (right panel). TMM, trehalose monomycolates; TDM, trehalose dimycolates. PE, phosphatidyl ethanolamine, CL – cardiolipin. TLC analysis was performed on Silica Gel plates in $\text{CHCl}_3/\text{CH}_3\text{OH}/\text{H}_2\text{O}$ (20:4:0.5).

solvent A: water, solvent B: MeOH, and flow rate 1.0 mL/min. Compounds were eluted with a gradient from 10 to 100% MeOH/water in 30 min, and purity was determined by the absorbance at 254 nm and 300 nm. All tested compounds have a purity of $\geq 98\%$ before sending for biological test.

3.1. Preparation of intermediate 2

To a solution of compound **1** (116 mg, 0.25 mmol) in EtOH/water (3:1, 8 mL) was added NH_4Cl (0.7 mg, 0.013 mmol) and Fe powder (142 mg, 2.54 mmol). The resulting mixture was heated at reflux and stirred for 1 h. After cooling to room temperature, the mixture was filtered through a pad of diatomaceous earth, which was then washed with more methanol (MeOH, 10 mL \times 3). The filtrate was concentrated under reduced pressure and the resulting aqueous fraction was extracted with dichloromethane (DCM, 20 mL \times 3). The combined extracts were washed with brine, dried (Na_2SO_4), filtered, and concentrated. The crude residue was purified by flash column chromatography on silica gel with DCM: MeOH (90:1) to afford intermediate **2** (88 mg, yield 82%) as a white solid: $R_f = 0.2$, $\text{CH}_2\text{Cl}_2/\text{MeOH}$: 90:1.

3.1.1. 2-(4-(Cyclohexylmethyl)piperazin-1-yl)-8-iodo-6-(trifluoromethyl)-4H-benzo[e][1,3]thiazin-4-one (C03)

To intermediate **2** (100 mg, 0.23 mmol) suspended in water (20 mL) at $0-5^\circ\text{C}$ was added dilute HCl (10%, 2 mL) and NaNO_2 (24 mg, 0.35 mmol, 1.5 equiv.) solutions successively, and the resulting reaction mixture was stirred for 1 h to complete the diazotization process. Then KI (78 mg, 0.47 mmol, 2.0 equiv.) was slowly added, and the reaction was stirred overnight at room temperature. The mixture was filtered and washed with distilled water (10 mL) and extracted with EtOAc (10 mL \times 3), and the combined organic layer was washed with 10% aqueous solution of Na_2SO_3 (15 mL) and then dried over anhydrous Na_2SO_4 , filtered, and concentrated. The crude residue was purified by flash column chromatography on silica gel with ethyl acetate (EtOAc) and petroleum ether (PET), EtOAc:PET (1:1) to afford compound **C03** (70 mg, yield 56%) as a yellow solid: $R_f = 0.2$, EtOAc:PET (1:1); ^1H NMR (400 MHz, CDCl_3) δ 8.75 (s, 1H), 8.18 (s, 1H), 4.43 (br, 2H), 4.09 (br, 2H), 2.62 (s, 4H), 2.26 (s, 2H), 1.81–1.75 (m, 6H), 1.71 (s, 1H), 1.33–1.21 (m, 2H), 0.92–0.87 (m, 2H); ^{13}C NMR (151 MHz, CDCl_3) δ 169.4, 161.7, 141.0, 138.3 (d, $J = 3.0$ Hz), 131.5 (d, $J = 34.7$ Hz), 127.2 (d, $J = 4.5$ Hz), 126.5, 125.2, 122.5 (q, $J = 273.3$ Hz), 94.9, 65.0, 52.9,

45.9, 34.8, 31.7, 26.6, 25.9; HRMS (ESI+) m/z $[\text{M} + \text{H}]^+$ calcd for $\text{C}_{20}\text{H}_{24}\text{F}_3\text{N}_3\text{O}_5$, 538.0631; found, 538.0610.

3.2. General procedure for the preparation of compound A01–05, A07 via Heck coupling reactions

To a solution of compound **C03** (1.0 equiv) in *N,N*-dimethylformamide (DMF) under a nitrogen atmosphere was added a series reagent containing propylene group (1.2 equiv; methyl acrylate, acrylamide, *N*-methacrylamide, *N,N*-dimethyl acrylamide, acrylonitrile, 2-vinylpyridine), triethylamine (2.0 equiv), palladium acetate (0.5 equiv). The reaction mixture was heated to 85°C for 3–6 h. After being cooled to room temperature, the solvent was evaporated under reduced pressure and diluted with ethyl acetate (20 mL) and washed with 10 mL H_2O . The solvents were removed. The products were purified using flash chromatography using mixtures of EtOAc and PET as eluent. The isolated yields were 56–92%.

3.2.1. Methyl (E)-3-(2-(4-(cyclohexylmethyl)piperazin-1-yl)-4-oxo-6-(trifluoromethyl)-4H-benzo[e][1,3]thiazin-8-yl)acrylate (A01)

The title compound was prepared from **C03** and methyl acrylate using the general procedure for Heck reaction (yield 92%) as a light white solid: $R_f = 0.24$, EtOAc:PET (1:1); ^1H NMR (400 MHz, CDCl_3) δ 8.75 (s, 1H), 7.91, 7.89 (d, $J = 16.0$ Hz, 1H), 6.54 (d, $J = 16.0$ Hz, 1H), 4.12 (br, 2H), 3.86 (s, 3H), 3.63 (br, 2H), 2.56 (s, 4H), 2.22 (d, $J = 4$ Hz, 2H), 1.80–1.67 (m, 6H), 1.51 (s, 1H), 1.32–1.28 (m, 2H), 0.93–0.87 (m, 2H); ^{13}C NMR (151 MHz, CDCl_3) δ 167.8, 166.1, 160.2, 137.1, 135.9, 132.5, 130.0 (q, $J = 33.2$ Hz), 128.5 (d, $J = 3.0$ Hz), 126.3 (d, $J = 3.0$ Hz), 124.3, 123.9, 123.2 (q, $J = 273.3$ Hz), 65.1, 52.9, 52.2, 46.1, 34.9, 31.7, 26.6, 26.0; HRMS (ESI+) m/z $[\text{M} + \text{H}]^+$ calcd for $\text{C}_{24}\text{H}_{29}\text{F}_3\text{N}_3\text{O}_5$, 496.1876; found 496.1893.

3.2.2. (E)-3-(2-(4-(Cyclohexylmethyl)piperazin-1-yl)-4-oxo-6-(trifluoromethyl)-4H-benzo[e][1,3]thiazin-8-yl)acrylamide (A02)

The title compound was prepared from **C03** and acrylamide using the general procedure for Heck reaction (yield 56%) as a brown solid: $R_f = 0.25$, EtOAc:PET (1:1); ^1H NMR (400 MHz, CD_3OD) δ 8.59 (s, 1H), 8.14 (s, 1H), 7.83 (d, $J = 15.2$ Hz, 1H), 6.83 (d, $J = 15.2$ Hz, 1H), 4.88 (s, 2H), 4.03 (br, 4H), 2.72 (br, 4H), 2.36 (s, 2H), 1.85–1.63 (m, 6H), 1.53 (br, 1H), 1.29–1.17 (m, 2H), 0.97–0.88 (m, 2H); ^{13}C NMR (100 MHz, CDCl_3) δ 167.1, 164.9, 159.5, 135.1, 134.1, 131.8, 128.8 (q, $J = 33.5$ Hz), 127.1 (d, $J = 3.3$ Hz), 125.0 (d, $J = 2.9$ Hz),

124.6, 123.2, 122.3 (q, $J = 271.3$ Hz), 64.1, 52.0, 33.9, 30.7, 28.7, 25.7, 25.0; HRMS (ESI⁺) m/z [M+H]⁺ calcd for C₂₃H₂₈F₃N₄O₂S, 481.1880; found, 481.1863.

3.2.3. (E)-3-(2-(4-(Cyclohexylmethyl)piperazin-1-yl)-4-oxo-6-(trifluoromethyl)-4H-benzo[e][1,3]thiazin-8-yl)-N-methylacrylamide (A03)

The title compound was prepared from **C03** and *N*-methyl acrylamide using the general procedure for Heck reaction (yield 56%) as a brown solid: $R_f = 0.23$, EtOAc-PET 1:1; ¹H NMR (400 MHz, CDCl₃) δ 8.66 (s, 1H), 7.83 (d, $J = 14.8$, 1H), 7.82 (s, 1H), 6.56 (d, $J = 15.2$ Hz, 1H), 6.45 (d, $J = 3.2$ Hz, 1H), 4.08 (br, 2H), 3.76 (br, 2H), 2.98 (d, $J = 4.4$ Hz, 3H), 2.49 (s, 4H), 2.16 (d, $J = 6.0$ Hz, 2H), 1.78–1.69 (m, 6H), 1.48 (br, 1H), 1.31–1.19 (m, 2H), 0.91–0.85 (m, 2H); ¹³C NMR (151 MHz, CDCl₃) δ 168.1, 164.9, 160.6, 136.0, 133.7, 133.2, 129.7 (q, $J = 28.2$ Hz), 129.0 (q, $J = 277.4$ Hz), 127.9 (d, $J = 3.6$ Hz), 126., 125.9 (d, $J = 2.7$ Hz), 124.2, 65.1, 53.1, 53.0, 34.9, 31.7, 29.7, 26.7, 26.0; HRMS (ESI⁺) m/z [M+H]⁺ calcd for C₂₄H₃₀F₃N₄O₂S, 495.2036; found: 495.2000.

3.2.4. (E)-3-(2-(4-(Cyclohexylmethyl)piperazin-1-yl)-4-oxo-6-(trifluoromethyl)-4H-benzo[e][1,3]thiazin-8-yl)-N,N-dimethylacrylamide (A04)

The title compound was prepared from **C03** (20 mg, 0.04 mmol) and *N,N*-dimethyl acrylamide using the general procedure for Heck reaction as a brown solid (yield 59%): $R_f = 0.5$, EtOAc-PET 1:1; ¹H NMR (400 MHz, CDCl₃) δ 8.74 (s, 1H), 7.91 (d, $J = 16.0$ Hz, 1H), 7.89 (s, 1H), 6.98 (d, $J = 16.0$ Hz, 1H), 4.13 (br, 2H), 3.81 (br, 2H), 3.23 (s, 3H), 3.12 (s, 3H), 2.54 (br, 4H), 2.21 (br, 2H), 1.81–1.71 (m, 6H), 1.52 (br, 1H), 1.33–1.25 (m, 2H), 0.94–0.88 (m, 2H); ¹³C NMR (151 MHz, CDCl₃) δ 168.1, 165.0, 160.7, 135.9, 135.2, 133.6, 129.8 (d, $J = 34.7$ Hz), 127.9 (d, $J = 3.0$ Hz), 125.9 (d, $J = 3.0$ Hz), 124.2, 123.5, 123.3 (q, $J = 273.3$ Hz), 65.1, 53.0, 46.4, 37.5, 36.1, 34.9, 31.7, 26.6, 26.0; HRMS (ESI⁺) m/z [M + H]⁺ calcd for C₂₅H₃₂F₃N₄O₂S, 509.2193; found 509.2207.

3.2.5. (E)-3-(2-(4-(Cyclohexylmethyl)piperazin-1-yl)-4-oxo-6-(trifluoromethyl)-4H-benzo[e][1,3]thiazin-8-yl)acrylonitrile (A05)

The title compound was prepared from **C03** and acrylonitrile using the general procedure for Heck reaction as a yellow solid (yield 76%): $R_f = 0.4$, EtOAc-PET 1:1; ¹H NMR (400 MHz, CDCl₃) δ 8.78 (s, 1H), 7.85 (s, 1H), 7.64 (d, $J = 16.0$ Hz, 1H), 6.05 (d, $J = 16$ Hz, 1H), 4.12 (br, 2H), 3.80 (br, 2H), 2.54 (br, 4H), 2.19 (s, 2H), 1.80–1.70 (m, 6H), 1.50 (br, 1H), 1.32–1.15 (m, 2H), 0.90–0.84 (m, 2H); ¹³C NMR (151 MHz, CDCl₃) δ 167.3, 159.5, 143.1, 135.7, 131.5, 130.2 (q, $J = 34.7$ Hz), 129.3 (d, $J = 3.0$ Hz), 125.8 (d, $J = 1.5$ Hz), 124.5, 123.0 (q, $J = 273.3$ Hz), 116.5, 103.0, 65.1, 53.0, 46.3, 34.9, 31.7, 26.7, 26.0; HRMS (ESI⁺) m/z [M+H]⁺ calcd for C₂₃H₂₆F₃N₄O₂S, 463.1774; found, 463.1783.

3.2.6. Methyl 3-(2-(4-(cyclohexylmethyl)piperazin-1-yl)-4-oxo-6-(trifluoromethyl)-4H-benzo[e][1,3]thiazin-8-yl)propionate (A06)

To a stirred solution of compound **C03** (20 mg, 0.04 mmol) in tetrahydrofuran (THF, 5 mL) was added methyl propionate (5 mg, 0.05 mmol, 1.2 equiv), potassium carbonate (10 mg, 0.08 mmol, 2.0 equiv), Pd(PPh₃)₂Cl₂ (2 mg, 0.2 equiv) and CuI (1 mg, 0.2 equiv) and the resulting mixture was stirred for 4 h at room temperature. The reaction mixture was then diluted with water (10 mL) and extracted with DCM (10 mL \times 3). The organic extracts were combined and dried over anhydrous MgSO₄ and concentrated under reduced pressure. The crude residue was purified by flash column chromatography on silica gel to afford compound **A06** (15 mg, yield 82%) as a brown solid: $R_f = 0.23$, EtOAc: PET = 1:5. ¹H NMR (400 MHz, CDCl₃) δ 8.78 (s, 1H), 7.99 (s, 1H), 4.15 (br, 2H), 3.90 (s, 3H), 3.78 (br, 2H), 2.57 (br, 4H), 2.22 (s, 2H), 1.80–1.71 (m, 6H), 1.51

(br, 1H), 1.24–1.15 (m, 2H), 0.90–0.87 (m, 2H); ¹³C NMR (151 MHz, CDCl₃) δ 167.3, 160.6, 153.3, 140.5, 133.1 (d, $J = 2.8$ Hz), 130.1 (q, $J = 34.4$ Hz), 129.3 (d, $J = 3.3$ Hz), 124.2, 122.8 (q, $J = 273.0$ Hz), 117.8, 88.8, 78.9, 65.1, 53.3, 53.0, 46.3, 35.0, 31.7, 26.7, 26.0; HRMS (ESI⁺) m/z [M+Na]⁺ calcd for C₂₄H₂₆F₃N₃O₃Na, 516.1539; found, 516.1521.

3.2.7. (E)-2-(4-(Cyclohexylmethyl)piperazin-1-yl)-8-(2-(pyridin-2-yl)vinyl)-6-(trifluoromethyl)-4H-benzo[e][1,3]thiazin-4-one (A07)

The title compound was prepared from **C03** and 2-vinylpyridine using the general procedure for Heck reaction as a brown solid (yield 57%): $R_f = 0.35$, EtOAc-PET 1:1; ¹H NMR (400 MHz, CDCl₃) δ 8.70 (s, 1H), 8.68 (d, $J = 4.0$ Hz, 1H), 8.01 (s, 1H), 7.90 (d, $J = 16.0$ Hz, 1H), 7.74 (t, $J = 8.0$ Hz, 1H), 7.40 (d, $J = 4.0$ Hz, 1H), 7.26 (s, 1H), 7.21 (d, $J = 12.0$ Hz, 1H), 4.07 (br, 2H), 3.83 (br, 2H), 2.51 (s, 4H), 2.17 (d, $J = 8.0$ Hz, 2H), 1.79–1.70 (m, 6H), 1.49 (br, 1H), 1.33–1.25 (m, 2H), 0.92–0.87 (m, 2H); ¹³C NMR (151 MHz, CDCl₃) δ 168.4, 161.0, 153.8, 149.9, 136.9, 135.1, 133.9, 129.8 (q, $J = 33.2$ Hz), 126.7, 125.5 (d, $J = 3.0$ Hz), 125.2, 124.0, 123.7, 123.5 (q, $J = 273.3$ Hz), 123.4, 65.0, 52.9, 45.8, 34.8, 31.7, 26.6, 25.9; HRMS (ESI⁺) m/z [M+H]⁺ calcd for C₂₇H₃₀F₃N₄O₂S, 515.2087; found 515.2078.

3.3. General procedure for the synthesis of compound C01, C02

A mixture of *tert*-butyl nitrite (1.25 equiv), copper (I) chloride or copper (II) bromide (1.25 equiv), in CH₃CN was heated to 60 °C, then treated with intermediate **2** (1.0 equiv) over 10 min, stirring is continued for 2 h. The mixture was cooled to room temperature, and diluted with ethyl acetate. The organic layer was washed with 10% hydrochloric acid and filtered, concentrated. The residue was applied to column chromatography to afford the title compound **C01** and **C02**.

3.3.1. 8-Chloro-2-(4-(cyclohexylmethyl)piperazin-1-yl)-6-(trifluoromethyl)-4H-benzo[e][1,3]thiazin-4-one (C01)

The title compound was prepared from intermediate **2** (100 mg, 0.24 mmol), copper (I) chloride (280 mg, 0.48 mmol, 2.0 eq) and *tert*-butyl nitrite (48 mg, 0.47 mmol, 2.0 eq) using the above procedure as a white solid (58 mg, yield 54%): $R_f = 0.68$, EtOAc-PET 1:1; ¹H NMR (400 MHz, CDCl₃) δ 8.73 (s, 1H), 7.97 (s, 1H), 4.13 (br, 2H), 3.81 (br, 2H), 2.54 (br, 4H), 2.20 (s, 2H), 1.81–1.71 (m, 6H), 1.40 (br, 1H), 1.25–1.15 (m, 2H), 0.90–0.88 (m, 2H); ¹³C NMR (151 MHz, CDCl₃) δ 168.3, 161.2, 137.7, 131.9 (d, $J = 1.5$ Hz), 130.9 (d, $J = 36.2$ Hz), 126.5 (d, $J = 3.0$ Hz), 126.0, 122.7 (q, $J = 273.3$ Hz), 120.4, 65.0, 52.8, 46.0, 34.7, 31.7, 26.5, 25.9; HRMS (ESI⁺) m/z [M+H]⁺ calcd for C₂₀H₂₄ClF₃N₃O₂S, 446.1275; found, 446.1294.

3.3.2. 8-Bromo-2-(4-(cyclohexylmethyl)piperazin-1-yl)-6-(trifluoromethyl)-4H-benzo[e][1,3]thiazin-4-one (C02)

The title compound **C02** was prepared from intermediate **2** (50 mg, 0.12 mmol), copper (II) bromide (34 mg, 0.24 mmol, 2.0 equiv) and *tert*-butyl nitrite (15 mg, 0.14 mmol, 1.2 equiv) using the above procedure. The product was obtained as a white solid (32 mg, yield 52%): $R_f = 0.48$, EtOAc-PET 1:1; ¹H NMR (400 MHz, CDCl₃) δ 8.72 (s, 1H), 7.97 (s, 1H), 4.15 (br, 2H), 3.85 (br, 2H), 2.59 (s, 4H), 2.24 (s, 2H), 1.77–1.71 (m, 6H), 1.53 (br, 1H), 1.41–1.25 (m, 2H), 0.88 (br, 2H); ¹³C NMR (151 MHz, CDCl₃) δ 168.3, 161.1, 137.9, 131.8 (d, $J = 3.0$ Hz), 130.8 (d, $J = 33.2$ Hz), 126.4 (d, $J = 3.0$ Hz), 126.1, 126.0 (d, $J = 273.3$ Hz), 120.3, 65.1, 53.0, 46.3, 34.9, 31.7, 26.7, 26.0; HRMS (ESI⁺) m/z [M+Na]⁺ calcd for C₂₀H₂₄BrF₃N₃O₂Na, 512.0590; found, 512.0755.

3.3.3. 2-(4-(Cyclohexylmethyl)piperazin-1-yl)-4-oxo-6-(trifluoromethyl)-4H-benzo[e][1,3]thiazine-8-carbonitrile (C04)

To a solution of compound **C03** (20 mg, 37.2 μ mol) in DMF

(10.0 mL) under nitrogen atmosphere was added zinc (II) cyanide (3 mg, 0.02 mmol) and tetrakis (triphenylphosphine)palladium (0) (2 mg, 10%). The reaction mixture was stirred at 90 °C for 4 h and was then diluted with toluene (10 mL) and the phases were separated. The aqueous phase was extracted twice with toluene (10 mL × 2). The combined organic phase was washed with brine (10 mL) and saturated aqueous ammonium hydroxide, dried over Na₂SO₄ and concentrated. The crude residue was purified by flash column chromatography on silica gel to afford compound **C04** (14 mg, yield 86%) as a white solid: *R*_f = 0.26, EtOAc: PET (1:5); ¹H NMR (400 MHz, CDCl₃) δ 8.91 (s, 1H), 8.08 (s, 1H), 4.15 (br, 2H), 3.78 (br, 2H), 2.54 (s, 4H), 2.19 (s, 2H), 1.80–1.71 (m, 6H), 1.67 (br, 1H), 1.28–1.18 (m, 2H), 0.90–0.87 (m, 2H); ¹³C NMR (151 MHz, CDCl₃) δ 166.3, 159.2, 140.5, 132.7 (d, *J* = 2.7 Hz), 131.5 (d, *J* = 3.0 Hz), 130.7 (q, *J* = 34.9 Hz), 124.6, 122.3 (q, *J* = 273.8 Hz), 113.9, 110.9, 65.0, 53.1, 35.0, 31.7, 29.7, 26.7, 26.0; HRMS (Cl⁺) *m/z* [M+H]⁺ calcd for C₂₁H₂₄F₃N₄O₅, 437.1617; found, 437.1614.

3.4. General procedure for the synthesis of compound **D01**, **D02**, **D03**

To a solution of compound A01, or A02 or A05 in methanol was added 20% Pd/C. The mixture was stirred under hydrogen at room temperature. After completion, the mixture was filtered through Celite and the filtrate was concentrated. The residue was applied to column chromatography for purification to afford the title compound **D01**, **D02**, **D03**.

3.4.1. Methyl-3-(2-(4-(cyclohexylmethyl)piperazin-1-yl)-4-oxo-6-(trifluoromethyl)-4H-benzo[e][1,3]thiazin-8-yl)propanoate (**D01**)

The title compound was prepared from **A01** (20 mg, 0.04 mmol) and Pd/C (4 mg, 20%) using the general procedure for reduction reaction (18 mg, yield 90%) as a cyan-blue solid: *R*_f = 0.34, EtOAc: PET 1:1; ¹H NMR (400 MHz, CDCl₃) δ 8.64 (s, 1H), 7.61 (s, 1H), 4.07 (br, 2H), 3.79 (br, 2H), 3.70 (s, 3H), 3.11 (t, *J* = 8.0 Hz, 2H), 2.73 (t, *J* = 8.0 Hz, 2H), 2.51 (s, 4H), 2.18 (d, *J* = 8.0 Hz, 2H), 1.79–1.70 (m, 6H), 1.49 (s, 1H), 1.27–1.22 (m, 2H), 0.89–0.86 (m, 2H); ¹³C NMR (151 MHz, CDCl₃) δ 172.1, 168.5, 160.7, 137.1, 135.3, 129.5 (q, *J* = 33.2 Hz), 128.1 (d, *J* = 3.0 Hz), 125.9 (d, *J* = 3.0 Hz), 123.8, 123.5 (q, *J* = 273.3 Hz), 65.1, 53.0, 51.9, 46.2, 34.9, 33.0, 31.7, 27.7, 26.7, 26.0; HRMS (ESI⁺) *m/z* [M+H]⁺ calcd for C₂₄H₃₁F₃N₃O₅S, 498.2033; found, 498.2009.

3.4.2. 3-(2-(4-(cyclohexylmethyl)piperazin-1-yl)-4-oxo-6-(trifluoromethyl)-4H-benzo[e][1,3]thiazin-8-yl)propanenitrile (**D02**)

The title compound was prepared from **A05** (20 mg, 0.04 mmol) and Pd/C (4 mg, 20%) using the general procedure for reduction reaction (18 mg, yield 95%) as a cyan-blue solid: *R*_f = 0.36, EtOAc: PET 1:1; ¹H NMR (400 MHz, CDCl₃) δ 8.70 (s, 1H), 7.65 (s, 1H), 4.10 (br, 2H), 3.79 (br, 2H), 3.17 (t, *J* = 8.0 Hz, 2H), 2.76 (t, *J* = 8.0 Hz, 2H), 2.52 (s, 4H), 2.18 (d, *J* = 8.0 Hz, 2H), 1.79–1.67 (m, 6H), 1.49 (br, 1H), 1.28–1.20 (m, 2H), 0.95–0.86 (m, 2H); ¹³C NMR (151 MHz, CDCl₃) δ 168.1, 159.9, 135.3, 134.7, 129.8 (q, *J* = 33.2 Hz), 128.5, 126.7, 124.1, 121.3 (q, *J* = 271.8 Hz), 117.8, 65.1, 53.0, 46.4, 35.0, 31.7, 28.4, 26.7, 26.0, 17.1; HRMS (ESI⁺) *m/z* [M+H]⁺ calcd for C₂₃H₂₈F₃N₄O₅, 465.1930; found, 465.1912.

3.4.3. 3-(2-(4-(Cyclohexylmethyl)piperazin-1-yl)-4-oxo-6-(trifluoromethyl)-4H-benzo[e][1,3]thiazin-8-yl)propanamide (**D03**)

The title compound was prepared from **A02** (20 mg, 0.04 mmol) and Pd/C (4 mg, 20%) using the general procedure for reduction reaction (19 mg, yield 98%) as a white solid: *R*_f = 0.28, EtOAc: PET 1:1; ¹H NMR (400 MHz, CDCl₃) δ 8.62 (s, 1H), 7.64 (s, 1H), 5.65 (s, 1H), 5.54 (s, 1H), 4.24 (br, 2H), 4.03 (br, 2H), 3.14 (s, 2H), 2.63 (s, 6H),

2.29 (s, 2H), 1.83–1.72 (m, 6H), 1.60 (s, 1H), 1.28–1.21 (m, 2H), 0.94–0.87 (br, 2H); ¹³C NMR (100 MHz, CDCl₃) δ 172.6, 168.6, 160.9, 137.5, 135.3, 128.1, 125.9, 123.8, 65.1, 52.9, 46.1, 34.4, 31.7, 29.7, 27.7, 26.6, 26.0; HRMS (ESI⁺) *m/z* [M+H]⁺ calcd for C₂₃H₃₀F₃N₄O₅S, 483.2036; found, 483.2062.

3.5. Preparation of intermediate **5**

Oxalyl chloride (165 mg, 1.3 mmol, 2.5 equiv) and catalytic amount of DMF were added successively to the suspension of 2,6-dichloronicotinic acid (100 mg, 0.52 mmol) in DCM (10 mL). The reaction was stirred at room temperature for 1 h and evaporated in vacuo. The residue was dissolved in 20 mL DCM and added to ammonium thiocyanate (59 mg, 0.78 mmol, 1.5 equiv) dropwise under stirring. A catalytic amount of PEG-400 was added to this suspension, it was then stirred at room temperature for 20 min. After consumption of the starting material, 1-(cyclohexylmethyl)piperazine (95 mg, 0.52 mmol) was added and stirred for 1 h at room temperature. The reaction mixture was diluted with water (30 mL) and extracted with DCM (20 mL × 3). The combined organic extracts were dried over anhydrous MgSO₄ and concentrated under reduced pressure. The residue was purified by column chromatography on silica gel with EtOAc:PET (1:3) to afford intermediate **5** as a colorless liquid (142 mg, yield 64%); *R*_f = 0.27, EtOAc: PET (1:3). MS(+ESI) *m/z* calcd for C₁₈H₂₅Cl₂N₄O₅ [M+H]⁺ = 415.10, found, 414.7.

3.6. Preparation of intermediate **6**

To a solution of intermediate **5** (20 mg, 0.04 mmol) in 10 mL toluene was added triethylamine (67 mg, 0.66 mmol, 2.0 equiv). The reaction mixture was stirred at 100 °C for 1 h and then diluted with 10 mL H₂O and the phases were separated. The aqueous phase was extracted twice with toluene (10 mL × 2). The combined organic phase was washed with brine and saturated aqueous ammonium hydroxide, dried over sodium sulfate and concentrated. The crude residue was purified by flash column chromatography on silica gel to afford intermediate **6** as a white solid (12 mg, yield 92%). EtOAc:PET (1:3, *R*_f = 0.24); ¹H NMR (400 MHz, CDCl₃) δ 8.57 (d, *J* = 8.2 Hz, 1H), 7.38 (d, *J* = 8.2 Hz, 1H), 4.12 (s, 2H), 3.69 (s, 2H), 2.51 (s, 4H), 2.17 (d, *J* = 6.8 Hz, 2H), 1.76 (d, *J* = 14.8 Hz, 4H), 1.69 (s, 2H), 1.48 (s, 1H), 1.28–1.21 (m, 2H), 0.93–0.85 (m, 2H).

3.6.1. 2-(4-(Cyclohexylmethyl)piperazin-1-yl)-4-oxo-4H-pyrido [3,2-*e*][1,3]thiazine-7-carbonitrile (**B01**)

To a 20 mL microwave vial containing a mixture of intermediate **6** (30 mg, 0.08 mmol), zinc cyanide (11 mg, 0.1 mmol, 1.2 equiv), zinc powder (4 mg, 0.02 mmol, 0.2 equiv), and DPPF (9 mg, 0.02 mmol, 0.2 equiv) was added DMSO (6 mL). The suspension was stirred with degassing under nitrogen for 5 min. Next, tris(dibenzylideneacetone)dipalladium (0) (7 mg, 0.01 mmol, 0.1 equiv) was added. The reaction mixture was sealed and stirred with heating at 100 °C (heat block) for 20 min. Then it was allowed to cool to RT, diluted with 20 mL of water, and adjusted to pH=8 with sat NaHCO₃, and extracted with DCM (10 mL × 3). The organic extracts were dried over anhydrous MgSO₄ and concentrated under reduced pressure. The residue was purified by column chromatography on silica gel to afford compound **B01** as a white solid (20 mg, yield 65%); EtOAc:PET (1:3, *R*_f = 0.23); ¹H NMR (400 MHz, CDCl₃) δ 8.75 (d, *J* = 8.0 Hz, 1H), 7.75 (d, *J* = 8.0 Hz, 1H), 4.15 (br, 2H), 3.72 (br, 2H), 2.53 (s, 4H), 2.18 (s, 2H), 1.79–1.70 (m, 6H), 1.49 (br, 1H), 1.27–1.20 (m, 2H), 0.92–0.87 (m, 2H); ¹³C NMR (151 MHz, CDCl₃) δ 167.6, 161.9, 156.5, 139.1, 135.7, 127.4, 122.6, 115.8, 65.0, 53.0, 34.9, 31.7, 29.7, 26.7, 26.0; HRMS (Cl⁺) *m/z* [M+H]⁺ calcd for C₁₉H₂₄N₅O₅, 370.1696; found, 370.1700.

3.6.2. 7-Chloro-2-(4-(cyclohexylmethyl)piperazin-1-yl)-4H-pyrimido[5,4-e][1,3]thiazin-4-one (**B02**)

To a solution of 2,4-dichloropyrimidine-5-carbonyl chloride (100 mg, 0.47 mmol) in DCM (10 mL) added ammonium thiocyanate (54 mg, 0.71 mmol, 1.5 equiv) dropwise under stirring. A drop of PEG-400 was added to the suspension, it was then stirred at room temperature for 20 min. After consumption of the starting material, 1-(cyclohexylmethyl)piperazine (86 mg, 0.47 mmol) was added. It was then stirred for 1 h at room temperature. The reaction mixture was then diluted with water (30 mL) and extracted with DCM (20 mL × 3). The organic extracts were dried over anhydrous MgSO₄ and concentrated under reduced pressure. The residue was purified by column chromatography on silica gel to afford compound **B02** as a white solid (159 mg, yield 89%); EtOAc-PET (1:3, *R_f* = 0.27); ¹H NMR (400 MHz, CDCl₃) δ 9.36 (s, 1H), 4.17 (br, 2H), 3.74 (br, 2H), 2.57 (s, 4H), 2.21 (s, 2H), 1.81–1.73 (m, 6H), 1.51 (br, 1H), 1.35–1.23 (m, 2H), 0.92–0.88 (m, 2H); ¹³C NMR (151 MHz, CDCl₃) δ 167.3, 166.6, 162.3, 161.0, 160.0, 115.9, 65.0, 53.0, 52.8, 47.0, 46.6, 35.0, 31.6, 26.7, 26.0; HRMS (CI⁺) *m/z* [M+H]⁺ calcd for C₁₇H₂₃ClN₅O₂S, 380.1306; found, 380.1317.

3.6.3. 2-(4-(Cyclohexylmethyl)piperazin-1-yl)-4-oxo-4H-pyrimido[5,4-e][1,3]thiazine-7-carbonitrile(**B03**)

To a solution of compound **B02** (50 mg, 0.13 mmol) in DMSO (5 mL) was added zinc cyanide (19 mg, 0.16 mmol, 1.2 equiv) and DPPF (14.59 mg, 26.32 μmol, 0.2 equiv). The suspension was stirred with degassing under nitrogen for 5 min. Next, tris(dibenzylideneacetone)dipalladium (0) (15 mg, 0.03 mmol, 0.2 equiv) was added. The reaction mixture was sealed and stirred with heating at 80 °C for 2 h. Then it was allowed to cool to RT, diluted with 20 mL of water, and adjusted to pH-8 with sat NaHCO₃, extracted with DCM (10 mL × 3). The organic extracts were dried over anhydrous MgSO₄ and concentrated under reduced pressure. The residue was purified by column chromatography on silica gel to afford compound **B03** (26 mg, yield 53%) as a white solid; EtOAc-PET (1:3, *R_f* = 0.28); ¹H NMR (400 MHz, CDCl₃) δ 9.48 (s, 1H), 4.13 (s, 2H), 3.72 (s, 2H), 2.56 (s, 2H), 2.50 (s, 2H), 2.17 (d, *J* = 6.8 Hz, 2H), 1.77–1.69 (m, 6H), 1.47 (br, 1H), 1.28–1.21 (m, 2H), 0.90–0.85 (m, 2H); ¹³C NMR (151 MHz, CDCl₃) δ 166.4, 165.8, 159.8, 159.1, 144.9, 118.3, 114.6, 64.9, 53.0, 52.8, 47.3, 46.8, 35.0, 31.6, 26.7, 26.0; HRMS (CI⁺) *m/z* [M+H]⁺ calcd for C₁₈H₂₃N₆O₂S, 371.1649; found, 371.1657.

3.7. Reactivity of compounds with methyl thioglycolate in PBS buffer

To assess the compound reactivity with methyl thioglycolate, the prepared compounds (10 mM) and methyl thioglycolate (50 mM) was incubated at 37 °C in 50 mM PBS buffer (pH 7.4) in a total volume of 160 μL. The reaction was monitored by TLC and analyzed by injection of aliquots to LC-MS/MS at predetermined intervals within a period of 48 h. Control reaction was run in the absence of methyl thioglycolate. The formation of methyl thioglycolate adduct was determined by detection of the corresponding MS adduct peak.

3.7.1. T_{1/2} Determination

The above reaction was monitored by HPLC. The disappearance of the parent compounds was monitored as % remaining relative to time zero, and the data were fitted to first-order kinetics by plotting the natural log of % remaining as a function of time. The pseudo-first-order rate constant (*k*), which is the negative slope of the linear fitting, was used to calculate the reaction half-life (*t*_{1/2} = 0.693/*k*).

3.7.2. MIC determination

M. tuberculosis H37Rv (ACTT 25618) strains were subcultured on Lowenstein–Jensen medium at 37 °C for 28 days. Bacterial suspension was adjusted to a turbidity equivalent to 1.0 McFarland standard, then further diluted 1:20 in Middle brook 7H9 broth supplemented with 10% (vol/vol) OADC enrichment and 0.2% (vol/vol) glycerol. MICs against replicating *M. tuberculosis* were determined by the microplate alamar blue assay (MABA) [19]. PBTZ 169 was used as positive control. Compound stock solutions (1.0 mg/mL) in DMSO were prepared and serially diluted in two-fold. For the most active compounds, the stock solution concentration was 3.2 μg/mL and the final testing concentration range was 2 to 0.002 μg/mL, respectively.

100 μL of bacterial culture suspension was added to the wells of the 96-well plate containing the corresponding drugs, and the plates were incubated at 37 °C. On day 7, 50 μL of 5% Tween 80 and 20 μL of alamar blue were added to all wells. After incubation for 24 h, the colors of all wells were recorded. A color change from blue to pink indicates bacterial growth. MIC was defined as the lowest concentration of the drug that showed no color change, which was the lowest concentration of drug capable of inhibiting the visible growth of tested isolates.

3.7.3. IC₅₀ determination

M. tuberculosis DprE1 was expressed and purified in *E. coli* cells, as previously reported [20]. Enzyme activity was determined using the Amplex Red/peroxidase coupled assay was performed according to published procedure [21]. Briefly, DprE1 (0.5 μM) was incubated at 30 °C in 20 mM glycylglycine pH 8.5, containing, 0.050 mM Amplex Red, and 0.35 μM horseradish peroxidase. The reaction was initiated by adding 500 μM FPR, and the formation of resorufin was followed at 572 nm ($\epsilon = 54,000 \text{ M}^{-1} \text{ cm}^{-1}$). Initial inhibition assays were carried out in the presence of 20 μM of each compound (dissolved in DMSO). DMSO was used as negative control, PBTZ169 as positive control. Compounds with more than 70% inhibitory activity at 20 μM were further analyzed for IC₅₀ calculated according to equation:

$$A_{[I]} = A_{[0]} \times \left(1 - \frac{[I]}{[I] + IC_{50}} \right)$$

where *A*_[I] is the activity of the enzyme at inhibitor concentration [I] and *A*_[0] is the activity of the enzyme without inhibitor. Otherwise, the activity was recorded as "a", as indicated in Table 1. All results are mean SD of three replicates.

3.7.4. Covalent modification

DprE1 (3 mg/mL, 100 μL) was incubated with 100 μM **A01** or **A02** at 30 °C for 30 min. The sample was dialyzed, concentrated to 20 μL, diluted 1:5 in methanol-water 1:1 containing 0.01% formic acid, and directly analyzed in mass spectrometry, using an Ion Trap (LCQ Fleet™) mass spectrometer with electrospray ionization (ESI) ion source controlled by Xcalibur software 2.2. Mass spectra, recorded for 2 min, were generated in positive ion mode under constant instrumental conditions: source voltage 5.0 kV, capillary voltage 46 V, sheath gas flow 20 (arbitrary units), auxiliary gas flow 10 (arbitrary units), sweep gas flow 1 (arbitrary units), capillary temperature 210 °C, tube lens voltage 105 V. MS/MS spectra, obtained by CID studies in the ion trap, were performed with an isolation width of 3 Da *m/z*, the activation amplitude was 35% of ejection RF amplitude that corresponds to 1.58 V.

Spectra deconvolution was performed using UniDec 3.2.0 software [22].

To identify the site of attachment of the compound the DprE1 reacted with **A01** and **A02** was digested with trypsin and then

peptides analyzed. Briefly, DprE1 (10 mg/mL, 100 μ l) was incubated with 300 μ M **A01** or **A02** at 30 °C for 60 min. As control the protein was incubated with DMSO, then samples were then incubated with 2 μ g trypsin (Trypsin Gold, Promega) at 37 °C overnight. Peptide analyses were carried out on an LC-MS (Thermo Finnigan, San Jose, CA, United States) system consisting of a thermostated column oven Surveyor autosampler controlled at 25 °C; a quaternary gradient Surveyor MS pump equipped with an UV/V is detector and an Ion Trap (LCQ Fleet™) mass spectrometer with electrospray ionization (ESI) ion source controlled by Xcalibur software 2.2. Analytes were separated by RP-HPLC on a Jupiter (Phenomenex, Torrance, CA, United States) C18 column (150 \times 2 mm, 4 μ m, 90 Å particle size) using a linear gradient (2–60% solvent B in 45 min; 60–98% B in 5 min and 98% B in 10 min) in which solvent A consisted of 0.1% aqueous formic acid and solvent B of acetonitrile containing 0.1% formic acid. Flow-rate was 0.2 mL/min. Mass spectra were generated by using the same conditions described above.

3.8. Metabolic labeling

M. tuberculosis H37Rv were grown in 7H9/ADC/Tween80 medium until OD = 1.04 (Experiment 1) or OD = 0.64 (Experiment 2). Metabolic labeling was performed in the final volume of the culture 100 μ l at concentration of the radiolabel 1 μ Ci/mL [¹⁴C]-acetate, (specific activity 106 mCi/mL, American Radiolabeled Chemicals, Inc.). Drug treatment, extraction of the lipids with organic solvents and their TLC analysis was performed as described [18].

Declaration of competing interest

The authors declare that they have no known competing financial interests or personal relationships that could have appeared to influence the work reported in this paper.

Acknowledgement

This work was supported by the National Natural Science Foundation of China (8187169); Italian Ministry of Education, University and Research (MIUR) (Dipartimenti di Eccellenza, Program 2018–2022) to Department of Biology and Biotechnology, “L. Spallanzani”, University of Pavia (to M.F., J.C.S., L.R.C.); and Slovak Research and Development Agency (APVV-15-0515, to K.M.).

Appendix A. Supplementary data

Supplementary data to this article can be found online at <https://doi.org/10.1016/j.ejmech.2020.112773>.

References

- [1] Global Tuberculosis Report, World Health Organization, 2019.
- [2] V. Makarov, G. Manina, K. Mikusová, U. Möllmann, O. Ryabova, B. Saint-Joanis, N. Dhar, M.R. Pasca, S. Buroni, A.P. Lucarelli, A. Milano, E. De Rossi, P. Belánová, A. Bobovská, P. Dianisková, J. Korduláková, C. Sala, E. Fullam, P. Schneider, J.D. McKinney, P. Brodin, T. Christophe, S. Waddell, P. Butcher, J. Albrethsen, I. Rosenkrands, R. Brosch, V. Nandi, S. Bharath, S. Gaonkar, R.K. Shandil, V. Balasubramanian, T. Balganes, S. Tyagi, J. Grosset, G. Riccardi, S.T. Cole, Benzothiazinones kill *Mycobacterium tuberculosis* by blocking arabinan synthesis, *Science* 324 (2009) 801–804.
- [3] B.A. Wolucka, M.R. McNeil, E. de Hoffmann, T. Chojnacki, P.J. Brennan, Recognition of the lipid intermediate for arabinogalactan/arabinomannan biosynthesis and its relation to the mode of action of ethambutol on mycobacteria, *J. Biol. Chem.* 269 (1994) 23328–23335.
- [4] L. Zhang, Y. Zhao, Y. Gao, L. Wu, R. Gao, Q. Zhang, Y. Wang, C. Wu, F. Wu, S.S. Gurucha, N. Veerapen, S.M. Batt, W. Zhao, L. Qin, X. Yang, M. Wang, Y. Zhu, B. Zhang, L. Bi, X. Zhang, H. Yang, L.W. Guddat, W. Xu, Q. Wang, J. Li, G.S. Besra, Z. Rao, Structures of cell wall arabinosyltransferases with the anti-tuberculosis drug ethambutol, *Science* 368 (2020) 1211–1219.
- [5] M. Brečić, I. Centárová, R. Mukherjee, G.S. Kolly, S. Huszár, A. Bobovská, E. Kilacková, V. Mokošová, Z. Svetlíková, M. Šarkan, J. Neres, J. Korduláková, S.T. Cole, K. Mikusová, DprE1 is a vulnerable tuberculosis drug target due to its cell wall localization, *ACS Chem. Biol.* 10 (2015) 1631–1636.
- [6] V. Makarov, B. Lechartier, M. Zhang, J. Neres, A.M. van der Sar, S.A. Raadsen, R.C. Hartkoorn, O.B. Ryabova, A. Vocat, L.A. Decosterd, N. Widmer, T. Buclin, W. Bitter, K. Andries, F. Pojer, P.J. Dyson, S.T. Cole, Towards a new combination therapy for tuberculosis with next generation benzothiazinones, *EMBO Mol. Med.* 6 (2014) 372–383.
- [7] C. Trefzer, H. Skovierová, S. Buroni, A. Bobovská, S. Nenci, E. Molteni, F. Pojer, M.R. Pasca, V. Makarov, S.T. Cole, G. Riccardi, K. Mikusová, K. Johansson, Benzothiazinones are suicide inhibitors of mycobacterial decaprenylphosphoryl-beta-D-ribofuranose 2'-oxidase DprE1, *J. Am. Chem. Soc.* 134 (2012) 912–915.
- [8] S.M. Batt, T. Jabeen, V. Bhowruth, L. Quill, P.A. Lund, L. Egging, L.J. Alderwick, K. Fütterer, G.S. Besra, Structural basis of inhibition of *Mycobacterium tuberculosis* DprE1 by benzothiazinone inhibitors, *Proc. Natl. Acad. Sci. USA* 109 (2012) 11354–11359.
- [9] a R.V. Chikhale, M.A. Barmade, P.R. Murumkar, M.R. Yadav, Overview of the development of DprE1 inhibitors for combating the menace of Tuberculosis, *J. Med. Chem.* 61 (2018) 8563–8593;
- b T. Barf, A. Kaptein, Irreversible protein kinase inhibitors: balancing the benefits and risks, *J. Med. Chem.* 55 (2012) 6243–6262.
- [10] Stephane De Cesco, Jerry kurian, Caroline Dufresne, Anthony K. Mittermaier, Nicolas Moïtessier, Covalent inhibitors design and discovery, *Eur. J. Med. Chem.* 138 (2017) 96–114.
- [11] S. Krishnan, R.M. Miller, B. Tian, R.D. Mullins, M.P. Jacobson, J. Taunton, Design of reversible, cysteine-targeted Michael acceptors guided by kinetic and computational analysis, *J. Am. Chem. Soc.* 136 (2014) 12624–12630.
- [12] a F.F. Fleming, L. Yao, P.C. Ravikumar, L. Funk, B.C. Shook, Nitrile-containing pharmaceuticals: efficacious roles of the nitrile pharmacophore, *J. Med. Chem.* 53 (2010) 7902–7917;
- b W.J. Metzler, J. Yanchunas, C. Weigelt, K. Kish, H.E. Klei, D. Xie, Y. Zhang, M. Corbett, J.K. Tamura, B. He, L.G. Hamann, M.S. Kirby, J. Marcinkiewicz, Involvement of DPP-IV catalytic residues in enzyme-saxagliptin complex formation, *Protein Sci.* 17 (2008) 240–250.
- [13] I.M. Serafimova, M.A. Pufall, S. Krishnan, K. Duda, M.S. Cohen, R.L. Maglathlin, J.M. McFarland, R.M. Miller, M. Frödin, J. Taunton, Reversible targeting of noncatalytic cysteines with chemically tuned electrophiles, *Nat. Chem. Biol.* 8 (2012) 471–476.
- [14] Neil E. Jacobsen, NMR spectroscopy explained, John Wiley & Sons, Inc (2007) 28.
- [15] R. Tiwari, P.A. Miller, L.R. Chiarelli, G. Mori, M. Šarkan, I. Centárová, S. Cho, K. Mikusová, S.G. Franzblau, A.G. Oliver, M.J. Miller, Design, syntheses, and anti-TB activity of 1,3-benzothiazinone azide and click chemistry products inspired by BTZ043, *ACS Med. Chem. Lett.* 7 (2016) 266–270.
- [16] J.A. Schwobel, D. Wondrousch, Y.K. Koleva, J.C. Madden, M.T. Cronin, G. Schürmann, Prediction of Michael-type acceptor reactivity toward glutathione, *Chem. Res. Toxicol.* 23 (2010) 1576–1585.
- [17] J.Y. Gauthier, N. Chautret, W. Cromlish, S. Desmarais, L.T. Duong, J.P. Falguyret, D.B. Kimmel, S. Lamontagne, S. Leger, T. LeRiche, C.S. Li, F. Masse, D.J. McKay, D.A. Nicoll-Griffith, R.M. Oballa, J.T. Palmer, M.D. Percival, D. Riendeau, J. Robichaud, G.A. Rodan, S.B. Rodan, C. Seto, M. Therien, V.L. Truong, M.C. Venuti, G. Wesolowski, R.N. Young, R. Zamboni, W.C. Black, The discovery of odanacatib (MK-0822), a selective inhibitor of cathepsin K, *Bioorg. Med. Chem. Lett.* 18 (2008) 923–928.
- [18] G. Karabanovich, J. Dusek, K. Savková, O. Pavlis, I. Pávková, J. Korábný, T. Kucera, H. Kocová, V. Vlčková, S. Huszár, Z. Konyariková, K. Konečná, O. Jandourek, J. Stolaríková, J. Korduláková, K. Vávrová, P. Pávek, V. Klimesová, A. Hrabálek, K. Mikusová, J. Roh, Development of 3,5-dinitrophenyl-containing 1,2,4-triazoles and their trifluoromethyl analogues as highly efficient antitubercular agents inhibiting decaprenylphosphoryl- β -D-ribofuranose 2'-oxidase, *J. Med. Chem.* 62 (2019) 8115–8139.
- [19] S.G. Franzblau, R.S. Witzig, J.C. McClaughlin, et al., Rapid, low-technology MIC determination with clinical *Mycobacterium tuberculosis* isolates by using the microplate Alamar Blue assay, *J. Clin. Microbiol.* 36 (1998) 362–366.
- [20] J. Neres, F. Pojer, E. Molteni, L.R. Chiarelli, N. Dhar, S. Boy-Röttger, S. Buroni, E. Fullam, G. Degiacomi, A.P. Lucarelli, R.J. Read, G. Zamoni, D.E. Edmondson, E. De Rossi, M.R. Pasca, J.D. McKinney, P.J. Dyson, G. Riccardi, A. Mattevi, S.T. Cole, C. Binda, Structural basis for benzothiazinone-mediated killing of *Mycobacterium tuberculosis*, *Sci. Transl. Med.* 4 (2012) 150ra121.
- [21] J. Neres, R.C. Hartkoorn, L.R. Chiarelli, R. Gadupudi, M.R. Pasca, G. Mori, D. Farina, S. Savina, V. Makarov, G.S. Kolly, E. Molteni, C. Binda, N. Dhar, S. Ferrari, P. Brodin, V. Delorme, V. Landry, A.L. Ribeiro, A. Venturelli, P. Saxena, F. Pojer, A. Carta, R. Luciani, A. Porta, G. Zanon, E. De Rossi, M.P. Costi, G. Riccardi, S.T. Cole, 2-Carboxyquinoxalines kill *Mycobacterium tuberculosis* through non-covalent inhibition of DprE1, *ACS Chem. Biol.* 10 (2015) 705–714.
- [22] M.T. Marty, A.J. Baldwin, E.G. Marklund, G.K. Hochberg, J.L. Benesch, C.V. Robinson, Bayesian deconvolution of mass and ion mobility spectra: from binary interactions to polydisperse ensembles, *Anal. Chem.* 87 (2015) 4370–4376.



***In vitro* Study of Bedaquiline Resistance in *Mycobacterium tuberculosis* Multi-Drug Resistant Clinical Isolates**

Giulia Degiacomi^{1*}, José Camilla Sammartino^{1,2}, Virginia Sinigiani¹, Paola Marra¹, Alice Urbani¹ and Maria Rosalia Pasca^{1*}

¹ Laboratory of Molecular Microbiology, Department of Biology and Biotechnology Lazzaro Spallanzani, University of Pavia, Pavia, Italy, ² Istituto Universitario di Studi Superiori-IUSS, Pavia, Italy

OPEN ACCESS

Edited by:

Marta Martins,
Trinity College Dublin, Ireland

Reviewed by:

Diana Machado,
New University of Lisbon, Portugal
Divakar Sharma,
Indian Institute of Technology, Delhi,
India

*Correspondence:

Giulia Degiacomi
giulia.degiacomi@unipv.it
Maria Rosalia Pasca
mariarosalia.pasca@unipv.it

Specialty section:

This article was submitted to
Antimicrobials, Resistance
and Chemotherapy,
a section of the journal
Frontiers in Microbiology

Received: 06 May 2020

Accepted: 26 August 2020

Published: 17 September 2020

Citation:

Degiacomi G, Sammartino JC,
Sinigiani V, Marra P, Urbani A and
Pasca MR (2020) *In vitro* Study
of Bedaquiline Resistance
in *Mycobacterium tuberculosis*
Multi-Drug Resistant Clinical Isolates.
Front. Microbiol. 11:559469.
doi: 10.3389/fmicb.2020.559469

Tuberculosis (TB) is one of the major causes of death related to antimicrobial resistance worldwide because of the spread of *Mycobacterium tuberculosis* multi- and extensively drug resistant (multi-drug resistant (MDR) and extensively drug-resistant (XDR), respectively) clinical isolates. To fight MDR and XDR tuberculosis, three new antitubercular drugs, bedaquiline (BDQ), delamanid, and pretomanid were approved for use in clinical setting. Unfortunately, BDQ quickly acquired two main mechanisms of resistance, consisting in mutations in either *atpE* gene, encoding the target, or in *Rv0678*, coding for the repressor of the MmpS5-MmpL5 efflux pump. To better understand the spreading of BDQ resistance in MDR- and XDR-TB, *in vitro* studies could be a valuable tool. To this aim, in this work an *in vitro* generation of *M. tuberculosis* mutants resistant to BDQ was performed starting from two MDR clinical isolates as parental cultures. The two *M. tuberculosis* MDR clinical isolates were firstly characterized by whole genome sequencing, finding the main mutations responsible for their MDR phenotype. Furthermore, several *M. tuberculosis* BDQ resistant mutants were isolated by both MDR strains, harboring mutations in both *atpE* and *Rv0678* genes. These BDQ resistant mutants were further characterized by studying their growth rate that could be related to their spreading in clinical settings. Finally, we also constructed a data sheet including the mutations associated with BDQ resistance that could be useful for the early detection of BDQ-resistance in MDR/XDR patients with the purpose of a better management of antibiotic resistance in clinical settings.

Keywords: *Mycobacterium tuberculosis*, bedaquiline, multi-drug resistance, Rv0678, MmpL5, AtpE

INTRODUCTION

According to the World Health Organization (WHO) report, in 2018, tuberculosis (TB), caused by *Mycobacterium tuberculosis*, was one of the major causes of death related to antimicrobial resistance (World Health Organization [WHO], 2019a). Globally, in 2018 about half a million TB infections were rifampicin-resistant, of which 78% were multi-drug resistant (MDR)-TB (World Health Organization [WHO], 2019a). Among these cases, 6.2% were estimated to have extensively drug-resistant (XDR)-TB (World Health Organization [WHO], 2019a). Even if it is a relatively small percentage of all MDR-TB cases, these infections are more complicated to treat and to manage and are a challenge for the health systems worldwide.

Recently, three new antitubercular drugs, bedaquiline (BDQ) (Janssen, Beerse, Belgium), delamanid (Otsuka, Tokyo, Japan), and pretomanid (TB Alliance) were approved for the treatment of MDR-TB (Li et al., 2019; Nieto Ramirez et al., 2020). Interestingly, several studies demonstrated that patients treated with a BDQ-containing regimen showed a high culture conversion rate (65–100%) (Li et al., 2019; Pontali et al., 2019).

BDQ is a diarylquinoline that targets *atpE* gene, coding for the subunit c of the ATP synthase complex (Andries et al., 2005). Its use reduces the mortality when added to treatment for MDR- and XDR-TB (Li et al., 2019; Conradie et al., 2020). The potential risk of BDQ of prolonging the QT interval has occurred in only 0.6% of treated patients; consequently, the advantage in its use is uncontested, even if it is still under investigation. In fact, many clinical studies are testing the effectiveness of new drug combinations, which include BDQ, to design the next generation regimens (Sharma et al., 2020).

In this context, WHO has recently updated the treatment for MDR-TB, by recommending two possible regimens (the longer regimen and the shorter one), both including BDQ and other drugs (Caminero et al., 2019; World Health Organization [WHO], 2019b). Interestingly, in a recent study, NIX-TB trial, a three-drug regimen including linezolid, BDQ and pretomanid was tested with XDR- and MDR-TB patients; the therapy was successful for 90% of patients (Conradie et al., 2020). As evident, BDQ use is rapidly spreading, and 90 countries reported having imported or started using BDQ by the end of 2018 (World Health Organization [WHO], 2019a).

In spite of its recent use in clinical practice, primary BDQ resistance appeared among *M. tuberculosis* clinical isolates (Veziris et al., 2017; Villellas et al., 2017; Zimenkov et al., 2017; Ismail et al., 2018). BDQ resistance is especially associated with mutations in *atpE* and *Rv0678* genes.

The most common mutations linked to low-level of BDQ resistance are present in *Rv0678* gene coding for the *M. tuberculosis* repressor of MmpS5-MmpL5 efflux system. This transporter pumps out of the cells also clofazimine and azoles (Milano et al., 2009; Hartkoorn et al., 2014; Smith et al., 2017). In some cases, *Rv0678* mutations occurred together with polymorphisms in other genes encoding the uncharacterized transporter Rv1979c and the cytoplasmic peptidase PepQ (Rv2535c), both associated with cross-resistance to clofazimine (CFZ) (Nieto Ramirez et al., 2020). Furthermore, a report demonstrated that mutations in *pepQ* gene confer low-level of BDQ resistance in mice (Almeida et al., 2016).

As expected, high BDQ resistance levels are caused by mutations in *atpE* gene, even if their frequency is extremely low among TB patients (Nieto Ramirez et al., 2020).

The surveillance of drug resistance during clinical management is mandatory in order to prevent the occurrence of BDQ resistance among TB patients. To this aim, *in vitro* studies could be a valuable tool for understanding the reasons linked to the spreading of BDQ resistance in particular amongst *M. tuberculosis* MDR and XDR clinical isolates. While acquiring resistance to first-line drugs such as rifampicin (RIF) and isoniazid (INH) is linked to a perturbation in the *M. tuberculosis* fitness (Kodjo et al., 2019), mutations in *Rv0678* and *atpE* have

not been yet demonstrated to have this behavior (Andries et al., 2014; Nieto Ramirez et al., 2020). On the other hand, the low frequency of *atpE* mutants in the clinical setting in comparison to *Rv0678* mutations could suggest a possible reduced fitness cost linked to some *atpE* mutations (Nieto Ramirez et al., 2020).

To better understand the spreading of BDQ resistance in MDR- and XDR-TB, we reported an *in vitro* generation of *M. tuberculosis* mutants resistant to BDQ starting from MDR clinical isolates as parental cultures, since BDQ is used to treat patients affected by MDR-TB. Moreover, we performed growth curves of both obtained BDQ resistant mutants and original MDR isolates to detect possible differences in strains harboring either *Rv0678* or *atpE* mutations. Furthermore, we compared these mutations to a compiled data sheet of previously published SNPs, deriving from *in vitro*, *in vivo* and clinically resistant strains, thus providing additional information for rapid and efficient detection of all known BDQ-resistance associated mutations to ensure an optimal treatment monitoring.

MATERIALS AND METHODS

Bacterial Strains, Growth Conditions and Drugs

Mycobacterium tuberculosis H37Rv and clinical isolates as well as their mutants were grown at 37°C in Middlebrook 7H9 broth (Becton Dickinson), supplemented with 0.05% w/v Tween 80 or on Middlebrook 7H11, both supplemented with 0.2% w/v glycerol, and 10% v/v Middlebrook OADC enrichment (oleic acid, albumin, D-glucose, catalase; Becton Dickinson). *M. tuberculosis* MDR clinical isolates were collected and characterized at the Sondalo Division of the Valtellina and Valchiavenna, Italy, hospital authority in 2012 (Menendez et al., 2013). Bedaquiline (D.B.A. Italia s.r.l.) was dissolved in DMSO (Sigma Aldrich).

All the experiments with *M. tuberculosis* were performed in Biosafety level 3 laboratory by authorized and trained researchers.

Genomic DNA Preparation and Whole-Genome Sequencing of *M. tuberculosis* Clinical Isolates

Genomic DNA of *M. tuberculosis* MDR clinical isolates (hereafter named IC1 and IC2) was extracted as previously described (Belisle and Sonnenberg, 1998). Genomic DNA samples were sequenced by using an Illumina HiSeq2000 technology at Fisabio (Valencia, Spain). Illumina reads were aligned to the annotated genome sequence of the wild-type H37Rv (Cole et al., 1998) (NC_000962.3) to identify SNPs. For the bioinformatic analysis of Illumina data, repetitive PE and PPE gene families were discarded as well as SNPs and indels with less than 50% probability. The possible polymorphisms associated to the resistance to the following drugs were investigated: streptomycin (*rrs*, *rpsL*, *gidB*), INH (*katG*, *inhA*, *ndh*, *nat*), RIF (*rpoB*), ethambutol (*embA*, *embB*, *embC*, *embR*), ethionamide (*ethA*, *inhA*, *ethR*), pyrazinamide (*pncA*, *rpsA*, *panD*), capreomycin (*thyA*, *rrs*), and BDQ (*Rv0678*, *atpE*, *pepQ*).

Determination of Minimal Inhibitory Concentration (MIC)

The drug susceptibility of *M. tuberculosis* strains was determined using the resazurin microtiter assay (REMA), as previously described (Palomino et al., 2002). Briefly, log-phase bacterial cultures were diluted to a theoretical OD₆₀₀ = 0.0005 and grown in a 96-well black plate (Fluoronunc, Thermo Fisher) in the presence of serial compound dilution. A growth control containing no compound and a sterile control without inoculum were also included. After 7 days of incubation at 37°C, 10 µl of resazurin (0.025% w/v) were added and fluorescence was measured after 24 h further incubation using a Fluoroskan™ Microplate Fluorometer (Thermo Fisher Scientific; excitation = 544 nm, emission = 590 nm). Bacterial viability was calculated as a percentage of resazurin turnover in the absence of compound.

Isolation and Characterization of *M. tuberculosis* Spontaneous Mutants Resistant to BDQ

Mycobacterium tuberculosis BDQ resistant mutants were isolated by plating approximately 10⁸ and 10⁹ CFU from exponential growth phase cultures of IC1 and IC2 clinical isolates onto solid medium containing drug at concentrations exceeding the MIC (5X, 10X, 20X MIC). Following 6–8 weeks of incubation, BDQ resistant colonies were streaked onto 7H11 medium. At the same time, these colonies were streaked also onto 7H11 medium plus the same BDQ concentration used for mutant isolation to confirm the resistant phenotype. BDQ MIC values were also assessed by REMA. Genomic DNA was extracted from each mutant and *Rv0678*, *atpE*, and *pepQ* genes were amplified by PCR (oligonucleotides in **Supplementary Table S1**), purified using Wizard® SV Gel and PCR Clean-Up System (Promega) and analyzed by conventional Sanger sequencing (Eurofins Genomics, Italy).

Growth Curves of *M. tuberculosis* BDQ Resistant Mutants and MDR Clinical Isolates

The cultures of *M. tuberculosis* mutants, as well as their corresponding parental strain, were inoculated in 7H9 medium in round bottom tubes at 37°C to reach an early exponential phase. Then, each strain was reinoculated in new 7H9 medium at final OD₆₀₀ = 0.06. The cultures were incubated in standing at 37°C for 8 days. After 24, 48, 96, 168, 192 h, the optical densities at 600 nm were recorded to plot growth curves. The H37Rv strain was also included as control.

Data Sheet Creation

The Medical Subject Headings vocabulary of biomedical terms (MeSH) search builder was used to construct the query for the terms “Bedaquiline,” “*Mycobacterium*,” and “Mutation”, with which the Pubmed and Pubmed Central databases were skimmed, then all the abstracts were downloaded in a MEDLINE format. The information gathered was then manually filtered in

two categories: relevant papers (i.e., original works, case studies, and clinical studies) and papers not pertinent to our purpose. The filtered-as-relevant papers were downloaded as full text, thoroughly analyzed and the type of mutations linked to BDQ resistance were annotated to set-up the data sheet.

RESULTS

Characterization of *M. tuberculosis* MDR Clinical Isolates

IC1 and IC2 strains are two *M. tuberculosis* MDR clinical isolates previously characterized (Menendez et al., 2013). In detail, IC1 is resistant to streptomycin (SM), INH, RIF, ethambutol (EMB), ethionamide (ETH); IC2 is resistant not only to the previously mentioned drugs, but also to pyrazinamide (PYR), and capreomycin (CM) (Menendez et al., 2013).

REMA was used to determine the BDQ MIC values of both isolates (MIC = 0.06 µg/ml, as for the H37Rv wild-type strain). This MIC value (0.06 µg/ml) for *M. tuberculosis* BDQ sensitive strains is in agreement with that proposed in 7H9 medium by both EUCAST and previously (Kaniga et al., 2016; EUCAST, 2020).

In order to pinpoint the SNPs responsible for their drug-resistance profile, the *M. tuberculosis* clinical strains were subjected to whole-genome sequencing (WGS) analysis. Using the obtained Illumina data, the genes involved in the resistance to the following drugs were checked: SM (*rrs*, *rpsL*, *gidB*), INH (*katG*, *inhA*, *ndh*, *nah*), RIF (*rpoB*), EMB (*embA*, *embB*, *embC*, *embR*), ETH (*ethA*, *inhA*, *ethR*), PYR (*pncA*, *rpsA*, *panD*), CAP (*tlyA*, *rrs*), and BDQ (*Rv0678*, *atpE*, *pepQ*).

For both *M. tuberculosis* isolates, the non-synonymous mutations found to be associated to their drug-resistance phenotype are enlisted in **Table 1**. As expected, no mutation was found in *Rv0678*, *atpE*, and *pepQ* genes according to their BDQ sensitivity.

Mycobacterium tuberculosis IC1 and IC2 clinical strains were used for further experiments because of their drug-resistance phenotype as well as their BDQ sensitivity.

Isolation and Phenotypic Characterization of Spontaneous *M. tuberculosis* Mutants Resistant to BDQ

Once shown their BDQ sensitivity, *M. tuberculosis* IC1 and IC2 clinical isolates were used to select and to isolate BDQ-resistant spontaneous mutants, since patients affected by MDR-TB are likely to receive BDQ as part of their therapy.

Mutants were selected onto solid medium containing high BDQ concentrations (0.3, 0.6, 1.2 µg/ml, corresponding to 5, 10, 20-fold MIC, respectively). *Mycobacterium tuberculosis* BDQ-resistant mutants were isolated at a frequency of about 1.8×10^{-8} for IC1 and 6×10^{-9} for IC2.

All the 12 isolated mutants showed to be BDQ resistant and their MIC value was confirmed by REMA, ranging from 0.25 µg/ml (4X MIC of sensitive strain) to 8 µg/ml (128X MIC of

TABLE 1 | Phenotypic and genotypic characteristics of *M. tuberculosis* IC1 and IC2 clinical isolates.

Resistance	Genome position (bp)	Gene	Mutation	Amino acid substitution
Clinical isolate IC1				
STR	4407880	<i>gjaB</i>	T323G	L108R
INH	2155168	<i>katG</i>	G944C	S315T
RIF	761155	<i>rpoB</i>	C1349T	S450L
EMB	4242803	<i>embC</i>	G2941C	V981L
EMB	4247429	<i>embB</i>	A916G	M306V
ETH	4327058	<i>ethA</i>	G416A	G139D
Clinical isolate IC2				
STR	781687	<i>rpsL</i>	A128G	K43R
INH	2155168	<i>katG</i>	G944C	S315T
RIF	761155	<i>rpoB</i>	C1349T	S450L
EMB	4242803	<i>embC</i>	G2941C	V981L
EMB	4247429	<i>embB</i>	A916G	M306V
PYR	2288807	<i>pncA</i>	C435G	D145E
PYR	2289106	<i>pncA</i>	G136A	A46T
ETH	4327058	<i>ethA</i>	G416A	G139D
CM	1918707	<i>tlyA</i>	insAG	Frameshift

sensitive strain) (Table 2). The different levels of drug-resistance could be linked to different associated mutations.

In order to investigate this possibility, *Rv0678*, *atpE*, and *pepQ* genes were amplified by PCR from the genomic DNA of *M. tuberculosis* BDQ resistant mutants and sequenced by Sanger method.

None of 12 *M. tuberculosis* resistant mutants had mutation in *pepQ* gene, while polymorphisms were found either in *atpE* or *Rv0678* genes (Table 2 and Supplementary Data Sheet S1).

In particular, seven strains carried a mutation in *AtpE*, the cellular BDQ target. Among them, five mutants harbored the same replacement of alanine at position 63 by a proline (A63P).

TABLE 2 | Phenotypic and genotypic characteristics of mutants resistant to BDQ obtained from *M. tuberculosis* clinical isolates IC1 and IC2.

<i>M. tuberculosis</i> strains	MIC (μ g/ml)	Mutation	Amino acid substitution
H37Rv	0.06		
IC1	0.06		
IC2	0.06		
IC1 B	8	<i>atpE</i> : g187c	A63P
IC1 C	4	<i>atpE</i> : g187c	A63P
IC1 D	4	<i>atpE</i> : g187c	A63P
IC1 F	4	<i>atpE</i> : g187c	A63P
IC1 G	4	<i>atpE</i> : g187c	A63P
IC1 H	2	<i>atpE</i> : a83c	D28A
IC2 Q	0.5	<i>atpE</i> : a83g	D28G
IC1 L	0.5	<i>rv0678</i> : c400t	R124Stop
IC1 M	0.5	<i>rv0678</i> : g120c	L40F
IC1 N	0.5	<i>rv0678</i> : a271c	T91P
IC1 O	0.5	<i>rv0678</i> : g61t	E21Stop
IC2 P	0.25	<i>rv0678</i> : g197a	G66E

IC2Q mutant had a substitution of the aspartic acid at position 28 with a glycine (D28G), while IC1H mutant presented at the same position a substitution with an alanine (D28A), (Table 2 and Supplementary Data Sheet S1). Furthermore, these mutants were characterized by a high level of BDQ resistance (2–8 μ g/ml) ranging from 32 to 128X MIC of the wild-type strain.

The other five isolated *M. tuberculosis* mutants harbored mutations in *Rv0678*, encoding the MmpR transcriptional repressor of the efflux pump MmpS5-MmpL5. These mutants were characterized by a low level of BDQ resistance (0.25–0.5 μ g/ml) corresponding to 4–8X MIC of the wild-type strain. Three mutants, IC1M, IC1N, and IC2P, presented an amino acid change: respectively, the leucine at position 40 was replaced by a phenylalanine, the tyrosine at position 91 by a proline, and, finally, the glycine at position 66 by a glutamate (Table 2 and Supplementary Data Sheet S1). The MmpR of the other two mutants, IC1L and IC1O, was truncated by a stop codon at position 400 and at position 61, respectively. Additional experiments to demonstrate the role of *Rv0678* in BDQ resistance were not performed. None of these *Rv0678* polymorphisms was already published, at the best of our knowledge.

Evaluation of the Possible Influence of *atpE* and *Rv0678* Mutations to the Growth Rate of *M. tuberculosis* BDQ Resistant Mutants

The growth curves of BDQ resistant mutants with respect to that of the *M. tuberculosis* H37Rv strain and the two parental MDR isolates were also evaluated (Figure 1).

As expected, IC1 and IC2 isolates presented a longer lag phase with respect to that of the wild-type strain. This is also in agreement with their lower growth rate (Figure 1A).

Interestingly, the rate of growth of IC2Q (*atpE* mutant) was lower than that of IC2 strain and of IC2P mutant (*Rv0678* mutant); on the other hand, IC2P grew faster than the other two strains (Figure 1C).

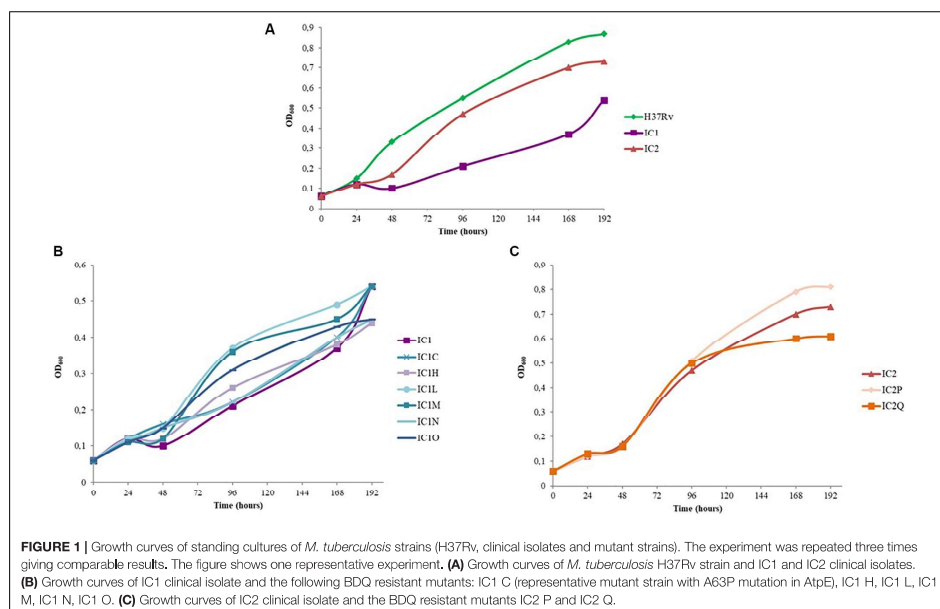
In the case of IC1-derived mutants, the lag phase length is similar between the mutants and the parental strain, while the rate of growth of IC1L, IC1M, IC1N, and IC1O (*Rv0678* mutants) was faster than that of IC1 (Figure 1B). These latter harbor mutations in *Rv0678* which do not perturb *M. tuberculosis* essential functions, whilst IC1C and IC1N (both *atpE* mutants) displayed a rate of growth similar to the parental one.

Overall, our data highlight that the *Rv0678* mutations do not affect growth rate of our parental strains, but could actually give an advantage in the growth rate.

Collection of All Known Polymorphisms Causing BDQ Resistance in *M. tuberculosis* and Other Mycobacteria

The previously published mutations associated with BDQ-resistance as well as the new ones found in this work were included in Supplementary Data Sheet S1.

BDQ is also active against non-tuberculous mycobacteria (NTM) belonging to the *Mycobacterium avium-intracellulare* complex (MAC) and the *Mycobacterium abscessus* complex



(MABSC) (Philly et al., 2015). Its possible use against these other mycobacterial species is under investigation. In NTM species BDQ presents the same mechanisms of resistance found in *M. tuberculosis*; consequently, the evaluation of the BDQ resistance associated polymorphisms could be useful also in these species. For this reason, in this collection, all the mycobacterial species in which an actual clinical use or possible use is under evaluation were included. Moreover, both *in vitro* isolated mutants and clinical isolates were added. At the end, all the mutations linked to BDQ resistance in mycobacteria have been considered in this data sheet that could be useful for the better understanding of BDQ resistance.

DISCUSSION

The current use of BDQ in the treatment for MDR- and XDR-TB reduces the mortality and it is highly effective (Ahmad et al., 2018; Conradie et al., 2020).

Nevertheless, the two main mechanisms of BDQ resistance, which are already widespread, are: modification of target (mutations in *atpE*, coding for the target) and over-expression of an efflux pump (mutations in *Rv0678* gene, coding for the repressor of MmpS5-MmpL5 efflux system). Several reports showed that the most spreading mechanism of BDQ resistance in clinical setting is represented by mutations in *Rv0678* gene even if with a low level of BDQ-resistance (Villellas et al.,

2017; Nieto Ramirez et al., 2020). To fight BDQ-resistance caused by *Rv0678* mutations and to allow its use for the largest possible part of patients, verapamil, an efflux inhibitor, could be the keystone, since it has been demonstrated to increase the efficacy of BDQ against both *M. tuberculosis* and *Mycobacterium abscessus* (Ghajavand et al., 2019; Viljoen et al., 2019).

In this study, an *in vitro* generation of *M. tuberculosis* mutants resistant to BDQ was performed starting from two MDR clinical isolates as parental cultures since patients affected by MDR-TB are eligible to receive BDQ as part of their therapy.

Polymorphisms were identified in both *Rv0678* and *atpE* genes. Our results confirm that these genes represent the main genetic drivers for the onset of BDQ-resistance, as previously pointed out.

Most *in vitro* isolated mutants harbored mutations in the BDQ target, AtpE at positions 28 and 63, according to previous multiple reports (Huitric et al., 2010; Segala et al., 2012; Zimenkov et al., 2017; Ismail et al., 2018). In particular, the mutation A63P was found in the first report regarding BDQ discovery (Andries et al., 2005). The 28 and 63 amino acid positions are considered mutation hotspots, as described in **Supplementary Data Sheet S1**. In fact, the AtpE D28 and A63 are not directly involved in the BDQ binding, but the disruption of the non-covalent bonds they form causes resistance (Preiss et al., 2015). Thanks to the previously published structure of complex crystals obtained by the co-crystallization of the *Mycobacterium phlei* c-ring with BDQ, it is well-known that BDQ forms an extensive amount

of van derWaals interactions with a stretch of nine residues (in *M. phlei*: G62, L63, E65, A66, A67, Y68, F69, I70, and L72) provided by two adjacent ϵ -subunits (Preiss et al., 2015). The mutations (D28A/G, A63P) harbored by BDQ-resistant mutants isolated in this study are positioned close to BDQ-binding site causing indirect structural interference with BDQ binding (Preiss et al., 2015), as evident by the higher MIC showed.

Different mutations could be linked to different levels of drug-resistance, as previously shown (Andries et al., 2005; Hartkoorn et al., 2014; Almeida et al., 2016). In general, *atpE* gene associated variants lead to high level of BDQ-resistance, but the most troublesome polymorphisms are linked to *Rv0678* gene, that are also the most represented ones found in clinical isolates even if the *Rv0678* mutations are linked to a lower level of BDQ resistance (Vilellas et al., 2017; Nieto Ramirez et al., 2020), as typical for efflux pump mechanism. When over-expressed, MmpS5-MmpL5 efflux system can extrude different classes of drugs, for example CFZ and azoles, further limiting the therapeutic options of patients affected by M/XDR-TB. As well exemplified also in this present study, different mutations were identified in *Rv0678* and were disseminated across the gene (Table 2 and Supplementary Data Sheet S1). Both the missense mutations and the nonsense mutations are reported to abolish the repressor activity of *Rv0678*, causing an over-expression of the MmpL5 efflux pump leading to drug extrusion (Zhang et al., 2015). It is worth noting that a G66 missense mutation was found not only in this study (G66E), but also in CFZ-resistant *M. tuberculosis* mutant isolated *in vitro* (G66V) (Zhang et al., 2015).

As responsible for BDQ resistance, mutations in the intergenic region between *Rv0678* and *MmpS5* as well as mutations in the genes encoding the efflux pump MmpS5/MmpL5 were also reported (Ghajavand et al., 2019).

Furthermore, several reports showed that *Rv0678* mutations could be present prior the BDQ treatment both *in vitro* and *in vivo* (Pang et al., 2017; Veziris et al., 2017; Vilellas et al., 2017; Xu et al., 2017; Chawla et al., 2018; Martinez et al., 2018). Consequently, it could be hypothesized that these mutations are adaptative or could improve the growth rate of the MDR mutants, representing an advantage for them. In this work, we evaluated the growth rate of our *M. tuberculosis* BDQ-resistant mutants in comparison with that of the parental strains (two MDR clinical isolates). The *atpE* mutants presented a growth rate similar or lower than that of the parental strains, since *atpE* is essential for *M. tuberculosis* growth, while *Rv0678* mutants showed either a similar growth rate as parental strains or better. Noteworthy, *Rv0678* gene is not essential for *M. tuberculosis* growth (Radhakrishnan et al., 2014). Finally, from our work the relative fitness of the mutants could be speculated. In fact, fitness cost determines in part the fate of resistance mutations (Melnyk et al., 2015). *In vitro* the *atpE* mutants seem to show a little decrease in fitness relative to that of the respective parental strain. On the opposite hand, *Rv0678* mutants seem to have the same fitness in comparison to the corresponding isolate or even a little advantage.

Previous studies showed that *Rv0678* repressor controls the expression of MmpS5-MmpL5 efflux system as well as of other

transporters such as IniAB and DrrA (Milano et al., 2009; Andries et al., 2014). Among the regulated proteins, there were also some essential enzymes and proteins important for the virulence (e.g., PimA, an antitoxin VapB1, etc.) (Andries et al., 2014), that could play a role in *M. tuberculosis* growth and/or infection. Apart from a genomic approach, proteomics-based approaches coupled with bioinformatics could be useful for the characterization of novel proteins which might be related to drug resistance, especially when no related mutations could explain it (Sharma et al., 2018).

CONCLUSION

The presented *in vitro* growth rate data could explain the spreading of *Rv0678* naturally occurring mutations in clinical settings also prior BDQ treatment, even if we cannot exclude the presence of other compensatory mutations that alleviate the cost of resistance without altering it. This evidence also suggests a role for fitness in BDQ-resistance spread, even if further investigations are needed to clearly elucidate this mechanism.

Overall, due to an increasing BDQ usage, it is urgent to implement a more extensive surveillance for such resistance in order to prevent the emergence of resistance in clinical settings. Our collection of polymorphisms responsible for BDQ resistance could be used as theranostics targets, such as in the development of a diagnostic kit for the early detection of BDQ resistant isolates to better manage the available therapeutic options.

DATA AVAILABILITY STATEMENT

All datasets presented in this study are included in the article/Supplementary Material.

AUTHOR CONTRIBUTIONS

GD and MP designed this study and interpreted the data. GD, JS, and MP wrote the manuscript. GD, JS, VS, PM, and AU performed experiments. All authors approved the final version of the manuscript.

FUNDING

GD is funded by a fellowship from the University of Pavia (FRG – Fondo Ricerca and Giovani: “Assegno di ricerca di tipo A”). This research was supported by the Italian Ministry of Education, University and Research (MIUR): Dipartimenti di Eccellenza Program (2018–2022) – Department of Biology and Biotechnology “Lazzaro Spallanzani”, University of Pavia.

SUPPLEMENTARY MATERIAL

The Supplementary Material for this article can be found online at: <https://www.frontiersin.org/articles/10.3389/fmicb.2020.559469/full#supplementary-material>

REFERENCES

- Ahmad, N., Ahuja, S. D., Akkerman, O. W., Alfenaar, J. C., Anderson, L. F., Baghaci, P., et al. (2018). Treatment correlates of successful outcomes in pulmonary multidrug-resistant tuberculosis: an individual patient data meta-analysis. *Lancet* 392, 821–834. doi: 10.1016/S0140-6736(18)31644-1
- Almeida, D., Joerges, T., Tyagi, S., Li, S. Y., Mdululi, K., Andries, K., et al. (2016). Mutations in pepQ Confer Low-level resistance to Bedaquiline and Clofazimine in *Mycobacterium tuberculosis*. *Antimicrob. Agents Chemother.* 60, 4590–4599. doi: 10.1128/AAC.00753-16
- Andries, K., Verhasselt, P., Guillemont, J., Gohlmann, H. W., Neefs, J. M., Winkler, H., et al. (2005). A diarylquinoline drug active on the ATP synthase of *Mycobacterium tuberculosis*. *Science* 307, 223–227. doi: 10.1126/science.1106753
- Andries, K., Villella, C., Coeck, N., Thys, K., Gevers, T., Vanrckx, L., et al. (2014). Acquired resistance of *Mycobacterium tuberculosis* to bedaquiline. *PLoS One* 9:e102135. doi: 10.1371/journal.pone.0102135
- Belisle, J. T., and Sonnenberg, M. G. (1998). Isolation of genomic DNA from *Mycobacteria*. *Methods Mol. Biol.* 101, 31–44. doi: 10.1385/0-89603-471-2:31
- Caminero, J. A., Garcia-Basteiro, A. L., Rendon, A., Piubello, A., Pontali, E., and Migliori, G. B. (2019). The future of drug-resistant tuberculosis treatment: learning from the past and the 2019 World Health Organization consolidated guidelines. *Eur. Respir. J.* 54:1901272. doi: 10.1183/13993003.01272-2019
- Chawla, K., Martinez, E., Kumar, A., Shenoy, V. P., and Sintchenko, V. (2018). Whole-genome sequencing reveals genetic signature of bedaquiline resistance in a clinical isolate of *Mycobacterium tuberculosis*. *J. Glob. Antimicrob. Resist.* 15, 103–104. doi: 10.1016/j.jgar.2018.09.006
- Cole, S. T., Brosch, R., Parkhill, J., Garnier, T., Churcher, C., Harris, D., et al. (1998). Deciphering the biology of *Mycobacterium tuberculosis* from the complete genome sequence. *Nature* 393, 537–544.
- Conradie, F., Diacon, A. I., Ngubane, N., Howell, P., Everitt, D., Crook, A. M., et al. (2020). Treatment of highly drug-resistant pulmonary tuberculosis. *N. Engl. J. Med.* 382, 893–902. doi: 10.1056/NEJMoa1901814
- EUCAST (2020). *Bedaquiline/Mycobacterium tuberculosis 7H9 International MIC Distribution - Reference Database 2020-08-09*. Available online at: <https://mic.eucast.org/Eucast2/regshow.jsp?id=44655> (accessed August 9, 2020).
- Ghahavand, H., Kargarpour Kamakoli, M., Khanipour, S., Pourazar Divaji, S., Masoumi, M., Rahimi Jamnani, F., et al. (2019). High prevalence of bedaquiline resistance in treatment-naive tuberculosis patients and verapamil effectiveness. *Antimicrob. Agents Chemother.* 63:e02530-18. doi: 10.1128/AAC.02530-18
- Hartkoorn, R. C., Uplekar, S., and Cole, S. T. (2014). Cross-resistance between clofazimine and bedaquiline through upregulation of MmpL5 in *Mycobacterium tuberculosis*. *Antimicrob. Agents Chemother.* 58, 2979–2981. doi: 10.1128/AAC.00037-14
- Huiltric, E., Verhasselt, P., Koul, A., Andries, K., Hoffner, S., and Andersson, D. I. (2010). Rates and mechanisms of resistance development in *Mycobacterium tuberculosis* to a novel diarylquinoline ATP synthase inhibitor. *Antimicrob. Agents Chemother.* 54, 1022–1028. doi: 10.1128/AAC.01611-09
- Ismail, N. A., Omar, S. V., Joseph, L., Govender, N., Blows, L., Ismail, F., et al. (2018). Defining Bedaquiline susceptibility, resistance, cross-resistance and associated genetic determinants: a retrospective cohort study. *Ebiomedicine* 28, 136–142. doi: 10.1016/j.ebiom.2018.01.005
- Kaniga, K., Cirillo, D. M., Hoffner, S., Ismail, N. A., Kaur, D., Lounis, N., et al. (2016). A multilaboratory, multicountry study to determine bedaquiline MIC quality control ranges for phenotypic drug susceptibility testing. *J. Clin. Microbiol.* 54, 2956–2962. doi: 10.1128/JCM.01123-16
- Kodio, O., Georges Togo, A. C., Sadio Sarro, Y. D., Fane, B., Diallo, F., Somboro, A., et al. (2019). Competitive fitness of *Mycobacterium tuberculosis* in vitro. *Int. J. Mycobacteriol.* 8, 287–291. doi: 10.4103/ijmy.ijmy_97_19
- Li, Y., Sun, F., and Zhang, W. (2019). Bedaquiline and delamanid in the treatment of multidrug-resistant tuberculosis: Promising but challenging. *Drug Dev Res.* 80, 98–105. doi: 10.1002/ddr.21498
- Martinez, E., Hennessy, D., Jelfs, P., Crighton, T., Chen, S. C., and Sintchenko, V. (2018). Mutations associated with in vitro resistance to bedaquiline in *Mycobacterium tuberculosis* isolates in Australia. *Tuberculosis* 111, 31–34. doi: 10.1016/j.tube.2018.04.007
- Melnyk, A. H., Wong, A., and Kassen, R. (2015). The fitness costs of antibiotic resistance mutations. *Evol. Appl.* 8, 273–283. doi: 10.1111/evo.12196
- Menendez, C., Rodriguez, F., Ribeiro, A. L., Zara, F., Frongia, C., Lobjois, V., et al. (2013). Synthesis and evaluation of α -ketotriazoles and α,β -diketotriazoles as inhibitors of *Mycobacterium tuberculosis*. *Eur. J. Med. Chem.* 69, 167–173. doi: 10.1016/j.ejmech.2013.06.042
- Milano, A., Pasca, M. R., Provvedi, R., Lucarelli, A. P., Manina, G., Ribeiro, A. L., et al. (2009). Azole resistance in *Mycobacterium tuberculosis* is mediated by the MmpS5-MmpL5 efflux system. *Tuberculosis* 89, 84–90. doi: 10.1016/j.tube.2008.08.003
- Nieto Ramirez, L. M., Quintero Vargas, K., and Diaz, G. (2020). Whole genome sequencing for the analysis of drug resistant strains of *Mycobacterium tuberculosis*: a systematic review for Bedaquiline and Delamanid. *Antibiotics* 9:E133. doi: 10.3390/antibiotics9030133
- Palomino, J. C., Martin, A., Camacho, M., Guerra, I., Swings, J., and Portaels, F. (2002). Resazurin microtiter assay plate: simple and inexpensive method for detection of drug resistance in *Mycobacterium tuberculosis*. *Antimicrob. Agents Chemother.* 46:2720.
- Pang, Y., Zong, Z., Huo, F., Jing, W., Ma, Y., Dong, L., et al. (2017). In vitro drug susceptibility of bedaquiline, delamanid, linezolid, clofazimine, moxifloxacin, and gatifloxacin against extensively drug-resistant tuberculosis in Beijing, China. *Antimicrob. Agents Chemother.* 61:e0900-17. doi: 10.1128/AAC.00900-17
- Phillely, J. V., Wallace, R. J. Jr., Benwill, J. L., Taskar, V., Brown-Elliott, B. A., and Thakkar, F. (2015). Preliminary Results of Bedaquiline as salvage therapy for patients with nontuberculous mycobacterial lung disease. *Chest* 148, 499–506. doi: 10.1378/chest.14-2764
- Pontali, E., Raviglione, M. C., Migliori, G. B., and The writing group members of the Global TB Network Clinical Trials Committee (2019). Regimens to treat multidrug-resistant tuberculosis: past, present and future perspectives. *Eur. Respir. Rev.* 28:190035. doi: 10.1183/16000617.0035-2019
- Preiss, L., Langer, J. D., Yildiz, O., Eckhardt-Strelau, L., Guillemont, J. E., Koul, A., et al. (2015). Structure of the mycobacterial ATP synthase Fo rotor ring in complex with the anti-TB drug bedaquiline. *Sci. Adv.* 1:e1500106. doi: 10.1126/sciadv.1500106
- Radhakrishnan, A., Kumar, N., Wright, C. C., Chou, T. H., Tringides, M. L., Bolla, J. R., et al. (2014). Crystal structure of the transcriptional regulator Rv0678 of *Mycobacterium tuberculosis*. *J. Biol. Chem.* 289, 16526–16540. doi: 10.1074/jbc.M113.538959
- Segala, E., Sougakoff, W., Nevejas-Chauffour, A., Jarlier, V., and Petrella, S. (2012). New mutations in the mycobacterial ATP synthase: new insights into the binding of the diarylquinoline TMC207 to the ATP synthase C-ring structure. *Antimicrob. Agents Chemother.* 56, 2326–2334. doi: 10.1128/AAC.016154-11
- Sharma, D., Bisht, D., and Khan, A. U. (2018). Potential alternative strategy against drug resistant tuberculosis: a proteomics prospect. *Proteomes* 6:26. doi: 10.3390/proteomes6020026
- Sharma, D., Sharma, S., and Sharma, J. (2020). Potential strategies for the management of drug-resistant tuberculosis. *J. Glob. Antimicrob. Resist.* 22, 210–214. doi: 10.1016/j.jgar.2020.02.029
- Smith, C. S., Aerts, A., Saunderson, P., Kawuma, J., Kita, E., and Virmond, M. (2017). Multidrug therapy for leprosy: a game changer on the path to elimination. *Lancet Infect. Dis.* 17:e00293-97. doi: 10.1016/S1473-3099(17)30418-8
- Veziris, N., Bernard, C., Guglielmetti, L., Le Du, D., Marigot-Outtandy, D., Jaspard, M., et al. (2017). Rapid emergence of *Mycobacterium tuberculosis* bedaquiline resistance: lessons to avoid repeating past errors. *Eur. Respir. J.* 49:1601719. doi: 10.1183/13993003.01719-2016
- Viljoen, A., Raynaud, C., Johansen, M. D., Roquet-Banères, F., Hierrmann, J. L., Daher, W., et al. (2019). Improved activity of bedaquiline by verapamil against *Mycobacterium abscessus* in vitro and in macrophages. *Antimicrob. Agents Chemother.* 63:e0705-19. doi: 10.1128/AAC.00705-19
- Villella, C., Coeck, N., Meehan, C. J., Lounis, N., de Jong, B., Rigouts, L., et al. (2017). Unexpected high prevalence of resistance-associated Rv0678 variants in MDR-TB patients without documented prior use of clofazimine or bedaquiline. *J. Antimicrob. Chemother.* 72, 684–690. doi: 10.1093/jac/dkw502

- World Health Organization [WHO] (2019a). *Global Tuberculosis Report*. Available online at: <https://apps.who.int/iris/bitstream/handle/10665/329368/9789241565714-eng.pdf?ua=1> (accessed October 17, 2019).
- World Health Organization [WHO] (2019b). *World Health Organization [WHO] Consolidated Guidelines on Drug-Resistant Tuberculosis Treatment*. Available at: <https://www.who.int/tb/publications/2019/consolidated-guidelines-drug-resistant-TB-treatment/en/> (accessed October 17, 2019).
- Xu, J., Wang, B., Hu, M., Huo, F., Guo, S., Jing, W., et al. (2017). Primary clofazimine and bedaquiline resistance among isolates from patients with multidrug-resistant tuberculosis. *Antimicrob. Agents Chemother.* 61:e0239-17. doi: 10.1128/AAC.00239-17
- Zhang, S., Chen, J., Cui, P., Shi, W., Zhang, W., and Zhang, Y. (2015). Identification of novel mutations associated with clofazimine resistance in *Mycobacterium tuberculosis*. *J. Antimicrob. Chemother.* 70, 2507–2510. doi: 10.1093/jac/dkv150
- Zimenkov, D. V., Nosova, E. Y., Kulagina, E. V., Antonova, O. V., Arslanbaeva, L. R., Isakova, A. I., et al. (2017). Examination of bedaquiline- and linezolid-resistant *Mycobacterium tuberculosis* isolates from the Moscow region. *J. Antimicrob. Chemother.* 72, 1901–1906. doi: 10.1093/jac/dkx094

Conflict of Interest: The authors declare that the research was conducted in the absence of any commercial or financial relationships that could be construed as a potential conflict of interest.

Copyright © 2020 Degiacomi, Sammartino, Sinigiani, Marra, Urbani and Pasca. This is an open-access article distributed under the terms of the Creative Commons Attribution License (CC BY). The use, distribution or reproduction in other forums is permitted, provided the original author(s) and the copyright owner(s) are credited and that the original publication in this journal is cited, in accordance with accepted academic practice. No use, distribution or reproduction is permitted which does not comply with these terms.



Contents lists available at ScienceDirect

Bioorganic Chemistry

journal homepage: www.elsevier.com/locate/bioorg

First triclosan-based macrocyclic inhibitors of InhA enzyme

Frédéric Rodriguez^{a,*}, Nathalie Saffon^b, José Camilla Sammartino^c, Giulia Degiacomi^c,
 Maria Rosalia Pasca^c, Christian Lherbet^{a,*}

^a LSPCMIB, UMR-CNRS 5068, Université Paul Sabatier-Toulouse III, 118 Route de Narbonne, 31062 Toulouse Cedex 9, France

^b Institut de Chimie de Toulouse, FR2599, 118 Route de Narbonne, 31062 Toulouse, France

^c Dipartimento di Biologia e Biotecnologie "Lazzaro Spallanzani", Via Ferrata 9, 27100 Pavia, Italy



ARTICLE INFO

Keywords:
 Macrocyclic
 Triclosan
 Enoyl-ACP-reductase
 InhA
Mycobacterium tuberculosis
 Marchantin analogue

ABSTRACT

Two macrocyclic derivatives based on the triclosan frame were designed and synthesized as inhibitors of *Mycobacterium tuberculosis* InhA enzyme. One of the two molecules **M02** displayed promising inhibitory activity against InhA enzyme with an IC_{50} of 4.7 μ M. Molecular docking studies of these two compounds were performed and confirmed that **M02** was more efficient as inhibitor of InhA activity. These molecules are the first macrocyclic direct inhibitors of InhA enzyme able to bind into the substrate pocket. Furthermore, these biaryl ether compounds exhibited antitubercular activities comparable to that of triclosan against *M. tuberculosis* H37Rv strain.

1. Introduction

Tuberculosis (TB) is a scourge and one of the top 10 causes of death and the leading cause from a single infectious agent worldwide [1]. In 2017, 1.6 million TB deaths including about 300,000 deaths among HIV-positive people were estimated. Even if the TB incidence is falling at about 2% per year, the number of TB infected people remain high. With the emergence of multidrug-resistant (MDR) and extensively drug-resistant (XDR) *Mycobacterium tuberculosis* (*Mtb*) strains, there is an urgent need to discover new drugs [2,3]. Enzymes involved in the biosynthesis of mycolic acids represent the main cellular targets, in particular proteins belonging to the Fatty Acid Synthesis (FASII) system, which is not present in humans [4]. One of them, InhA enzyme, essential for *Mtb* survival [5], catalyzes the reduction of the NADH-dependent stereospecific reduction of 2-*trans*-enoyl-ACP (acyl-carrier-protein) [6]. The current anti-TB front-line drug, isoniazid (INH) is one of the most efficient compound to treat TB and inhibits indirectly InhA. Indeed, INH acts as a prodrug requiring an oxidative activation by KatG, a catalase-peroxidase to generate the isonicotinoyl radical. This radical species covalently reacts with NAD resulting in an isonicotinoyl-NADH adduct (INH-NADH), acting as the real inhibitor of InhA enzyme [7,8]. Different classes of direct inhibitors of InhA enzyme were investigated such as Triclosan (TCL, Fig. 1B) [9,10] and derivatives, GEQ analogues [11–14], triazoles [15] or thiazoles [16]. Surprisingly, little attention has been paid to macrocyclic InhA inhibitors although the active site of InhA is large and buried deeply. It can accommodate the cofactor NADH and also the long fatty

acid intermediates [17]. Taking advantage of this large binding site, pyridomycin [18] produced by *Streptomyces pyridomyceticus* [19] is the sole macrocyclic inhibitor of InhA enzyme (Fig. 2A). This natural product acts as a competitive inhibitor at both the lipid substrate- and NADH cofactor-binding pockets of InhA.

In 2003, Kuo et al. reported the X-ray structure (1P45) of two molecules of Triclosan in the binding site of InhA enzyme (Fig. 2) [13]. Based on this structure, we decided to design macrocyclic inhibitors of InhA, involving two molecules of triclosan, as an alternative approach compared to those existing for analogues of triclosan as inhibitors of InhA (Fig. 2). These new TCL-based macrocyclic molecules represent regioisomer analogues of macrocyclic molecules such as riccardins, neomarchantins or isomarchantins, member of the macrocyclic bis(benzyl) natural products (Fig. 1B) [20]. It is noteworthy that these natural bisbenzyl products exhibit broad biological activities; in fact, they are anticancers [21,22], antibacterials [23,24] or antifungals [25].

In this work, we reported the design, the synthesis and the biological evaluation of two macrocyclic biaryl-ether-based molecules, inspired from TCL, as inhibitors of InhA enzyme and as antitubercular agents.

2. Results and discussion

2.1. Design of the macrocyclic inhibitors

In 2003, unexpectedly, two triclosan molecules were found in the substrate binding site of InhA enzyme [13]. One molecule of triclosan

* Corresponding authors.

E-mail addresses: build@chimie.ups-tlse.fr (F. Rodriguez), lherbet@chimie.ups-tlse.fr (C. Lherbet).

<https://doi.org/10.1016/j.bioorg.2019.103498>

Received 14 October 2019; Received in revised form 2 December 2019; Accepted 5 December 2019

Available online 06 December 2019

0045-2068/ © 2019 Elsevier Inc. All rights reserved.

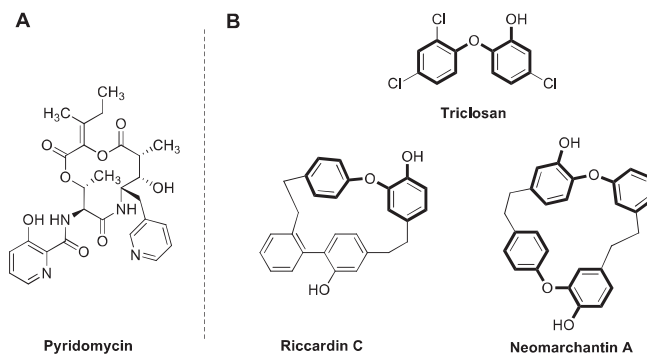


Fig. 1. A: Pyridomycin, a macrocyclic inhibitor of InhA enzyme. B: Triclosan and examples of macrocyclic biarylethers: Riccardin C and Neomarchantin A.

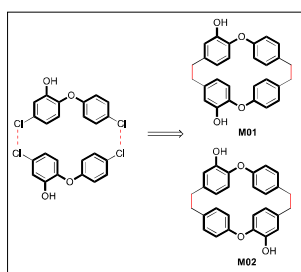
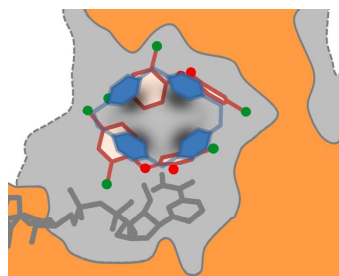


Fig. 2. Schematics based on X-Ray structure of the two molecules of triclosan (dark red) found in the binding cavity (grey) of InhA enzyme (structure 1P45, chain A, orange) in the presence of cofactor NAD (gray). The picture is clipped and oriented with major portal to the left (opened) and minor portal (closed) to the right. The main design's idea is to reproduce the global envelop of the two triclosan molecules (dark red) by a family of macrocyclic compounds (blue). Right: Schema for the synthesis of macrocyclic analogues **M01** and **M02** based on the structures of marchantin derivatives.

occupies the same space as the substrate. The phenol ring forms a stacking interaction with NADH and his hydrogen bonded to the phenolic group of Tyr158. The second molecule of triclosan is found in chain A of the structure 1P45 and binds at the position of the aliphatic part of the substrate analogue THT in an almost entirely hydrophobic area. The two hydroxyl groups on each triclosan are not oriented in the same way. Based on the structure reported by Kuo et al. [13], Fig. 2 shows that simple metrics such as distances between atoms could provide informations on the predisposition of the molecules toward macrocyclic compounds. In our case, chloride atoms bind in close proximity to each other and could be replaced by methylene groups. Consequently, two candidates, i.e. macrocycles **M01** or **M02**, have been selected as potential macrocyclic inhibitors of InhA enzyme. As for these designed molecules, marchantins and analogues have the particularity to possess two methylene groups as linkers between each biaryl moiety.

2.1.1. Synthesis of the precursors 4, 5 and 7

Different methods were developed to synthesize macrocyclic bis-benzyl-based molecules such as riccardins, marchantins, neomarchantins or isomarchantins [20]. Not surprisingly, the most difficult step is the macrocyclization step. Just by looking at the precedent synthesis of the aforementioned compounds, the most reliable macrocyclisation step was realized through Wittig olefination or related methodologies, followed by hydrogenation of the double bond. This strategy has been recently illustrated by the contributions of the groups of Lou [26] and Miyachi [27].

On this basis, the initial steps started by the synthesis of the precursors 4, 9 and 12 that will be used for the Wittig olefination. Vanillin was initially converted to its acetal 3, as described. The resulting phenol was condensed with either 4-fluorobenzaldehyde either methyl 4-

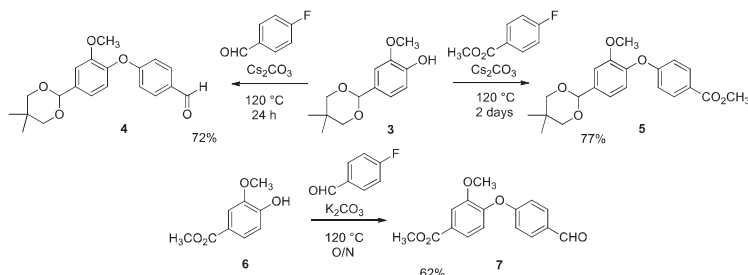
formylbenzoate to afford biaryl ethers 4 and 5. In a same way, biaryl ether 7 was synthesized from the commercially available phenol 6 (see Scheme 1).

Aldehyde 7 was reduced to its corresponding alcohol derivative 8 by NaBH₄ and treated with triphenylphosphine hydrobromide (Fig. 4). The same protocol was used for compound 5 to afford compound 12, except that acetal derivative 5 was previously deprotected in the presence of PPTS (Scheme 2).

2.1.2. Synthesis of the macrocycles

The general procedures for the synthesis of the two macrocycles are outlined in Schemes 3 and 4.

The union of intermediates 9 and 12 with compound 4 was accomplished using Wittig reaction to afford the corresponding stilbene intermediates that were subsequently hydrogenated to give compounds 13 and 18. Then, these compounds were reduced by LiAlH₄ and PPTS treatment provided the two aldehydes 15 and 20. Reactions with triphenyl phosphine hydrobromide furnished compounds 16 and 21 in very good yields. Macrocyclic compounds 17 and 22 were synthesized in two steps from 16 and 21, respectively. Firstly, compounds 16 and 21 were cyclized via an intramolecular Wittig reaction between a biaryl-ether aldehyde and a phosphonium salt, according to a reported method [26]. Then the stilbene intermediates were reduced by hydrogenation to afford compounds 17 and 22. Double demethylation of compounds 17 and 22 by BBr₃ at low temperature gave desired compounds **M01** and **M02** in good yield. The structure of compound **M01** was confirmed through X-ray crystallography (Fig. 3; for detailed crystallographic data, see the Supporting Information). Unfortunately, it was not possible to obtain single crystals of **M02**: all attempts to crystallize **M02** led to the formation of a polycrystalline material.



Scheme 1. Synthesis of the intermediates 4, 5 and 7 for the synthesis of the two macrocycles.

2.2. Biological evaluation of the macrocycles and intermediates

The molecules were evaluated as inhibitors of InhA enzyme and *Mycobacterium tuberculosis* H37Rv strains. The inhibitory potencies against InhA enzyme of the two macrocyclic molecules were measured spectrophotometrically, accordingly to a procedure already reported [11]. TCL was used as control. In our assays, macrocycle **M01** showed modest inhibition of InhA activity with 52% inhibition at $50\ \mu\text{M}$ (see Table 1). But, to our delight, macrocycle **M02** was clearly more active than **M01** and showed inhibitory activity with a IC_{50} value of $4.7\ \mu\text{M}$ (see Figs. 1 and 4). MICs to **M01** and **M02** were determined against *Mtb* H37Rv growth; **M01** and **M02** activities were comparable to that found for TCL. Considering an approximative IC_{50} of $0.5\ \mu\text{M}$ for TCL (58% at $0.5\ \mu\text{M}$) against InhA, **M02** remains 10 times less active than TCL while the same molecule is half as active against mycobacteria. **M01** has the same antitubercular activity as TCL but its lack of inhibition on InhA suggests another target for this compound.

2.3. In silico studies of macrocycles M01 and M02 with InhA enzyme

To better understand the binding mode of these macrocycles into the InhA active site, we performed docking experiment to reveal the possible interactions into the protein.

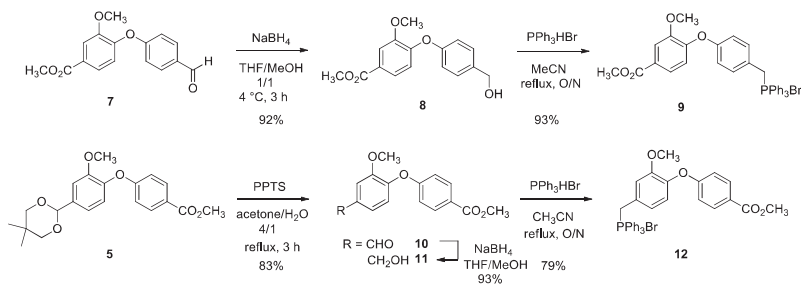
The active site of InhA [7,28] is characterized by a large volume, two variable entries (major and minor portals) at opposite sides of binding cavity, the ability to make structural transitions involving the substrate binding loop (SBL: residues 195–210) and the presence of NAD cofactor interacting with the protein and substrate (or inhibitors). The inhibition schemes include prodrugs that bind to NAD to form an adduct [8,29], direct inhibitors (i.e. some diphenyl ethers derivatives) involved in reversible association with the cofactor [13,30,31], long

time residence inhibitors associated with induced-fit [32–34], or whether the displacement of cofactor [18]. Several keys aspects have emerged among literature, such as the involvement of TYR158, PHE49, the conformation (open or closed states) of helix H6 or the reordering of the SBL loop. But despite classification studies [17,35,36] using different approaches, these different binding and inhibition pathways are not obviously correlated to structure-function relationships (i.e. ligand chemical structures vs. binding site topology) and can be slightly affected by minor changes in ligand structure. All of these elements make docking studies difficult, especially as the best reproduction of crystallographic data by docking methods involves a balance between intermolecular contributions, sometimes antagonist, of ligand-protein and ligand-cofactor interactions.

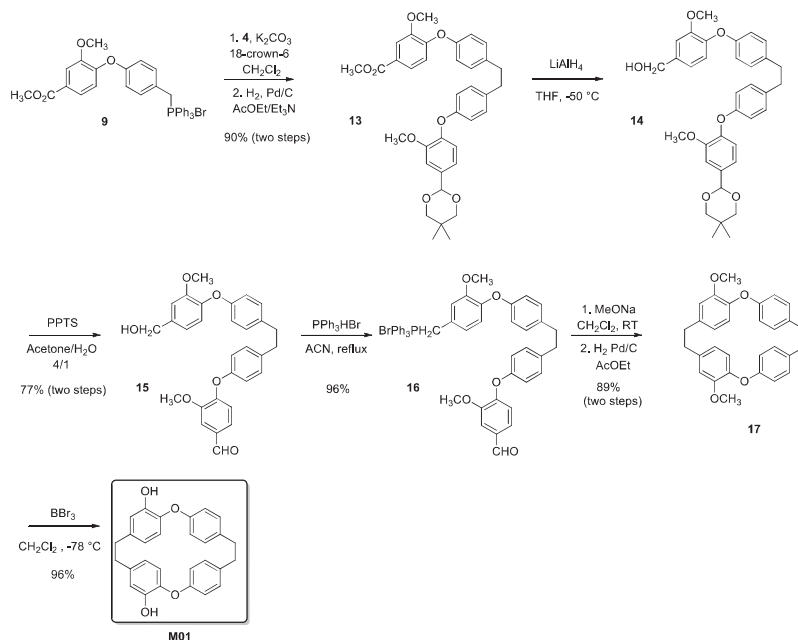
Knowing this intrinsic complexity and the subsequent limitations, docking studies were performed in order to explore the potent insertion of macrocyclic compounds in the binding site of InhA. We used 1P45a (1P45, chain A) [13] as receptor; this structure includes not one but two triclosan (TCL) ligands, interacting upper the cofactor. This arrangement of two triclosan molecules was used as a basis for the design of macrocyclic compounds. We consider also 1P45a as an open structure (relatively to SBL dynamics and major portal, minor portal is closed) able to embed relatively large ligands.

The first result is that **M01** (*cis*) and **M02** (*trans*) molecules are able to dock deeply in the hydrophobic pocket (occupied by most known co-crystallized ligands) near cofactor and TYR158 and can make interactions with both the cofactor and the protein. After docking calculations, most of the poses show that the areas of the hydroxyl and ether groups are positioned along a vertical axis, with one, ether and hydroxyl groups, at the top of the cavity in the hydrophobic pocket and the other at the bottom, close to the cofactor (nicotinamide-ribose part).

In the case of the *cis* compound (**M01**, Fig. 5A and B) the hydroxyl



Scheme 2. Synthesis of the phosphonium bromide intermediates 9 and 12.

Scheme 3. Synthesis of the dimeric macrocyclic triclosan derivative **M01**.

groups are oriented towards the major portal and on the same side than the TYR158 residue. So, interactions with TYR158 and cofactor (2'-OH of ribose) are possible in the case of B1 + topology (see experimental section) by the mean of the bottom hydroxyl group of **M01**. The poses related to A1 topology (see experimental section) have this hydroxyl group too far from TYR158 but interactions with cofactor (nicotinamide) involving ether group are possible.

In the case of the *trans* compound (**M02**, Fig. 5C) the bottom hydroxyl group is headed to the other side and interactions with TYR158 are not possible. But the poses show strong interactions with cofactor (phosphate, ribose) by the mean of this hydroxyl group. The best poses for **M02** display the same A2 topology (see supporting information), a very stable configuration (*N.B.*: this was not the case for **M01**) and give significantly better docking scores and scores contribution (Ligand-Cofactor and Ligand-Protein) than for **M01** compound.

Interestingly, if we compare A topologies (see experimental section) for **M01** and **M02** compounds (Fig. 5D) with C16-fatty acyl substrate (THT, 1BVR [7]) and diaryl ether direct inhibitor such as **PT70** (TCU, 2X22, long time residence inhibitor [32]) we notice that the envelop of **M01** and **M02** is able to share the same chain pathways than these inhibitors in the hydrophobic binding pocket.

Finally, according to score values, interaction patterns and conformational stability (A topology) of poses, the docking experiments show that compound **M02** is more optimized for the binding site than **M01**. These results are in accordance with experimental data; the difference in activity by comparison with triclosan could be correlated with the rigidity of our macrocycles. A longer spacer group i.e. three methylene groups instead of two, would allow for greater flexibility, which could facilitate binding into the substrate binding site.

3. Conclusion

In conclusion, two macrocyclic potential inhibitors of InhA enzyme were designed, based on the X-ray structure of the InhA/TCL couple. These two macrocycles incorporating two biaryl compounds were synthesized and the final macrocyclisation step was realized through Wittig olefination. Both molecules were evaluated as inhibitors of InhA enzyme and *Mtb* growth. We found that one of them, macrocycle **M02**, was able to inhibit InhA enzyme with an affinity (IC_{50}) in the micromolar range. Furthermore, molecular docking studies were carried out to understand the difference in bioactivities between both compounds. The results suggest that **M02** binds in the active site. However, in order to increase its enzymatic activity, the molecule could be optimized by considering two approaches: modulating flexibility or modulating substituents on the phenyl moiety (including hydroxyl group and/or chlorine substituents). MIC values for macrocycles **M01** and **M02** were found to be similar to that of TCL. This result is very promising for the upcoming implementation of macrocyclic compounds as direct inhibitors of InhA enzyme.

4. Experimental section

4.1. Material and methods

All chemicals were obtained from Aldrich-Sigma, Acros Organics or Alfa Aesar and used without further purification. Anhydrous solvents were freshly distilled before use or were obtained from the M. Braun Solvent Purification System (MB-SPS-800). The melting points were determined on a Mettler Toledo MP50 melting point system and are uncorrected. NMR spectroscopic data were recorded on advance 300

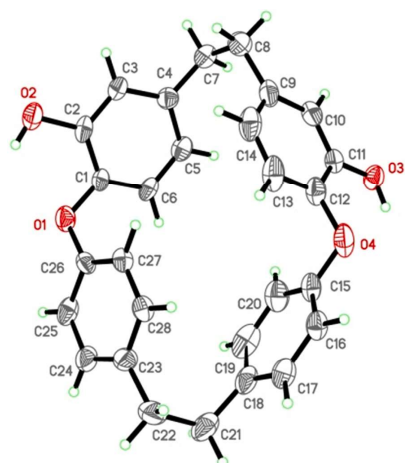
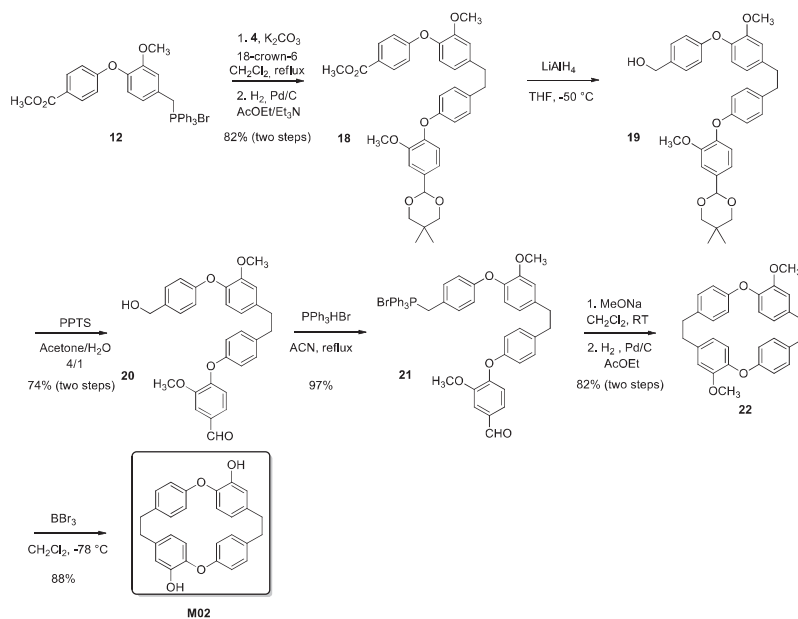


Fig. 3. Molecular view of the X-ray crystal structure of **M01** (Scheme 3), with thermal ellipsoids drawn at the 30% probability level. Only one of the 7 molecules of the asymmetric unit of **M01** is shown and solvent molecules (CH_2Cl_2) are omitted for clarity.

Table 1

Activities against InhA enzyme and *Mtb* H37Rv strain.

Compound	% Inhibition at 50 μM (IC_{50})	<i>Mtb</i> MIC ($\mu\text{g}/\text{mL}$)
Macrocyle 1 (M01)	52	20
Macrocyle 2 (M02)	93 ($4.7 \pm 0.4 \mu\text{M}$)	40
Triclosan (TCL)	100/58% at 0.5 μM	20
Streptomycin	–	0.25

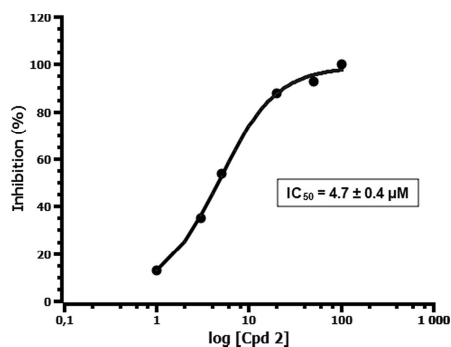


Fig. 4. Determination of IC_{50} of macrocyle **M02** against InhA enzyme.

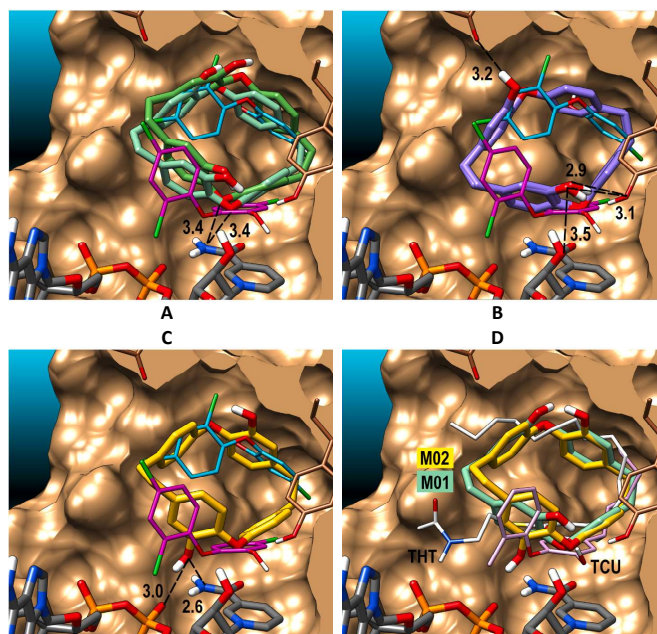


Fig. 5. Docking results showing the four best poses in the case of **M01** (up) and **M02** (down) compounds. The 1P45a (1P45, chain A) structure (brown depicted surfaces) is used, major portal of InhA at left, minor portal at right of the picture. The cofactor NAD (gray) is shown at bottom and the TYR158 and GLN 100 residues (brown) are highlighted. Triclosan molecules, co-crystallized in 1P45 are shown in pink (TCL 500) and cyan (TCL 450). The TCL 500 conformation is known to be typical for many triclosan-based inhibitors. Interatomic distances are expressed in Å (cutoff of 3.5 Å). **A** – Poses {00, 12} for **M01** (green) showing variations of macrocycle topology: type A1. The ether group is interacting (putative hydrogen bond) with the nicotinamid moiety of the cofactor. **B** – Poses {29, 04} for **M01** (purple) for B1+ type topology. The position of hydroxy group in front of the view allows the typical interaction with TYR158 (right). The ligand interacts also with cofactor, additional interaction with GLN100 (up). **C** – Poses {17, 36, 06, 13} for **M02** (yellow) classified with A2 topology. In this case, the hydroxy group engaged in interactions with the cofactor is placed behind the macrocycle. **D** – Comparison of poses {12} for **M01** and {17} for **M02**. The overall topologies (type A) are similar but the position of hydroxy groups are different. The THT compound (substrate, white) from 1BVRa [7] and the TCU (inhibitor, light pink) from 2X22a [32] aligned structures are shown.

spectrometer (Bruker, Billerica, MA, USA) operating at 300 MHz for ^1H NMR analysis and 75 MHz for ^{13}C NMR analysis (APT). Chemical shifts (δ) were reported in ppm, using the solvent residual peak as internal reference: CDCl_3 $\delta = 7.26$ ppm/77.0 ppm, MeOD $\delta = 3.31$ ppm/49.0 ppm. spin-spin coupling constants (J) are reported in Hz, while multiplicities are abbreviated by s (singlet), bs (broad singlet), d (doublet), bd (broad doublet), dd (doublet of doublets), t (triplet), td (triplet of doublets), m (multiplet). Mass spectra (DCI/NH $_3$) were obtained on a DSQ ThermoFisher Scientific. For MS–ESI spectra, a Dionex ultimate 3000 UPLC system with an ABSciex Q TRAP 4500 was used. High-resolution mass spectra (HRMS) were recorded on a UPLC Xevo G2 Q-TOF (Waters) or on a GCT Premier (Waters). IR spectra were recorded on a ThermoScientific Nicolet IS50 – ATR diamant from ThermoFisher Scientific. The desired product was purified by flash column chromatography with PuriFlash 430 system using puriFlash® columns from Interchim. The enzymatic evaluation was performed on a Cary Bio 300.

4.1.1. Synthesis of precursors 4, 5 and 7

4.1.1.1. 4-[4-(5,5-Dimethyl-1,3-dioxan-2-yl)-2-methoxyphenoxy]benzaldehyde (4)

To a solution of 4-(5,5-dimethyl-1,3-dioxan-2-yl)-2-methoxyphenol (0.485 g, 3.1 mmol) in DMF (20 mL), were added 4-fluorobenzaldehyde (1.1 eq) and cesium carbonate (1.2 eq). The solution was stirred for 24 h at 120 °C under argon. The solvent was removed under reduced pressure. Ethyl acetate was added to the mixture and the mixture solution was washed with water and brine, dried using magnesium sulfate and filtered. The solution was concentrated and the desired product was purified by flash chromatography (linear gradient 95/5 to 60/40 petroleum ether/ethyl acetate) and was isolated as a white powder (0.521 g, 72%). Rf: 0.57 (petroleum ether/ethyl acetate 7/3). Mp: 115–117 °C. $\nu_{\text{max}}/\text{cm}^{-1}$:

2966; 2955; 2864; 1684; 1611; 1596; 1583; 1498; 1396; 1280; 1230; ^1H NMR (300 MHz, CDCl_3) δ 9.88 (s, 1H); 7.78 (m, 2H); 7.22 (d, $J = 1.7$ Hz, 1H); 7.13 (dd, $J = 8.1$ Hz, $J = 1.7$ Hz, 1H); 7.08 (d, $J = 8.1$ Hz, 1H); 6.96 (m, 2H); 5.40 (s, 1H); 3.80 (s, 3H); 3.70 (m, 2H); 3.64 (m, 2H); 1.31 (s, 3H); 0.81 (s, 3H); ^{13}C NMR (75 MHz, CDCl_3) δ 190.7; 163.4; 151.5; 143.0; 136.9; 131.7; 130.8; 122.2; 119.2; 116.1; 110.7; 101.1; 77.6; 55.8; 30.2; 23.0; 21.8; HRMS (DCI-CH $_4$) Calculated for $\text{C}_{20}\text{H}_{23}\text{O}_5$ (MH^+): 343.1545. Found: 343.1547.

4.1.1.2. Methyl 4-(4-formyl-2-methoxyphenoxy)benzoate (5) To a solution of 4-(5,5-dimethyl-1,3-dioxan-2-yl)-2-methoxyphenol (0.485 g, 3.1 mmol) in DMF (20 mL), were added methyl 4-fluorobenzoate (1.5 eq) and cesium carbonate (1.5 eq). The solution was stirred for two days at 120 °C under argon. The solvent was removed under reduced pressure. Ethyl acetate was added to the mixture and the mixture solution was washed with water and brine, dried using magnesium sulfate and filtered. The solution was concentrated and the desired product was purified by flash chromatography (linear gradient 95/5 to 70/30 petroleum ether/ethyl acetate) and was isolated as a white powder (0.600 g, 77%). Rf: 0.50 (petroleum ether/ethyl acetate 7/3). Mp: 128–130 °C. $\nu_{\text{max}}/\text{cm}^{-1}$: 2959; 2907; 2870; 1712; 1597; 1502; 1455; 1432; 1410; 1279; 1229; ^1H NMR (300 MHz, CDCl_3) δ 7.94 (m, 2H); 7.21 (d, $J = 1.8$ Hz, 1H); 7.12 (dd, $J = 8.1$ Hz, $J = 1.8$ Hz, 1H); 7.06 (d, $J = 8.1$ Hz, 1H); 5.40 (s, 1H); 3.87 (s, 3H); 3.81 (s, 3H); 3.79 (m, 2H); 3.67 (m, $J = 10.9$ Hz, 2H); 1.31 (s, 3H); 0.81 (s, 3H); ^{13}C NMR (75 MHz, CDCl_3) δ 166.6; 162.1; 151.5; 143.6; 136.5; 131.4; 123.9; 122.0; 119.1; 115.7; 110.7; 101.2; 77.7; 55.8; 51.9; 30.2; 23.1; 21.8; HRMS (DCI-CH $_4$) Calculated for $\text{C}_{21}\text{H}_{25}\text{O}_6$ (MH^+): 373.1651. Found: 373.1643.

4.1.1.3. Methyl 4-(4-formylphenoxy)-3-methoxybenzoate (7) To a

solution of methyl ester derivative **6** (1.5 g, 8.2 mmol) in DMF (30 mL), were added 4-fluorobenzaldehyde (1.2 eq) and potassium carbonate (2 eq). The solution was stirred overnight at 120 °C under argon. The solvent was removed under reduced pressure. Ethyl acetate was added to the mixture and the mixture solution was washed with water and brine, dried using magnesium sulfate and filtered. The solution was concentrated and the desired product was purified by flash chromatography (linear gradient 95/5 to 70/30 petroleum ether/ethyl acetate) and was isolated as a white powder (1.460 g, 62%). Mp: 104–106 °C. $\nu_{\text{max}}/\text{cm}^{-1}$: 2960; 1713; 1698; 1608; 1596; 1584; 1499; 1435; 1297; 1270; 1224; $^1\text{H NMR}$ (300 MHz, CDCl_3) δ 9.91 (s, 1H); 7.82 (m, 2H); 7.70 (s, 1H); 7.68 (m, 1H); 7.08 (m, 1H); 7.01 (m, 2H); 3.92 (s, 3H); 3.85 (s, 3H); $^{13}\text{C NMR}$ (75 MHz, CDCl_3) δ 190.6; 166.2; 162.4; 151.2; 147.2; 131.8; 131.5; 127.9; 123.1; 121.4; 116.9; 113.9; 56.0; 52.3; HRMS (DCI- CH_4) Calculated for $\text{C}_{16}\text{H}_{15}\text{O}_5$ (MH^+): 287.0919. Found: 287.0909.

4.1.2. Synthesis of macrocycle **1**

4.1.2.1. Methyl 4-[4-(hydroxymethyl)phenoxy]-3-methoxybenzoate (8). To a solution of compound **7** (0.8 g, 2.8 mmol) in a mixture THF/MeOH (1/1, 20 mL) at 4 °C, was added NaBH_4 (0.5 eq). The reaction mixture was stirred for 3 h at room temperature before quenching with saturated aqueous solution of NH_4Cl . The reaction mixture was then concentrated under reduced pressure. The product was extracted with ethyl acetate and the organic phase was washed with H_2O , dried over MgSO_4 , filtered and concentrated in vacuo to afford compound **8** as a white solid upon standing (0.740 mg, 92%). Rf: 0.14 (petroleum ether/ethyl acetate 7/3). $^1\text{H NMR}$ (300 MHz, CDCl_3) δ 7.65 (d, $J = 1.8$ Hz, 1H); 7.58 (dd, $J = 8.2$ Hz, $J = 1.9$ Hz, 1H); 7.32 (m, 2H); 6.97 (m, 2H); 6.85 (d, $J = 8.3$ Hz, 2H); 4.64 (s, 2H); 3.90 (s, 3H); 3.89 (s, 3H); 2.12 (br s, 1H); $^{13}\text{C NMR}$ (75 MHz, CDCl_3) δ 166.6; 155.8; 150.3; 150.1; 136.3; 128.6; 125.6; 123.0; 118.7; 118.3; 113.4; 64.6; 56.0; 52.1; HRMS (DCI- CH_4) Calculated for $\text{C}_{16}\text{H}_{17}\text{O}_5$ (MH^+): 289.1076. Found: 289.1071.

4.1.2.2. ([4-[2-methoxy-4-(methoxycarbonyl)phenoxy]phenyl]methyl)triphenylphosphonium bromide (9). Compound **8** (0.800 g, 2.77 mmol) was mixed with triphenylphosphonium bromide (2.77 mmol, 1 eq) in acetonitrile for 4 h and then cooled to room temperature. The reaction mixture was evaporated to afford compound **9** as a white powder which was purified by flash chromatography (gradient ethyl acetate/MeOH 100 to 80/20) to give white powder (1.470 g, 93%). Mp: 101–103 °C. $^1\text{H NMR}$ (300 MHz, CDCl_3) δ 7.66–7.70 (m, 9H); 7.51–7.61 (m, 8H); 7.07 (dd, $J = 8.3$ Hz, $J = 2.7$ Hz, 2H); 6.77 (d, $J = 8.2$ Hz, 1H); 6.70 (d, $J = 8.2$ Hz, 2H); 5.37 (d, $J = 14.1$ Hz, 2H); 3.85 (s, 3H); 3.82 (s, 3H); $^{13}\text{C NMR}$ (75 MHz, CDCl_3) δ 166.3; 156.5 (d, $J = 4.1$ Hz); 150.2; 149.1; 134.9 (d, $J = 2.92$ Hz); 134.2 (d, $J = 9.9$ Hz); 132.9 (d, $J = 5.5$ Hz); 130.1 (d, $J = 12.5$ Hz); 129.9; 126.1; 122.9; 122.1 (d, $J = 8.6$ Hz); 122.0; 118.6; 118.5 (d, $J = 3.2$ Hz); 118.1; 117.0; 113.4; 55.9; 52.1; 29.9 (d, $J = 46.9$ Hz); HRMS (ESI) Calculated for $\text{C}_{34}\text{H}_{30}\text{O}_4\text{P}$ (M^+): 533.1882. Found: 533.1881.

4.1.2.3. Methyl 4-[4-(2-[4-(5,5-dimethyl-1,3-dioxan-2-yl)-2-methoxyphenoxy]phenyl)ethyl]phenoxy]-3-methoxybenzoate (13). The title compound was prepared from compounds **9** and **4**, by following a published procedure [26]. To a solution of phosphonium salt **8** (1.05 eq) in anhydrous dichloromethane (50 mL), were added successively aldehyde **4** (0.690 g, 2.01 mmol, 1 eq), K_2CO_3 (2 eq) and a spatula tip of 18-crown 6. The reaction mixture was stirred for 24 h under reflux and argon. The solution was concentrated in vacuo and the desired product was purified by flash chromatography (gradient petroleum ether/ethyl acetate 9/1 to 5/5). The resulting sticky oil was diluted in AcOEt (8 mL). Palladium on activated carbon (Pd/C 10%, 100 mg/mmol) and triethylamine (1 mL) were added and the resulting solution was stirred for 24 h under H_2 at 0.4 MPa pressure. The mixture was filtered into a filter funnel containing celite. The resulting solution

was evaporated to afford compound **13** as a gummy solid (1.085 g, 90% over two steps). Mp: 127–128 °C. $^1\text{H NMR}$ (300 MHz, CDCl_3) δ 7.66 (d, $J = 1.9$ Hz, 1H); 7.58 (dd, $J = 8.1$ Hz, $J = 1.9$ Hz, 1H); 7.18 (d, $J = 1.8$ Hz, 1H); 7.12 (m, 2H); 7.02–7.07 (m, 3H); 6.92 (m, 2H); 6.81–6.87 (m, 3H); 5.38 (s, 1H); 3.94 (s, 3H); 3.91 (s, 3H); 3.87 (s, 3H); 3.72 (m, 4H); 2.87 (s, 4H); 1.31 (s, 3H); 0.81 (s, 3H); $^{13}\text{C NMR}$ (75 MHz, CDCl_3) δ 166.5; 155.8; 154.2; 151.0; 150.6; 150.0; 145.7; 137.3; 135.7; 134.9; 129.7; 129.3; 125.1; 123.0; 120.2; 118.9; 117.6; 117.3; 113.3; 110.4; 101.3; 77.6; 56.0; 55.9; 52.0; 37.2; 37.1; 30.1; 23.0; 21.8; HRMS (DCI- CH_4) Calculated for $\text{C}_{36}\text{H}_{30}\text{O}_8$ (MH^+): 599.2645. Found: 599.2615.

4.1.2.4. {4-[4-(2-[4-(5,5-dimethyl-1,3-dioxan-2-yl)-2-methoxyphenoxy]phenyl)ethyl]phenoxy]-3-methoxyphenyl}methanol (14). To a suspension of lithium aluminium hydride (2 eq) in dry tetrahydrofuran (20 mL) at –40 °C, was added dropwise a solution of compound **13** (0.768 g, 1.28 mmol, 1 eq). The reaction mixture was allowed to warm to room temperature and was stirred for 3 h. Then a saturated aqueous solution of NH_4Cl was added and the resulting mixture was concentrated to give crude oil. The crude oil was dissolved in ethanol and HCl (0.1 N) was added and the mixture was stirred for 2 h at room temperature. After concentration of the solution, the residue was dissolved in AcOEt and the organic phase was washed with water and brine, dried over MgSO_4 , filtered and concentrated. Compound **14** (0.742 g) was directly engaged in the next step without further purification.

4.1.2.5. 4-[4-(2-[4-(4-(hydroxymethyl)-2-methoxyphenoxy]phenyl)ethyl]phenoxy]-3-methoxybenzaldehyde (15). Compound **14** (0.742 g, 1.3 mmol) was dissolved in a mixture acetone/ H_2O (20/5 mL) and pyridinium *para*-toluene sulfonate (PPTS, 0.40 eq). The solution was stirred under reflux for 3 h and cooled down. The solution was then concentrated in vacuo to remove acetone and ethyl acetate was added. The organic phase was washed with water and brine, dried over MgSO_4 , filtered and concentrated in vacuo to give colorless oil. The residue was purified by flash chromatography (gradient petroleum ether/ethyl acetate 9/1 to 4/6) to afford compound **15** as a colorless oil (0.474 g, 77% over two steps). Rf: 0.58 (petroleum ether/ethyl acetate: 6/4). $^1\text{H NMR}$ (300 MHz, CDCl_3) δ 9.88 (s, 1H); 7.51 (d, $J = 1.8$ Hz, 1H); 7.36 (dd, $J = 8.1$ Hz, $J = 1.8$ Hz, 1H); 7.15 (m, 2H); 7.08–7.05 (m, 3H); 6.96 (m, 2H); 6.85–6.89 (m, 5H); 4.68 (s, 2H); 3.97 (s, 3H); 3.86 (s, 3H); 2.90 (br s, 4H); $^{13}\text{C NMR}$ (75 MHz, CDCl_3) δ 190.9; 155.9; 153.6; 152.7; 151.3; 150.7; 144.9; 138.0; 137.3; 135.7; 131.9; 130.0; 129.5; 125.8; 120.3; 119.6; 119.4; 117.4; 117; 111.5; 110.5; 65.1; 56.1; 56.0; 37.3; 37.1; HRMS (DCI- CH_4) Calculated for $\text{C}_{30}\text{H}_{28}\text{O}_6$ (M^+): 484.1886. Found: 484.1887.

4.1.2.6. {[4-(4-(2-[4-(4-formyl-2-methoxyphenoxy)phenyl]ethyl)phenoxy)-3-methoxyphenyl]methyl}triphenylphosphonium bromide (16). The title compound was prepared by following the procedure used for compound **9** and was isolated as white foam (0.760 g, 96%). Rf: 0.53 (dichloromethane/methanol: 9/1). Mp: 119–121 °C. $^1\text{H NMR}$ (300 MHz, CDCl_3) δ 9.86 (s, 1H); 7.71–7.78 (m, 9H); 7.57–7.63 (m, 6H); 7.48 (d, $J = 2.0$ Hz, 1H); 7.34 (dd, $J = 8.3$ Hz, $J = 2.0$ Hz, 1H); 7.11 (d, $J = 8.7$ Hz, 2H); 7.05 (m, 1H); 7.03 (d, $J = 8.7$ Hz, 2H); 6.93 (d, $J = 8.7$ Hz, 2H); 6.84 (d, $J = 8.2$ Hz, 1H); 6.77 (d, $J = 8.5$ Hz, 2H); 6.64 (d, $J = 8.2$ Hz, 1H); 6.55 (dt, $J = 8.2$ Hz, $J = 2.3$ Hz, 1H); 5.42 (d, $J = 14.1$ Hz, 2H); 3.93 (s, 3H); 3.49 (s, 3H); 2.85 (br s, 4H); HRMS (ESI) Calculated for $\text{C}_{48}\text{H}_{42}\text{O}_2\text{P}$ (M^+): 729.2770. Found: 729.2782.

Macrocycle 17. The macrocycle **17** was synthesized in two steps. **First step (cyclization):** Compound **17** (0.250 g, 0.309 mmol) in dry dichloromethane (45 mL) was added over 10 min, to a cold solution of sodium methoxide (8 eq) in dry dichloromethane (100 mL). The mixture was stirred at room temperature for 18 h and was then concentrated under reduced pressure. The product was extracted with ethyl acetate and the organic phase was washed with H_2O , dried over MgSO_4 , filtered and concentrated in vacuo to give a viscous oil which was not

further purified. **Second step (reduction)**: The aforementioned oily product was dissolved in ethyl acetate (10 mL) and palladium on activated carbon (10% Pd, 100 mg/mmol) was added. The resulting suspension was stirred under H₂ at 0.4 MPa pressure for 24 h at room temperature. The reaction mixture was filtered and concentrated to afford a crude oil. The resulting residue was purified by flash chromatography (gradient petroleum ether/ethyl acetate 95/5 to 50/50) to furnish compound **17** as a white oil (0.124 g, 89% over two steps). Rf: 0.65 (petroleum ether/ethyl acetate: 8/2). ¹H NMR (300 MHz, CDCl₃) δ 6.57–6.60 (m, 4H); 6.47–6.51 (m, 6H); 6.41 (d, *J* = 8.1 Hz, 2H); 6.03 (dd, *J* = 8.0 Hz, *J* = 1.8 Hz, 2H); 3.73 (s, 6H); 2.83 (s, 4H); 2.77 (s, 4H); ¹³C NMR (75 MHz, CDCl₃) δ 157.3; 150.4; 145.8; 136.5; 134.9; 130.3; 121.8; 120.0; 118.2; 113.4; 55.9; 37.8; 37.6; HRMS (DCI-CH₄) Calculated for C₃₀H₂₉O₄ (MH⁺): 453.2066. Found: 453.2064.

Macrocycle M01. To a solution of compound **17** (117 mg, 0.26 mmol), was added BBr₃ (1 M in dichloromethane, 6 eq) at 78 °C. After 2 h30 at this temperature, the reaction mixture was cooled down and stirred for additional 12 h. Cold water was carefully added and the reaction mixture was stirred for 30 min. The solution was diluted with dichloromethane, washed with water then brine, dried over magnesium sulfate and concentrated to afford macrocycle **M01** as a yellow oil. The residue was purified by flash chromatography (gradient petroleum ether/ethyl acetate 9/1 to 5/5) to afford macrocycle **M01** as a lightly yellow solid (0.106 g, 96%). Rf: 0.2 (petroleum ether/ethyl acetate: 8/2). Mp: 177–179 °C. $\nu_{\max}/\text{cm}^{-1}$: 3547; 3410; 3029; 2923; 2855; 1599; 1504; 1334; 1268; 1219; ¹H NMR (300 MHz, CDCl₃) δ 6.68 (d, *J* = 2.1 Hz, 2H); 6.62 (m, 4H); 6.5 (m, 4H); 6.24 (d, *J* = 8.2 Hz, 2H); 5.86 (dd, *J* = 8.1 Hz, *J* = 2.1 Hz, 2H); 5.43 (br s, 2H); 2.79 (s, 4H); 2.77 (s, 4H); ¹³C NMR (75 MHz, CDCl₃) δ 156.8; 147.1; 143.8; 137.2; 135.8; 130.6; 122.2; 118.6; 115.8; 37.7; 37.5; HRMS (ESI) Calculated for C₂₈H₂₃O₄ [M–H]⁺: 423.1596. Found: 423.1595.

CCDC-1958250 (**M01**) contains the supplementary crystallographic data (see supporting information). These data can be obtained free of charge from The Cambridge Crystallographic Data Centre via www.ccdc.cam.ac.uk/data_request/cif.

Selected data for M01: C₂₈H₂₃O₄, 1/2 CH₂Cl₂, *M* = 466.93, monoclinic, space group *P*2₁/*n*, *a* = 19.560(2) Å, *b* = 45.650(5) Å, *c* = 20.292(2) Å, β = 101.668(3)°, *V* = 17745(3) Å³, *Z* = 28, crystal size 0.16 × 0.10 × 0.08 mm³, 243,390 reflections collected (32575 independent, *R*_{int} = 0.2405), 2229 parameters, 197 restraints, *R*₁ [*I* > 2σ(*I*)] = 0.1066, *wR*₂ [all data] = 0.3350, largest diff. peak and hole: 0.577 and –0.507 eÅ^{–3}.

4.1.3. Synthesis of macrocycle M02

4.1.3.1. Methyl 4-(4-formyl-2-methoxyphenoxy)benzoate (10). This compound was synthesized by a similar method (pyridinium *para*-toluenesulfonate, acetone/H₂O, reflux) to that used for the preparation of compound **15**. Compound **10** isolated as a white powder (0.348 g, 83%) was used for the next step without further purification. Rf: 0.58 (petroleum ether/ethyl acetate 6/4). Mp: 115–118 °C. $\nu_{\max}/\text{cm}^{-1}$: 2950; 2920; 1714; 1699; 1612; 1593; 1495; 1283; 1230; ¹H NMR (300 MHz, CDCl₃) δ 9.94 (s, 1H); 8.02 (m, 2H); 7.54 (d, *J* = 1.8 Hz, 1H); 7.46 (dd, *J* = 8.1 Hz, *J* = 1.8 Hz, 1H); 7.11 (d, *J* = 8.1 Hz, 1H); 6.98 (m, 2H); 3.89 (s, 3H); 3.90 (s, 3H); ¹³C NMR (75 MHz, CDCl₃) δ 190.8; 166.4; 160.5; 151.8; 149.7; 133.7; 131.7; 125.5; 125.3; 120.5; 117.3; 111.1; 56.1; 52.1; HRMS (DCI-CH₄) Calculated for C₁₆H₁₅O₅ (MH⁺): 287.0919. Found: 287.0910.

4.1.3.2. Methyl 4-(4-(hydroxymethyl)-2-methoxyphenoxy)benzoate (11) [26]. Compound **11** was synthesized by a similar method to that used for the preparation of compound **8** and was isolated as a colorless oil (0.320 g, 93%). Compound **11** was engaged in the next step without further purification. ¹H NMR (300 MHz, CDCl₃) δ 7.96 (d, *J* = 9.0 Hz, 2H); 7.07 (d, *J* = 1.9 Hz, 1H); 7.07 (d, *J* = 8.1 Hz, 1H); 6.94 (dd, *J* = 8.1 Hz, *J* = 1.9 Hz, 1H); 6.89 (d, *J* = 8.9 Hz, 2H); 4.70 (s, 2H); 3.87 (s, 3H); 3.79 (s, 3H); ¹³C NMR (75 MHz, CDCl₃) 166.7; 162.2;

121.7; 142.6; 139.0; 131.5; 123.8; 122.2; 119.5; 115.7; 11.6; 64.9; 55.8; 51.9; HRMS (DCI-CH₄) Calculated for C₁₆H₁₇O₅ (MH⁺): 289.1076. Found: 289.1069.

4.1.3.3. ((3-Methoxy-4-[4-(methoxycarbonyl)phenoxy]phenyl)methyl)triphenylphosphonium bromide (12) [26]. This compound was synthesized by a similar method to that used for the preparation of compound **9** and it was isolated as a white foam (0.572 g, 79%). The resulting product was used for the next step without further purification. ¹H NMR (300 MHz, CDCl₃) δ 7.94 (m, 2H); 7.75–7.83 (m, 8H); 7.60–7.67 (m, 6H); 7.21 (m, 1H); 6.80 (m, 2H); 6.63 (m, 1H); 5.52 (d, *J* = 13.9 Hz, 2H); 3.87 (s, 3H); 3.47 (s, 3H); HRMS (ESI) Calculated for C₃₄H₃₀O₄P [M]⁺: 533.1882. Found: 533.1879.

4.1.3.4. Methyl 4-[4-(2-(4-[4-(5,5-dimethyl-1,3-dioxan-2-yl)-2-methoxyphenoxy]phenyl)ethyl)-2-methoxyphenoxy]benzoate (18). The title compound was prepared by following the same procedure to that used for the preparation of compound **13** and was purified by flash chromatography (gradient petroleum ether/ethyl acetate 9/1 to 7/3) to furnish compound **18** as a colorless oil (0.471 g, 82% over two steps). ¹H NMR (300 MHz, CDCl₃) δ 7.96 (m, 2H); 7.19 (d, *J* = 1.8 Hz, 1H); 7.03–7.10 (m, 3H); 6.86–6.98 (m, 6H); 6.76–6.79 (m, 2H); 5.39 (s, 1H); 3.89 (s, 3H); 3.88 (s, 3H); 3.79 (d, *J* = 11.1 Hz, 2H); 3.73 (s, 3H); 3.66 (d, *J* = 11.0 Hz, 2H); 2.91 (s, 4H); 1.30 (s, 3H); 0.81 (s, 3H); ¹³C NMR (75 MHz, CDCl₃) δ 166.7; 162.4; 156.0; 151.3; 151.1; 145.7; 141.3; 139.9; 135.6; 135.0; 131.4; 129.4; 123.6; 122.1; 121.0; 120.3; 117.3; 115.6; 113.3; 110.4; 101.4; 77.7; 55.9; 55.8; 51.8; 37.8; 37.1; 30.2; 23.1; 21.8; HRMS (DCI-CH₄) Calculated for C₃₆H₃₉O₈ (MH⁺): 599.2645. Found: 599.2636.

4.1.3.5. 4-[4-(2-(4-[4-(2-Dimethyl-1,3-dioxan-5-yl)-2-methoxyphenoxy]phenyl)ethyl)phenoxy]-3-methoxyphenylmethanol (19). The title compound was prepared from compound **18** (0.468 g, 0.782 mmol), by following the same procedure to that used for the preparation of compound **14**. Compound **19** (0.449 g) was directly engaged in the next step without further purification.

4.1.3.6. 4-[4-(2-(4-[4-(Hydroxymethyl)phenoxy]-3-methoxyphenyl)ethyl)phenoxy]-3-methoxybenzaldehyde (20). The title compound was prepared by following the same procedure to that used for the preparation of compound **15** and was purified by flash chromatography (gradient petroleum ether/ethyl acetate 9/1 in 15 min) to furnish compound **20** as a colorless oil (0.280 g, 74%). ¹H NMR (300 MHz, CDCl₃) δ 9.9(s, 1H); 7.51 (d, *J* = 1.8 Hz, 1H); 7.35 (dd, *J* = 1.8 Hz, *J* = 8.2 Hz, 1H); 7.27 (m, 2H); 7.17 (m, 2H); 6.97 (m, 2H); 6.85–6.91 (m, 4H); 6.76 (d, *J* = 1.8 Hz, 1H); 6.71 (dd, *J* = 2.9 Hz, *J* = 1.8 Hz, 1H); 4.62 (s, 2H); 3.96 (s, 3H); 3.77 (s, 3H); 2.93 (s, 4H); ¹³C NMR (75 MHz, CDCl₃) δ 190.9; 157.7; 153.7; 152.6; 151.1; 150.7; 142.8; 138.5; 137.7; 134.7; 131.9; 129.9; 128.5; 125.7; 121.1; 120.9; 119.5; 117.0; 116.8; 113.2; 110.5; 64.9; 56.1; 55.9; 37.7; 37.2; HRMS (DCI-CH₄) Calculated for C₃₀H₂₈O₆ (M⁺): 484.1886. Found: 484.1874.

4.1.3.7. (([4-(4-(2-[4-(4-Formyl-2-methoxyphenoxy)phenyl]ethyl)-2-methoxyphenoxy]phenyl)methyl]triphenylphosphonium bromide (21). The title compound was prepared by following the same procedure to that used for the preparation of compound **9**. Compound **21** was isolated as a colorless foam (0.114 g, 97%). ¹H NMR (300 MHz, CDCl₃) δ 7.67–7.77 (m, 9H); 7.57–7.64 (6H); 7.50 (d, *J* = 1.7 Hz, 1H); 7.35 (dd, *J* = 8.0 Hz, *J* = 1.8 Hz, 1H); 7.15 (d, *J* = 8.6 Hz, 2H); 7.00 (dd, *J* = 8.8 Hz, *J* = 2.7 Hz, 2H); 6.95 (d, *J* = 8.6 Hz, 2H); 6.85 (d, *J* = 8.2 Hz, 1H); 6.81 (d, *J* = 7.8 Hz, 1H); 6.65–6.71 (m, 4H); 5.31 (d, *J* = 13.9 Hz, 2H); 3.95 (s, 3H); 3.73 (s, 3H); HRMS (ESI) Calculated for C₄₈H₄₂O₅P [M]⁺: 729.2770. Found: 729.2766.

Macrocycle 22. The title compound was prepared by following the same procedure to that used for the preparation of macrocycle **17**. The

resulting residue was purified by flash chromatography (gradient petroleum ether/ethyl acetate 9/1 to 5/5) to afford macrocycle **22** as a white oil (0.112 g, 82% over two steps). ^1H NMR (300 MHz, CDCl_3) δ 6.55 (d, $J = 8.1$ Hz, 2H); 6.52 (br s, 8H); 6.40 (d, $J = 1.8$ Hz, 2H); 6.13 (dd, $J = 8.1$ Hz, 2 Hz, 2H); 3.65 (s, 6H); 2.81 (br s, 8H); ^{13}C NMR (75 MHz, CDCl_3) δ 158.2; 151.4; 144.1; 137.9; 133.8; 129.9; 122.2; 121.9; 116.4; 114.0; 55.9; 38.0; 37.3; HRMS (DCI-CH_4) Calculated for $\text{C}_{30}\text{H}_{29}\text{O}_4$ (MH^+): 453.2066. Found: 453.2067.

Macrocycle M02. The title compound was prepared by following the same procedure than those for macrocycle **M01**. The crude product was purified by flash chromatography (gradient petroleum ether/AcOEt 9/1 to 2/8 in 20 min) to provide macrocycle **M02** as a lightly yellow solid (0.091 g, 88%). Rf: 0.69 (TLC petroleum ether/ethyl acetate 7/3). $\nu_{\text{max}}/\text{cm}^{-1}$: 3442; 3056; 3030; 2925; 2855; 1741; 1596; 1499; 1206; ^1H NMR (300 MHz, MeOD) δ 6.54 (m, 8H); 6.49 (d, $J = 2.0$ Hz, 2H); 6.37 (d, $J = 8.2$ Hz, 2H); 5.83 (dd, $J = 8.2$ Hz, $J = 1.9$ Hz, 2H); 2.75 (m, 8H); ^{13}C NMR (75 MHz, MeOD) δ 159.5; 150.0; 144.5; 139.0; 135.6; 131.1; 123.0; 122.4; 118.3; 117.9; 38.9; 38.3; HRMS (DCI-CH_4) Calculated for $\text{C}_{28}\text{H}_{25}\text{O}_4$ (MH^+): 425.1753. Found: 425.1746.

4.2. Biology

4.2.1. InhA activity inhibition

Triclosan and NADH were obtained from Sigma-Aldrich. Stock solutions of all compounds were prepared in DMSO such that the final concentration of this co-solvent was constant at 5% v/v in a final volume of 1 mL for all kinetic reactions. Kinetic assays were performed using *trans*-2-dodecenoyl-coenzyme A (DDCoA) and wild type InhA as previously described [37]. Briefly, reactions were performed at 25 °C in an aqueous buffer (30 mM PIPES and 150 mM NaCl pH 6.8) containing additionally 250 μM cofactor (NADH), 50 μM substrate (DDCoA) and the tested compound (at 50 μM or 10 μM). Reactions were initiated by addition of InhA (100 nM final) and NADH oxidation was followed at 340 nm. The inhibitory activity of each derivative was expressed as the percentage inhibition of InhA activity (initial velocity of the reaction) with respect to the control reaction without inhibitor. Triclosan was used as a positive control. All activity assays were performed in triplicate. For the most potent compounds, IC_{50} values were determined using the 4-parameter curve-fitting software XLFit (IDBS) with at least six points.

4.2.2. MIC determination in *M. tuberculosis* growth inhibition

M. tuberculosis H37Rv was used as the reference strain. *M. tuberculosis* strain was grown at 37 °C in Middlebrook 7H9 broth (Difco), supplemented with 0.05% Tween 80, or on solid Middlebrook 7H11 medium (Difco) supplemented with oleic acid-albumin-dextrose-catalase (OADC). MICs for the new compounds were determined by means of the REMA method [38].

Two independent *M. tuberculosis* cultures were grown approximately to mid-log phase, then diluted to a final $\text{OD}_{600} = 0.0005$ and used to determine MIC in microtiter. Streptomycin and triclosan were used as control. Concentrations assayed were: 40-20-10-5-2.5-1.25-0.6-0.3-0.15 $\mu\text{g}/\text{ml}$, 0 as control. After an incubation of 7 days at 37 °C, resazurin was added at a final concentration of 0.0025%. After 1 day of incubation, plates were read (Ex 544 nm, Em 590 nm, Fluoroskan ThermoScientific).

4.2.3. Molecular docking

Molecular graphics were performed with the UCSF Chimera package [39]. Chimera is developed by the Resource for Biocomputing, Visualization, and Informatics at the University of California, San Francisco (supported by the NIGMS P41-GM103311).

The protein structures used in this paper were structurally aligned with the PDB [40] entry 1BVRa [7] (1BVR, chain A) set as reference and using UCSF Chimera/Matchmaker [41] program. The protein structures, in this reference space, were prepared (structure checks,

rotamers, hydrogenation) using Biovia Discovery Studio 2016 (<http://accelrys.com/>) and UCSF Chimera.

The new compounds were sketched using ChemAxon Marvin 16.5, (<http://www.chemaxon.com>). All ligands (extracted from protein structures or new) were checked (hybridization, hydrogenation, some geometry optimizations, 3D sketching) and were merged in SDF libraries using Discovery Studio.

Molecular modeling studies were carried with Molegro Virtual Docker 6 (<http://www.clcbio.com>) software using 1P45a (1P45, chain A) structure [13] as target. A search space (sphere of 15 Å radius) surrounding the binding cavity was used and the ligands were set flexible during the docking. The docking process uses the MolDock [42] function (Moldock [grid] with a resolution of 0.3 Å) for scoring. The Moldock optimizer (6000 iteration steps, population size of 100, 40 independent runs, other parameters let as default) was used for searches. The Tabu clustering was pushed to 1.5 Å (RMSD threshold) in order to increase sensitivity. Post-minimization and post-optimization of H-Bonds parameters were activated; other parameters of this docking protocol were let with default values. No water molecules (entropy penalty) were taken in account in the study [43].

The poses issued from the calculations were ranked, filtered and annotated according to the following sequential rules: {A} the MolDock, Rerank, contributions terms (Interaction, Protein, Cofactor) issued from MolDock calculations were selected to give a table of poses/scores. {B} The table was ranked according to MolDock scores. {C} For all types of scores/contributions, the values were distributed into ranges (as a histogram) of 5 units (giving a scale color in tables). {D} Each pose of the table was compared to others and the poses with the same conformation (in this case a ring topology) were classified. Eventually, a given pose was defined as representative for each topology group. {E} Each pose of interest was manually inspected for the interactions with cofactor NAD, TYR158 and other protein residues. The poses were tagged (+ sign) if a typical network of hydrogen bonds involving TYR158 was possible. {F} The first four best MolDock scores were retained as typical results, and PLANTS [44] score was calculated (re-scoring).

These macrocyclic compounds are relatively rigid molecules; therefore, false positives are known to occur when a full flexibility (softened potentials) scheme is enabled. The protocol takes in account this kind of bias using non flexible (residues) searches. However, after step {E} of protocol, checks were done using a strong minimization (ligand, residues and backbone) in order to ensure that the best pose's conformations do not vary significantly.

The poses were analyzed and compared to different inhibitors co-crystallized in InhA structures, particularly the two triclosan residues (TCL500, TC450) found in 1P45a, the c16 fatty acyl substrate (THT) found in 1BVRa and the inhibitor PT70 (TCU) found in 2X22a (2X22, chain A) [32] structures.

The poses were classified on the basis of macrocycle topology defined by a letter, a number and a sign. The letter (A or B in this paper) is related to the overall macrocycle envelope in space, the associated number (i.e. A1 or A2) is related to the position of hydroxyl groups (in space). The topologies were tagged (+) if, at least, one hydrogen bond is found possible between the pose and TYR158.

Declaration of Competing Interest

There are no conflicts to declare.

Acknowledgements

The authors are grateful to financial support from the CNRS and the Université Paul Sabatier.

Appendix A. Supplementary material

Supplementary data to this article can be found online at <https://doi.org/10.1016/j.bioorg.2019.103498>.

References

- [1] World Health Organization, Global Tuberculosis Report 2018, World Health Organization, Geneva, Switzerland, 2018.
- [2] E. Pontali, M.C. Raviglione, G.B. Migliori, and the writing group members of the Global TB Network Clinical Trials Committee. Regimens to treat multidrug-resistant tuberculosis: past, present and future perspectives, *Eur. Respir. Rev.* 28 (2019) 190035.
- [3] C. Lange, K. Dheda, D. Chesov, A.M. Mandalakas, Z. Udawadia, C.R. Horsburgh Jr., Management of drug-resistant tuberculosis, *Lancet* 394 (2019) 953–966.
- [4] M. Jankute, J.A. Cox, J. Harrison, G.S. Besra, Assembly of the mycobacterial cell wall, *Annu. Rev. Microbiol.* 69 (2015) 405–423.
- [5] C. Vilchèze, H.R. Morbidoni, T.R. Weisbrod, H. Iwamoto, M. Kuo, J.C. Sacchettini, W.R. Jacobs Jr., Inactivation of the *inhA*-encoded fatty acid synthase II (FASII) enoyl-acyl carrier protein reductase induces accumulation of the FASII end products and cell lysis of *Mycobacterium smegmatis*, *J. Bacteriol.* 182 (2000) 4059–41067.
- [6] A. Quémard, J.C. Sacchettini, A. Dessen, C. Vilchèze, R. Bittman, W.R. Jacobs Jr., J.S. Blanchard, Enzymic characterization of the target for isoniazid in *Mycobacterium tuberculosis*, *Biochemistry* 34 (1995) 8235–8241.
- [7] D.A. Rozwarski, C. Vilchèze, M. Sugantino, R. Bittman, J.C. Sacchettini, Crystal structure of the *Mycobacterium tuberculosis* enoyl-ACP reductase, *InhA*, in complex with NAD⁺ and a C16 fatty acyl substrate, *J. Biol. Chem.* 274 (1999) 15582–15589.
- [8] A. Chollet, L. Mourey, C. Lherbet, A. Delbot, S. Julien, M. Baltas, J. Bernadou, G. Pratiel, L. Maveyraud, V. Bernardes-Génisson, Crystal structure of the enoyl-ACP reductase of *Mycobacterium tuberculosis* (*InhA*) in the apo-form and in complex with the active metabolite of isoniazid pre-formed by a biomimetic approach, *J. Struct. Biol.* 190 (2015) 328–337.
- [9] L.A. Spagnuolo, S. Eltschkner, W. Yu, F. Daryaei, S. Davoodi, S.E. Knudson, E.K. Allen, J. Merino, A. Pechibul, B. Moree, N. Thivalapill, J.J. Truglio, J. Salafsky, R.A. Slayden, C. Kisker, P.J. Tonge, Evaluating the contribution of transition-state destabilization to changes in the residence time of Triazole-based *InhA* inhibitors, *J. Am. Chem. Soc.* 139 (2017) 3417–3429.
- [10] C.W. Levy, A. Roujeinikova, S. Sedelnikova, P.J. Baker, A.R. Stuijter, A.R. Slabas, D.W. Rice, J.B. Rafferty, Molecular basis of triclosan activity, *Nature* 398 (1999) 383–384.
- [11] A. Chollet, G. Mori, C. Menendez, F. Rodríguez, I. Fabing, M.R. Pasca, J. Madacki, J. Kordulakova, P. Constant, A. Quémard, V. Bernardes-Génisson, C. Lherbet, M. Baltas, Design, synthesis and evaluation of new GQO derivatives as inhibitors of *InhA* enzyme and *Mycobacterium tuberculosis* growth, *Eur. J. Med. Chem.* 101 (2015) 218–235.
- [12] T. Matviuk, F. Rodríguez, N. Saffon, S. Mallet-Ladeira, M. Gorichko, A.L. de Jesus Lopes Ribeiro, M.R. Pasca, C. Lherbet, Z. Voltenko, M. Baltas, Design chemical synthesis of 3-(9H-fluoren-9-yl)pyrrolidine-2,5-dione derivatives and biological activity against enoyl-ACP reductase (*InhA*) and *Mycobacterium tuberculosis*, *Eur. J. Med. Chem.* 70 (2013) 37–48.
- [13] M.R. Kuo, H.R. Morbidoni, D. Alland, A. Sneddon, S.F. Sneddon, B.B. Gourlie, M.M. Staveski, M. Leonard, J.S. Gregory, A.D. Janjigian, C. Yee, J.M. Musser, B. Kreiswirth, H. Iwamoto, R. Perozzo, W.R. Jacobs Jr., J.C. Sacchettini, D.A. Fidock, Targeting tuberculosis and malaria through inhibition of Enoyl reductase: compound activity and structural data, *J. Biol. Chem.* 278 (2003) 20851–20859.
- [14] T. Matviuk, J. Madacki, G. Mori, B.S. Orena, C. Menendez, A. Kysil, C. André-Barris, F. Rodríguez, J. Kordulakova, S. Mallet-Ladeira, Z. Voltenko, M.R. Pasca, C. Lherbet, M. Baltas, Pyrrolidinone and pyrrolidine derivatives: evaluation as inhibitors of *InhA* and *Mycobacterium tuberculosis*, *Eur. J. Med. Chem.* 123 (2016) 462–475.
- [15] C. Menendez, A. Chollet, F. Rodríguez, C. Inard, M.R. Pasca, C. Lherbet, M. Baltas, Chemical synthesis and biological evaluation of triazole derivatives as inhibitors of *InhA* and antituberculosis agents, *Eur. J. Med. Chem.* 52 (2012) 275–283.
- [16] P.S. Shirude, P. Madhavapetti, M. Naik, K. Murugan, V. Shinde, R. Nandishah, A. Bhat, A. Kumar, S. Hameed, G. Holdgate, G. Davies, H. McMiken, N. Hegde, A. Ambady, J. Venkataraman, M. Panda, B. Bandodkar, V.K. Sambandamurthy, J.A. Read, Methyl-thiazoles: a novel mode of inhibition with the potential to develop novel inhibitors targeting *InhA* in *Mycobacterium tuberculosis*, *J. Med. Chem.* 56 (2013) 8533–8542.
- [17] A. Chollet, L. Maveyraud, C. Lherbet, V. Bernardes-Génisson, An overview on crystal structures of *InhA* protein: apo-form, in complex with its natural ligands and inhibitors, *Eur. J. Med. Chem.* 146 (2018) 318–343.
- [18] R.G. Hartkoorn, F. Pojer, J.A. Read, H. Gingell, J. Neres, O.P. Horlacher, K.C. Altman, S.T. Cole, Pyridomycin bridges the NADH⁺ and substrate-binding pockets of the enoyl reductase *InhA*, *Nat. Chem. Biol.* 10 (2014) 96–98.
- [19] K. Maeda, H. Kosaka, Y. Okami, H. Umezawa, A new antibiotic, Pyridomycin J. Antibiot., Ser. A 6 (1953) 140.
- [20] D.C. Harrowen, S.L. Kostik, Macroyclic bisbenzyl natural products and their chemical synthesis, *Nat. Prod. Rep.* 29 (2012) 223–242.
- [21] Y.Q. Shi, C.J. Zhu, H.Q. Yuan, B.Q. Li, J. Gao, X.J. Qu, B. Sun, Y.N. Cheng, X. Li, S. Li, H.X. Lou, Marchantin C, a novel microtubule inhibitor from liverwort with anti-tumor activity both in vivo and in vitro, *Cancer Lett.* 276 (2009) 160–170.
- [22] X. Xue, D.F. Sun, C.C. Sun, H.P. Liu, B. Yue, C.R. Zhao, H.X. Lou, X.J. Qu, Inhibitory effect of riccardin D on growth of human non-small cell lung cancer: in vitro and in vivo studies, *Lung Cancer* 76 (2012) 300–308.
- [23] A. Cheng, L. Sun, X. Wu, H. Lou, The inhibitory effect of a macrocyclic bisbenzyl riccardin D on the biofilms of *Candida albicans*, *Biol. Pharm. Bull.* 32 (2009) 1417–1421.
- [24] K. Fujii, D. Morita, K. Onoda, T. Kuroda, H. Miyachi, Minimum structural requirements for cell membrane leakage-mediated anti-MRSA activity of macrocyclic bis(benzyls), *Bioorg. Med. Chem. Lett.* 26 (2016) 2324–2327.
- [25] M. Iwashita, S. Fujii, S. Ito, T. Hirano, H. Kagechika, Efficient and diversity-oriented total synthesis of Riccardin C and application to develop novel macrolactam derivatives, *Tetrahedron* 67 (2011) 6073–6082.
- [26] B. Sun, L. Li, Q.-W. Hu, H.-B. Zheng, H. Tang, H.-M. Niu, H.-Q. Yuan, H.-X. Lou, Design, synthesis, biological evaluation and molecular modeling study of novel macrocyclic bisbenzyl analogues as antitubulin agents, *Eur. J. Med. Chem.* 129 (2017) 186–208.
- [27] K. Onoda, H. Sawada, D. Morita, K. Fujii, H. Tokiwa, T. Kuroda, H. Miyachi, Anti-MRSA activity of isopropylcholin-type macrocyclic bis(benzyls) is mediated through cell membrane damage, *Bioorg. Med. Chem.* 23 (2015) 3309–3316.
- [28] A. Dessen, A. Quémard, J.S. Blanchard, W.R. Jacobs, J.C. Sacchettini, Crystal structure and function of the isoniazid target of *Mycobacterium tuberculosis*, *Science* 267 (1995) 1638–1641.
- [29] D.A. Rozwarski, G.A. Grant, D.H. Barton, W.R. Jacobs Jr., J.C. Sacchettini, Modification of the NADH of the isoniazid target (*InhA*) from *Mycobacterium tuberculosis*, *Science* 279 (1998) 98–102.
- [30] T.J. Sullivan, J.J. Truglio, M.E. Boyne, P. Novichenok, X. Zhang, C.F. Stratton, H.J. Li, T. Kaur, A. Amin, F. Johnson, R.A. Slayden, C. Kisker, P.J. Tonge, High affinity *InhA* inhibitors with activity against drug-resistant strains of *Mycobacterium tuberculosis*, *ACS Chem. Biol.* 1 (2006) 43–53.
- [31] J.S. Freundlich, F. Wang, C. Vilchèze, G. Gulter, R. Langley, G.A. Schiehsler, D.P. Jacobus, W.R. Jacobs, J.C. Sacchettini, Triclosan derivatives: towards potent inhibitors of drug-sensitive and drug-resistant *Mycobacterium tuberculosis*, *ChemMedChem* 4 (2009) 241–248.
- [32] S.R. Luckner, N. Liu, C.W. am. Ende, P.J. Tonge, C. Kisker, A slow, tight binding inhibitor of *InhA*, the enoyl-acyl carrier protein reductase from *Mycobacterium tuberculosis*, *J. Biol. Chem.* 285 (2010) 14330–14337.
- [33] C.T. Lai, H.-J. Li, W. Yu, S. Shah, G.R. Bommineni, V. Perrone, M. Garcia-Diaz, P.J. Tonge, C. Simmerling, Rational modulation of the induced-fit conformational change for slow-onset inhibition in *Mycobacterium tuberculosis* *InhA*, *Biochemistry* 54 (2015) 4683–4691.
- [34] H.-J. Li, C.T. Lai, P. Pan, W. Yu, N. Liu, G.R. Bommineni, M. Garcia-Diaz, C. Simmerling, P.J. Tonge, A structural and energetic model for the slow-onset inhibition of the *Mycobacterium tuberculosis* enoyl-ACP reductase *InhA*, *ACS Chem. Biol.* 9 (2014) 986–993.
- [35] C.A. Merget, C.A. Striffler, Slow-onset inhibition of *Mycobacterium tuberculosis* *InhA*: revealing molecular determinants of residence time by MD simulations, *PLoS One* 10 (2015) 1–25.
- [36] P. Pan, P.J. Tonge, Targeting *InhA*, the FASII Enoyl-ACP reductase: SAR studies on novel inhibitor scaffolds, *Curr. Topics Med. Chem.* 12 (2012) 672–693.
- [37] S.D. Joshi, D. Kumar, S.R. Dixit, N. Tgadi, U.A. More, C. Lherbet, T.M. Aminabhavi, K.S. Yang, Synthesis, characterization and antitubercular activities of novel hydrazones and their Cu-complexes, *Eur. J. Med. Chem.* 121 (2016) 21–39.
- [38] J.C. Palomino, A. Martin, M. Camacho, H. Guerra, J. Swings, F. Portaels, Resazurin microtiter assay plate: simple and inexpensive method for detection of drug resistance in *Mycobacterium tuberculosis*, *Antimicrob. Agents Chemother.* 46 (2002) 2720–2722.
- [39] E.F. Pettersen, T.D. Goddard, C.C. Huang, G.S. Couch, D.M. Greenblatt, E.C. Meng, T.E. Ferrin, UCSF chimera – a visualization system for exploratory research and analysis, *J. Comput. Chem.* 25 (2004) 1605–1612.
- [40] H.M. Berman, J. Westbrook, Z. Feng, G. Gilliland, T.N. Bhat, H. Weissig, I.N. Shindyalov, P.E. Bourne, The protein data bank, *Nucl. Acids Res.* 28 (2000) 235–242.
- [41] E.C. Meng, E.F. Pettersen, G.S. Couch, C.C. Huang, T.E. Ferrin, Tools for integrated sequence-structure analysis with UCSF Chimera, *BMC Bioinform.* 7 (2006) 339–349.
- [42] R. Thomsen, M.H. Christensen, MolDock: a new technique for high-accuracy molecular docking, *J. Med. Chem.* 49 (2006) 3315–3321.
- [43] M.A. Lie, R. Thomsen, C.N.S. Pedersen, B. Schlott, M.H. Christensen, Molecular docking with ligand attached water molecules, *J. Chem. Inf. Model.* 51 (2011) 909–917.
- [44] O. Korb, T. Stützle, T.E. Exner, Empirical scoring functions for advanced protein-ligand docking with PLANTS, *J. Chem. Inf. Model.* 49 (2009) 84–96.